UNIVERSIDAD DE MURCIA

ESCUELA INTERNACIONAL DE DOCTORADO

MELANOCORTIN 1 RECEPTOR AS REGULATOR OF PROTECTIVE RESPONSES AGAINST OXIDATIVE STRESS AND UVR-INDUCED DNA DAMAGE

El receptor de Melanocortinas 1 (MC1R) como regulador de respuestas de defensa frente al estrés oxidativo, daño inducido por la radiación ultravioleta

Dª María Castejón Griñán

2019

UNIVERSIDAD DE MURCIA

FACULTAD DE MEDICINA

Departamento de Bioquímica y Biología Molecular B e Inmunología

MELANOCORTIN 1 RECEPTOR AS REGULATOR OF PROTECTIVE RESPONSES AGAINST OXIDATIVE STRESS AND UVR-INDUCED DNA DAMAGE

El Receptor de Melanocortinas 1 (MC1R) como regulador de respuestas de defensa frente al estrés oxidativo, daño inducido por la radiación ultravioleta

Memoria presentada por **María Castejón Griñán**

para optar al grado de **Doctora por la Universidad de Murcia**

(Tesis Doctoral con Mención Europea)

Murcia, Mayo 2019

FACULTAD DE MEDICINA

UNIVERSIDAD DE MURCIA

Departamento de Bioquímica y Biología Molecular B e Inmunología

Doña **Cecilia Mª Herraiz Serrano**, Profesora Ayudante Doctora de Universidad del Área de Bioquímica y Biología Molecular en el Departamento de Bioquímica y Biología Molecular B e Inmunología y Don **José Carlos García-Borrón Martínez**, Catedrático de Universidad del Área de Bioquímica y Biología Molecular en el Departamento de Bioquímica y Biología Molecular B e Inmunología,

AUTORIZAN

La presentación de la Tesis Doctoral titulada "**El Receptor de Melanocortinas 1 (MC1R) como regulador de respuestas de defensa frente al estrés oxidativo, daño inducido por la radiación ultravioleta**", realizada por Doña María Castejón Griñán bajo nuestra inmediata dirección y supervisión, en el Departamento de Bioquímica y Biología Molecular B e Inmunología, y que presenta para la obtención del grado de Doctora por la Universidad de Murcia.

En Murcia, a 23 de Mayo de 2019

Fdo Cecilia Mª Herraiz Serrano

José Carlos García-Borrón

The experimental work exposed in this Doctoral Thesis has been supported by grants SAF2012-32134 and SAF2015-67092-R from MINECO (Spain) and FEDER (European Community) and 19875/ GERM/15 from Fundación Seneca, Comunidad Autónoma de la Región de Murcia (CARM).

María Castejón Griñán holds a pre-doctoral fellowship from the Fundación Séneca (Research Coordination Centre, Murcia, Spain), under the FPI (Formation of Investigative Personnel) Programme (F19850/FPI/15)

Publications

Some of the results are included in the following publications:

1. Cecilia Herraiz, Conchi Olivares, **María Castejón-Griñán**, Marta Abrisqueta, Celia Jiménez-Cervantes, José Carlos García-Borrón.
   Functional Characterization of MC1R-TUBB3 Intergenic Splice Variants of the Human Melanocortin 1 Receptor.
   PLoS One 2015 Dec 11; 10(12):e0144757.
   https://doi.org/10.1371/journal.pone.0144757

2. **María Castejón-Griñán**, Cecilia Herraiz, Conchi Olivares, Celia Jiménez-Cervantes and Jose Carlos García-Borrón.
   cAMP-independent non-pigmentary actions of variant melanocortin 1 receptor: AKT-mediated activation of protective responses to oxidative DNA damage.
   Oncogene 2018; **37**, 3631–3646. https://doi.org/10.1038/s41388-018-0216-1

Other publications:

Marta Abrisqueta, Concepción Olivares, Cecilia Herraiz, **María Castejón-Griñán**, Julia Sirés-Campos, José Carlos García-Borrón, Celia Jiménez-Cervantes.
Human melanocortin 1 receptor-mediated ubiquitination of nonvisual arrestins. Role of Mahogunin Ring Finger 1 E3 ligase.
Biochim. Biophys. Acta - Mol. Cell Res. 2018 Jan; 1865(1):76-94.
https://doi.org/10.1016/j.bbamcr.2017.09.013

Participation in meetings

MC1R controls mitochondrial function and oxidative stress in melanoma. Margalida Torrens-Mas, Mercedes Nadal-Serrano, **María Castejón-Griñán**, Pilar Roca and Jordi Oliver. Oxygen Club of California World Congress "oxidants and antioxidants in biology (24/06/2015 to 26/06/2015, Valencia, Spain).

Functional interactions of β-arrestin isoforms and human Melanocortin 1 receptor. Marta Abrisqueta, Conchi Olivares, Julia Sirés Campos, **María Castejón-Griñán**, Cecilia Herraiz, Jose Carlos García-Borrón, Celia Jiménez-Cervantes. XXXVIII Spanish Society for Biochemistry and Molecular Biology Meeting (07/09/2015 to 10/09/2015, Valencia, Spain).

Non-Pigmentary roles of Melanocortin 1 Receptor signaling in melanocytes: Regulation of Defensive Responses to Oxidative Damage. **María Castejón-Griñán**, Marta Abrisqueta, Julia Sirés-Campos, Concepción Olivares, Celia Jimenez-Cervantes, Jose Carlos García-Borrón, Cecilia Herraiz. XXXVIII Spanish Society for Biochemistry and Molecular Biology Meeting (07/09/2015 to 10/09/2015, Valencia, Spain).

Mgrn1-dependent downregulation of pigmentation is a cell autonomous process involving changes in melanosome and melanogenesis enzymes maturation. Julia Sirés-Campos, **María Castejón**, Marta Abrisqueta, Cecilia Herraiz, José C. García-Borrón, Celia Jiménez-Cervantes, Conchi Olivares. XXXVIII Spanish Society for Biochemistry and Molecular Biology Meeting (07/09/2015 to 10/09/2015, Valencia, Spain).

cAMP-independent non-pigmentary actions of Melanocortin 1 Receptor signaling in melanocytes: Regulation of Defensive Responses to Oxidative Damage. **María Castejón-Griñán**, Marta Abrisqueta, Julia Sirés-Campos, Concepción Olivares, Celia Jimenez-Cervantes, José Carlos García-Borrón, Cecilia Herraiz. 20th European Society for Pigment Cell Research Meeting (12/09/2016 to 15/09/2016, Milan, Italy).

Mahogunin RING Finger 1 regulates the melanosomal pH and decreases pigmentation by acidification of the melanosome. Julia Sirés-Campos, **María Castejón-Griñán**, Marta Abrisqueta, Dorothy C. Bennett, Elena V. Sviderskaya, Cecilia Herraiz, Celia Jiménez-Cervantes, José Carlos García-Borrón, Conchi Olivares. 20th European Society for Pigment Cell Research Meeting (12/09/2016 to 15/09/2016, Milan, Italy).

Genome instability and aberrant cell cycle progression in Mahogunin Ring Finger-1 null mouse melanocytes. Idoya Martínez-Vicente, Cecilia Herraiz, Marta Abrisqueta, **María Castejón-Griñán**, Julia Sirés-Campos, Elena V. Sviderskaya, Dorothy C. Bennett, Conchi Olivares, José Carlos García-Borrón, Celia Jiménez-Cervantes. International Pigment Cell Conference (IPCC) (26/08/2017 to 30/08/2017, Denver, Colorado, USA).

Mahogunin Ring Finger-1 controls Tyrosinase activity and melanin synthesis by regulation of melanosomal pH. Julia Sirés-Campos, Conchi Olivares, Ana Lambertos, Cecilia Herraiz, Marta Abrisqueta, **María Castejón-Griñán**, Idoya Martínez-Vicente, Elena V. Sviderskaya, Dorothy C.

Bennett, Rafael Peñafiel, Celia Jiménez-Cervantes, José Carlos García-Borrón. International Pigment Cell Conference (IPCC) (26/08/2017 to 30/08/2017, Denver, Colorado, USA).

cAMP-independent Non-Pigmentary actions of variant Melanocortin 1 Receptor: Activation of Protective Responses to Oxidative DNA Damage. **María Castejón-Griñán**, Cecilia Herraiz, Concepción Olivares, Celia Jimenez-Cervantes and Jose Carlos García-Borrón. Chromosomal Instability: From Molecular Mechanisms to Disease workshop (13/11/2017 to 15/11/2017, Baeza, Spain).

MSH activates BER pathway through a NOX/AKT- mediated mechanism in human melanoma cells harboring MC1R- variants, to decrease oxidative DNA damage. **María Castejón-Griñán,** Cecilia Herraiz, Celia JiménezCervantes, José Carlos García-Borrón. 21st European Society for Pigment Cell Research Meeting (24/09/2018 to 27/09/2018, Rennes, France).

Induction of a senescent- like phenotype by loss of MGRN1 expression in mouse melanocytes. Idoya Martínez, Marta Abrisqueta, **María Castejón-Griñán,** Conchi Olivares, Cecilia Herraiz, José Carlos García-Borrón, Celia Jiménez-Cervantes. 21st European Society for Pigment Cell Research Meeting (24/09/2018 to 27/09/2018, Rennes, France).

Downregulation of MGRN1 expression decreases the metastatic potential of melanoma cells in vitro and in vivo. Cecilia Herraiz; Idoya Martínez; **María Castejón-Griñán**; Conchi Olivares; Marta Abrisqueta; Celia Jiménez-Cervantes; José Carlos García-Borrón. 21st European Society for Pigment Cell Research Meeting (24/09/2018 to 27/09/2018, Rennes, France).

A mi familia, especialmente a mis padres

Juan Luis y María, a mi hermana Lola y a Guille

Agradecimientos

Gracias, en primer lugar, a mi tutora Celia y a mis directores Cecilia y José Carlos. A Celia y José Carlos por toda su dedicación, su sabiduría y su motivación, pero sobretodo por confiar en mi desde que el primer momento, por apoyarme siempre y por ayudarme a crecer. A Cecilia por estar siempre dispuesta a ayudarme y permanecer al pie del cañón. Por todos tus buenos consejos y tu preocupación por mí, por transmitirme tu capacidad de trabajo y hacerlo todo siempre con alegría. Eres un ejemplo profesional y personal.

Gracias a mis compañeras de laboratorio, las que están aquí y las que se han ido. A Julia, Marta, Ana, Conchi e Idoya. Y a Cecilia de nuevo, que también incluyo en este grupo. ¡Por todo! Por hacer del laboratorio un sitio agradable, por escuchar mis agobios, compartir mis preocupaciones y celebrar mis alegrías. A Marta por ayudarme desde que llegué a hacer el TFG y cederme una parte de su laboratorio ¡con lo que sabemos que le cuesta!, por los cafés y por las risas. A Conchi por su apoyo y sus ratos de conversaciones que tanto ayudan. A Ana por transmitirme su alegría, tranquilidad y bondad a la par que su capacidad de trabajo y esfuerzo. A Julia por todos los ratos compartidos, nuestras innumerables charlas, por entenderme tan bien y por preocuparse por mi incluso después de haberse marchado, en definitiva, muchas gracias por ser mi amiga más allá del laboratorio. A Idoya, mi copiloto en la última etapa, por estar codo con codo en el laboratorio cada día y ser tan buena conmigo. Gracias por esos viajes a Copenhague y París. Tengo la gran suerte de que todas nos entendamos tan bien y de que nos apoyemos tanto. Muchas gracias de corazón.

A todos los miembros del departamento de Bioquímica y Biología Molecular B e Inmunología, es especial a Paco Arques, Fernando, Trini y Rafa.

Gracias a los vecinos de pasillo, el departamento de Biología Celular e Histología. A Manolo, José Ángel, María, Emma, Blanca, Rebeca, Paula, Julieta y Leo por esos ratos a la hora de la comida, que siempre se hacen más llevaderos con nuestras conversaciones y por ayudarme siempre que he necesitado algo, aunque os lleve buscar un anticuerpo en el último congelador del laboratorio. A los doctorandos por nuestras charlas sobre la situación de la investigación y por compartir nuestras ganas de crecer profesionalmente.

A todos los miembros del Servicio de Apoyo a la Investigación de la Universidad de Murcia. Especialmente a los de los servicios de Cultivo de Tejidos, a los de Microscopía, a los de Biología Molecular y a los de Análisis de Imagen, que me ayudaron especialmente en los primeros años.

A todos los componentes del Centro de Estabilidad Cromosómica de la Universidad de Copenhague. En especial a Andrés, David y Stephanie. A Andrés por confiar en mí, por enseñarme tanto y hacerme sentir un miembro más de su grupo. A David y Stephanie por ayudarme dentro del laboratorio y fuera de él. Por todos los buenos ratos, las risas, por tratarme con tanto cariño, por preocuparos por mí y por ser mis amigos.

A mis amigas Lidia, Miriam, Elena y Raquel. Por entenderme siempre, aunque os quede tan lejano lo que hago. A Lidia y Miriam por estar siempre ahí, por compartir mis alegrías y mis penas, y por motivarme y alegrarme.

Gracias a mi familia por entender que tenía que "dar de comer a las células" cuando llegaba tarde y preocuparse tanto por mí.

A Guille por apoyarme en todas mis decisiones, aunque eso conlleve estar a distancia, y siempre hacerlo con una sonrisa, por motivarme y creer en mí siempre, por celebrar mis alegrías y ayudarme con mis problemas y por quererme.

A mis padres y a mi hermana por tantas horas aguantándome hablando del trabajo, por aconsejarme a tomar decisiones, por ayudarme en todo lo posible, por vuestro apoyo y vuestro cariño. Y no solamente en esta etapa sino siempre, por educarme en los valores del esfuerzo, la constancia y la honestidad para conseguir lo que me proponga y celebrarlo conmigo.

INDEX

Index

LIST OF ACRONYMS

List of Acronyms

The acronyms used in this PhD thesis are listed below in alphabetical order:

53BP1: 53-binding protein 1

6-4PPs: pyrimidine (6-4) pyrimidone photoproducts

8-oxodG: 8-oxo-7,8-dihydroguanine

$O_2^{\bullet-}$: superoxide radical anion

AC: adenylyl cyclase

ACTH: adrenocorticotropic hormone

AKAP12: A-kinase-anchoring protein 12

ALM: acral lentiginous melanoma

ATM: ataxia telangiectasia mutated

ATR: ataxia telangiectasia and Rad3-related protein

ASR: age-standardized incidence rated

APE-1/Ref1: AP-endonuclease 1

APS: ammonium persulfate

ARRB: β-arrestin

ASIP: agouti signal protein

BCA: bicinchoninic acid

BER: base excision repair

bFGF: basic fibroblast growth factor

BSA: bovine Serum Albumin

cAMP: cyclic adenosine monophosphate

CAT: catalase

CCND1: cyclin D1

CDKN2A: cyclin-dependent kinase inhibitor 2A

CDK4: cyclin-dependent kinase 4

Chx: cycloheximide

CPDs: cyclobutane pyrimidine dimers

CRE: cAMP-responsive element

CREB: cAMP-responsive element binding

Cys: cysteine

CysDOPA: cysteinylDOPA

ΔΔCt: comparative Ct Method for Relative Quantification

dbcAMP: dibutyryl-cAMP

DC: DOPAchrome

DCFDA: 2′7′dichlorodihydrofluoresceindiacetate

DCT (TYRP2): DOPAchrome tautomerase

DDA: 2′,5′-dideoxyadenosine

DDB1: damaged DNA binding protein 1

DDB2: damaged DNA binding protein 2

DDR: DNA damage response

DHI: 5,6-dihydroxyindole

DHICA: 5,6-dihydroxyindole-2-carboxylic acid

DMEM: dulbecco's modified eagle medium

DNA: deoxyribonucleic acid

DNA-PK: DNA-dependent protein kinase

DPI: diphenylepodium

DQ: L-DOPAquinone

DSB: double DNA strand break

ECIS: European Cancer Information System

ECL: enhanced chemiluminescence

EDTA: ethylenediaminetetraacetic acid

ENDBR: endothelin-B receptor

Endo H: endoglycosidase H

ER: endoplasmic reticulum

ERK: extracellular signal-regulated kinase

ET-1: endothelin-1

FBS: fetal bovine serum

FGF: fibroblast growth factor

FGFR: fibroblast growth factor receptor

FSK: forskolin

γ-GCS: γ-glutamylcysteine synthase

GPCR: G protein-coupled receptor

GPx: glutathione peroxidase

GRK: G protein-coupled receptor kinase

GSTPi: glutathione-S-transferase Pi

GSH: glutathione

H_2O_2: hydrogen peroxide

HBD3: β-defensin 3

HBSS: hank's balanced salt solution

HGF: hepatocyte growth factor

HMCs: human melanoma cells

HO-1: hemeoxygenase-1

HR: homologous recombination

HRP: horseradish peroxidase

IAA: iodoacetamide

IBMX: 3-isobutil-1-metilxantina

IL: interleukin

iNOX: nitric oxide synthase

IR: ionizing radiation

KITLG: KIT ligand

KRPG: krebs-ringer phosphate

L-DOPA: L-3,4-dihydroxyphenylalanine

LB: Lysogeny Broth

LMM lentigo maligna melanoma

LOF: loss-of-function

Luperox: tert-butyl hydroperoxide

LRO: lysosome-related organelles

MAPK: mitogen-activated protein kinase

MC: melanocortin

MC1R: melanocortin 1 receptor

MGRN1: mahogunin Ring Finger-1

MITF: microphthalmia-associated transcription factor

MMPs: metalloproteinases

Mr: molecular weight

αMSH: α-melanocyte stimulating hormone

MTT: 3-(4,5-dimethylthiazol-2-yl)-2,5-diphenyltetrazolium bromide

NDP-MSH: [Nle4, D-Phe7]-αMSH

NEM: N-Ethylmaleimide

NER: nucleotide excision repair

NGS: next generation sequencing

NHEJ: non-homologous-end-joining

NHMs: normal human melanocytes

NM: Nodular melanoma

NOX: NADPH oxidase

NOXA1: NADPH oxidase activator 1

NR4A2: nuclear Receptor Subfamily 4 Group A Member 2

Nrf2: nuclear factor (erythroid-derived 2)-like 2)

OGG: 8-oxoguanine DNA glycosylase

ORF open Reading Frame

PBS: phosphate buffered saline

PCR: polymerase chain reaction

PDK1: 3-phosphoinositide-dependent protein kinase 1

PGC-1α: peroxisome proliferator-activated receptor γ coactivator-1α

PI3K: phosphoinositide-3-kinase

PIP_2: phosphatidylinositol-(3,4)-biphosphate

PIP_3: phosphatidylinositol-(3,4,5)-triphosphate

PKA: protein kinase A

PKB: protein kinase B

PKC: protein kinase C

PMSF: phenylmethanesulfonyl fluoride

Polδ: DNA polymerase delta *XPAB1*

POMC: Pro-opiomelanocortin

Prx1: peroxiredoxin1

PTEN: phosphatase and tensin homolog deleted on chromosome 10

PVDF: polyvinylidene difluoride

Rb1: retinoblastoma

RGP: radial Growth Phase

RHC: red hair color

RNA: ribonucleic acid

RNS: Reactive Nitrogen Species

ROS: reactive oxygen species

RT: room temperature

RT-PCR: real time polymerase chain reaction

RTK: tyrosine kinase receptor

SB: DNA strand break

SC79: 2-amino-6-chloro-α-cyano-3-(ethoxycarbonyl)-4H-1-benzopyran-4-acetic acid ethyl ester

SCF: stem cell factor

SDS: sodium dodecil sulfate

TERT: telomerase reverse transcriptase

XPA: xeroderma pigmentosum A

SDS-PAGE: discontinuous sodium dodecyl sulfate polyacrylamide gel electrophoresis

SEM: standard error of mean

SNV: single nucleotide variants

SOD1: superoxide dismutase

SSB: single DNA strand break

SSM: superficial spreading melanoma

TAE: tris-acetate-EDTA buffer

TBS: tris Buffer Saline

TEMED: tetramethylethane-1,2-diamine

TGFβ: transforming growth factor beta

TM: transmembrane

TMB: 3,3′,5,5′Tetrametilbencidina

TNFα: tumor necrosis factor alpha

TP53: tumor protein P53

TPA: 12-O-Tetradecanoylphorbol 13-acetate

TUBB3: Tubulin-β-III

TYR: tyrosinase

TYRP: tyrosinase-related protein

UVR: ultraviolet radiation

VGP: Vertical Growth Phase

WES: whole-exome sequencing

WGS: whole-genome sequence

Wip1: p53-induced phosphatase 1

WT: wild type

XPC: xeroderma pigmentosum C

INTRODUCTION

The skin

The skin is the largest organ of the body accounting for approximately 15% of the adult body weight. Its primary role is to act as an intact surface between our body and the external environment protecting human life from exposure to various damaging environmental stimuli, such as toxic substances, ultraviolet radiation (UVR) and microorganisms. The skin is also the largest sensory organ of the body and performs metabolic functions, such as vitamin D production. This organ consists of three different layers: epidermis, dermis and hypodermis (Figure 1).

1. The **epidermis** is a stratified epithelium mostly consisting of keratinocytes (80-90% of the overall epidermal cell population), which produce keratins, proteins that contribute to the physical protective properties of skin. The layers of the epidermis are: the **stratum corneum**, a thick layer of flattened cells; the **stratum lucydum**, which helps produce friction between the stratum corneum and the granulosum; the **stratum granulosum** composed of cells which have lost the nucleus and are filled with keratin; **the stratum spinosum**, the largest layer of the epidermis where the **squamous** cells are located, whose function is to strengthen the epidermis and to assist in intercellular communication; and **the basal layer (stratum germinativum, basement membrane)**, a single cell layer and the deepest of the epidermis. The basal layer is the only layer with proliferative potential. Stem cells undergo continuous cell division (mitosis), detach from the underlying basement membrane and differentiate as they migrate through the epidermis. Therefore, keratinocytes from the skin surface periodically detach and are continually replaced by inner cells moving outward in a process called desquamation[1]. The basal layer also contains **melanocytes** (~5%), dendritic-like cells responsible for producing melanin, the pigment that gives skin color and photoprotection; Merkel cells (~3-5%) which are cutaneous sensory cells, and Langerhans immune cells (~5-8%).
2. The **dermis**, beneath the epidermis, contains tough connective tissue, hair follicles, and sebaceous and sweat glands. It is mainly composed by fibroblasts, which synthesize extracelular matrix components (collagen and elastin) to confer elasticity and mechanic resistance to the skin, and by immune cells.
3. The deeper subcutaneous tissue, the **hypodermis**, containing vascular vessels and nerve endings, is made of connective tissue and fat that protects against physical lesions and prevents heat lost.

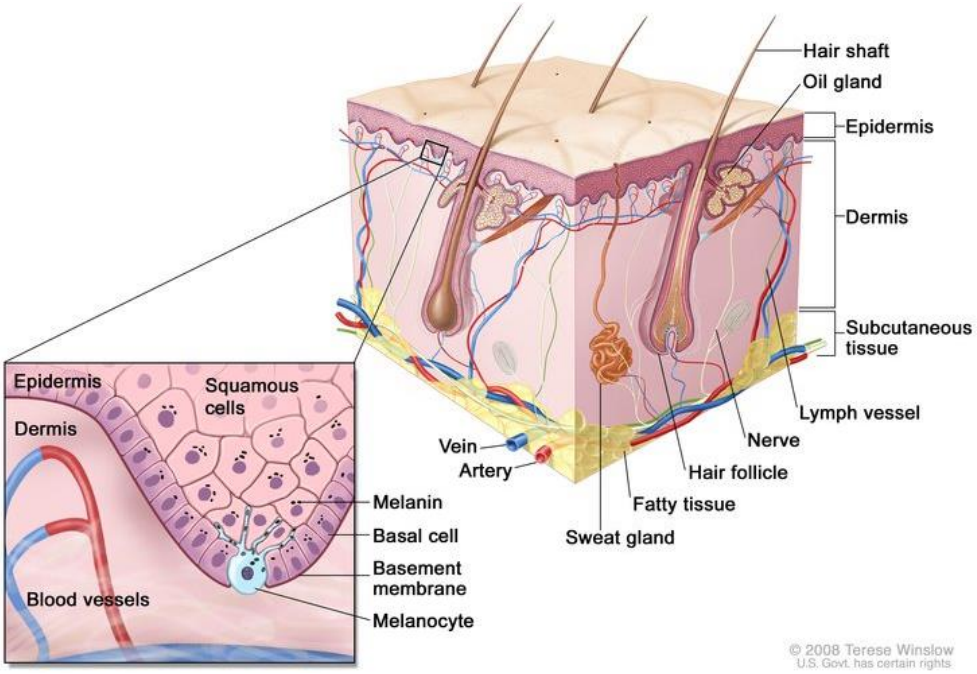

Figure 1. Schematic representation of normal skin and layers. Detail showing basement membrane where melanocytes are located. Adapted from *National Cancer Institute*, available online: https://visualsonline.cancer.gov/details.cfm?imageid=8284.

Melanocytes

Melanocytes are specialized cells derived from the neural crest that migrate to the epidermis, hair follicles and the eye during embryogenesis[2]. But melanocytes are also located in mucosa, cochlea, brain, heart, lung and even in adipose tissue (reviewed by[3]). The best-known role of these dendritic-like cells is to produce pigments called melanins in response to certain stimuli, such as UVR, and to transfer these pigments to the surrounding keratinocytes to protect them from UVR-induced DNA damage[4,5]. Melanocytes have also been considered "sensory" and regulatory cells that contribute to the maintenance of human epidermal homeostasis[6], but these biological functions will not be further discussed here.

2.1. Melanins and melanosomes

Melanins are polyphenolic pigments derived from oxidation and cyclation of the amino acid tyrosine[7,8]. Melanocytes can produce two types of melanin: the black-brown photoprotective eumelanin and the yellow-red poorly photoprotective pheomelanin[2,9]. Both melanins are synthetized within melanocytes through a complex enzymatic process named Raper-Mason

pathway[10] (Figure 2). The type of melanin formed depends on the activity of the melanogenic enzymes: tyrosinase (TYR), and the tyrosinase-related proteins (TYRP1 and TYRP2); and on the availability of substrates, such as tyrosine and sulfhydryl groups[11,12]. TYR is the rate-limiting enzyme of this pathway and catalyzes the first two reactions: the hydroxylation of L-tyrosine to L-3,4-dihydroxyphenylalanine (L-DOPA), and the conversion of this later into L-DOPAquinone (DQ) by oxidation (reviewed by[13,14]). Then, the pathway progresses to eu- or pheomelanin production depending on the sulfhydryl compounds content[15]. In the absence of low molecular weight sulfhydryl compounds (cysteine or glutathione), intramolecular cyclization of DQ leads to DOPAchrome (DC) which spontaneously loses its carboxylic group generating 5,6-dihydroxyindole (DHI). DHIs are oxidized and further polymerize producing DHI melanins, dark brown insoluble polymers. However, in the presence of TYRP2 (also named DC tautomerase, DCT), this enzyme catalyzes the keto-enolic tautomerization of DC into 5,6-dihydroxyindole-2-carboxylic acid (DHICA)[16], which is then oxidized and polymerizes to yield the light brown moderately-soluble DHICA-melanins[17–19]. Thus, during eumelanogenesis a mix of DHI-DHICA melanin is formed in a ratio determined by TYRP2 activity. On the other hand, pheomelanogenesis is favored in the presence of high levels of cysteine (Cys) or glutathione (GSH). A reductive addition of Cys to DQ to give CysteinylDOPA (CysDOPA) occurs, and oxidation of this product leads to benzothiazine intermediates that polymerize forming pheomelanin[20,21]. Both types of melanin are synthesized within melanocytes simultaneously; therefore melanogenesis is better described as 'mixed melanogenesis'.

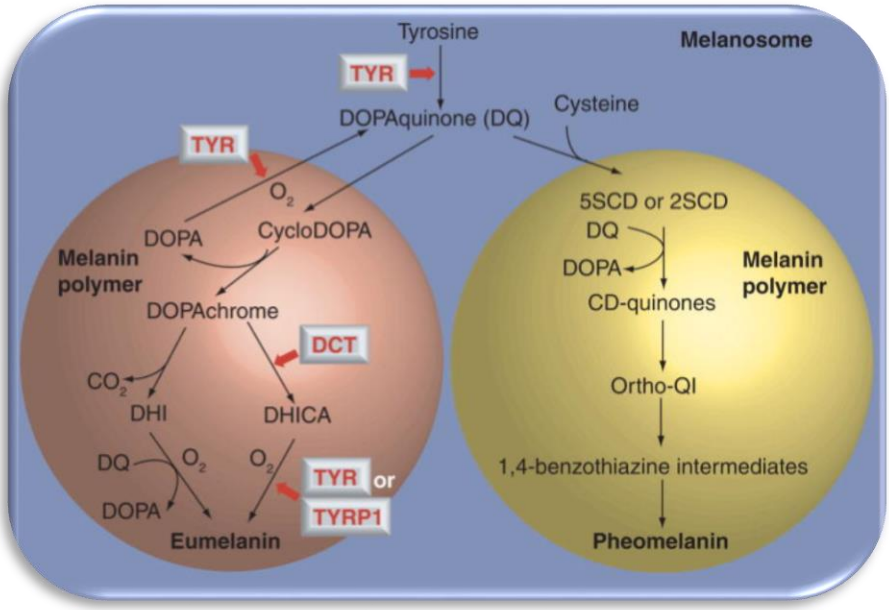

Figure 2. Biosynthetic pathways of eumelanin and pheomelanin. Adapted from Kondo and Hearing, 2011[9].

Within melanocytes, melanin production, storage and transport takes place in specialized membrane-bound organelles termed melanosomes. Melanosome morphology depends on the type of melanin synthetized (Figure 3). Eumelanin-containing melanosomes (eumelanosomes) are elliptical, with longitudinal deposition of pigments over an intraluminal fibrillar matrix[22,23]. Conversely, pheomelanin-containing pheomelanosomes, are less regularly shaped and compact than eumelanosomes, predominantly spherical, with granular deposition of pigments[23–25]. Eu- and pheomelanosomes also differ in their luminal pH. Melanosomes derived from melanocytes of light-skinned individuals are more acidic and have lower TYR activity than melanosomes from dark skin, which have a more neutral pH and higher TYR activity[26,27]. Melanosomes are Lysosome-Related Organelles (LRO) which contain acid-dependent hydrolases and lysosomal-associated membrane proteins[28]. All LROs progressively mature from precursors by acquisition of specialized cargoes and generation of a luminal environment supporting their function[29]. Non-pigmented melanosome precursors, or premelanosomes, are produced via the trans-Golgi network and/or endocytosis. Premelanosomes mature by acquiring melanogenic enzymes and effectors required for motility or secretion. According to their degree of maturation, melanosomes are classified in four well-characterized stages[30]. Stage I melanosomes correspond to perinuclear and spherical premelanosomes with poor or absent matrix organization. Stage II eumelanosomes are ovoid organelles containing longitudinally organized matrix fibers without melanin. In pheomelanosomes, melanin is already formed at this stage. In stage III, there are deposits of melanin and TYR activity is maximal. Finally, stage IV melanosomes are opaque, completely filled with melanin and no longer have TYR activity[9,31] (Figure 3). In melanocytes, the 'late' melanosomes (stages III and IV) bind to microtubules and undergo actin-dependent transport towards the cell periphery, where they are transferred to keratinocytes[9,31].

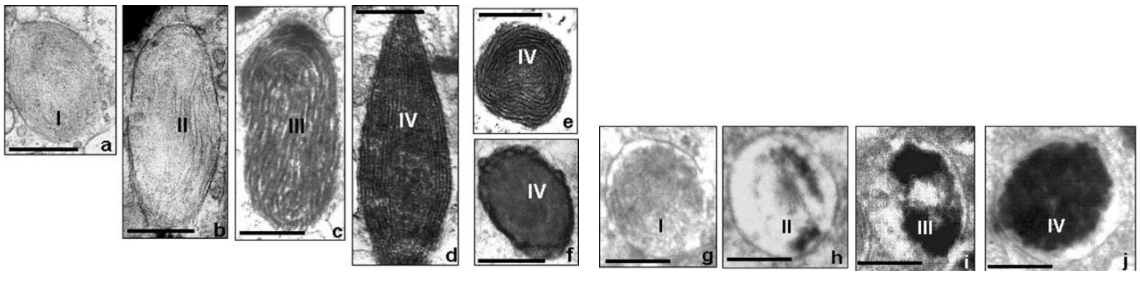

Figure 3. Melanosomes at different maturation stages. Electron microscopy images showing the different stages of eumelanogenesis (a-f) and pheomelanogenesis (g-j). Adapted from Slominski et al., 2004[32].

2.2. Epidermal melanin unit

Melanocytes are in intimate physical and functional contact with keratinocytes, as described by Fitzpatrick and Breathnach[33] who introduced the concept of "epidermal melanin unit". They proposed that each melanocyte interacts with 30-40 keratinocytes to achieve skin pigmentation[3,34] and to distribute melanin-containing melanosomes throughout the epidermis. In keratinocytes, melanosomes are distributed around the nucleus to protect it from UVR (Figure 4). In fact, skin color does not depend on the number of melanocytes, which is similar among individuals with different phenotypes, but relies on the type, number and size of melanosomes, as well as on their correct transfer, distribution and organization through the epidermis[35,36].

However, the "epidermal melanin unit" involves a much more complex interaction between melanocytes and keratinocytes than pigment transfer and distribution. Keratinocytes not only regulate pigment formation within melanocytes but also their differentiation, proliferation and DNA damage responses (DDRs), among other processes[37]. These regulatory interactions will be discussed in section 3.

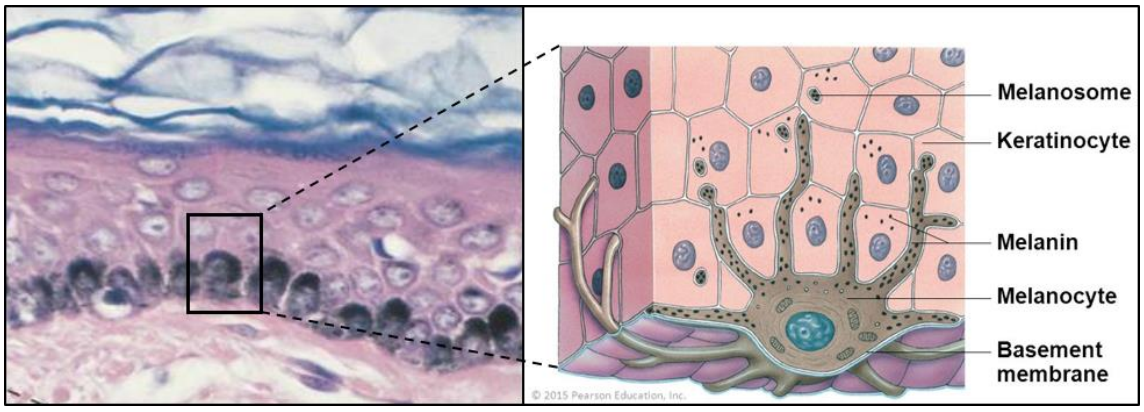

Figure 4. The epidermal melanin unit. Adapted from Pearson Education, 2015.

2.3. Cutaneous response to UVR: focus on the role of melanin

Cumulative UVR exposure contributes to UV-induced DNA damage, oxidative stress, and inflammation in the skin. Therefore, overexposure to UVR is a major risk factor for melanoma and non-melanoma skin cancer development.

UVR causes different types of DNA lesions. Direct absorption of UV photons by DNA triggers the formation of dimerized pyrimidine bases, mainly cyclobutane pyrimidine dimers (CPDs), the most frequent UVR-induced lesions in cellular DNA[38], and pyrimidine (6-4) pyrimidone photoproducts (6-4PPs)[39,40]. A third type of photoproduct has been identified, the Dewar valence isomer, formed

by absorption by 6-4PPs of an additional photon[41]. Formation of other DNA lesions, such as adenine dimers[42,43] or adenine–thymine dimers[42,44,45] has been reported as minor photoreactions. UVR also damages DNA indirectly by production of reactive oxygen species (ROS). This oxidative stress also causes CPDs, oxidative base lesions mainly 8-oxo-7,8-dihydroguanine (8-oxodG) and DNA strand breaks (SBs) as well as lipid and protein oxidation. The type of lesion induced by UVR depends on its wavelength. The UV wavelength range extends from 100 to 400 nm and has three components: UVC (100-280 nm), UVB (280-315 nm) and UVA (315-400 nm). The UVR components relevant for human health are UVB and the least energetic UVA, since UVC is absorbed by oxygen and ozone in the atmosphere. If unrepaired, UVR-induced DNA lesions lead to mutations in proto-oncogenes and tumor suppressor genes and malignant transformation of skin cells. Therefore, UVR is considered a "complete carcinogen", but the contribution of each type of radiation to melanoma and non-melanoma skin cancers initiation and development and the mechanisms accounting for these processes are still controversial.

2.3.1. DNA lesions induced by UVB radiation

The least penetrant UVB wavelength mainly induces pyrimidine dimer formation by direct absorption of photons by DNA. Although absorption is maximal at 260 nm (in the UVC range), DNA also absorbs effectively in the UVB region[46] (Figure 5). In UVB-irradiated double-stranded DNA, 6-4PPs are 3- to 5-fold less frequent than CPDs[47,48]. Occurrence of oxidative stress in human skin and cultured keratinocytes exposed to UVB radiation has also been demonstrated by detection of ROS, mainly superoxide radical anion ($O_2^{\bullet -}$) and hydrogen peroxide (H_2O_2)[49–55]. It has been proposed that UVB-induced ROS and Reactive Nitrogen Species (RNS) are generated by cyclooxygenase, NADPH oxidase (NOX)[53,56,57] or nitric oxide synthase (iNOX)[55,58–61]. In addition, UVB was able to induce bystander effect in non-target neighbor cells. As a result, UVB radiation is able to induce the formation of 8-oxodG in the DNA of skin and cultured cells[62–69], but the relevance of UVB-induced oxidative lesions is still debated. Indeed, UVB-related oxidative lesions are considered of limited quantitative relevance since 8-oxodG levels represent 1% of total DNA damage compared to CPDs and 6-4PPs following UVB excitation[70]. However, a significant biological role is strongly suggested by several observations, such as the increased susceptibility to UVR-induced skin cancer in 8-oxoguanine DNA glycosylase 1 (OGG1) knockout mice[71]. This enzyme recognizes oxidized bases and activates their repair. Therefore, the actual contribution of oxidative lesions to UVB-induced skin carcinogenesis requires further study. Formation of UVB-

induced DNA SBs has also been reported. UVB induces DNA SBs indirectly by accumulation of unrepaired CPDs. During replication, these unrepaired CPDs promote collapse of replication forks leading to formation of DNA SBs[72].

In summary, it is well established that excessive UVB exposure is strongly implicated in skin cancers[73], mainly by the promotion of CPD-derived mutations. In fact, these mutations are considered "UV-signature mutations". However, the participation of UVA in skin carcinogenesis is also accepted[74], although its specific mechanisms remain unclear[75].

2.3.2. UVA-induced DNA lesions

Even though UVA photons are much more weakly absorbed than UVB (Figure 5), the total absorption of UVA wavelengths by DNA is only 4.2-fold lower than that of UVB wavelengths[46,76]. This points out the likely relevance of UVA-induced CPDs, which may have been underestimated for long. Several studies have indicated that UVA radiation can induce CPDs[77,78] by oxidative mechanisms[79–81] and by direct absorption[82–84]. On the other hand, 6-4PPs are produced in very low amounts or not at all in the UVA range[76,84]. However, UVA photons have been shown to be more efficient than UVB photons in converting UVB-generated 6-4PPs into highly mutagenic Dewar valence isomers[85], thus suggesting that UVA can be mutagenic per se and also by cooperation with UVB.

Much of the UVA-dependent DNA damage is attributed to oxidative stress. UVA generation of CPDs by redox processes has been reported[38,79–81]. A mechanism involving a photosensitizing role of melanin has been recently proposed[79,86]. This mechanism seems possible since other non-DNA chromophores present in human skin cells also absorb UVA photons, leading to the formation of photo-excited states with subsequent generation of ROS and RNS, organic free radicals and other toxic photoproducts. The role of pheomelanin in melanomagenesis will be further discussed in the section 2.3.4. As described for UVB, UVA can also induce ROS through bystander effects and enzymatic activities[78,87,88].

UVA-induced oxidative stress also promotes the formation of the main DNA oxidation product, 8-oxodG, and in a minor extent single-SBs (SSB)[89] and pyrimidine oxidation products[85,90]. Although it appears quite unlikely that DSBs may be generated directly by low energy UVA photons, their formation in UVA-irradiated cells has been reported[91], probably as a result of unrepaired CPDs that could be converted into DSBs during replication[92].

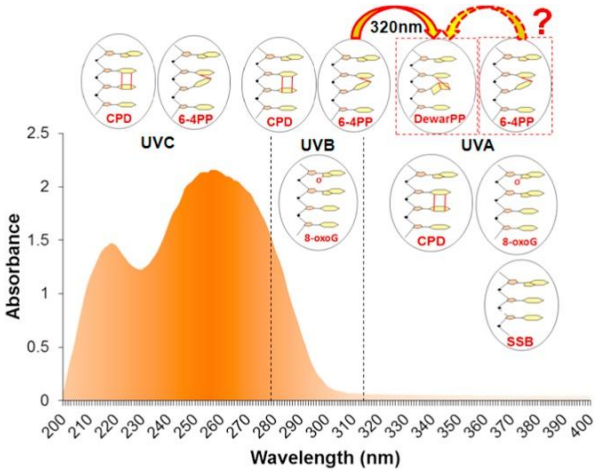

Figure 5. DNA absorption spectrum and the main types of DNA lesions induced by each UV band. Adapted from Schuch et al., 2017[46].

The relative contribution of each DNA lesion to the overall DNA damage burden induced by UVR and its consequences on skin carcinogenesis are not clear. Particularly, the information on UVA-generated damage to cellular DNA is still scarce. UVB mainly induces highly mutagenic CPDs, responsible for "UVR mutation signatures" (C to T transitions), associated with 90% of non-melanoma skin cancers. However, only 60% of melanomas seem related to UV mutation signatures[5,93,94]. It has been proposed that the different mutational spectrum of melanomas and keratinocyte-derived tumors arises from a different class of DNA damage. This hypothesis suggests an important role for oxidative lesions, mainly induced by UVA, in melanoma. In this line, a study showed that the ratio between CDPs and 8-oxodG in melanocytes was 1.4[77], whereas in other skin cell types CPDs are the major DNA lesions, possibly because as much as 99% of UVA reaches the basal lamina of the epidermis, where melanocytes are located, compared with only 1% of UVB. Consistent with this notion, UVB fingerprint mutations and CPDs were largely confined to non-basal cells of human squamous-cell carcinomas and solar keratoses, while 8-oxodG and its resulting mutations (G to T) were at least as common in the deeper (dermal) parts of the lesions as in the distal layers[95]. Nevertheless, some reports identified CPDs as the major photolesions caused by UVA in cells[85] and in skin[96,97] and these have been considered potentially more mutagenic than those induced by UVB[98]. Therefore, a role of UVA-induced CPDs in solar genotoxicity cannot be ruled out.

Altogether, these results strongly suggest that UVA is involved in melanomagenesis. However, further investigation about the relative contribution of UVA and UVB to melanomagenesis, and quantitative and qualitative information about DNA lesions induced by each UV wavelength, would help to better understand melanomagenesis and to develop rational strategies for melanoma prevention and treatment.

2.3.3. Cutaneous photoprotective mechanisms

The accumulation of unrepaired DNA damage increases the frequency of mutations, thus contributing to carcinogenesis. Nevertheless, the mutational burden not only depends on the rate of formation of DNA lesions, but also on the activation of complex systems that cells have developed to avoid the deleterious effects of sunlight. These systems include antioxidants, that protect DNA, and mechanisms of DNA damage repair and tolerance. The antioxidant defense comprises a series of molecules that act to detoxify ROS and to prevent their subsequent reactions. Cellular antioxidants include enzymes, non-enzymatic substances (reduced glutathione-GSH, ascorbate, tocopherols, carotenoids, albumin, uric acid and bilirubin), proteins, chelating agents, and phenolic and aromatic molecules. A major antioxidant is GSH, a reducing agent reacting directly with several ROS. GSH also participates in the reduction of H_2O_2 catalyzed by the enzyme glutathione peroxidase (GPx). GPx catalyzes the GSH-dependent reduction of H_2O_2 to form oxidized glutathione (GSSG) and H_2O. GSSG is recycled by glutathione reductase, which converts GSSG into GSH at the expense of NADPH[99–101]. Other important antioxidant enzymes are catalase (CAT), which reduces H_2O_2 to H_2O and O_2, and superoxide dismutase (SOD) that inactivates $O_2^{\bullet-}$ anions[102].

On the other hand, after generation of DNA lesions, several DNA repair mechanisms are activated. In fact, in human cells, DNA damage initiates many cellular responses (DNA damage responses, DDR), which include cell cycle arrest (mostly in G1/S and S/G2), DNA repair and cell death by apoptosis[76,84]. CPDs and 6-4PPs can be recognized and repaired by the nucleotide excision repair (NER) pathway[103]. In this pathway, DNA damage-sensing proteins, including Xeroderma pigmentosum C (XPC), damaged DNA binding protein 1 (DDB1), damaged DNA binding protein 2 (DDB2) and Xeroderma pigmentosum A (XPA), bind to sites of DNA damage and recruit repair machinery to the lesion[104]. The importance of NER to limit CPD-dependent carcinogenesis is well illustrated by the susceptibility of NER defective human patients to skin cancer[105]. UVR-induced oxidative DNA damage is recognized by the lesion-specific glycosylase OGG1 and repaired by base excision repair (BER)[106]. Briefly, after altered or inappropriate bases are

recognized by OGG1, this enzyme or AP-endonuclease (APE-1/Ref1) cleaves the damaged base from the sugar and phosphodiester backbone resulting in an apurinic/apyrimidinic site, which is then processed and repaired by DNA polymerases and DNA ligases using the complementary strand as a template to ensure fidelity. Homologous recombination (HR) and Non-homologous-end-joining (NHEJ) are the pathways responsible for DSBs repair. Regulation of antioxidant defenses and DNA repair pathways is a major area of investigation, since they are critical in determining cutaneous responses to UVR.

2.3.4. Differential role of eu- and pheomelanins in photoprotection

The cutaneous response to sun exposure is highly dependent on skin color diversity and skin phenotypes[107]. The "Fitzpatrick Scale", developed in 1975, classifies 6 phototypes based on basal complexion, melanin level, inflammatory response to UVR and cancer risk[33,108] (Figure 6). Fair skin phenotypes (Fitzpatrick Scale type I and II) are strongly associated with UV sensitivity and skin cancer risk, including melanoma, whereas dark-skinned individuals have a lower skin cancer risk and are more UVR-resistant[14]. In fact, dark skin has an intrinsic UVB protection factor of 13.4, and a UVA protective factor of 5.7 compared to 3.4 and 1.8, respectively, in light skin[109–111].

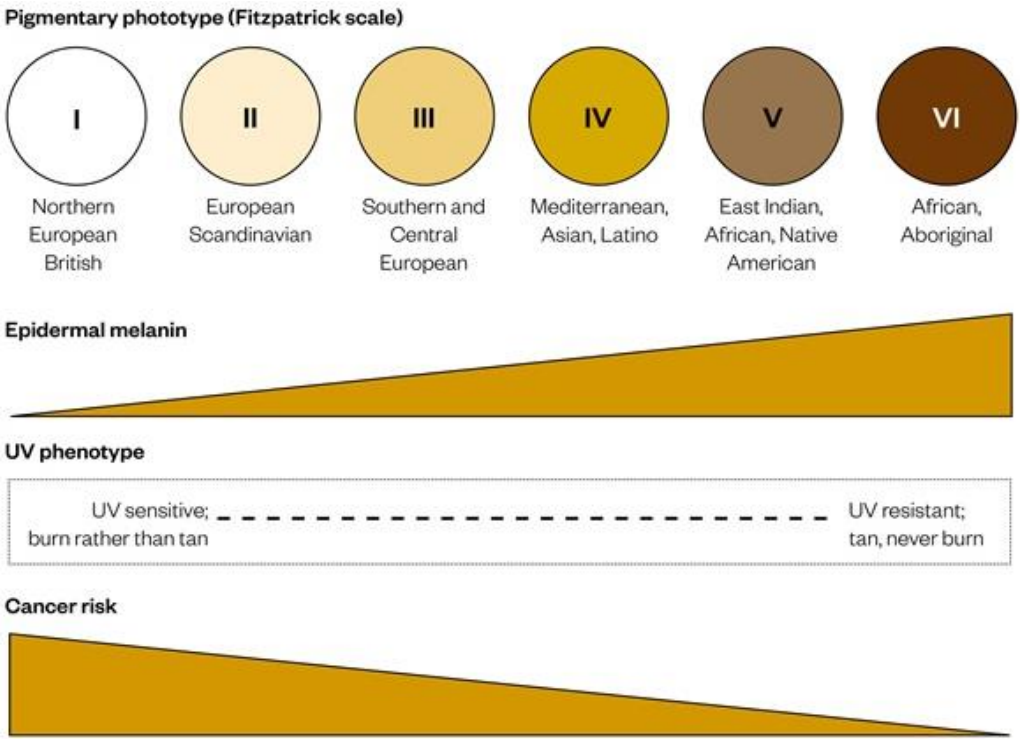

Figure 6. Fitzpatrick scale: Classification of pigmentary phenotypes. Adapted from D'Orazio et al., 2013[5].

Human skin color is mainly determined by the ratio between the dark eumelanin and the lighter pheomelanin[5,12,107,112]. The photoprotective behaviour of eumelanin is well established and relies on limiting the extent of UVR penetration within the epidermis[113] and scavenging ROS[107]. In contrast, pheomelanin is weakly photoprotective against UVR and might even behave as a photosensitizer by enhancing the UVR-induced production of ROS[107,114–116].

Eumelanin is efficient at blocking UVR, by absorption and scattering of incident light. Eumelanin displays a characteristic broad-band optical absorption throughout the UV-visible spectrum, decreasing monotonically with increasing wavelength[117]. Light absorption by eumelanin is followed by thermal relaxation that quenches potentially harmful photochemical reactions[118]. Epidermal eumelanin shields nuclei forming "supranuclear melanin caps" in melanocytes and keratinocytes[119]. In addition, eumelanin is stable whereas pheomelanin is prone to photodegradation[120,121]. In dark skin, eumelanin-rich melanosomes persist in keratinocytes throughout the epidermal layers. In contrast, in lightly pigmented skin, melanosomes with low eumelanin content are degraded, and only "melanin dust", presumed to be the degradation product of pheomelanin, is found in the epidermis. Moreover, the sulfhydryl groups in Cys are prone to oxidation, which further reduces the stability of pheomelanin. In this line, it has been shown that dark skin transmits 7.4% of UVB and 17.5% of UVA, compared to 29.4% and 55.5%, respectively, in light skin[109–111]. Apart from the UVR-blocking ability of eumelanin, its chemical characteristics confer antioxidant and free radical scavenger properties[122–125].

The photoprotective role of eumelanin against UVA-and UVB-induced damage[126] is well documented**.** In an *in vivo* study comparing the levels of UVR-induced DNA damage (and its clereance) in the skin of human individuals with different pigmentation and ethnic origin, an inverse correlation between melanin content and the levels of CPD was demonstrated[127]. *In vitro* experiments analyzing the responses of human melanocyte cultures derived from donors with different skin phototypes and different total melanin and eumelanin contents to the same doses of UVR are in agreement with these results[128].

The higher susceptibility to skin cancer of red hair individuals seems to be due not only to the reduced eumelanin content, but also to the toxic properties of pheomelanins, especially upon exposure to UVR. As explained above, pheomelanin is prone to photodegradation[21,120,129] and is believed to contribute to the damaging effects of UVR by promoting oxidative stress (Figure 7). After UVR exposure, pheomelanin acts as a photosensitizer exacerbating UVR-induced ROS production[122,130,131]. It has been proposed that the UVA-excited pheomelanin chromophore generates $O_2^{\bullet-}$ anion via electron transfer to molecular oxygen, which then generates H_2O_2 and hydroxyl radicals[132]. Generation of singlet oxygen ($^1O_2$) by photoexcitation of pheomelanin with

UVA has also been reported[133,134]. Maresca and coworkers[135] showed that pheomelanin content correlates inversely with the levels and activity of the antioxidant enzyme CAT in human melanocytes, making lightly pigmented melanocytes more susceptible to accumulate oxidative damage after UVR exposure[135]. Indeed, several studies suggest that the phototoxic properties of pheomelanin contribute to UVR-induced DNA damage and melanomagenesis. Pheomelanin increased SSB induction in UVA-irradiated human melanocytes derived from skin phenotype I[89] and participated actively in CPD formation in melanocytes long after UVR exposure[86]. A recent study has suggested that melanin could be involved in UVA-induced "dark" CPDs in human skin *in vivo*[79] and that the increase of UVA-induced CPD with epidermal depth in human skin *in vivo* is related to the increase of melanin concentration with epidermal depth[80,136]. In addition, pheomelanin increased apoptosis in murine skin[137] and another study, revealed that UVA-irradiated mice required melanin to develop melanoma[81].

In summary, it seems well established that UVR-dependent ROS generation by pheomelanin increases oxidative stress, thus contributing to melanomagenesis. In this line, there is increasing evidence supporting that oxidative stress is important for melanoma formation. Dysplastic nevi, considered precursors of melanoma, have higher pheomelanin content and express more ROS than normal human melanocytes (NHMs)[138]. A study in which the genomes of human melanomas were sequenced found that ROS-type mutations, originating predominantly from oxidized guanine, were the second most common mutations found in a human melanoma[93]. In fact, it has been proposed that the most common driver somatic mutation in melanoma $BRAF^{V600E}$ is caused by increased generation of ROS[139]. Moreover, several studies have recently revealed that pheomelanin promotes oxidative stress and ultimately melanomagenesis by UVR-independent mechanisms (Figure 7). These mechanisms would explain why some melanomas arise in shielded areas of the body. Mitra et al. (2012) showed that conditional mice with a red/yellow phenotype bearing a conditional $BRAF^{V600E}$ mutant allele developed invasive melanoma at higher rates than albino mice with the same genetic background even in the absence of UVR[140]. In addition, the same study demonstrated that the skin of pheomelanic mice contained higher levels of oxidative DNA damage and lipid peroxidation than albino mice[140].

Two non-mutually exclusive mechanisms for the induction of oxidative stress and melanomagenesis by pheomelanin in the dark have been proposed[141]. On the one hand, pheomelanin could promote the formation of damaging ROS (Figure 7). On the other, the pigment could deplete protective antioxidants, making the cell more vulnerable to elevated ROS levels[141].

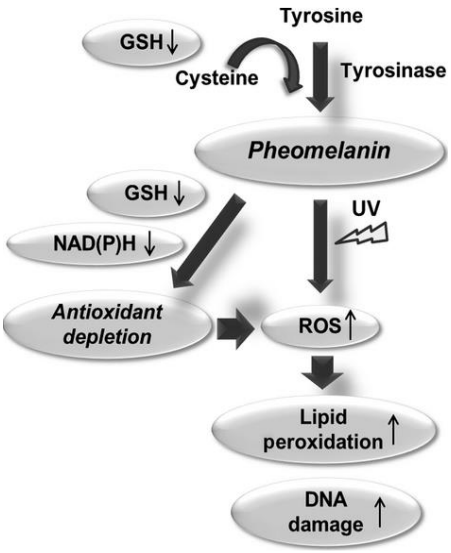

In this line, Panzella et al. demonstrated that pheomelanin can induce depletion of NADH and GSH by a redox cycling mechanism without UVR[142,143] and that the synthetic pathway of pheomelanin, which consumes GSH-derived Cys with consequent depletion of GSH[114,140] contributes to antioxidant depletion (Figure 7). The pro-oxidant ability of pheomelanin has been recently confirmed, as well as its role as pro-inflammatory agent independently from light exposure[144,145], supporting that pheomelanogenesis might be associated with chronic oxidative damage, inflammation and carcinogenesis.

Figure 7. Overall view of the role of pheomelanin in triggering an oxidative stress under light exposure or in the dark conditions. Adapted from Napolitano et al., 2014[114].

In conclusion, a direct relationship between UVR exposure and melanomagenesis is established. On the one hand, the photoprotective effect of eumelanin is documented, but pheomelanin exacerbates UVA-induced oxidative stress, DNA damage and melanomagenesis[81]. Moreover, UVR-independent events involving pheomelanin may also play a significant role in skin carcinogenesis and support the notion that melanoma is not completely UVR-dependent.

Melanocyte-Keratinocyte crosstalk

As explained above, in the epidermal melanin unit, keratinocytes and melanocytes are in tight physical and functional contact. Melanocytes synthesize melanin pigments within melanosomes, and transfer them to keratinocytes through prominent dendritic processes. Conversely, melanocytes strongly depend on keratinocytes for their correct function. Keratinocytes act as paracrine regulators of melanocyte survival, proliferation, differentiation and melanogenesis through secretion of paracrine factors, such as growth factors, hormones and

cytokines. These keratinocyte-derived paracrine factors have key roles in regulating melanocyte function through receptor-mediated signaling pathways. Moreover, this melanocyte-keratinocyte complex interaction can be modulated by environmental stimuli, mainly UVR[34,146].

3.1. Regulation of melanocyte proliferation

Melanocytes are differentiated cells with poor ability to proliferate and a long lifespan in the epidermis[147]. However, keratinocytes synthesize growth factors and cytokines to induce melanocyte proliferation and their synthesis is usually increased upon UVR exposure[34,146]. These include endothelin-1 (ET-1), hepatocyte growth factor (HGF), basic fibroblast growth factor (bFGF, also known as FGF2), the stem cell factor (SCF, or KIT ligand, KITLG), and melanocortins (MCs)[34]. These mitogens act in synergy activating their cognate receptors that trigger different intracellular signal transduction cascades to promote proliferation. Thus, NHMs require the crosstalk of different signaling pathways in order to proliferate.

ET-1 is a 21 amino acid peptide synthesized by keratinocytes[148]. This mitogen binds to a G-protein coupled receptor, the Endothelin-B receptor (ENDBR) on melanocytes[149,150]. Activation of this receptor increases intracellular inositol triphosphate formation and calcium mobilization, and stimulates protein kinase C (PKC), leading to phosphorylation of the extracellular signal-regulated kinases 1 and 2 (ERK1/2)[151,152].

The growth factors HGF[37], FGF2[153] and SCF[154] are also secreted by keratinocytes. They bind to their specific tyrosine kinase receptors (RTKs), cMET, FGFR and cKIT, respectively, to promote melanocyte proliferation[155]. Activation of cell surface RTKs triggers various signal transduction pathways, notably the RAS/RAF/MER/ERK cascade, which stimulates melanocyte proliferation and the phosphoinositide-3-kinase (PI3K)/AKT, pathway crucial for proliferation and survival[155].

Overall, activation of the RTKs, cKIT, cMET, and FGFR receptors, as well as stimulation of PKC by ET-1, results in activation of the ERK1/2 kinases in human melanocytes[149]. Therefore, ERK1/2 pathway is critical for the mitogenic response of melanocytes. In fact, the ERK signaling pathway is the most commonly mutated pathway in melanoma[156]. Mutations or molecular alterations in members of this pathway, notably BRAF and NRAS, drive aberrant growth and survival in malignant melanocytes, and are frequent key events in melanoma initiation and progression[84,155].

Alpha-melanocyte-stimuling hormone (αMSH), synthesized by melanocytes and keratinocytes, stimulates proliferation of melanocytes through a synergistic potentiation of the mitogenic effects of growth factors[157–161]. αMSH role in regulation of melanocyte function will be further discussed in the next section.

3.2. Regulation of melanocyte differentiation

3.2.1. Melanocortins

Melanocyte differentiation is mainly induced by the keratinocyte-derived MC, αMSH. The MC family of small peptides hormones is formed by MSH peptides (αMSH, βMSH, and γMSH) and adrenocorticotropic hormone (ACTH). Structurally, all of them present the amino acid sequence -Tyr-x-Met-x-His-Phe-Arg-Trp-, containing the tetrapeptide His-Phe-Arg-Trp (HFRW), critical for melanotropic activity[32,162].

MCs derive as cleavage products of the Pro-opiomelanocortin (POMC) protein, a 225 amino acid protein expressed in pituitary, nervous system and the skin[32]. UVR exposure promotes POMC expression and processing in epidermal melanocytes and keratinocytes[163,164] (Figure 8). The resulting MC binds to the Melanocortin 1 receptor (MC1R), a G-protein coupled receptor expressed on melanocytes[165,166]. The various MCs vary in their binding affinity to the MC1R, being αMSH and ACTH the two major agonists for MC1R followed by βMSH and γMSH[167].

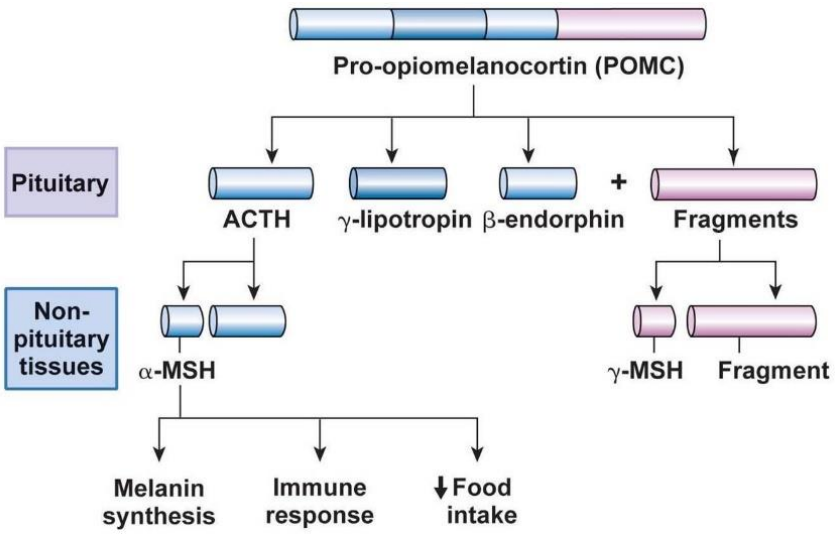

Figure 8. Melanocortin biosynthesis through proopiomelanocortin processing.

Within melanocytes, αMSH or ACTH binding to MC1R activates intracellular signaling pathways to induce proliferation, eumelanin synthesis and dendritogenesis. Activation of MC1R promotes Gαs protein dissociation and activation of the cyclic adenosine monophosphate (Camp) pathway to stimulate eumelanogenesis and pigment transfer to keratinocytes. Therefore, MC1R signaling determines the amount and type of pigment produced within melanocytes with low or absent MC1R activity associated with pheomelanogenesis, and strong signaling with eumelanogenesis[4].

3.2.2. Structure of the MC1R

MC1R belongs to the class A subfamily of G-protein coupled receptors (GPCRs). It is expressed in the surface of melanocytes and melanoma cells, although low levels of expression are also detected in many other skin cell types including human keratinocytes, fibroblasts, and immune cells[168]. MC1R is a 317 amino acids seven-αhelical transmembrane protein with the structural hallmarks of the GPCRs: an extracellular N-terminus, seven transmembrane (TM) fragments, three extracellular loops (els), three intracellular loops (ils) and an intracellular C-terminus (Figure 9).

The N-terminus functions as a non-cleavable signal anchor directing traffic of the protein to the endoplasmic reticulum (ER) membrane[169]. This N-terminus is conserved in the mature protein, and accordingly a flag-epitope fused to the N-terminus of MC1R is not cleaved during the processing of the protein in HEK293T cells[170]. MC1R contains two putative glycosylation sites, Asn15 and Asn29[171,172], both occupied by two structurally different glycans. Glycosylation regulates the availability of MC1R molecules on the cell surface[173].

The els and ils are formed between the TM regions. In MC1R, these els are relatively short compared with most GPCRs and their limited size seems related to the high constitutive activity of the receptor, particularly for el2[167,174]. The interface between il2 and TM3 contains the critical tripeptide 141DRY143, characteristic of all class A receptors and required for MC1R function. Moreover, Thr157 phosphorylation and other elements in il2 seem crucial for MC1R export to plasma membrane, since mutations in il2 impair MC1R trafficking to the plasma membrane with dramatically reduced cell surface levels[175–177].

The MC-binding site is a pocket located below the plasma membrane–extracellular medium interface, formed with the contribution of several TM fragments. It is formed by a highly charged region containing Glu94 (TM2), Asp117 and Asp121 in the TM3 and a network of

aromatic residues located near the extracellular side of TM4, TM5 and TM6. The negatively charged region interacts with an Arg residue in the HFRW pharmacophore core shared by the natural MCs[178], whereas the aromatic residues interact with the aromatic residues of the pharmacophore[178].

The intracellular C-terminus is only 19 amino acids in length, with the last 5 amino acids containing a tripeptide CSW conserved in all MCRs. This domain mediates the interaction with Gs proteins[179,180]; participates in receptor desensitization and internalization through GPCR kinase (GRK)-mediated phosphorylation of its Thr308 and Ser316 residues[175]; and is involved in the correct disposition of the receptor within the plasma membrane by acylation (palmitoylation or myristoylation) of Cys residues and integration of the acyl chain within the lipid bilayer[181,182]. Deletion of the terminal pentapeptide, dramatically decreases plasma membrane MC1R expression and MC1R function[170].

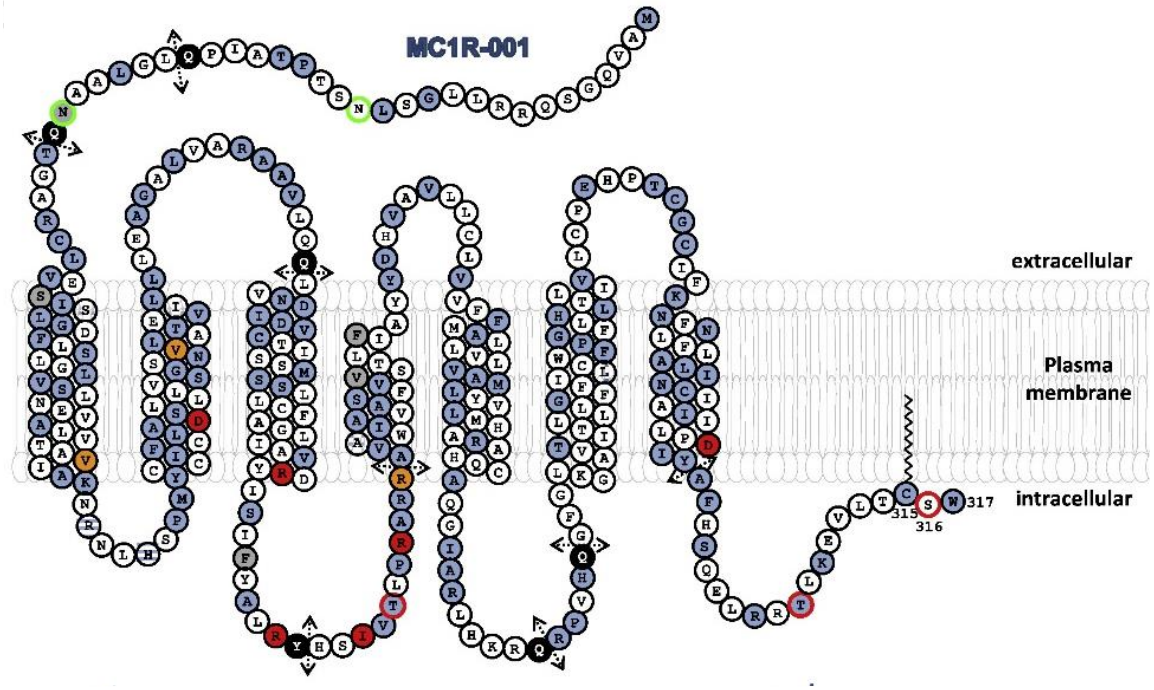

Figure 9. Structure of MC1R and protein sequence changing polymorphisms. The positions for TM helices are drawn according to the two-dimensional model of Ringholm et al., 2004[183]. The amino acid sequence corresponds to the WT MC1R (ID number ENST00000555147). Polymorphic positions for which no reliable association studies are available are indicated in blue. Positions of R and r variants are shown in red and orange, respectively. Residues shown in gray correspond to indels and black circles with white lettering followed by broken arrows to premature stop codons. Positions where both an indel and a point mutation have been found are shown as blue circles hatched in white. Ser/Thr residues presumably phosphorylated are highlighted with a red border. The two Asn residues glycosylated are indicated with a green border. Adapted from Herraiz et al., 2017[184].

3.2.3. MC1R signaling

MC1R signaling is pleiotropic with activation of cAMP, p38 stress activated-kinase and ERK1/2 pathways. Moreover, functional coupling to PI3K/AKT pathway has been proposed (Figure 10).

Most physiological effects of MC1R on melanocytes, notably including induction of eumelanogenesis, appear mediated by the cAMP pathway[185]. Upon binding of αMSH, Gαs protein dissociates from MC1R and activates AC. The resulting increase in intracellular cAMP levels activates protein kinase A (PKA), followed by PKA-dependent phosphorylation of cAMP-responsive element binding (CREB) proteins. Phosphorylated CREB proteins bind to gene promoters containing the CRE (cAMP-responsive element) sequences to activate expression of several genes. CREB mediates activation of microphthalmia-associated transcription factor (MITF)[186], a key transcription factor that positively regulates melanocyte differentiation markers. It upregulates expression of the melanogenic enzymes TYR, TYRP1 and TYRP2/DCT[186–189], and the expression of Rab27a, a small GTPase involved in melanosome transport[190,191]. Therefore, activation of MITF through the cAMP pathway, promotes eumelanin synthesis and its distribution throughout the skin[192], the main processes responsible for skin pigmentation.

In melanocytes, αMSH-mediated cAMP pathway has been shown to target another important transcriptional regulator. The peroxisome proliferator-activated receptor γ coactivator-1α (PGC-1α) is a member of a small family of transcriptional coactivators which interact with many nuclear receptors and transcription factors and are critically involved in the regulation of mitochondrial biogenesis, liver and brown adipose tissue metabolism, and detoxification of ROS[193–195]. αMSH and cAMP were shown to strongly increase PGC-1α expression both in melanoma cells and NHMs, by two complementary mechanisms involving transcriptional activation of *PGC-1α* gene expression and stabilization of the PGC-1α protein. This post-translational effect most likely resulted from direct phosphorylation of PGC-1α by PKA. PGC-1α and the related PGC-1β stimulated MITF and Tyr expression, as well as melanin pigment production[193]. This series of investigations firmly established PGC-1α as a new and important downstream target of MC1R signaling via the cAMP pathway (Figure 10).

MC1R displays some degree of agonist-independent constitutive activity[167], a common feature among GPCRs[196,197]. In constitutively active GPCRs, like MC1R, inverse agonists compete with activatory ligands for the same binding site in the receptor, decreasing constitutive signaling. The main inverse agonist for MC1R is agouti signal protein (ASIP), which suppresses melanogenesis[198,199]. The neutral MC1R antagonist β-defensin 3 (HBD3) also regulates MC1R

signaling. This peptide prevents αMSH and ASIP binding to MC1R[200] and thus, was shown to inhibit αMSH-mediated increases in cAMP and in the activity of TYR in melanocytes[201].

MC1R activation also triggers the activation of p38 and ERK1/2 kinases, but the mechanisms involved are different. Activation of p38 downstream of MC1R is cAMP-dependent[202,203]. Conversely, in human melanocytes and melanoma cells, ERK activation by αMSH relies on transactivation of cKIT and is independent on cAMP and G-protein activation[161] (Figure 10). Within melanocytes, ERK1 and ERK2 catalyze MITF phosphorylation to enhance its transcriptional activity[204]. ERK1/2-dependent MITF phosphorylation also targets MITF for ubiquitination and degradation by the proteasome[205]. The resulting decrease in MITF levels downregulates the melanogenic enzymes and inhibits melanogenesis after prolonged stimulation of the ERKs. Thus, the cAMP and ERK signals originating independently from MC1R might converge on MITF.

Activation of PI3K/AKT signaling downstream of MC1R has been proposed. The PI3K-AKT (also known as protein kinase B, PKB) pathway is involved in a variety of important processes leading to cell cycle progression and proliferation, cell migration and survival[206]. Activated RTKs bind to and activate PI3K, which catalyzes the conversion of phosphatidylinositol-(3,4)-biphosphate (PIP_2) lipids to phosphatidylinositol-(3,4,5)-triphosphates (PIP_3). These lipid messengers activate 3-phosphoinositide-dependent protein kinase 1 (PDK1) and AKT to trigger cell survival and proliferation. The level of active phospho-AKT reflects the balance between the opposing actions of activatory kinases working in a PIP3-PI3K-dependent manner on one hand, and dephosphorylation by phosphatases on the other[155]. The phosphatase and tensin homolog deleted on chromosome 10 (PTEN), a PIP_3 phosphatase, terminates PI3K signaling by hydrolysis of the lipid messenger and thus, negatively regulates the PI3K-AKT pathway. The balance of PI3K and PTEN activity, which determines the strength and duration of AKT activation, is frequently lost in many types of cancer, including melanoma[207].

It has been reported that activation of AKT after αMSH binding to MC1R mediates pro-survival and anti-apoptotic effects[208,209]. Treatment of melanocytes with αMSH before exposure to UVR activated the PI3K/AKT pathway, as measured by phosphorylation of Bad, a known AKT substrate. This treatment reduced the levels of H_2O_2 and enhanced the repair of CPDs induced by UVR[208]. Moreover, stimulation of retinal pigment epithelium cells with αMSH reduced H_2O_2-induced cell damage and apoptosis through activation of AKT and mTOR pathways[209].

In melanocytes, the mechanisms downstream of MC1R accounting for AKT regulation are still unknown, but involvement of cKIT or PTEN has been proposed. A mechanism of regulation of AKT activity involving the direct interaction of MC1R with PTEN has been reported[210]. Following UVR in αMSH-treated melanocytes, wild type (WT) MC1R would recruit PTEN to prevent its ubiquitination by WWP2, thereby protecting the phosphatase from proteasomal degradation and downregulating AKT signaling[210]. In addition, a mechanism involving MC1R/cKIT/PI3K pathway might participate in AKT regulation, since transactivation of cKIT by MC1R has been reported[161] and RTKs including cKIT are functionally connected with AKT[211]. Thus, AKT activation by αMSH might be at least carried out via two complementary MC1R-dependent mechanisms.

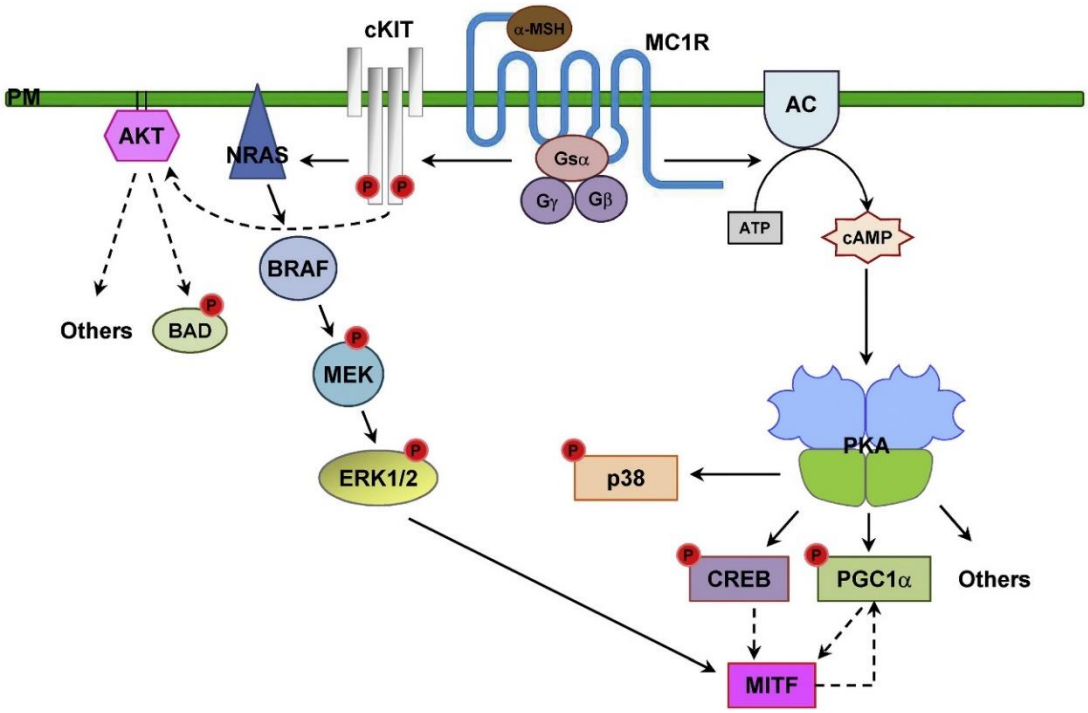

Figure 10. Signaling pathways triggered by MC1R agonists. Adapted from Herraiz et al., 2017[184].

3.2.4. Regulation of MC1R

MC1R function is tightly regulated at different levels (Figure 11). The *MC1R* genotype provides a first level of regulation of MC1R signaling. The *MC1R* gene is unusually polymorphic and many of the natural variants are functionally relevant[4]. Moreover, it has also been shown that αMSH switches expression of *MC1R* transcripts from the canonical MC1R-001 form encoding for the fully active receptor to chimeric MC1R-TUBB3 transcripts Iso1/2, generated by intergenic splicing of *MC1R* and *Tubulin-β-III* (*TUBB3*) genes[212,213]. The function of this chimeric proteins

remains largely unknown. MC1R polymorphisms and MC1R-TUBB3 isoforms function will be discussed in section 5.

In addition, MC1R activity can be modulated at a transcriptional level by several paracrine and endocrine factors that control MC1R expression, as well as by the UVR. MCs, ET-1, interleukin-1α (IL-1α), interleukin-1 β (IL-1β), and UVR stimulate *MC1R* gene expression[201,214–216]. αMSH stimulates *MC1R* gene expression at least in part due to activation of MITF, which binds the promoter of *MC1R* to stimulate its activity[217]. Conversely, two cytokines TNFα[218] and TGFβ[219], and low concentrations of H_2O_2[220] repress *MC1R* expression.

MC1R processing and forward trafficking determine the expression of MC1R on the cell surface or the retention in intracellular compartments[4]. During this anterograde traffic, MC1R undergoes a series of post-translational modifications including oligomerization, glycosylation and phosphorylation. MC1R is newly synthetized in the rough ER where several quality control systems check for completion of posttranslational processing and determine the intracellular retention of misfolded or misprocessed mutants. Within the ER, MC1R undergoes dimerization[171,221] by both non-covalent domain swap-type interactions and covalent disulfide bonds between the Cys35, Cys267, Cys273 and C275, although only Cys35 is required for MC1R traffic to the plasma membrane[221]. Moreover, dimerization between MC1R variants and WT MC1R may cause a dominant-negative effect on MC1R signaling[171]. Another maturation step within the ER is N-glycosylation in two Asn residues in the N-terminus[173]. The glycosylated oligomers are transported to the Golgi apparatus where the glycan chains are not processed to complex oligosaccharides, since mature and active WT MC1R is sensitive to endoglycosidase H (Endo H)[173,222], an enzyme that cleaves core high-mannose N-glycan chains and hybrid-type chains but not the complex oligosaccharides. Glycosylation has a strong effect on the availability of MC1R molecules on the plasma membrane, most likely by a combination of improved forward trafficking and decreased internalization[173]. Efficient MC1R export is regulated by Thr157 phosphorylation[176], a critical step in MC1R migration to the plasma membrane.

Once in the plasma membrane, MC1R function is primarily controlled by the interaction of the receptor with the activatory MCs or the inhibitory ASIP and HBD3. Ligand binding triggers other regulatory events including homologous desensitization of signaling and receptor internalization. GPCR desensitization is a strong attenuation of signaling following short exposure of its agonist, normally in a GRK-dependent manner[223]. Upon agonist binding, MC1R undergoes desensitization by GRK2 and GRK6-mediated phosphorylation[224], but only GRK6 promotes internalization by phosphorylation of Thr308 and Ser316 target residues[175]. GRK6 also appears to inhibit MC1R constitutive signaling. Moreover, the non-visual adaptor protein β-arrestin 2

(ARRB2) stimulates receptor internalization by sequestration in endocytic vesicles whose likely destination seems to be the recycling to the plasma membrane. The highly homologous β-arrestin 1 (ARRB1) lacks significant effect, but is able to bind to the receptor. Therefore, a mechanism of MC1R functional regulation based on the competition of the inhibitory ARRB2 and the functionally neutral ARRB1 has been proposed[225]. MC1R signaling is also negatively modulated by the E3-ubiquitin ligase Mahogunin Ring Finger-1 (MGRN1), mainly by a mechanism involving competition between MGRN1 and Gs for binding to MC1R[226]. Recently, our group has reported that MGRN1 ubiquitylates ARRB2 in the presence of MC1R[227]. MC1R- and MGRN1-dependent ARRB ubiquitylation allows a stable MC1R-ARRB interaction rather than promoting proteasomal degradation.

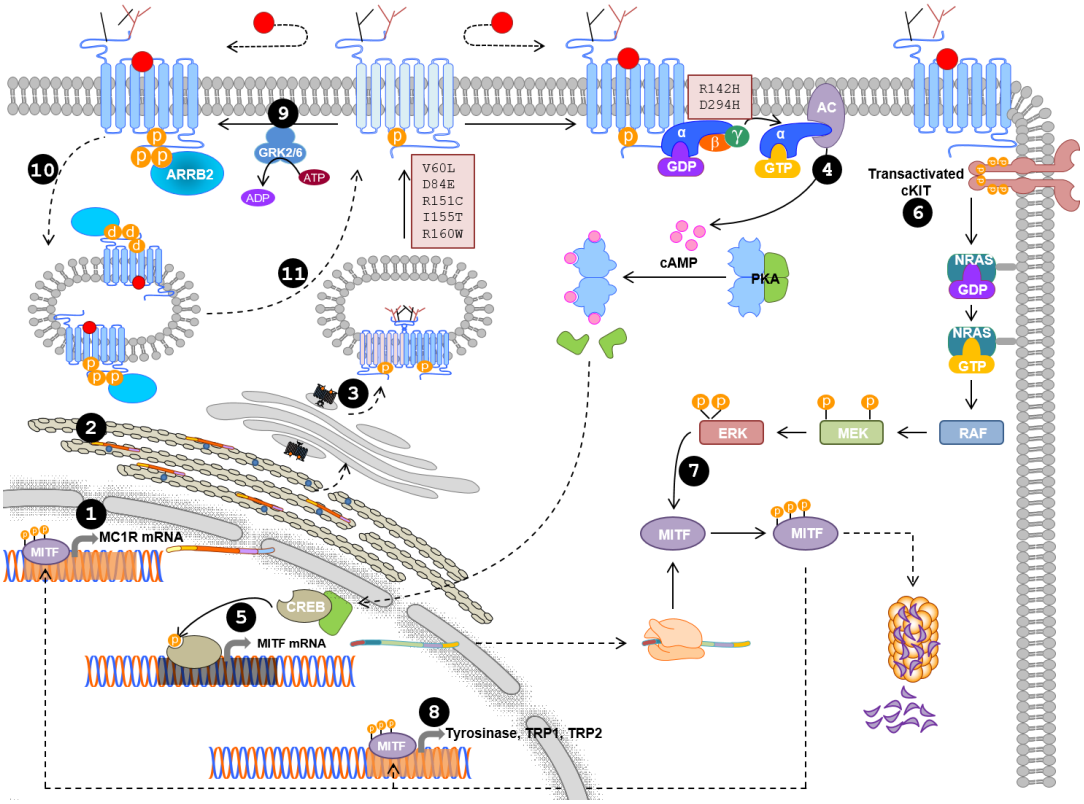

Figure 11. Scheme of the main steps in MC1R biosynthesis, functional coupling and regulation. (1) Transcription of the *MC1R* gene. (2) Translation and post-translational modifications including oligomerization and glycosylation in the rough ER. (3) Forward trafficking of glycosylated oligomers to the plasma membrane. (4) Activation of the cAMP signaling pathway upon agonist binding. (5) Activation of CREB transcription factors in the nucleus by PKA catalytic subunits, which in turn increase the rate of transcription of the *MITF* gene. (6) Transactivation of cKIT by agonist-activated MC1R to trigger the NRAS-BRAF-MEK-ERK cascade. (7) Phosphorylation of MITF by active ERKs to increase its transcriptional activity and its proteasome-dependent degradation. (8) Transcription of the genes encoding for melanogenic enzymes and for *MC1R* triggered by active MITF. (9) Desensitization of agonist-bound MC1R by GRK2 or GRK6-dependent phosphorylation. (10) ARRB2 recruitment followed by sequestration in endocytic vesicles (11) whose likely destination is recycling to the cell surface. Adapted from Garcia-Borron et al., 2014[4].

3.3. Tanning response

The tanning response is a relevant photoprotective mechanism against UVR-induced carcinogenesis that consists of the darkening of UVR-exposed skin. UVR-mediated skin pigmentation is actually biphasic. First, it occurs by rapid modification of preexisting melanin precursors and redistribution of melanosomes throughout the skin. Then, UVR induces a delayed tanning response that begins several hours to days after UVR exposure, and involves activation of melanocyte differentiation, eumelanogenesis and dendritogenesis. This process is complex and results from the direct effect of UVR on melanocytes and paracrine interactions with keratinocytes[34]. UVR stimulates the production of ET-1 and POMC by keratinocytes and those factors can then act in a paracrine manner to stimulate melanocyte function.

In this line, MC1R plays a central role in determining the UVR-induced adaptative tanning since this receptor is responsible for the switch from basal pheomelanogenesis to the eumelanin synthesis and promotes pigment transfer to keratinocytes. In keratinocytes, UVR-induced DNA damage leads to stabilization and increased activity of p53, which in turn, activates the transcription of the *POMC* gene[228]. POMC-derived αMSH and ACTH activate preexisting MC1R in melanocytes and upregulate the expression of *MC1R*[201,216,229]. In response to agonist binding, activation of the cAMP pathway increases MITF transcription via CREB proteins, leading to high expression of the melanogenic enzymes[186–189] and of proteins involved in melanosome transport[190,191]. Melanocytes transfer eumelanin to keratinocytes, where these pigments form protective caps around the nucleus of keratinocytes to protect DNA from further UVR-induced damage.

Keratinocyte-derived ET-1 also participates in the adaptive tanning response. Activation of ENDBR by ET-1 enhances the UVR-induced phosphorylation of p38 with subsequent increase in p53 expression, and activates PKC leading to phosphorylation of ERK1/2, CREB and MITF upregulation[149,208]. PKC has also been proposed to phosphorylate and activate the melanogenic enzyme TYR[230]. Another important effect of ET-1 is upregulation of MC1R expression[158,201]. Thus, the synergistic interaction of ENDBR with MC1R involves enhanced activation of MITF and p53, resulting in increased melanocyte pigmentation among other processes[158,160,208].

Melanoma

4.1. Incidence

Cutaneous melanoma is a lethal skin cancer that arises from malignant transformation of melanocytes located in the basal lamina of the epidermis and in the eye. The incidence of melanoma has increased rapidly over the last decades, with an ever-seen annual incidence increase of 4-6% in many fair-skinned populations and an overall growth of 237% over the last 30 years (https://seer.cancer.gov/)[231–233]. The number of new cases of melanoma was 22.8 per 100,000 persons in 2018 in the USA where 91,270 new cases were diagnosed for 2018 accounting for 5.3% of all cancers and 9,320 deaths[233,234]. The trend in Europe was similar; more than 10^5 new cases of melanoma were diagnosed in 2018 and more than 22,000 European citizens died due to the disease (http://gco.iarc.fr/today)[235]. Increases in incidence rates differ between ethnic groups, regions, gender and ages. Melanoma is more common among individuals of fair complexion compared to dark-skinned individuals. The United States illustrate well the differences in melanoma incidence among races and ethnicities[233,236]. This disease is most commonly diagnosed in non-Hispanic whites, with an annual incidence rate of 26 (per 100,000), compared to 4 in Hispanics and 1 in blacks[233,234]. Melanoma incidence also varies by geographic location with the highest incidence rates in North America, Australia and New Zealand[235] (Figure 12).

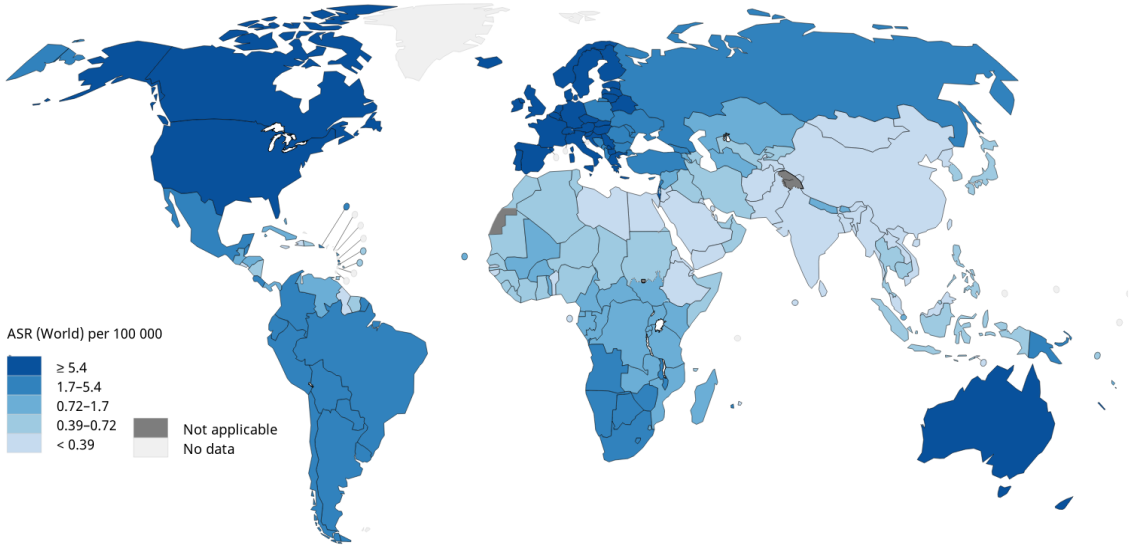

Figure 12. Estimated worldwide melanoma age-standardized incidence rated (ASR) in 2018. ASR (world) is expressed per 100,000 persons. Adapted from Globocan 2018. Graph production: IARC 2018[235].

Furthermore, in Europe, there is a gradual reduction in melanoma incidence from north to south[237] (Figure 13). This difference is attributed to the predominant phenotype of each region, with more prevalent fairer-skinned individuals in Scandinavia compared to a majority of olive-skinned population in southern Europe[232]. However, since UVR incidence is low in northern European regions, the fact that individuals from these countries spend recreational periods in countries with high UV incidence, may contribute to this high incidence.

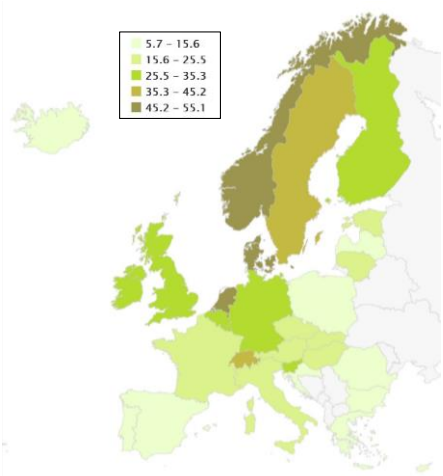

Figure 13. Estimated melanoma age-standardized incidence rates in Europe in 2018. ASR (world) is expressed per 100,000 persons. Adapted from ECIS, 2018 (https://ecis.jrc.ec.europa.eu/)[237].

Similar differences by region, ethnicity, age, and sex are observed in mortality rates of melanoma, but melanoma mortality has not risen as dramatically as incidence over the years. However, melanoma is a very aggressive cancer that tends to metastasize rapidly. Unfortunately, although invasive melanoma represents only 4% of all skin cancers, it still accounts for 80% of skin cancer deaths. Survival rates highly depend on the stage of progression when melanoma is diagnosed. Early detection of melanoma allows for resection of the localized tumor and is crucial for a good prognosis, with five-year survival rates higher than 95%. On the contrary, in advanced stages, surgery is no longer sufficient and the five-year relative survival rate decreases until 20%[233].

4.2. Melanoma progression and histological classification

Melanocyte transformation progresses through a series of well-defined steps characterized by histological and genetic changes[238,239] (Figure 14). However, a subset of melanomas do not present a lineal progression and can metastatize even though they skip intermediate steps in progression. Genes involved in cancer-relevant processes such as proliferation, differentiation, cell adhesion, cell cycle and apoptosis, which usually rely on keratinocyte-melanocyte crosstalk, are frequently mutated during melanoma initiation and progression[240].

According to the standard linear model, the first step is the proliferation of melanocytes to form **benign nevi** by the acquisition of mutations in oncogenic drivers, mainly BRAF and NRAS. After an initial phase of increased growth, BRAF or NRAS-mutated melanocytes undergo oncogene-induced senescence. Melanocytic cells eventually overcome senescence, usually by dysregulation of cell growth, DNA repair, and the susceptibility to cell death. As a result, the lesion progresses to **dysplastic nevi** with aberrant differentiation and melanocytic nuclear atypia. Genetic lesions that inactivate *cyclin-dependent kinase inhibitor 2A* (*CDKN2A*), retinoblastoma *(Rb1)* and *PTEN*, have been associated with transformation of benign to dysplastic nevi[240].

Then cells grow intraepidermally during the **Radial Growth Phase (RGP)**; a phase characterized by the enlargement of the tumor at its periphery. Mutations in the *telomerase reverse transcriptase* (*TERT*) promoter are more frequently associated with this phase[241,242].
If RGP melanomas are not cured by surgery, they progress to the **Vertical Growth Phase (VGP)**, associated with invasion of the dermis and acquisition of the ability to metastasize. In this phase, cells become independent of keratinocytes and acquire molecular alterations in genes encoding for cell adhesion proteins (*cadherins* and *integrins*) and *matrix metalloproteinases* (*MMPs*), which confer the metastatic ability.

Finally, **metastatic melanoma** spreads to distant organs such as liver, lung and brain, where melanoma cells can colonize to stablish a metastatic focus. At this stage, the disease is usually refractory to therapies and has bad prognosis.

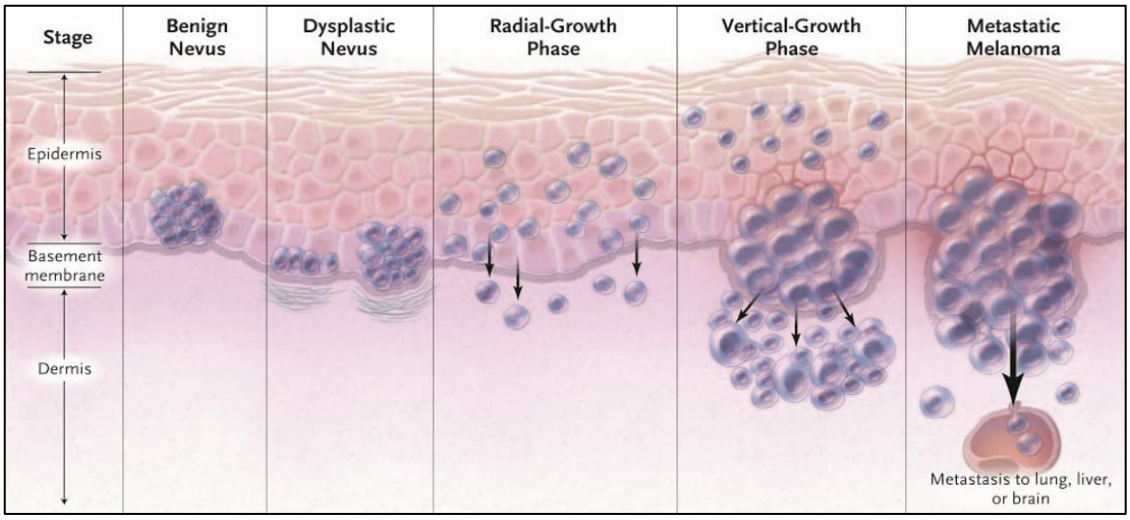

Figure 14. Melanoma progression. Adapted from Miller and Mihm., 2006[239].

There are four main clinical subtypes of melanoma based on their histological appearance and behaviour[243] (Figure 15):

- **Superficial spreading melanoma (SSM)** is the most common form of melanoma in Caucasian population, corresponding to about 70% of all melanomas. SSM usually derives from preexisting nevi and is associated with intermittent exposure to UVR with episodes of severe sunburn, especially at an early age.
- **Lentigo maligna melanoma (LMM)** arises on chronically sun-exposed damaged skin: in the head and neck region, arms and upper trunk. The precursor of LMM, the Lentigo maligna (LM) is generally flat in appearance and grows slowly in diameter over 5 to 20 years or longer before it actually forms the LMM. Thus, it is most often diagnosed in elderly people.
- **Acral lentiginous melanoma (ALM)** is the most common subtype of melanoma in people of Asian or African descent, but it is not frequent in fair-skinned people. It is mainly found in non-UVR exposed areas of the body, such as the palms of the hands, the soles of the feet and the nail bed[244].
- **Nodular melanoma (NM)** is the second most common type of melanoma accounting for 10-30% of all melanomas. The lesion is recognized as a nodule that may arise on any site, but it is commonly found on sun-exposed areas of the head and neck. It is the most aggressive form because of its short or absent RGP.

Figure 15. Malignant Melanoma histological subtypes. From left to right: Superficial Spreading Melanoma, Lentigo maligna Melanoma, Acral Melanoma and Nodular Melanoma. Adapted from Alasadi and Alsafy, 2017; and *Dermatoweb* (http://dermatoweb.udl.es/)[245,246].

In addition to the four main histopathological subtypes, there are other, less frequent types of melanomas, such as ocular melanomas[247], spitzoid melanoma[248] and the desmoplastic melanoma[249].

4.3. External and genetic risk factors

The interactions of genetic, phenotypic and environmental risk factors determine the susceptibility to melanoma. The main environmental risk factor is the UVR, with the highest risk associated with intense intermittent UVR exposure, from sunlight or use of indoor tanning devices[250], and with severe sunburns during childhood[251–253]. Major familiar risk factors include a fair skin phenotype (natural blond or red hair color, difficulty to tan and propensity to sunburn), the presence of atypical, large, or numerous (more than 50) moles and personal or family history of melanoma. Risk is also increased for people aged over 30 years (particularly older than 50 years) with a history of excessive sun exposure, including sunburns; a past history of skin cancer, and diseases or treatments that suppress the immune system[254–256].

Approximately, 5-10% of melanoma patients exhibit an autosomal-dominant hereditary form of the disease. Two highly penetrance genes that confer high risk of melanoma were first identified 20 years ago: *CDKN2A* and *cyclin-dependent kinase 4* (*CDK4*)[156,257,258]. Mutations in the *CDKN2A* locus are found in 25-40% of families with familial melanoma[259], whereas mutations in *CDK4* are uncommon and have only been described in a few families worldwide[260,261].

In addition, next-generation sequencing (NGS) germline mutations to multiple genes involved in telomere maintenance in melanoma-prone families: *TERT*[241], *protection of telomeres 1* (*POT1*)[262], *adrenocortical dysplasia homologue* (*ACD*) and *telomere repeat binding factor 2 interacting protein* (*TERF2IP*)[263]. However, mutations in these genes are rare, with each contributing to <1% of all familial clustering of melanoma.

Other low-penetrance genes such as *ASIP*, *oculocutaneous albinism II* (*OCA2*), *HECT and RLD domain containing E3 ubiquitin protein ligase 2* (*HERC2*), *TYR*, *TYRP1* and *SLC45A2* (m*elanoma antigen AIM1*) and moderate penetrance genes such as *MIT*F and *MC1R*, have been associated with familial melanoma[263].

Among these, *MC1R* is a major melanoma susceptibility gene, since it is very frequently mutated in the population. This gene is unusually polymorphic, with almost 50% of people of Caucasian descent carrying at least one variant allele. As explained before, MC1R determines the eumelanin/pheomelanin ratio and, thus, the pigmentation phenotype. Many natural variants have compromised activation of eumelanin synthesis resulting in higher contents of photosensitizer yellow-reddish pheomelanin. These variants are strongly associated with the "Red Hair Color" (RHC) phenotype, characterized by fair skin pigmentation, red hair color, freckles, propensity to sunburn and inability to tan. According to their penetrance for the RHC phenotype, MC1R variants have been classified into strong "R" alleles, weaker "r" forms, and

pseudoalleles with no significant effect on the phenotype[264]. In addition to this phenotypic effect, an association between *MC1R* genotype and melanoma susceptibility, independent on fair phenotype, has been reported[265–268]. Since WT MC1R has been shown to activate antioxidant defenses, DNA repair mechanisms and survival pathways, while MC1R variants have been linked to inefficient DNA repair[4], the risk conferred by these MC1R variants, even in dark-skinned populations, might be related to these non-pigmentary roles. These MC1R-mediated pigmentation-independent mechanisms will be further discuss in section 5. The melanoma risk conferred by R variants is additive, thus carriers of two R alleles have a higher risk than individuals harboring one or none of these variants[269].

Furthermore, *MC1R* can interact with other melanoma susceptibility genes. *MC1R* variants appear to modify the penetrance of *CDKN2A* mutations in melanoma prone families. Individuals harboring both an *MC1R* variant and a *CDKN2A* mutation, showed an increased risk and a significantly decreased age of onset of melanoma compared with individuals carrying only a *CDKN2A* mutation[270,271].

4.4. Mutational burden of melanoma and frequent somatic alterations

Despite the relevance of germinal mutations in familial melanoma, almost 90% of melanomas are sporadic and result from somatic mutations, the catalogue of somatic mutations in melanoma reflects the mutational processes accounting for the malignant transformation of melanocytes, from the initial lesion to the metastatic melanoma. Exome sequencing has shown that the main mutational process in melanoma is the exposure to the highly mutagenic UVR that mainly promotes C>T or CC>TT transitions, corresponding to a UVR induced mutation signature and accounting for 70% of mutations in melanoma[5,93]. Because of the major role of mutagenic UVR, the mutational burden of cutaneous melanomas is very high, with rates of 18-38 mutations/Mb[84,272]. In fact, Lawrence and coworkers compared the frequency of somatic mutations across a panel of human cancer types. This study revealed that melanoma and lung cancer were the tumor types with the highest mutation rates, mainly attributable to the effect of carcinogens, UVR light and tobacco smoke, respectively (Figure 16)[273].

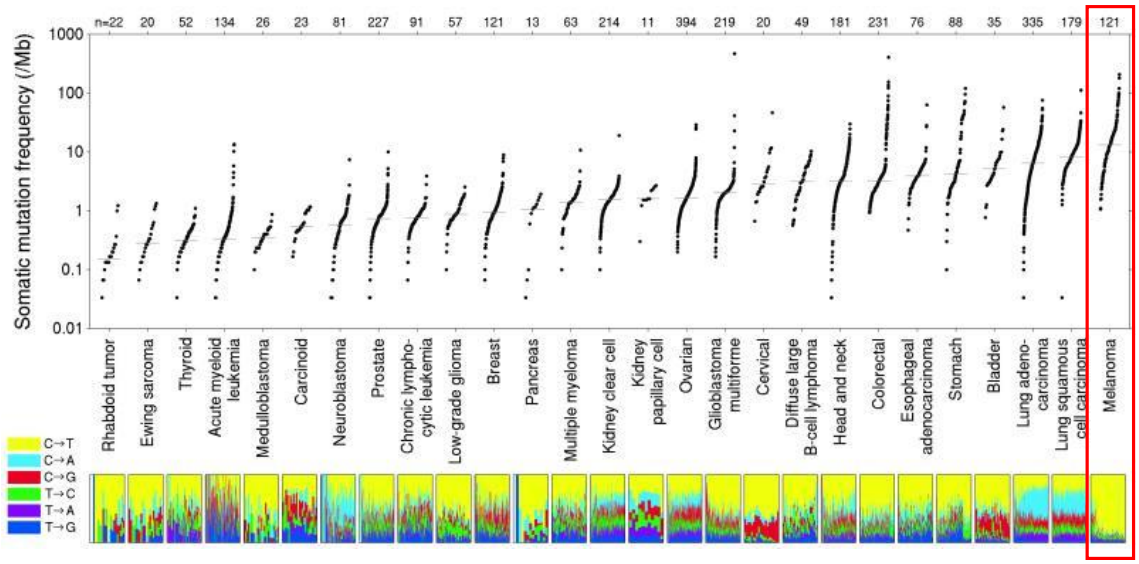

Figure 16. Somatic mutation frequencies observed in exomes from 3,083 tumor-normal pairs. Each dot corresponds to a tumor-normal pair, with vertical position indicating the total frequency of somatic mutations in the exome. The lower panel shows the relative proportions of the six different possible base-pair substitutions, as indicated in the legend on the left. Adapted from Lawrence et al., 2013[273].

Moreover, a significant association between mutation burden in melanoma and body site has been established[272,274,275]. Exome sequencing of 147 melanomas revealed that melanomas arising from sun-exposed areas exhibited higher somatic mutation rates than acral, mucosal and uveal melanomas (median count of 171 mutations per sun-exposed tumor and 9 mutations per sun-shielded tumor), with the former linked to UV signature mutations[274]. These results were recently supported by the analysis of whole-genome sequences (WGS) derived from cutaneous, acral and mucosal melanomas[272]. In this study, genetic alterations differed between cutaneous and acral melanomas (Figure 17). Mutational signatures of UVR exposure, single nucleotide variants (SNV) and indels, dominated cutaneous melanomas (49.2 mutations/Mb in cutaneous versus 2.64 in acral melanoma), while structural variants were more frequent in acral and mucosal melanomas (342 in acral compared to 101 in cutaneous melanoma)[272].

In addition to body site, *MC1R* genotype is an important factor that influences the mutational load in melanoma[275,276]. Accordingly, carrying either at least one r (low penetrance) or R allele, increases the mutation burden in cutaneous melanoma for both UVR signatures and non-UVR base pair substitutions. Each *MC1R* variant allele additively increases mutation burden with the highest mutation load in melanomas heterozygote for R alleles followed by R/r and r/r genotypes[275].

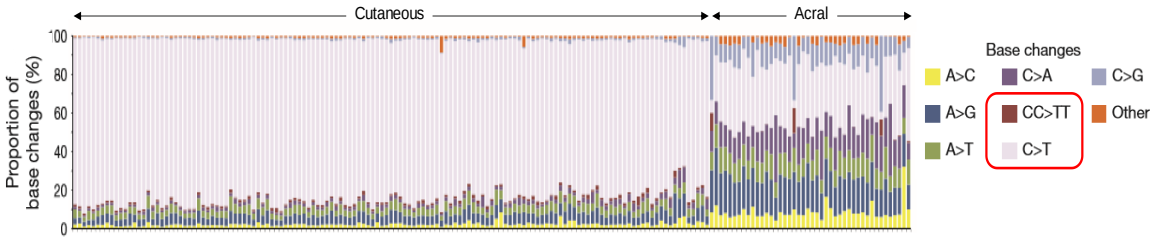

Figure 17. Proportion of somatic base changes. Melanomas segregate into two groups with nearly all cutaneous melanomas showing a high proportion of C> T transitions. Adapted from Hayward et al., 2017[272].

This molecular heterogeneity and high mutation load of melanoma has complicated the identification of *bona fide* driver mutations. Nevertheless, major oncogenic events of early melanocyte transformation are known and allow for a classification of melanomas in 4 molecular subtypes, the BRAF, NRAS, NF1 and triple WT subtypes[84,277].

Before the era of NGS, activating mutations in the oncogenes *BRAF* and *NRAS* had already been discovered. These genes, encoding the serine/threonine kinase BRAF and the GTPase NRAS, respectively, are mutated in 70-80% of sporadic melanomas leading to activation of the ERK signaling pathway. In fact, this signaling pathway is the most commonly mutated in melanoma (80-90% of sporadic melanomas)[156]. The most frequent mutation in *BRAF* occurs in the V600 codon with the substitution of a Valine for a Glutamic, Lysine or Arginine, with the former being the predominant form[278]. Mutations in the RAF isoforms *ARAF* and *CRAF* have not been reported. *NRAS* hotspot mutations in Q61, G12 and G13 codons are also frequent in melanoma accounting for 20-30% of sporadic melanomas whereas mutations in other RAS isoforms, *HRAS* and *KRAS*, are much less common.

Loss-of-function (LOF) mutations in *NF1* also account for the hyperactivity of the ERK1/2, since *NF1* is a tumor suppressor gene encoding a protein that acts as a negative regulator of RAS[279]. It is the third most frequent mutation in melanoma, present in about 14% of melanomas. *BRAF* hot-spot mutations and *NRAS* hot-spot mutations do not co-occur in melanomas, but *NF1*-mutated melanomas may show concurrent *NRAS* mutations, and more infrequently *BRAF* hot-spot mutations.

Triple-WT melanomas, as well as acral and mucosal melanomas, are more heterogeneous, less enriched in the UVR mutational signature and occasionally harbor mutations in the KIT RTK, or deregulation of signaling downstream of other RTKs, also leading to activation of the ERKs[272].

Other less common events in melanoma causing dysregulated mitogen-activated protein kinase (*MAPK*) signaling include mutations in *GNAQ* and *GNA11*, enriched in the triple-WT group[280] and predominant genetic lesions in uveal melanoma[281]. *MAP2K1 and MAP2K2*, encoding MEK1 and MEK2, accounting for 6% and 2% melanomas, respectively, have also been reported[282]. Moreover, RASopathy genes *PTPN11*, *RASA1*, *RASA2*, and *SOS1* , as well as another RAS domain-containing gene *RASSF2* appear co-mutated with NF1[242,280,283,284], hence providing further support for this family of genes being important regulators of melanomagenesis.

The PI3K/AKT signaling pathway is also frequently hyperactivated in melanoma, promoting antiapoptotic and prosurvival effects. This signaling pathway can be activated through mutations in *NRAS*, loss of the tumor suppressor *NF1*, and by alterations in other members downstream of NRAS, such as, *PTEN*, *PIK3CA*[285] (altered in 5% of samples) and *AKT*[286] (8% of samples, most are copy-number gains). The most frequent molecular alteration in this signaling pathway in melanoma is the loss of PTEN, occurring in up to 30-50% of melanomas[287]. *PTEN* mutations and deletions are usually linked to BRAF-mutant melanomas[288], whereas amplification and mRNA overexpression of AKT3 are more frequent in NRAS, NF1, and triple-WT compared to the BRAF subtype[277].

In addition to molecular alterations in signaling members of RAS/RAF/MEK/ERK and PI3K/AKT pathways, driver mutations of relevance are linked to other known cancer-related molecular processes dysregulated in melanoma (Figure 18). Genetic alterations in pigmentation/differentiation, telomere maintenance, cell cycle, cell death and DNA damage response pathways have been reported. Among these, some genes and pathways altered somatically and those with germline mutations overlap to increase susceptibility to melanoma.

Several studies have revealed somatic mutations in *TERT* promoter, all linked to a UVB signature[84,241,272,277,289–291]. *TERT* dysregulation is less frequent in the triple-WT subtype compared to BRAF, NRAS and NF1 subtypes.

Aberrations in at least one of the members of the CDKN2A/CDK4/CCND1/RB1 pathway have been found. The suppressor gene *CDKN2A* is mutated or deleted in almost half of TCGA melanomas, whereas mutations and amplifications of *CDK4*, amplifications of *Cyclin D1* (*CCND1)* and *RB1* deletions or mutations are less common[84,272].

Tumor protein P53 (TP53) aberrations have been widely documented[274,277,289,292]. In TCGA melanomas, this tumor suppressor appears deleted or mutated in around 50% of samples. *MDM2* amplifications have also been observed, mainly in the triple WT subtype, while *TP53* alterations are predominant in BRAF, NRAS and NF1 subtypes.

Moreover, new driver genes in melanoma were identified simultaneously in several independent whole-exome sequencing (WES) studies: *RAC*1, *PPP6C*, *ARID2*, *IDH*[274,292], with the TCGA study supporting these findings[277] (Figure 18). Among these, *RAC1* and *PPP6C* result from C>T transitions. RAC1 is a member of the Rac subfamily of Rho GTPases that functions as a molecular switch, cycling between active GTP-bound and inactive GDP-bound states. This GTPase regulates cytoskeleton rearrangement and, thus, it plays important roles in cellular adhesion, migration and invasion. A recurrent activating mutation in *RAC1* changing Proline 29 to Serine was identified[274,292]. This mutant protein favors the GTP-bound state increasing its binding to downstream effectors and accelerating cell proliferation and migration.

PPP6C seems to have a crucial role in chromosomal segregation and cell cycle control. This phosphatase regulates progression from G1 to S phase of the cell cycle, in part through control of cyclin D1 and is the major phosphatase for Aurora A[293–295]. This mitotic kinase controls spindle pole formation, centrosome maturation, chromosomal segregation and cytokinesis during mitosis[294]. Mutations are localized to highly conserved regions within or near the active site, or the surrounding substrate recognition area, leading to inactivation of the protein and, consequently, promoting chromosome instability[274]. These mutations usually co-occur with mutations in *BRAF* or *NRAS*[296].

ARID2 gene encodes a member of the SWI/SNF chromatin-remodeling complex. LOF mutations in *ARID2*[296–298] have been found in 12% of melanomas[84], suggesting a role for dysregulation of chromatin remodeling in melanomagenesis.

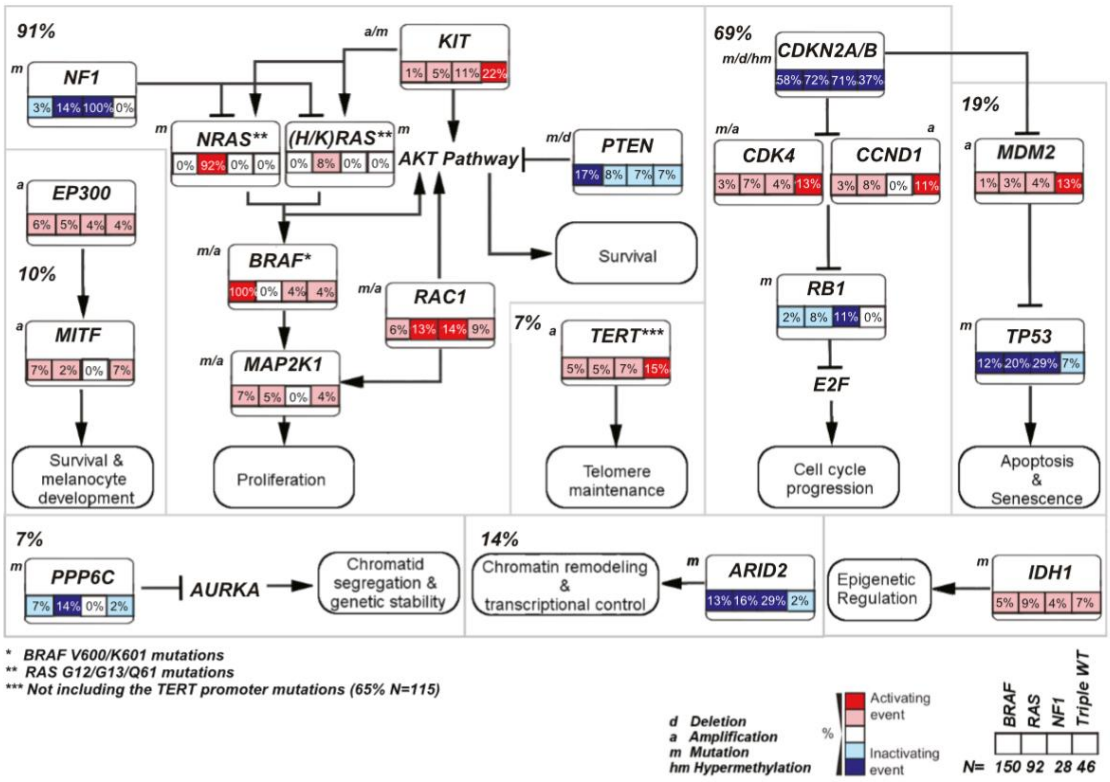

Figure 18. Pathways altered in melanoma. Percentage of recurrently altered pathways in the four melanoma subtypes (*BRAF* = V600/K601 mutants, *RAS* [*N/H/K*] = G12, G13, and Q61 mutants) through integration of mutation, copy-number variation, and hypermethylation data are indicated (n = 316). a, amplification; d, deletion, m, mutation. Adapted from Akbani et al.,2015[277].

Overall, these findings identify the major genes and pathways altered in melanoma. However, the number of WES and WGS studies is still insufficient and a bigger sample size is needed. Moreover, a deeper knowledge of the stepwise acquisition of molecular alterations is crucial to decipher the mechanisms accounting for initiation and progression of melanoma, and will have important implications for prognosis and therapy. Indeed, these genes and their downstream effectors are potential pharmacological targets and may provide biomarkers for a better prognostic assessment.

MC1R and genomic instability

5.1. Splice variants and polymorphisms

The human *MC1R* gene (MIM# 155555, Ensembl ID ENSG00000258839) is located in the 16q24 region. Its structure is quite complex, as it displays several splice variants and a high degree of polymorphism. It comprises 4 exons and yields several transcripts as a result of intra- and intergenic splicing. The major transcript contains a 951 nucleotides (nt) coding region[299] and is formed by exons 2, 3 and 4, with retention of two unspliced intervening sequences between exons 2–3 and 3–4 (Figure 19A). This canonical *MC1R* encodes for the 317 amino acid GPCR whose structure and functional properties have been explained before (consensus sequence CDS 56011.1), and is named along this memory as either, WT MC1R or MC1R-001. As minor forms, three intragenic spliced variants have been described[300]. Tan and coworkers reported an alternative spliced MC1R form designated as MC1R-002 (ID ENST00000555427) which contains exons 1–4 resulting in a 1149 nt-long ORF encoding for a 382 amino acids protein[300]. This splice isoform is identical to MC1R-001 up to Ser316, followed by an additional 65 amino acids C-terminal extension (Figure 19C). Another splice variant, named MC1R-350, was isolated from cultured NHMs and skin sections[301]. This isoform shares with MC1R-001 and MC1R-002 the sequence up to Cys315, but shows a different 35 amino acids C-terminal extension (Figure 19C). Finally, the MC1R-003 transcript (ENST00000539976) lacks a functional ORF and is most likely a non-coding defective transcript.

Two spliced intergenic variants have also been described[213]. Formation of intergenic isoforms is favored by the dense packing in the 16q34 region bearing the *MC1R* gene, where less than 8 kb separate the coding 3' end of the next upstream gene and the *MC1R* initiation codon, and the intervening DNA fragment located between *MC1R* and the downstream *TUBB3* is only 2.5 kb-long. This dense packing together with an unusual and inefficient polyadenylation signal in human *MC1R,* have been shown to promote *MC1R* intergenic splicing with its downstream neighbor *TUBB3*[212,213]. The intergenic splicing produces two MC1R-TUBB3 quimeras, Iso1 and Iso2, containing the complete MC1R sequence fused to TUBB-derived C-terminal extensions, in frame for Iso1 and out of frame for Iso2[213]. The transcript Iso1 contains *MC1R* exons 3 and 4 fused to *TUBB3* exons 3, 4 and 5 (Figure 19A). This transcript (also called RP11-566K11.2-001 transcript, ID ENST00000556922) encodes for a 797 amino acids in-frame fusion chimera corresponding to the first 366 residues of MC1R-002 and most of the TUBB3 sequence (Figure 19B). The other intergenic splice variant, named Iso2, arises by out-of-frame fusion of *MC1R* exon 3 and exon 3

of *TUBB3* (Figure 19A), yielding a 432 amino acids protein where the first 316 residues match the MC1R-001 sequence. The remaining 116 C-terminal residues share no homology with known proteins[213] (Figure 19B). Significantly, treatment with αMSH or activation of the p38-MAPK, both key molecules associated with UVR responses, results in a shift in expression from canonical MC1R in favor of chimeric MC1R-TUBB3 isoforms[212,213], which might lead to novel phenotypes required for tanning. So far little or any information is available on the functional properties of the chimeric proteins.

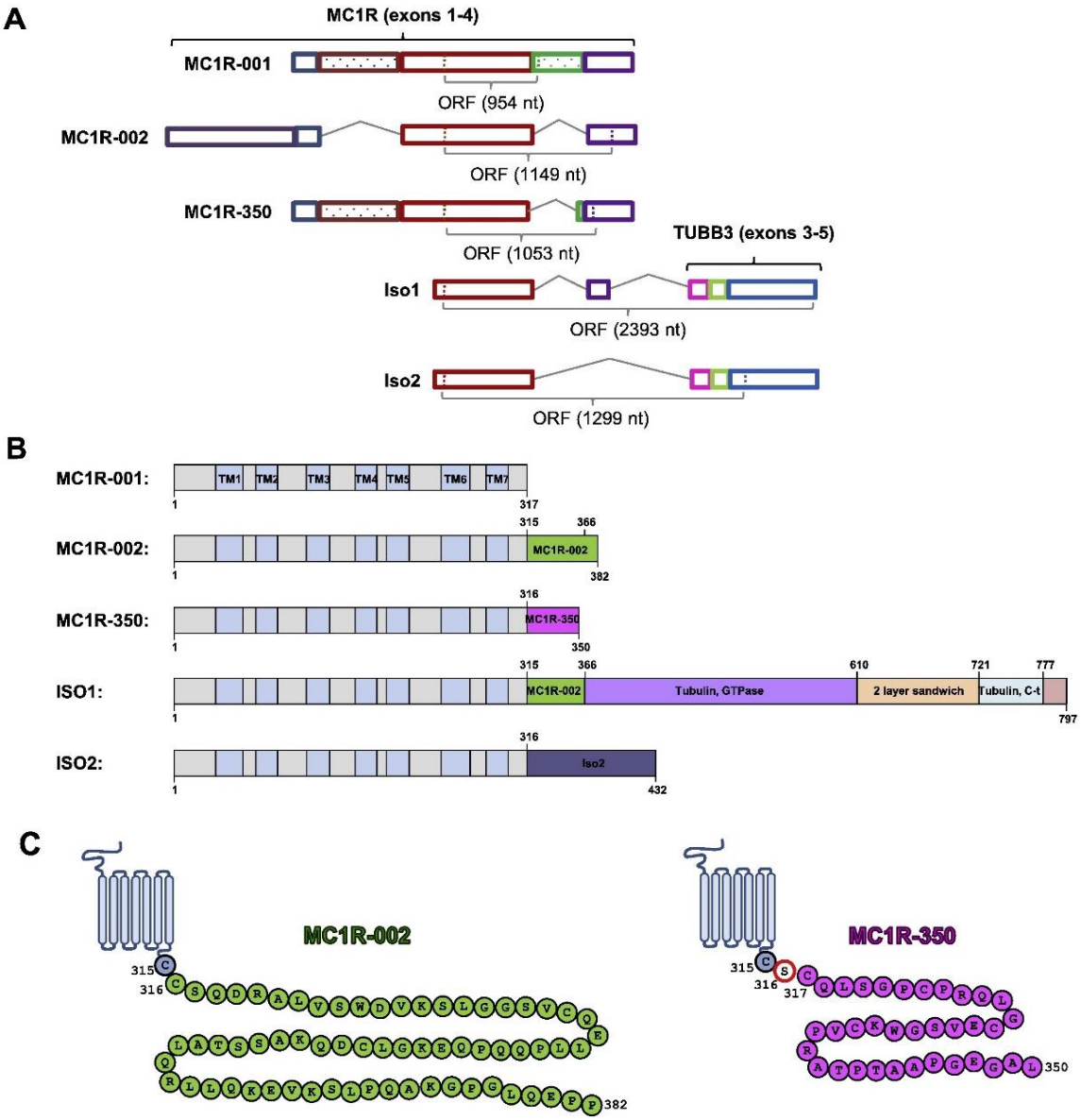

Figure 19. Structure of the *MC1R* gene and MC1R isoforms. (A) Exon organization of *MC1R* splice variants (*MC1R-001*, *MC1R-002* and *MC1R-350*) and *MC1R-TUBB3* intergenic transcripts, *Iso1* and *Iso2*. Exons of all *MC1R*-derived transcripts are depicted in colored boxes and the number of nucleotides in the corresponding ORF is shown below. (B) Structural domains of *MC1R* gene-derived proteins. (C) Amino acid sequence, coding sequence polymorphisms and possible arrangement of TM regions in MC1R intragenic splice isoforms. Ser/Thr residue presumably phosphorylated is highlighted with a red border. The sequence of MC1R-350 and MC1R-002 proteins is identical to MC1R-001 up to Cys315. For MC1R-350 and MC1R-002, only the sequence of their specific cytosolic extensions is shown (pink and green, respectively). Adapted from Herraiz et al., 2017[184].

On the other hand, human *MC1R* is highly polymorphic (reviewed by[4,184]), with around 200 nonsynonymous coding region variants in virtually all the structural domains of the protein described to date (Figure 9), and over 50 polymorphisms in 3′ and 5′ untranslated regions whose potential effects on *MC1R* gene expression or mRNA processing and/or stability remain unknown.

As mentioned before, Valverde et al., first reported the association of some allelic variants with a strong RHC phenotype and increased melanoma and non-melanoma skin cancer risk[172,302]. These highly penetrant variants for RHC phenotype, considered as "R" variants, include D84E, R142H, R151C, R160W and D294H. The mutant alleles V60L, V92M and R163Q are "r" variants, less penetrant for the RHC phenotype.

The frequencies of specific alleles show significant variations in different populations. The R variants R142H, R151C, R160W and D294H and the r mutant allele V60L, are present in around 30% of individuals of northern European descent and, overall they account for more than 60% of all individuals with red hair[303]. Conversely, V92M and particularly R163Q are extremely common in Asian populations, with frequencies around 14% and higher than 60%, respectively[304,305]. On the contrary, nonsynonymous variants are infrequent in dark-skinned African individuals, whereas synonymous variants are found in dark-skinned African populations at a relatively high frequency compared with Caucasians[306,307]. In this line, a positive selection for certain RHC variants associated with lighter skin pigmentation in regions of lower UVR incidence have been proposed[308] whereas extensive genetic studies strongly suggest the occurrence of purifying selection at the *MC1R* gene in Africans[308]. This is in accordance with the hypothesis that migration from Africa to northern latitudes involved the transition towards progressively less pigmented phenotypes favoring the formation of active vitamin D under conditions of limited exposure to UVR[309].

5.2. Variant MC1R signaling

The cAMP pathway is the canonical signaling pathway activated by αMSH binding to MC1R and mediates differentiation. *MC1R* polymorphisms that correlate with the RHC phenotype are associated with impaired functional coupling to the cAMP pathway, consistent with their inefficient activation of eumelanogenesis. Both R and r MC1R variants show decreased or undetectable functional coupling to cAMP pathway in response to MC1R agonists when assayed in heterologous systems, human melanoma cells (HMCs) or NHMs of defined genotype[4,202,229]. Since cells that harbor R variants failed to efficiently activate cAMP production upon MC stimulation, R variants have been considered LOF mutants[202,229]. However, they often display a certain residual activity when they are overexpressed in heterologous systems[171,176,177,183,310–313]. This residual coupling varies from an almost complete LOF for penetrant RHC variants such as D84E and D94H, to 25-50% residual activity for other R forms, particularly R151C or R161W. The degree of functional impairment in activation of cAMP synthesis grossly correlates with penetrance[314]. In fact, the evaluation of agonist-promoted cAMP synthesis has been proposed as a method for classification of MC1R variants according to penetrance. Since all the R forms analyzed thus far have levels of α-MSH-induced cAMP production below 50% of WT when assayed in heterologous systems, whereas the r alleles retain higher residual activities[4], a 50% residual signaling potential may set the threshold between R and r alleles.

Our group, in collaboration with others, has characterized the functional coupling to the cAMP pathway of several MC1R variants, as well as their trafficking behaviour[176,177,184,315]. The main cause of functional impairment for the major RHC alleles R161C, R161W, I155T and D84E may be a decreased cell surface expression[177,268,313,316], due to deficient anterograde trafficking or increased desensitization and internalization[171,176,317]. The R151C variant is retained in the ER and the R160W in the Golgi apparatus[176,318]. On the contrary, certain alleles show decreased functional coupling with normal plasma membrane density. Among these, MC1R variants that bind agonists with reasonable affinity but do not undergo the transition to an active conformation competent for Gs protein activation such as D294H[318], and variants correctly trafficked but unable to bind MC1R agonists such as C289R[176], have been described. These variants can be expressed on the cell surface at densities even higher than WT, most likely because of inefficient recognition by the GRKs and the internalization machinery.

In addition, MC1R undergoes constitutive dimerization during its anterograde trafficking to the cell surface (see section 3.2.4). Co-expression of RHC variants with WT MC1R yielded forms with altered agonist binding affinity and reduced functional coupling to AC. At least the major

RHC variants R151C, R160W and D294H efficiently heterodimerize with the WT form to modify its trafficking and functional properties[171], thus allowing for a pseudodominant-negative behaviour[316].

The best-characterized r alleles are V60L, V92M and R163Q. The effects of V92M and R163Q substitutions on functional coupling to the cAMP cascade are not significant[177,216183]. Only the V60L mutation has been consistently found to result in significant LOF, with a residual ability to activate cAMP synthesis approximately 50% of WT when assessed in heterologous cells[177] as well as in homozygous human melanocytes[216]. This moderate functional impairment can be accounted for by misstrafficking with significant intracellular retention.

RHC mutant alleles also show impaired p38 activation upon MC binding, according to their decreased ability in activating cAMP pathway[202]. On the other hand, most RHC alleles are able to positively couple to ERK1/2 in response to their agonists in NHMs or HMCs, as well as when transfected in heterologous systems[161,310], despite their reduced ability in activating cAMP pathway. These findings confirm the cAMP-independent activation of the ERKs[177] and are in line with the minor effect of this pathway on MC1R-dependent pigmentation in human skin, as compared with activation of cAMP pathway[184]. Accordingly, most RHC variants should be best considered as imbalanced signaling forms rather than as LOF mutants. Moreover, it has been shown that WT MC1R, but not several major RHC alleles, might prevent proteasomal degradation of PTEN[210], suggesting the possibility of a differential capability to activate AKT signaling.

Therefore, MC1R variants hypomorphic in activation of cAMP cascade, can still achieve efficient signaling to other pathways. Further investigation of functional coupling of these variants to cAMP-independent pathways, as well as the physiological consequences of their activation would help to elucidate the roles of MC1R variants as determinants of melanoma risk.

It has been demonstrated that UVR increases expression of MC1R-TUBB3 quimeras[212,213]. However, the biological role of these isoforms as well as their coupling to downstream signaling pathways are still unknown.

5.3. MC1R role in DNA repair

As explained before, inefficient cAMP signaling of MC1R-RHC variants, results in inappropriate activation of photoprotective eumelanin synthesis in response to UVR. This pigmentation-dependent effect might be partially responsible of an increased melanoma susceptibility in carriers of RHC variants[266,268,319,320]. However, as discussed above (see section 4.3), melanoma risk not only relies on eumelanin content and pigmentation phenotype[128,321,322],

but also on impaired pigmentation-independent actions triggered by WT MC1R. Genetic epidemiological studies showed that a significant association of *MC1R* variants and melanoma persists after stratification for pigmentation, and carrying *MC1R* allelic variants also increases melanoma risk in dark-skinned population of European origin, thus pointing to pigment-independent actions of MC1R[265–269,319,323–325].

Concerning these pigmentation-independent actions, MC1R orchestrates a complex series of events to induce antioxidant defenses[216,326] and DNA repair mechanisms (BER and NER pathways) in UVR-exposed melanocytes (recently reviewed in[116,184,327]). Moreover, several studies demonstrated that αMSH can prevent UVR-induced apoptosis in melanocytes[208,216,328,329]. All together, these effects are expected to reduce genomic instability and mutagenesis in melanocytes.

On the contrary, melanocytes carrying MC1R RHC variants have been reported to activate inefficiently or not at all these mechanisms and thus, have been linked to increased UVR-induced apoptosis and defective DNA repair[4]. In this respect, microarray experiments comparing melanocytes carrying MC1R variant alleles (R160W/D294H) with WT MC1R, showed differentially regulated expression of a large number of genes involved in oxidative stress, DNA repair, cell cycle and apoptosis. In WT-MC1R melanocytes, stimulation with αMSH had the opposite effect of UVR on the expression of many genes involved in these functional categories. In contrast, in RHC MC1R melanocytes treated with αMSH and irradiated with UVR, gene expression did not change compared with melanocytes irradiated with UVR in the absence of αMSH treatment, suggesting lack of modulation of the UVR response by αMSH in these cells[216]. In addition, it has been shown that skin cell co-cultures established from carriers of *MC1R* variants showed de-regulated expression of a large number of genes, notably including genes related with cellular management of oxidative stress and DNA damage[330].

Therefore, it appears that several pigment-independent effects of αMSH require expression of *WT MC1R* and are absent in melanocytes expressing 2 *RHC* alleles[208,216,331]. Moreover transfection of melanocytes expressing 2 RHC alleles with the WT MC1R restored their ability to respond to MSH and normalized their response to UVR[329]. In addition, most of these pigment-independent effects are thought to rely on activation of cAMP pathway, since they were mimicked by the AC agonist, FSK[216,332–334]. However, the involvement of other signaling pathways in the activation of antioxidant defenses, DNA repair and survival pathways by MC1R cannot be ruled out. Indeed, it has been shown that activation of PI3K/AKT signaling pathway by MC1R also mediated antiapoptotic effects in melanocytes by increasing Bcl2 protein levels[216,332]. In retinal

pigment epithelium cells, αMSH decreased oxidative stress and increased survival through activation of AKT-mTOR signaling[209].

In conclusion, expression of WT MC1R protects melanocytes against the genotoxic effects of UVR by pigment-dependent and independent mechanisms that synergistically act to maintain genomic stability and ensure survival of melanocytes[208,216,328,329,331,335,336] (Figure 20). In this respect, it has been proposed that the pigment-independent mechanisms represent an early and immediate response to UVR to prevent genomic instability of melanocytes, whereas adaptive UVR tanning is a delayed response, which protects against the genotoxic effects of subsequent UVR exposure[116]. Accordingly, MC1R variants with reduced cAMP signaling would compromise the DNA repair[208,328,337–339] and antioxidant capacities[216,329,331326] of human melanocytes and fail to activate efficiently the UVR-adaptive eumelanin synthesis (Figure 20). All of these impaired MC1R-directed functions are believed to result in increased cellular damage, genomic instability and risk for malignant transformation, and might explain why the mutation load in MC1R variant melanomas is higher compared with WT MC1R melanomas[275,276,338].

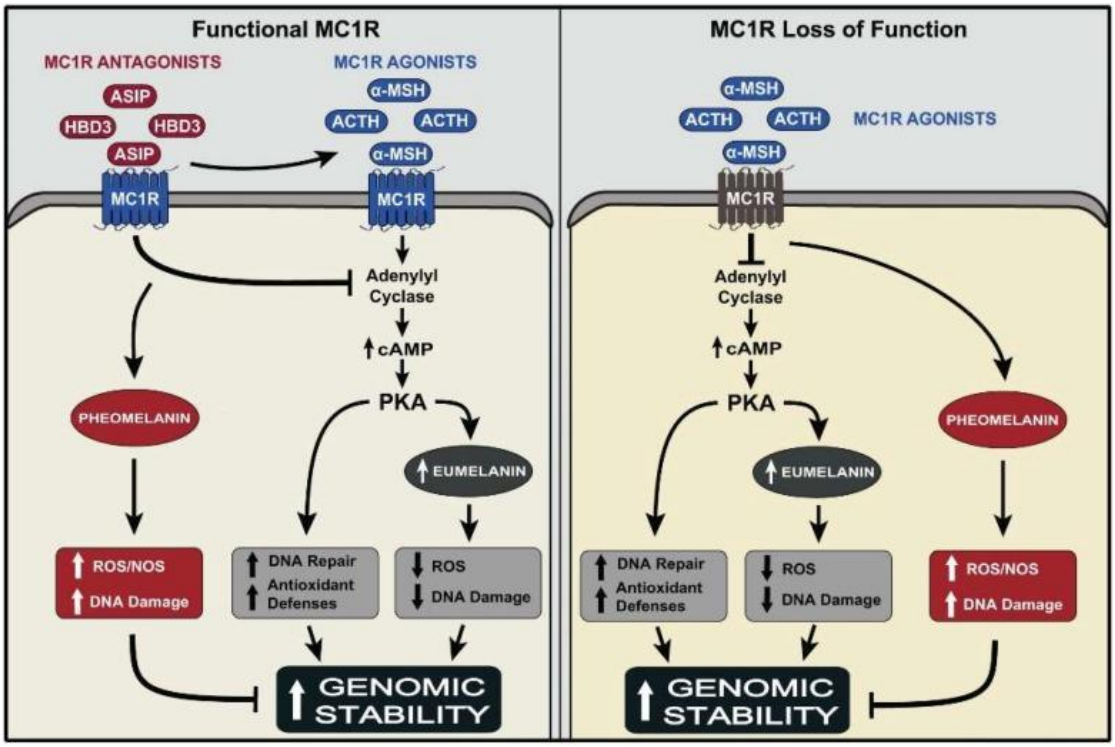

Figure 20. Summary of the current view of the effects of the MC1R agonists αMSH and ACTH and the antagonists ASIP and HBD3 on functional MC1R, and the impact of LOF of MC1R on these effects. Upward arrows: increase in the effect; T bar: blocking the effect. Adapted from Swope and Abdel-Malek., 2018[116].

5.3.1. Induction of antioxidant defenses

As mentioned before (see section 2.3), oxidative stress is implicated in melanomagenesis[140,340]. This oxidative stress results from the balance between the production of prooxidant species in cells and the reduction of cellular antioxidant capacity (Figure 21). Within melanocytes, UVR, melanin synthesis and pheomelanin are important sources of ROS that contribute to an excessive oxidative stress. In this line, it is important to decipher the molecular mechanisms of melanocytes to avoid the deleterious effects of oxidative stress.

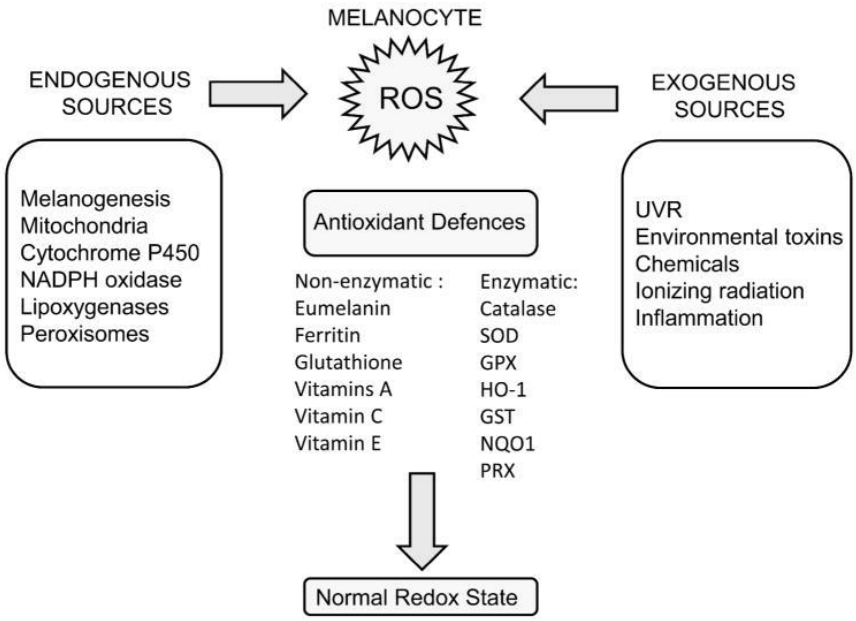

Figure 21. Induction of ROS by endogenous and exogenous sources and antioxidant defenses that restore normal redox state in melanocytes. Adapted from Denat et al., 2014[330].

αMSH has been shown to protect against the UVR-induced oxidative stress by: i) inhibition of generation of H_2O_2[208,216,326,329] ii) activation of antioxidant enzymes, mainly catalase[326,331], and iii) up regulation of expression of antioxidant genes[329,331].

In human melanocytes, release of H_2O_2 after UVR exposure was attenuated by MSH[208,216,331]. Moreover, using keratinocytes transfected with MC1R, Henri et al. reported that MSH decreased UVA-induced ROS levels in WT-MC1R cells compared to cells that stably express the MC1R R151C variant. Interestingly, this mechanism was PKA-dependent and involved the enzyme NOX1. PKA-dependent NOXA1 (NADPH oxidase activator 1) phosphorylation which promoted inhibition of the ROS-producer enzyme NOX1[341] was increased in cells expressing the WT receptor compared with cells harboring the R151C variant and inhibition of PKA in

keratinocytes overexpressing the WT-MC1R resulted in a marked increase of ROS production after UVA irradiation[342].

Antioxidant enzymes are considered the first line of defense against an increase in ROS. Reduction in H_2O_2 levels by MSH may also be at least partially due to increased levels and activity of the antioxidant enzyme catalase[331]. MSH also induced catalase activity and protein levels in B16F10 mouse melanoma cells, through a cAMP/PKA-dependent post-transcriptional mechanism[326]. Activation of MC1R by MSH also enhanced protein levels of the antioxidant proteins peroxiredoxin1 (Prx1)[216], which reduces endogenous peroxides, and ferritin[331] in NHMs. H_2O_2 can be converted in the presence of iron, into the highly reactive hydroxyl radical via the Fenton reaction[343,344]. Increased levels of ferritin would sequester free iron that acts as a catalyst for hydroxyl radical generation[331,343,344].

In addition, MC1R reduces the extent of oxidative damage by induction of transcriptions factors known to regulate the redox state of melanocytes. Kokot and colleagues showed that MSH increased the expression of *Nuclear factor (erythroid-derived 2)-like 2* (*Nrf2*) gene, as well as its target genes, *hemeoxygenase-1* (*HO-1*), *γ-glutamylcysteine synthase* (*γ-GCS*) and *glutathione-S-transferase Pi* (*GSTPi*)[335] in both keratinocytes and melanocytes, and blocked the inhibitory effects of UVR on these genes. γ-GCS is the rate-limiting enzyme for the synthesis of the antioxidant GSH[345] and GSTPi mediates the reduction of ROS-induced oxidized proteins[335]. Regulation of another transcription factor, p53, a major sensor of DNA damage, is a mechanism by which αMSH exerts its antioxidant effects in melanocytes[329]. Indeed, Kadekaro et al. showed that pretreatment with αMSH prior to UVR exposure resulted in accumulation of p53 above the levels achieved by irradiation with UVR in the absence of the hormone[329]. αMSH also increased the activatory p53 phosphorylation at Ser15 with nuclear translocation of the protein, resulting in enhanced transcriptional activity, as shown by higher levels of the p53 targets p21 and GADD45[329]. Pharmacological inhibition of p53 activation by PFT or silencing of *p53* gene, abolished the inhibitory effect of αMSH on reduction of H_2O_2 generation by UVR exposure and H_2O_2-induced oxidative DNA damage[329]. This p53 induction seems to be dependent on p38 activation, since αMSH increased the UVR-induced phosphorylation of p38, whereas its inhibition abolished the increased accumulation of p53 induced by MSH[329].

Taken together, these data suggest that melanocytes regulate oxidative stress by different mechanisms many of which rely on activation of cAMP signaling. Overall, these mechanisms appear crucial to decrease the burden of UVR-induced oxidative damage.

5.3.2. Activation of DNA repair

MC1R activation by αMSH has been shown to activate the BER pathway, responsible for clearance of oxidized bases, and the NER pathway, the major pathway that removes bulky DNA lesions that distort the DNA double helix, including UVR-induced CPDs and 6,4-PPs[346].

Reduced generation and enhanced repair of CPDs by αMSH was first suggested independently by two groups[328,332]. However, the mechanisms by which αMSH mediates activation of the NER pathway have not been completely elucidated yet, although they have been widely investigated in the last years. Several groups have reported that MC1R function and cAMP signaling regulates the efficiency of NER[128,327,334,337,347–350].

The NER repair proteins DDB1, DDB2 and XPC, have all been shown to be upregulated after cAMP stimulation in WT MC1R melanocytes grown together with keratinocytes in co-culture[351]. WT MC1R regulated DDB2 protein levels through activation of p38 signaling, but these effects were absent in MC1R R/R variant melanocytes[351].

Abdel-Malek's group also reported an increase in DDB1 levels following αMSH stimulation[216], which confirms the enhancement of expression of this DNA repair gene found in microarray experiments[216].

Further studies from the same laboratory showed that MC1R activation also led to increased levels of γH2AX and XPC, promoting formation of DNA repair complexes in human melanocytes[350] (Figures 22). It was demonstrated that DDB2 and XPC are required for the recruitment and phosphorylation of ataxia telangiectasia and Rad3-related protein (ATR) and ataxia telangiectasia mutated (ATM) kinases to initiate DNA repair during NER[352]. Moreover, it was reported that the presence of XPC and XPA factors is important for γH2AX formation and that ATR mediates induction of γH2AX by UVR[352,353], all together suggesting a role of γH2AX in repair of photoproducts. Within melanocytes, αMSH induction of γH2AX was dependent on the p53-induced phosphatase 1 (Wip1) and on ATM and ATR DNA damage sensing proteins. Following MSH stimulation, the levels of Wip1, which dephosphorylates γH2AX, correlated inversely with γH2AX[350]. On the other hand, treatment of melanocytes with ATR and ATM inhibitors, partially but significantly, blocked the increase in γH2AX induced by UVR alone or together with αMSH[350].

Melanocytes treated with αMSH also increased the activatory phosphorylation of ATR, ATM and DNA-dependent protein kinase (DNA-PK)[329,350], the three major sensors of DNA damage and activators of p53[354], as well as the ATM and ATR downstream kinases Chk1 and Chk2, which are involved in cell cycle arrest[329,350]. In fact, phosphorylation of p53 at Ser15 in an ATM and DNA-PK dependent manner by MSH was reported[329,350].

Again, these effects were apparently dependent on a WT *MC1R* genotype, as they were less evident in *MC1R-variant* melanocytes. However, in this study, the variants expressed in the melanocyte cultures were not specified, and given the functional non-equivalence of variant *MC1R* alleles, a residual DNA repair activity of some of them cannot be ruled out.

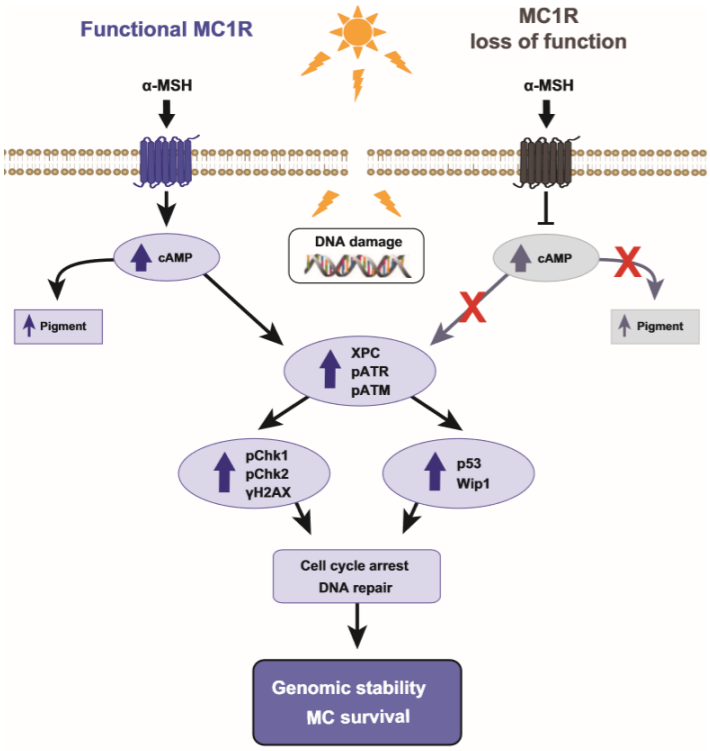

Figure 22. Summary of the effects of αMSH and MC1R on the DDR of human melanocytes described by Abdel-Malek group. Adapted from Swope et al., 2014[350].

Involvement of ATR phosphorylation in MC1R-induced NER was further supported by the findings of D'Orazio and coworkers. This research group has extensively investigated the mechanisms by which the MC1R/cAMP axis induces NER activation. They reported post-translational modifications of NER proteins to stimulate immediate responses.

Stimulation of MC1R, which results in activation of the cAMP-dependent PKA, induced the phosphorylation of ATR on Ser435. Phosphorylation of this site induced association of ATR with XPA[334] and directed the recruitment of XPA to sites of UVR-induced DNA lesions to enhance DNA repair by NER[334]. In fact, Ser435 is part of a PKA target sequence within ATR's predicted nuclear localization sequence, suggesting that its phosphorylation might impact ATR's nuclear localization[355] (Figure 23).

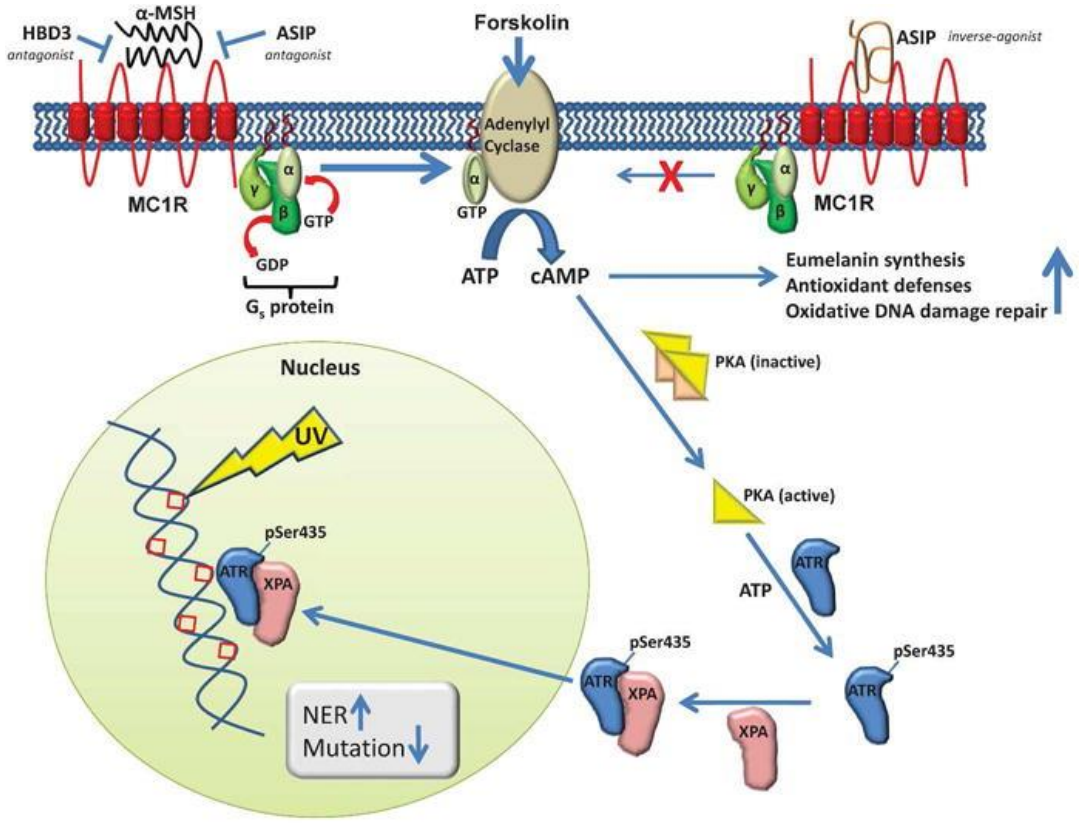

Figure 23. MC1R signaling controls repair of UV-induced DNA damage and suppression of mutations via elevation of intracellular levels of cAMP. Adapted from Cassidy et al., 2015[356].

D'Orazio's group also identified the A-kinase-anchoring protein 12 (AKAP12) as a critical protein that interacts with and promotes phosphorylation of ATR[357]. AKAP12 binds to both PKA and ATR thereby scaffolding the PKA-ATR interaction. The AKAP12-ATR complex moves from the cytosol to the nucleus, where it interacts with UVR-induced photoproducts and promotes the recruitment of XPA and other NER factors[357].

Overall, the data summarized in this section show that in human melanocytes, MSH accelerates repair of UV-induced DNA damage in MC1R-WT melanocytes by activating NER, whereas melanocytes carrying *MC1R variants* do not enhance NER efficiency following ligand stimulation (Figure 24). The effects of αMSH can be mimicked when cAMP levels are induced pharmacologically via AC activation (by FSK) either in WT MC1R or variant melanocytes.

Activation of MC1R signaling also enhances transcriptional expression of several NER pathway components. By combining chromatin immunoprecipitation coupled to high throughput sequencing (ChIP-seq) and RNA sequencing analyses, MITF was shown to directly regulate a set of genes required for DNA repair. Loss of MITF reduced expression of NER factors, including *XPA*, *RPA*, *DNA ligase I* and *DNA polymerase delta* (*Polδ*)[358]. Moreover, *XPAB1* gene expression was

down-regulated in neonatal whole skin of C57BL/6J recessive yellow mice with LOF MC1R[359]. In contrast with the immediate responses mediated by post-translational modifications, the transcriptional induction would allow melanocytes and skin to cope with further UVR-induced DNA damage[338].

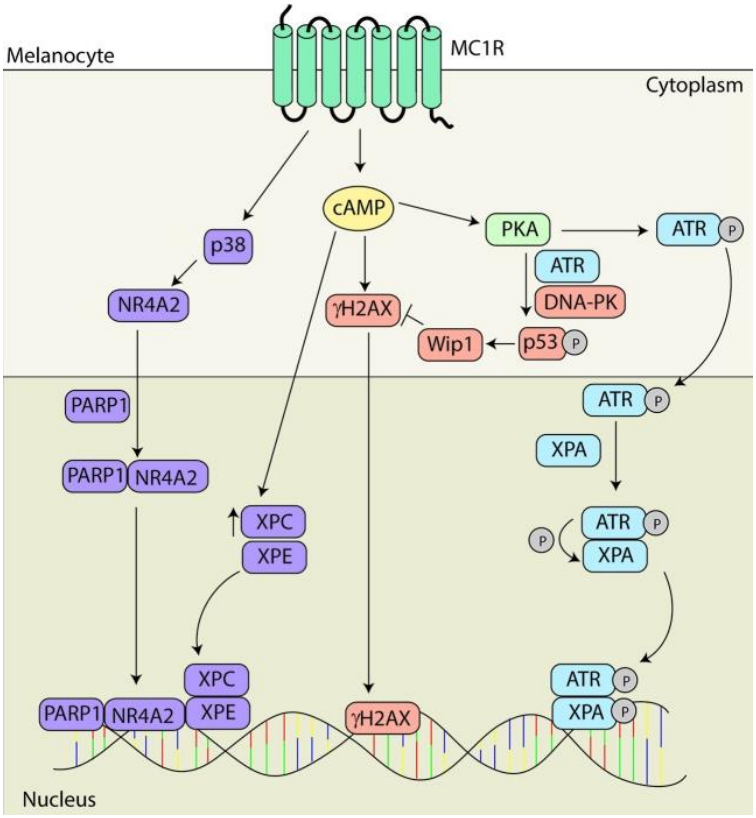

Figure 24. MC1R signaling activates NER and promotes genomic stability through multiple mechanisms. Adapted from Wolf Horrel et al., 2016[360].

On the other hand, ROS-induced lesions, mainly 8-oxodG, are cleared by the BER pathway. Studies on the effects of MC1R signaling on the activity of the BER pathway are scarce. Nevertheless, it has been shown that within melanocytes, MC1R activation mediates the repair of oxidative DNA damage by increasing the expression of OGG1 and APE-1/Ref-1, two essential enzymes involved in BER[329]. These induction relies at least partially on p53 activation since silencing of p53 abolished the stimulating effect of αMSH[329]. Furthermore, It has been shown that 8-oxodG occurs in clusters on stretched chromatin fibers following exposure to UVR resulting in disruption to the chromatin structure that may cause SSBs and DSBs[361]. These DNA lesions are considered minor lesions induced by UVR, but they are extremely genotoxic and compromise cell viability.

DSBs are mainly repaired by the NHEJ and HR pathways. Interestingly, hormone-treated melanocytes were protected against generation of DNA SBs, as estimated by comet assay[329,331]. Although mechanistic work about αMSH-mediated activation of HR and NHEJ pathways has not been performed, αMSH was shown to activate several HR and NHEJ-related factors. Melanocytes were reported to respond to UVR exposure with increased phosphorylation of two members of the PIKK family of DNA damage sensor proteins, DNA-PK and ATM(Ser1981)[329,350]. DNA-PK is a kinase activated specifically by DSBs and the first enzyme involved in NHEJ pathway. ATM also participates in the repair of DSBs, resulting in the phosphorylation of H2AX within minutes[362].

Interestingly, the nuclear receptors Nuclear Receptor Subfamily 4 Group A Member 2 (NR4A2) are recruited to novel nuclear foci to participate in DSBs repair upon ionizing radiation (IR). Co-localization experiments revealed that, upon exposure to IR, NR4A2 foci co-localized with γH2AX and 53-binding protein 1 (53BP1)[363], both markers of DSBs[362,364]. Within foci, NR4A2 receptors also interacted with PARP and DNA-PK proteins. Downregulation of PARP1 by siPARP1 severely disrupted the recruitment of NR4A2 to sites of DSB[363]. Upon exposure to IR, NR4A2 interacted with and was phosphorylated in Ser337 residue by DNA-PK. This phosphorylation promoted DNA repair. Within melanocytes the NR4A2 nuclear receptors are transcriptionally induced by αMSH[365] suggesting a role of MC1R signaling in activating DSBs repair through NR42A receptors.

In summary, a wealth of data prove that MC1R signaling through the cAMP pathway results in a potent activation of NER. This cAMP-dependent induction of NER would be compromised in melanocytes carrying *MC1R variants* with impaired signaling to cAMP. However, it is still unclear whether MC1R variants can still activate NER by cAMP-independent mechanisms. Moreover, the ability of MC1R (WT or variant) to promote BER or clearance of DNA SBs appears likely, but remains largely unexplored. A deeper knowledge of these effects of MC1R is needed to understand the relationship of *MC1R* genotype and melanoma risk.

AIMS

Aims

The protective responses of the melanocytes to UVR are multiple and complex. Many of them are triggered by keratinocyte-secreted signaling molecules that activate receptors in the melanocytes' surface. Among these, the MC1R plays a key role in the protection against UVR-induced damage. In response to its natural ligands, mainly αMSH, it mediates the activation of eumelanogenesis and triggers pigmentation-independent mechanisms such as induction of DNA repair pathways and antioxidant enzymes. These processes have been thought to rely on the cAMP-pathway and are triggered by WT MC1R to maintain genomic stability. Moreover, UVR may cause a MC1R isoform switch by promoting the expression of MC1R-TUBB3 intergenic splice variants of unknown functional properties.

The efficient activation of these processes depends on the *MC1R* genotype. In this context, there are still some topics that remain to be explored. On the one hand, the biological role of intergenic and intragenic splice variants have not been elucidated yet. On the other hand, although MC1R RHC variants fail to increase eumelanogenesis, their role in the induction of pigmentation-independent effects requires further investigation.

Within this framework, the present work aimed at:

1. **Analyzing the trafficking and signaling properties of the MC1R-TUBB3 chimeric proteins** in order to decipher their possible physiological role.

2. **Assessing the MC1R-dependent protection against oxidative DNA damage in human melanoma cells and epidermal melanocytes of defined *MC1R* genotype**, by comparing the ability of variant and WT MC1R to promote:

   2a – Induction of antioxidant enzymes.
   2b- Repair of oxidized bases.
   2c- Clearance of DNA strand breaks.

3. **Identifying the signaling pathways, if any, responsible for activation of DNA repair downstream of variant MC1R.** This would help to better understand the role of *MC1R* as a melanoma susceptibility gene.

MATERIALS AND METHODS

Reagents

The companies suppliers of reagents and kits used are described in the following list:

- **Amersham (Little Chalfont, Buckinghamshire, UK):** The radioligand [^{125}I]-NDP-MSH specific activity 2000 Ci/mmol.
- **AppliChem GMBH (Darmstad, Alemania):** Ethylenediaminetetraacetic acid (EDTA) and sodium dodecil sulfate (SDS).
- **Arbor Assays (Eisenhower Place, Michigan, USA):** Direct cyclic AMP Enzyme Immunoassay Kit.
- **Biotools, B & M Labs (Madrid, Spain):** DNA polymerase.
- **BioRad (Richmond, VA, USA):** reagents used for SDS-PAGE and Western blot: ammonium persulfate (APS), TEMED, Tween 20 and Extra Thick Blot Paper Protean XL Size.
- **Calbiochem (Darmstad, Alemania):** phosphatase inhibitors (imidazole, sodium fluoride, sodium o-vanadate and β-Glycerol phosphate) and the protein synthesis inhibitor, cycloheximide.
- **DAKO Corporation (Glostrup, Denmark)**: mounting medium for immunostaining.
- **Fermentas (Barcelona, España):** DNA ladder and restriction endonucleases.
- **Invitrogen (Carlsbad, CA, USA):** Lipofectamine™ 2000, Library Efficiency DH5α, DNA ligase, Alexa conjugate antibodies, pcDNA3.1 plasmid, SYBR™ Green I Nucleic Acid Gel Stain 10,000X, cDNA SuperScript First-Strand Synthesis System for RT-PCR, 2'7'dichlorodihydrofluorescein diacetate, AmplexUltraRed and DAPI.
- **Labotaq (Sevilla, Spain):** RedSafe™ Nucleic Acid Staining Solution (20,000x).
- **Merck (Darmstadt, Alemania):** ethanol and isopropanol.
- **Millipore (Billerica, MA, USA):** Polyvinylidene difluoride (PVDF) membrane Immobilion-Ny+ Blotting Membrane (Immobilon-P).
- **Prolabo (Barcelona, Spain)**: acrylamide/bisacrylamide.
- **Pronadisa (Madrid, España):** Agarose, Lysogeny Broth (LB) agar medium, Super Optimal Broth (SOB) medium.
- **QIAGEN (Hilden, Alemania):** QIAquick Gel Extraction Kit and RNeasy® Mini Kit.
- **Roche Applied Sciences (Mannheim, Alemania**): complete™ Mini EDTA-free Protease Inhibitor Cocktail tablets.
- **Sigma-Aldrich (St Louis, MO, USA):** Igepal CA-630, Bovine Serum Albumin (BSA), Phenylmethanesulfonyl fluoride (PMSF), iodoacetamide (IAA), N-Ethylmaleimide (NEM),

EZview Red ANTI-FLAG M2 Affinity Gel beads, *tert*-Butyl hydroperoxide solution (Luperox® TBH70X), ampicillin and kanamicine antibiotics, β-mercaptoethanol, anti-FLAG M2–Peroxidase conjugate antibody, MTT, GenElute HP Plasmid Maxiprep Kit and GenElute HP Plasmid Miniprep Kit.

- **Thermo Fisher Scientific (Waltham, Massachusetts, USA):** ECL Plus Western blot Detection System, Pierce™ bicinchoninic acid (BCA) Protein Assay Reagent A, 16% p-formaldehyde, Tris, glycine and PageRuler Prestained Protein Ladder.
- **Teknokroma Analítica S.A. (Barcelona, Spain):** Oligonucleotide sequences.
- **Trevigen (Gaithersburg, MD, USA):** Alkaline Comet Assay and 8-oxodG antibody.
- **VWR (Radnor, Pennsylvania):** Plastic used for cell culture.
- **Zymo Research (Orange, CA, USA):** Kit DNA Clean & Concentrator™.

Reagents not described in this list are specified in the corresponding sections.

Activators and inhibitors

Activators and inhibitors used are shown in Figure 1 and listed below:

- The protein synthesis inhibitor, **cycloheximide** (Chx, 0.1 mM) was from Amersham.
- The synthetic α melanocyte stimulating hormone (αMSH) analogue [Nle4, D-Phe7] αMSH (**NDP-MSH**) (Calbiochem) used at 10^{-7} M from a stock solution of 10^{-3} M in HCl 0.01 N.
- The adenylyl cyclase (AC) activator, forskolin (**FSK**) (Calbiochem) was used at 10^{-5} M, from a stock solution 10^{-2} M.
- The analog of cyclic AMP (dibutyryl-cAMP, **dbcAMP**) from Santa Cruz Biotechnology at $3x10^{-6}$ M.
- The AC inhibitor 2',5'-dideoxyadenosine (**DDA**), was resuspended at 200 mM in DMSO and then diluted until final concentration $2.5x10^{-3}$ M.
- The AKT1/2/3 inhibitor **MK-2206** and the PI3K inhibitor **LY294002** from Apexbio Technology LLC were used at $5x10^{-6}$ M and $2x10^{-5}$ M, respectively.
- The AKT activator (2-amino-6-chloro-α-cyano-3-(ethoxycarbonyl)-4H-1-benzopyran-4-acetic acid ethyl ester) **SC79** from Sigma was used at 10 μg/ml.
- The MAPK kinase inhbitor MEK, **PD98059** (Sigma), was used at final concentration 50 μM.
- The NOX1/4 inhibitor **GKT137831** from Apexbio Technology LLC was used at 10^{-4} M.
- The NOX inhibitor Diphenylepodium (**DPI**) from Sigma was used at 10^{-4} M.

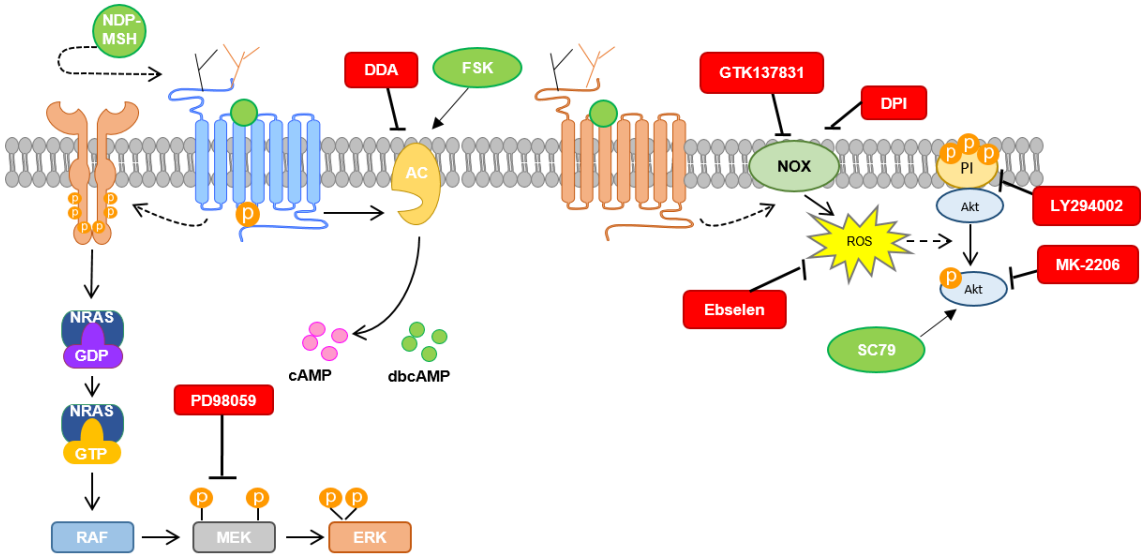

Figure 1. Activators and inhibitors used. Activators are shown in green and inhibitors are shown in red.

Cell culture

Human HEK293T cells, PC12 cells, HBL (LOCE-MM1, established in the LOCE, Université Libre de Bruxelles, Belgium, a gift from Prof. G. Ghanem), A375, SKMEL28 and C8161 HMCs were grown in DMEM with 10% fetal bovine serum (FBS), 100 U/ml penicillin and 100 µg/ml streptomycin sulfate.

Human epidermal melanocytes, Hermes, (kindly provided by Prof. J.N. Rodríguez López, University of Murcia, Spain) were cultured in Melanocyte Medium-2 enriched with 5% FBS, 10% Melanocyte Growth Supplement-PMA-free, 100 U/ml penicillin and 100 µg/ml streptomycin sulfate. Serum and Melanocyte Growth Supplement were removed 1 day before, and for the duration of each experiment.

All cells were incubated at 5% CO_2 and 37 °C in a ThermoQuest incubator (Forma Scientific, Marietta, OH, USA).

To maintain cell lines, cells were seeded in a 75 cm^2 flask (5 x 10^5 cells) or 25 cm^2 flask (1.5 x 10^5 cells) with 10 ml of complete medium and grown until 85% confluency. Then, cells were washed with phosphate buffered saline, PBS, (137 mM NaCl, 2.7 mM KCl, 10 mM Na_2HPO_4, 1 mM KH_2PO_4, pH 7.2) to remove all traces of serum, which contains trypsin inhibitor, detached with trypsin-EDTA solution (0.5% trypsin, 0.2% EDTA in PBS) and centrifuged at 300 g for 5 min. The resulting cellular pellet was resuspended in complete growth medium and appropriate aliquots of the cell suspension were added to new culture vessels. Trypsin-EDTA treatment was not used to detach HEK293T cells.

Cell culture reagents used for melanoma cells and trypsin/EDTA were from Gibco, and reagents used for HEM culture were from Gentaur.

Expression constructs

All expression constructs were prepared in pcDNA3 (Invitrogen, Carlsbad, California, USA). The preparation of Flag-tagged WT-MC1R[222] , R151C and D294H[318], V60L and V92M[161] expression constructs have been previously described. N-terminal 3xHA-labeled MC1R-001 construct was from the Missouri University of Science and Technology cDNA Resource Center (Rolla, MO). MC1R/TUBB3 locus constructs inserted into the pcDNA3.1-His expression vector were kindly provided by Prof A. Furger (University of Oxford, UK) and have been previously described[213]. Expression constructs used and previously described are listed in Table 1.

Expression constructs	Overexpressed gene	Supplier
Flag-tagged WT-MC1R	WT-MC1R	Research group[222]
Flag-tagged R151C-MC1R	Variant-MC1R R151C	Research group [318]
Flag-tagged D294H-MC1R	Variant-MC1R D294H	Research group [318]
Flag-tagged V60L-MC1R	Variant-MC1R V60L	Research group [161]
Flag-tagged V92M-MC1R	Variant-MC1R V92M	Research group [161]
N-terminal 3xHA-labeled MC1R-001	WT-MC1R	Missouri University of Science and Technology cDNA Resource Center.
MC1R/TUBB3 in pcDNA3.1-His (Iso1)	MC1R Iso1	Prof A. Furger[213]
MC1R/TUBB3 in pcDNA3.1-His (Iso2)	MC1R Iso2	Prof A. Furger[213]

Table 1. Expression constructs used and previously described, overexpressed gene and supplier (company or laboratory). Papers that described plasmid generation are specified.

To obtain mutant S83P-MC1R, site-directed mutagenesis was performed.

To generate the Flag-tagged constructs, MC1R-TUBB3 chimeric transcripts were subcloned into pcDNA3 (Invitrogen) using EcoRI and XbaI as restriction enzymes. Site-directed mutagenesis was performed to ablate BamHI restriction site within TUBB3 gene in pIso1 and pIso2. N-terminal Flag epitope Iso1 and Iso2 constructs were obtained using a Flag-WT MC1R-001 as template and cleaving with BamHI and XbaI.

4.1. Expression constructs by site-directed mutagenesis

Site-directed mutagenesis using the QuikChange XL Site-Directed Mutagenesis kit (Agilent, Santa Clara, CA) was performed to obtain mutant S83P-MC1R and to ablate BamHI restriction site within TUBB3 gene in pIso1 and pIso2.

First, Mutant Strand Synthesis Reaction (Thermal Cycling) was performed using 2.5 U PfuTurboDNA Polymerase, 10 ng of template and 125 ng primers containing the desired mutation (Table 2). The oligonucleotide primers, each complementary to opposite strands of the vector, were extended during temperature cycling. Incorporation of the oligonucleotide primers generates a mutated plasmid containing staggered nicks. The PCR program consisted of: primer hybridization at 95 ºC for 1 min, 18 rounds of PCR followed by a 7 min extension at 68º C. Following temperature cycling, the product was treated with Dpn I endonuclease at 37 ºC for 1 h to digest methylated and hemimethylated DNA from parental DNA template and to select for mutation-containing synthesized DNA.

The nicked vector DNA incorporating the desired mutation was then transformed into DH5α competent cells. To select positive plasmid-containing bacteria, several colonies previously formed in LB agar plate were grown in 4 ml of SOB medium with 100 µg/ml ampicillin with gently shaking for 18 h at 37 ºC. Then, plasmid DNA was isolated using GenElute HP Plasmid Miniprep kit. This kit consists of modified alkaline-SDS lysis procedure followed by adsorption of the plasmid DNA onto silica in the presence of high salt concentration.

DNA concentration was determined by measuring the absorbance at 260 nm with the spectophotometer Thermo Scientific™ NanoDrop 2000c (Thermo Thermo Scientific). The purity of DNA was examined by the ratio of the measurement at 260 nm and 280 nm. Pure DNA has an A_{260}/A_{280} ratio of 1.9–2. Constructs were verified by double strand automated sequencing (section 8.2).

Construct	Template	Oligo sequence 5' → 3'
Iso1 in pcDNA3	Iso1 in pcDNA3 without BamHI restriction site	CTACTTCGTGGAGTGGATTCCCAACAACGTGAA
Iso2 in pcDNA3	Iso2 in pcDNA3 without BamHI restriction site	CTACTTCGTGGAGTGGCTCCCCAACAACGTG
Flag-tagged S83P-MC1R	Flag-WT-MC1R	GCTGCCTGGCCTTGCCGGACCTGCTGGTG

Table 2. Expression constructs generated by site-directed mutagenesis. Templates and forward primers used to obtain the constructs are described.

4.2. Expression constructs subcloned into pcDNA3

MC1R-TUBB3 chimeric transcripts (inserted into the pcDNA3.1-His expression vector and kindly provided by Prof A. Furger[213]) were subcloned into pcDNA3 (Invitrogen) using EcoRI and XbaI restriction enzymes. First, MC1R-TUBB3 chimeric transcripts in the pcDNA3.1-His expression vector and pcDNA3.1 expression vector were double-digested separately with EcoRI and XbaI restriction enzymes by incubation at 37 ºC for 1 h. Each digestion product was electrophoresed in a 1% agarose gel (see section 8) and the corresponding bands were extracted with QIAquick Gel Extraction Kit, according to manufacturer's instructions. Then, the eluted products concentrations and purities were determined as described above.

Ligation of DNA and pcDNA3.1 was performed using 30 ng of the expression vector and the insert in a molar ratio of 1:5 (vector: insert) incubating at RT for 4 h with 1 U of T4 DNA ligase. Finally, 10 ng of ligation mixture were transformed into ampicillin resistant DH5α competent cells. The process follows as described above.

To generate the Flag-tagged constructs, after ablation of BamHI restriction site in pIso1 and pIso2 (see section 4.1), N-terminal Flag epitope Iso1 and Iso2 constructs were subcloned into pcDNA3 using a Flag-WT MC1R-001 as a template and cleaving with BamHI and XbaI following the same protocol explained above.

Transient transfection

The reagent used for plasmid DNA transient transfection was Lipofectamine 2000 (Invitrogen) at 1 mg/ml. Transfection was performed according to the following protocol: Plasmid DNA and Lipofectamine 2000 were diluted in Opti-MEM (Gibco) and incubated for 10 minutes at room temperature (RT) to increase transfection efficiency. Then, plasmid DNA and lipofectamine solutions were mixed for 20 minutes at RT to allow the formation of plasmid DNA-lipid complexes. Finally, the mix was added to cells previously grown in DMEM with 10% FBS and without antibiotics. Cells were collected 24 or 48 h after transfection.

Cells grown to approximately 80% confluence were transfected with Plasmid DNA and Lipofectamine 2000 quantities described in Tables 3 and 4:

Plate format	Plasmid DNA (µg)	Lipofectamine 2000 (µl)	Final volume (µl)
24-well plate	0.3	1	350
12-well plate	0.5	1.5	500
6-well plate	1	2	1000

Table 3. DNA plasmid and Lipofectamine quantities used according to plate format for HBL HMCs transient transfection.

Plate format	Plasmid DNA (µg)	Lipofectamine 2000 (µl)	Final volume (µl)
24-well plate	0.15	0.75	350
12-well plate	0.3	1	500
6-well plate	0.6	1.5	1000

Table 4. DNA plasmid and Lipofectamine quantities used according to plate format for HEK293T and PC12 cells transient transfection.

RNA extraction

Total RNA was extracted with the commercial kit RNeasy® Mini Kit (QIAGEN, Hilden, Germany). Around $5x10^6$-10^6 cells grown in a p6 well or a 25 cm^2 flask were disrupted with 350 µl Buffer RLT (provided by the kit), a salt solution containing guanidinium that allows cell lysis and inhibition of endogenous RNases, and homogenized with gentle shaking. A volume of 350 µl of 70 % ethanol was added to the lysates to promote selective binding of RNA to the RNeasy membranes. Samples were then applied to the RNeasy Mini spin column and centrifuged at 9000 g for 15 s. The supernatant was discarded and the samples bound to the column were washed 3 times by centrifugation at 9000 g for 15 s. Finally, high quality RNA was eluted in RNase-free water and its concentration was determined by measuring the absorbance at 260 nm with the spectophotometer Thermo Scientific™ NanoDrop 2000c (Thermo Thermo Scientific). The purity of RNA was determined by the ratio of the reading at 260 nm and 280 nm. Pure RNA has an A_{260}/A_{280} ratio of 1.9–2.

cDNA synthesis

RNA was reverse transcribed into cDNA using The SuperScript® First-Strand Synthesis System for RT-PCR kit (Invitrogen Life technologies) according to manufacturer's instructions. One ug of RNA was denaturalized at 65 ºC for 5 min in presence of oligo(dT)12-18 and dNTPs, then samples were cooled down slowly and placed on ice for 5 minutes. The samples were incubated at 42 ºC for 2 min with a mix containing retrotranscriptase buffer, DTT, $MgCl_2$ and RNase OUT. Then, 1 µl of SuperScript II Retrotranscriptase enzyme was added. cDNA synthesis reaction was performed at 42 ºC for 50 min and, terminated at 70 ºC for 15 min. To eliminate the remaining RNA, samples were incubated with 1 µl of RNase H at 37 ºC for 20 min.

Semi-quantitative PCR and sequencing

8.1. Semi-quantitative PCR

The sequences of NRAS and exon 15 of BRAF have been previously described by our research group[177]. Full-length *NRAS* ORF was amplified from cDNA, whereas for *BRAF*, exon 15 was amplified using genomic DNA as template.

The complete coding sequences of *MC1R* and *PTEN* were amplified from cDNA (50 ng, obtained as described in sections 6 and 7), using 1.5 mM $MgCl_2$, 200 µM of each dNTP, 0.5 µg of each primer and 1 U of DNA polymerase (Biotools). For MC1R, 30 rounds of PCR were performed (denaturation for 1 min at 95º C, annealing 1 min at 60º C and extension 1 min at 72º C) followed by a 10 min extension at 72º. For PTEN, the same conditions were used except that the annealing temperature was 54 ºC.

Primers used for amplification of *MC1R*, *PTEN*, *NRAS* and *BRAF* sequences are described in Table 5 as well as the annealing temperature of each primer.

Target	Oligo sequence 5' → 3'	Annealing Temperature (ºC)
MC1R forward	ATGGCTGTGCAGGGATCCCAG	60
MC1R reverse	TCACCAGGAGCATGTCAGCAC	60
PTEN forward	ATGACAGCCATCATCAAAGAGATC	54
PTEN reverse	TCAGACTTTTGTAATTTGTGTATGCTGAT	54
NRAS forward	CGGATCCGAAATGACTGAGTACAAAC	54
NRAS reverse	TGAATTCTTACATCACCACACATG	54
BRAF exon 15 forward	TCATAATGCTTGCTCTGATAGGA	57
BRAF exon 15 reverse	GGCCAAAAATTTAATCAGTGGA	57

Table 5. Oligonucleotide sequences used for *MC1R*, *PTEN, NRAS* and *BRAF* amplification by PCR. Target gene, oligonucleotide sequence and annealing temperature used for PCR are described.

Detection of the amplified products was performed at the end of the reaction by electrophoresis and image analysis. For agarose electrophoresis, 20 µl of sample were loaded into a 1% agarose gel containing 1% Red Safe nucleic acid staining reagent solution (20,000x) and electrophoresis was performed using 1X TAE buffer (40 mM Tris, 1 mM EDTA, and 30 mM acetic acid (0.175% v/v)) at 100 V for 30-40 min. PCR product was detected using a UV Gel Doc 1000 transilumintor from BioRad (Richmond, VA, USA) and purified using DNA Clean & ConcentratorTM kit following manufacturer's instructions. DNA concentration was determined as specified above.

8.2. Sequencing

MC1R, PTEN, NRAS and *BRAF* mutation status were determined using automated sequencing of PCR amplified products (Molecular Biologoy Platform, University of Murcia). Sequences were compared with WT sequences obtained from ensemble database (https://www.ensembl.org/index.html). Primers used for sequencing are described in Table 6. Mutation status was confirmed by resequencing separately amplified DNA aliquots.

Target	Oligo sequence 5' → 3'	Annealing Temperature (ºC)
MC1Rint forward	AGCAACGTGCTGGAGAC	54
MC1Rint reverse	GCGTAGAAGATGGAGATGTAG	62
PTENint forward	GGACGAACTGGTGTAATGATATGTG	58
PTENint reverse	TCTGTTTGTGGAAGAACTCTACTTTGAT	59
NRASint forward	CCATGAGAGACCAATAC	50
NRASint reverse	GGTACATCATCCGAGTC	52
BRAF exon 15 forward	TCATAATGCTTGCTCTGATAGGA	57
BRAF exon 15 reverse	GGCCAAAAATTTAATCAGTGGA	57

Table 6. Oligonucleotide sequences used for *MC1R*, *PTEN, NRAS* and *BRAF* gene sequencing. Target gene, oligonucleotide sequence and annealing temperature used are shown.

Gene expression analysis by Real-time PCR

9.1. Experimental design: Primer design and validation

A good primer design is one of the most important parameters in RT-PCR. Primers were designed according to manufacturer´s guidelines (Applied Biosystems):

- Primers were specific for the target sequence. To confirm the specificity of primers, we performed a BLAST search against public databases to be sure that our primers only recognized the target of interest.
- Primers had between 18-28 base pairs length.
- Primers annealed to two different exons to allow differentiation between amplification of cDNA and potential contaminating genomic DNA.
- Primers were selected to amplify sequences between 50-150 base pairs.
- Primers were designed to avoid stretches of homopolymer sequences (e.g., poly (dG)) or repeating motifs, as these can hybridize inappropriately.
- Primer pairs contained approximately 30-80 % GC content, since primers with high GC content can form stable imperfect hybrids.
- Primers had melting temperatures around 58-60 ºC.
- The last 5 nucleotides in 3' end of the primer did not have more than two G or C.

All primers used for analysis of gene expression by RT-PCR were from Biolegio BV (Nimega, Nertherlands) and are described in Table 7.

Oligo name	Oligo sequence 5' → 3'	Length	%GC	Tm
MC1R-001 forward	GCCCTCATCATCTGCAATGC	20	55	58
MC1R-001 reverse	CCCTCTGCCCAGCACACTTA	20	60	60
Iso1 forward	GCTCCTGCAAAAGGAGTTCTG	21	52	58
Iso1 reverse	GCTCGAGGCACGTACTTGTG	20	60	59
Iso2 forward	TGCTGACATGCTCCTGTTCTG	21	53	59
Iso2 reverse	GCTCGAGGCACGTACTTGTG	20	60	59
MITF forward	GGCAGACCTTGGTTTCCATA	20	50	58
MITF reverse	ATGAGGAAATCTTGGGCTTGA	21	44	58
CAT forward	CATCGCCACATGAATGGATA	20	45	59
CAT reverse	CCAACTGGGATGAGAGGGTA	20	55	59
SOD1 forward	TTTGGAGATAATACAGCAGGCTGTAC	26	42	59
SOD1 reverse	TAGACACATCGGCCACACCAT	21	52	60
GPx1 forward	CGGCGGCCCAGTCGGTGTAT	17	65	60
GPx1 reverse	TTCATCTGGGTGTAGTCCCG	20	50	58
β-actin forward	GACAGGATGCAGAAGGAGATCA	22	50	57
β-actin reverse	GCTCAGGAGGAGCAATGATCTT	22	50	58

Table 7. Primers for analysis of human gene expression by real time PCR. Length, annealing temperature and GC content for each primer are shown.

A dilution series of known template concentrations was used to establish a **standard curve** for assessing the reaction efficiency. The slope of the log-linear phase of the amplification reaction was a measure of reaction **efficiency** according to the equation: Efficiency = $10^{(-1/\text{slope})}$ -1. All primers used showed an efficiency between 90% and 110%, which corresponds to a slope between -3.58 and -3.10. The specificity of the RT-PCR reaction was confirmed using melting curve analysis. **Melting curve** analysis can identify the presence of primer-dimers, because they exhibit a lower melting temperature than the amplicon. None of the designed primers showed primer dimerization.

An example of parameters studied is shown in Figure 2.

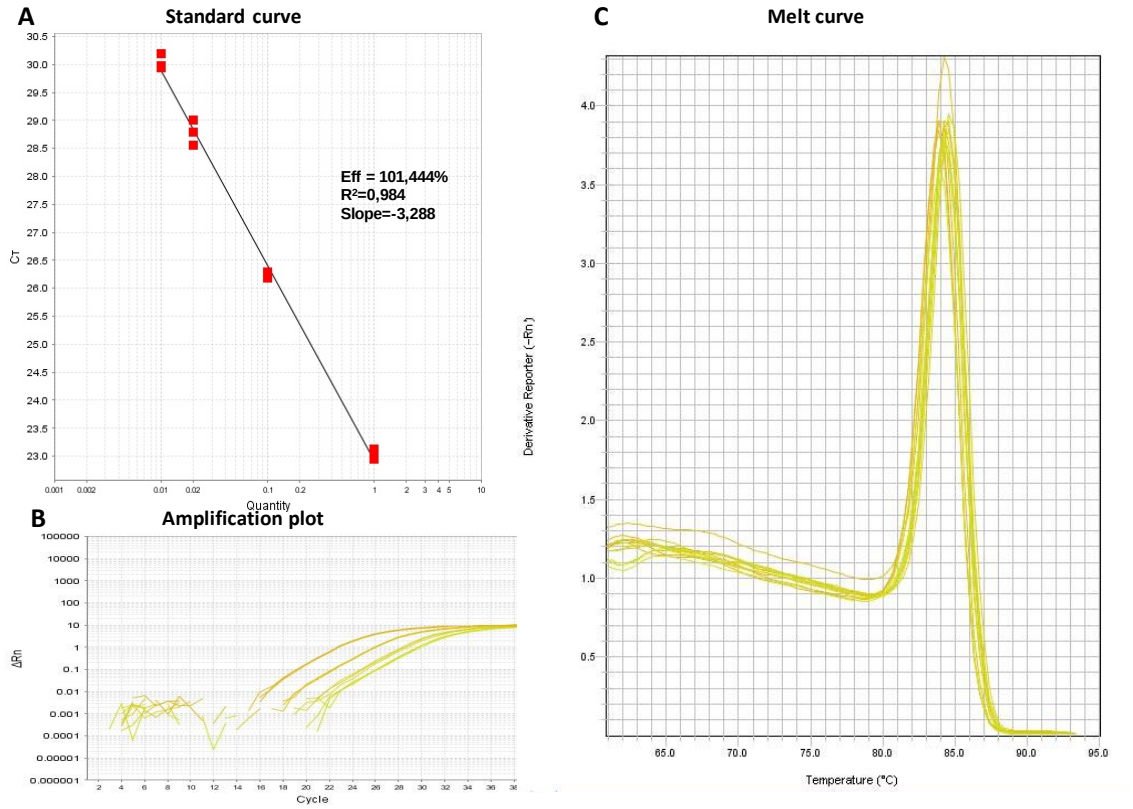

Figure 2. Amplification of GPx1 from cDNA obtained from A375 melanoma cells. RT-PCR of serial dilutions of a human cDNA was performed using Power SYBR Green PCR Master Mix (Applied Biosystem) under standard thermal cycling conditions on ABI 7500 Fast Real Time PCR System. **A. Standard curve.** The log of each known concentration in the dilution series (x-axis) is plotted against the Ct value for that concentration (y-axis). From this standard curve, information about the performance of the reaction as well as various reaction parameters (including slope and correlation coefficient) were determined. **B. Amplification plot.** Fluorescence is plotted against the cycle number to generate an amplification plot that represents the accumulation of product over the duration of the entire PCR reaction. **C.Melting Curve.** The -ΔF/ΔT (change in fluorescence/ change in temperature) is plotted against temperature to obtain a clear view of the melting dynamics.

9.2. Plate preparation

RT-PCR was performed using the Power SYBR Green PCR Master Mix (Applied Biosystem, Warrington, UK). A 96 well-plate was used to mix the reagents. Eight µl of diluted cDNA were loaded into each well (final sample concentration was 2.5 ng/µl or 0.25 ng/µl depending on the gene analyzed). Then, a mix containing 10 µl of Power SYBR Green PCR Master Mix and 2 µl of 0.5 µM primers solution (final concentration 50 nM) were added. The plate was centrifuged at 200 g for 5 min in a Hermle Z326 plate centrifuge and the RT-PCR was performed on ABI 7500 Fast Real Time PCR System with the following cycling conditions: 95° C for 30 s and 40 cycles of 95° C for 5 s and 60° C for 60 s. β-actin gene was used as endogenous reference gene.

9.3. Data analysis: Comparative Ct Method for Relative Quantification (ΔΔCt)

Gene expression was analyzed using the Comparative Ct Method for Relative Quantification (ΔΔCt). Gene of interest Cts ($C_{t\ GOI}^{s}$) were compared with reference gene Cts ($C_{t\ reference}^{s}$), (ΔCt) in every sample studied. Then, ΔCt of the experimental sample was compared with ΔCt of the control sample. The resulting value ΔΔCt was used to determine gene expression values relative to control, fold change=$2^{-\Delta\Delta Ct}$. Cts values over 35 were not included.

$$C_{t\ GOI}^{s} - C_{t\ reference}^{s} = \Delta C_{t\ sample}$$

$$C_{t\ GOI}^{c} - C_{t\ reference}^{c} = \Delta C_{t\ control}$$

$$\Delta Ct_{\ sample} - \Delta Ct_{\ control} = \Delta\Delta Ct$$

Protein extraction and quantification

10.1. Protein extraction

Three different methods were used to solubilize cells depending on post-translational modifications and subcellular localization of target proteins:

1. For extraction and detection of **phosphorylated proteins**, cells were washed with cold PBS and resuspended in lysis buffer I (50 mM Tris-HCl pH 8, 1% Igepal, 1 mM EDTA, 0.1 mM PMSF) supplemented with 10 mM IAA, 10 mM NEM and phosphatase inhibitors (200 mM imidazol, 100 mM NaF, 100 mM sodium o-vanadate and 1 M β-Glycerol phosphate). Then, lysis extracts were centrifuged at 15000 g for 20 minutes at 4 ºC in a Labnet Prism-R C2500-R Refrigerated centrifuge. Supernatants were collected for protein measurement.

2. For extraction and detection of **nuclear proteins**, cells were washed with cold PBS and resuspended in lysis buffer II (150 mM sodium chloride, 1.0 Triton X-100, 0.5% sodium deoxycholate, 0.1% SDS, 50 mM Tris, pH 8.0) supplemented with 10 mM IAA, 10 mM NEM and phosphatase inhibitors (200 mM imidazol, 100 mM NaF, 100 mM sodium o-vanadate and 1 M β-Glycerol phosphate). Then, lysis extracts were processed as described in method 1.

3. For extraction and detection of **membrane proteins**, cells were collected and centrifuged at 300 g 4 ºC for 5 min. Then, cellular pellet was resuspended in lysis buffer I (50 mM Tris-HCl pH 8, 1% Igepal, 1 mM EDTA, 0.1 mM PMSF) supplemented with 10 mM IAA, 10 mM NEM and phosphatase inhibitors (200 mM imidazol, 100 mM NaF, 100 mM sodium o-vanadate and 1 M β-Glycerol phosphate). Lysis extracts were incubated for at least 1 h at 4 ºC with gentle shaking, then centrifuged at 15000 g for 30 minutes at 4º C in a Labnet Prism-R C2500-R Refrigerated centrifuge. Supernatants were collected for protein measurement.

10.2. Protein measurement

The total amount of protein was determined by BCA assay according to supplier's instructions. The principle of the assay is the reduction of Cu^{+2} to Cu^{+1} by proteins in an alkaline solution (the Biuret reaction) resulting in a purple color formation by BCA. First, diluted BSA protein standards and working reagent (WR) solution were prepared. A set of standards for a range from 0 to 30 µg/ml of BSA were diluted from a stock solution of 2 mg/ml BSA. The WR was prepared by mixing the BCA reagent A, containing sodium carbonate, sodium bicarbonate, bicinchoninic acid and sodium tartrate in 0.1 M sodium hydroxide, with BCA reagent B, containing 4% cupric sulfat, in a ratio 50:1, reagent A:B. Then, 15 µl of each BSA standard and protein sample duplicate were pipetted into a 96-well microplate. A volume of 285 µl of WR was added to each well and microplate was incubated at 37 °C for 30 min. Finally, absorbance was measured at 562 nm on a BioTek™ ELx800™ microtiter plate reader (BioTek, Bedfordshire, UK). Protein µg were calculated using linear regression analysis with GraphPad Prism (GraphPad Software, San Diego California, USA, www.graphpad.com).

Immunoblotting and Immunoprecipitation

11.1. Protein electrophoresis

Discontinuous sodium dodecyl sulfate polyacrylamide gel electrophoresis (SDS-PAGE) was carried out according to Laemmli method with some modifications and using Miniprotean II or III cells and PowerPac Basic power supply, both from Biorad.

A resolving and a stacking gel mixture were prepared. The resolving gel had 6 cm height, 1 mm thickness and 8-12% acrylamide/bisacrylamide depending on the size of the protein of interest. The stacking gel had 1 cm height, 1 mm thickness and 4% acrylamide/bisacrylamide. Polymerization was initiated by APS and TEMED. TEMED accelerates the rate of formation of free radicals from persulfate and these in turn catalyze polymerization.

Cell lysates containing 20 µg protein were incubated (4:1 ratio) in 4X loading sample buffer (250 mM Tris pH 6.8, 8% SDS, 20% glycerol, 0.08% bromophenol blue and 3.2 M β-mercaptoethanol) for at least 20 min at RT or boiled at 95 ºC for 5 min (membrane protein samples were not boiled). For SDS-PAGE electrophoresis, 20 µl of samples were loaded into each well. Next, electrophoresis was performed using a dissociacion running buffer (25 mM Tris, 190 mM glicine, 0.1% SDS, pH 8.3), at 100 V for around 2 h.

11.2. Transfer and protein detection

After electrophoresis, the separated proteins were transferred onto a PVDF membrane (Immobilon-P) 0.45 µm pore size (Millipore). PVDF membranes were activated with ethanol prior to submersion into transfer buffer (48 mM Tris, 39 mM Glicine, 0.04% SDS, 20% methanol) and gels matrix were incubated in transfer buffer for 5 min. Electrotransfer was performed in a semi-dry transfer system from Bio-Rad (Trans-Blot® Turbo™ Transfer System), using 22 V and 1.3 A for 20 min.

The resulting membranes were blocked with blocking buffer (Table 8) for 1 h with moderate shaking to prevent non-specific binding of the antibody to the membrane surface. Membranes were then incubated with the primary antibody diluted in blocking buffer (Table 8) overnight at 4 ºC with moderate shaking. Next, membranes were washed several times with 1%Tween-20 1x Tris Buffer Saline, TBS (20 mM Tris, 137 mM NaCl, pH 7.4) or 1%Tween20 1x PBS (both named as washing buffer) for 5-10 minutes with gentle shaking, and incubated with a secondary antibody bound to a detection probe (horse radish peroxidase, HRP) for 1 h. Membranes were washed again prior to protein detection. For primary antibodies bound to HRP, secondary antibodies were not used.

For detection of the protein of interest, we used Enhanced chemiluminescence (ECL) method using ECL Plus reagent (Thermo Fisher Scientific) and light emitted was captured with Fusion

Solo.6S (Vilber-Lourmat, Collégien, France). In the chemiluminescence reaction HRP enzyme catalyzes the oxidation of luminol into a reagent that emits light when it decays.

Primary antibodies anti-ERK2 or anti-GAPDH were used as loading control. After detection of target protein, membranes were stripped with 0.5 M NaOH treatment for 10 min with gentle shaking and a final 10-min wash with H_2O was performed to remove antibodies from Western blot membranes. Reprobing membranes with new antibodies was performed following the same protocol as for target antibodies.

Relative abundance of protein target quantification was measured with ImageJ software (National Institutes of Health, Bethesda, MA, USA. Measurements for the protein of interest were normalized to the loading control.

Antibodies used for Western blot are summarized in Table 8.

Primary Antibody	Blocking buffer	Dilution	Secondary antibody
Flag M2 monoclonal (Sigma-Aldrich)	5% milk in TBST	1:10000	————
HA-peroxidase conjugate (Sigma-Aldrich)	5% milk in TBST	1:10000	————
APE-1/Ref1 (Santa Cruz)	2% BSA in TBST	1:2000	**anti-mouse IgG-HRP** (Santa Cruz)
p-AKT1/2/3 (Santa Cruz)	2% BSA in TBST	1:5000	**anti-rabbit IgG-HRP** (Millipore)
AKT1/2/3 (Santa Cruz)	2% BSA in TBST	1:1000	**anti-rabbit IgG-HRP** (Millipore)
Catalase (Santa Cruz)	2% BSA in TBST	1:2000	**anti-rabbit IgG-HRP** (Millipore)
cKIT (Cell Signaling)	2% BSA in TBST	1:1000	**anti-rabbit IgG-HRP** (Millipore)
p-ERK1/2 (Santa Cruz)	2% BSA in TBST	1:5000	**anti-rabbit IgG-HRP** (Millipore)
ERK2 (Santa Cruz)	2% BSA in PBST	1:10000	**anti-rabbit IgG-HRP** (Millipore)
GAPDH (Santa Cruz)	2% BSA in TBST	1:10000	**anti-rabbit IgG-HRP** (Millipore)
NOX1 (Novus biologicals)	2% BSA in TBST	1:2000	**anti-mouse IgG-HRP** (Santa Cruz)
OGG1/2 (Santa Cruz)	2% BSA in TBST	1:2000	**anti-mouse IgG-HRP** (Santa Cruz)
PTEN (Cell Signaling)	2% BSA in TBST	1:1000	**anti-rabbit IgG-HRP** (Millipore)
SOD1 (Santa Cruz)	2% BSA in TBST	1:1000	**anti-mouse IgG-HRP** (Santa Cruz)
Tubulin-β-III (Sigma-Aldrich)	2% BSA in TBST	1:5000	**anti-rabbit IgG-HRP** (Millipore)

Table 8. Antibodies used for detection of proteins by SDS-Page and Western blot. Manufacturer, blocking buffer, dilution and secondary antibody used for each primary antibody are described. Secondary antibodies were used at 1:10,000 dilution.

11.3. Immunoprecipitation

Cells grown in 6-well plates were washed and solubilized as described in section 10.1. A 10% volume of supernatant was mixed (2:1 ratio) with loading sample buffer and used as protein loading control (input). The remaining supernatant was incubated with 20 µl of EZview Red ANTI-FLAG M2 Affinity Gel beads for 1 h at 4 ºC with orbital shaking to allow protein binding to the

beads. The protein-beads mixture was centrifuged for 30 s at 15000 g and washed five times with lysis buffer I supplemented with 300 mM NaCl and 0.1% Tween20. Then, the supernatant was discarded and the mixture was eluted with pre-heated (95° C) loading sample buffer. Finally, 20 µl of the protein extract eluted and the protein loading control were electrophoresed and blotted as above.

11.4. Determination of protein half-lifes

Protein half-lifes were determined analysing the decay of MC1R-001, Iso1 and Iso2 in HEK293T cells treated with the protein synthesis inhibitor Chx. HEK293T were transiently transfected to express Flag-labeled WT MC1R-001, Iso1 and Iso2. Cells were then incubated with the protein synthesis inhibitor Chx (10^{-4} M in complete DMEM) for different times ranging from 0 to 6 h and lysed at each time point as described in section 10.1. The levels of residual proteins in cell extracts were detected by SDS-PAGE and Western blot. To calculate the half-lives, a semi-log graph was performed. The intensity of receptor bands in the blots was measured with ImageJ and the semi-log of residual signals was plotted against time. Half-life (t½) values correspond to the slope of the resulting lines.

Binding and internalization assays

12.1. Radioligand binding assay

In order to quantify the number of binding sites to MSH in the plasma membrane, a competition assay was performed using [I^{125}]-NDP-MSH as the radioactive tracer and unlabeled NDP-MSH as competing peptide.

Cells grown in triplicate wells of 12-well plates were transfected as required. Twenty-four hours after transfection, cells were serum deprived for 3 h and incubated with ^{125}I-labeled NDP-MSH ($5x10^{-11}$ M) (0.1 µCi/well), in a final volume of 0.5 ml of serum-free medium, and increasing concentrations of non-labeled competing NDP-MSH diluted in serum-free medium, from 10^{-12} to 10^{-7} M for 1 h at 37°C. Cells were washed with DMEM, harvested and counted for radioactivity in a gamma counter (Wizard 1470 Automatic Gamma Counter, Perkin Elmer) (specific binding). Nonspecific binding was estimated with excess unlabeled NDP-MSH (10^{-6} M), or cells transfected with empty vector, with similar results. Parallel dishes were employed to determine cell number

and total protein. Maximal binding (Bmax) values and dissociation constants were calculated by non-linear regression, with the GraphPad Prism software (San Diego, CA, USA).

12.2. Internalization assay

To estimate internalization of agonist–receptor complexes, an acid wash procedure was used[175]. Cells serum-deprived for at least 3 h, were incubated (90 min, 37° C) with [^{125}I]-NDP-MSH isotopically diluted to a final concentration of 10^{-9} M and 10^{5} cpm, washed with cold serum-free DMEM followed by two 2–3 min ice-cold acid washes with acid wash buffer (0.5 ml of 50 mM glycine and 150 mM NaCl, pH 3.0). Acid washes promote release of ligand bound to the receptor on the cell surface without cell lysis. Acid washes were pooled and counted to determine the amount of non-internalized ligand bound to the cell surface. Cells were trypsin-harvested and counted for internalized receptor. Internalization indexes were defined as the percentage of internal relative to total ligand bound.

$$Internalization\ index\ (\%) = \frac{\text{cells cpm}}{\text{acid washes cpm} + \text{ cells cpm}}$$

cAMP assay

Binding αMSH to MC1R activates Gs protein which in turn activates AC leading to an increase of cAMP levels. Therefore, to analyze MC1R positive coupling to cAMP pathway, intracellular cAMP levels were determined using a commercial ELISA immunoassay.

For cAMP assays, cells were grown in 12-well plates, transfected as indicated, serum deprived for at least 3 h, and stimulated as required. The medium was aspirated and the cells quickly washed with ice-cold PBS. Stimulated cells were lysed with 200 µl 0.1 N HCl (preheated at 70°C) and scraped. The heat shock and the acidic medium allows cell lysis, cAMP release and phosphodiesterase inhibition. The mix was freeze dried in a Speed-Vac Concentrador SVC100H, washed with H_2O and freeze-dried again twice. The samples were resuspended in the right volume of lysis buffer (provided by the commercial kit) for cAMP detection.

Intracellular cAMP levels were determined using a commercial ELISA immunoassay from Arbor Assays (Eisenhower Place, Michigan, USA), as supplier's instructions. Briefly, a special Plate Primer

was added to all the wells, and standards (a known concentration of cAMP-peroxidase conjugate) or samples were pipetted into the microtiter plate. A cAMP-peroxidase conjugate was added to the standards and samples in the wells. The binding reaction was initiated by the addition of an antibody to cAMP. After incubation for 2 h at RT with gentle shaking, microplate was washed and the substrate TMB (3,3′,5,5′-Tetramethylbenzidine) was added. The substrate reacts with the bound cAMP-peroxidase conjugate and after a short incubation (30 min), the reaction was stopped and the absorbance was measured at 450 nm in a BioTek™ ELx800™ microtiter plate reader. Parallel dishes were used for protein determination performed with the BCA method (section 10.2). Data are shown as pmoles cAMP per µg protein relative to the control.

Flow cytometry

14.1. Cell surface expression analysis

Cells previously seeded and treated as required, were collected and centrifuged for 5 min at 250 g at 4 ºC. Supernatant was discarded and pellet was resuspended in 300 µl of 1x PBS. After cell counting, approximately 10^5 cells were seeded in a 96 well plate and incubated in a final volume of 100 µl with anti-Flag M2 (1:25) for 30 min at 4º C. Cells were washed twice (2% fetal bovine serum, 0.01% NaN_3 in PBS), and further incubated with a phycoerythrin-labeled anti-mouse IgG at a final dilution of 1:50, for 30 min at 4º C. Then, cells were washed, resuspended in 500 µl of 1x PBS and analyzed in a Becton Dickinson FACScan system.

14.2. Cell cycle analysis

Cells previously seeded and treated as required, were collected and centrifuged for 5 min at 300 g at 4 ºC. Supernatant was discarded and pellet was resuspended in 70% ethanol in 1XPBS for fixation. After incubation for 30 min, cells were centrifuged for 10 min at 250 g at 4 ºC and resuspended in 1XPBS. Finally, cells were incubated with 1 µg/µl RNAase and 400 µg/ml propidium yodide for 30 min at 37º C and analyzed in a Becton Dickinson FACScan system.

14.3. Flow cytometry analysis

The data were acquired with BD CellQuest Pro software (FACScalibur). Briefly, cell populations were selected according to size (FSC) and complexity (SSC) from a FSC vs SSC dot plot and

histograms were created to analyze emitted fluorescence from each condition. The resulting data were analyzed using the flow cytometry data analysis software, Flowing Software (Cell Imaging Core, Turku Centre for Biotechnology).

Reactive oxygen species measurement

ROS levels were determined by two fluorescent methods depending on ROS subcellular localization.

15.1. Intracellular ROS assay

Production of intracellular ROS was assessed with 2′7′-dichlorodihydrofluorescein diacetate (DCFDA) (Molecular Probes, Invitrogen). DCFDA is a cell-permeable non-fluorescent probe. This dye is de-esterified by intracellular esterases and turns to highly fluorescent 2′,7′-dichlorofluorescein (DCF) upon oxidation by ROS.

Cells were grown in DMEM without phenol red (Gibco) in a 96-well white microplate (Corning™ Cell Culture, Thermo Fisher Scientific), serum-deprived for at least 3 h and treated as required. Then cells were washed with PBS and incubated with 10 µM DCFDA dye in Hank's Balanced Salt Solution (HBSS) (Gibco) for 45 min at 37 ºC and 5 % CO_2 protected from light, washed again and treated with luperox or NDP-MSH, depending on the experiment. Cells were washed with PBS 3 times and fluorescence was measured at 492 nm excitation and 517 nm emission in a CLARIOstar microplate reader (BMG LABTECH, Ortenberg Germany). Cells incubated with HBSS without DCFDA were used as negative control.

15.2. Extracellular ROS assay

AmplexUltraRed (Molecular Probes, Invitrogen) is an impermeant reagent that can be oxidized by hydrogen peroxide (H_2O_2) in the presence of HRP enzyme to produce resorufin, a fluorescent reaction product. Thus, the fluorescence intensity of resorufin corresponds to the amount of H_2O_2 produced outside cells.

Cells were grown in DMEM without phenol red (Gibco) in a 96-well white microplate, serum-deprived for at least 3h and treated as required. Then cells were washed with PBS and a work-solution (WS) containing 50 µM Amplex® Red reagent and 0.1 U/ml HRP in Krebs-Ringer phosphate (KRPG) (145 mM NaCl, 5.7 mM sodium phosphate, 4.86 mM KCl, 0.54 mM $CaCl_2$, 1.22

mM $MgSO_4$, 5.5 mM glucose, pH 7.35) was added into each well. Fluorescence was measured at 530 nm excitation and 590 nm emission at multiple time points to follow the kinetics of the reaction in a CLARIOstar microplate reader. As negative controls, we used cells incubated with KRPG without AmplexUltrared and HRP and wells without cells containing WS.

15.3. Crystal violet assay

To normalize fluorescence intensity signals for cell number, crystal violet assay was performed. After fluorescence determination, 20 µl of 0.5 % crystal violet solution in acetic acid was added into each well containing 100 µl of the corresponding buffer and microplate was incubated for 10 min at RT protected from light. Cells were washed twice with water and after allowing to air dry, methanol was added to solubilize stained cells. Absorbance was measured at 562 nm on a BioTek™ ELx800™ microtiter plate reader.

15.4. ROS measurement analysis

Fluorescence data were normalized for cell number, with crystal violet and were corrected for background signal by subtracting fluorescence signals derived from negative control from samples fluorescence values.

Cell viability assay

The assay relies on the reduction of MTT (3-(4,5-dimethylthiazol-2-yl)-2,5-diphenyltetrazolium bromide), a yellow water-soluble tetrazolium dye to purple colored formazan crystals, primarily by the mitochondrial dehydrogenases.

Cells were grown in 96-well plates and serum deprived for at least 3 h. Then, cells were treated as required, washed twice with PBS and incubated with 1 mg/ml MTT solution at 37º C and 5% CO_2 for 4 h in the dark. After incubation, culture media containing non-metabolized MTT was removed and DMSO was added to solubilize the formazan crystal formed by living cells. Absorbance at 570 nm was measured using BioTek™ ELx800™ microtiter plate reader. Data are shown as % of live treated cells relative to live untreated control cells.

Comet assay

The Alkaline Comet Assay was performed according to the manufacturer's protocol (Trevigen). Briefly, cells harvested and resuspended in PBS at $1x10^5$ cells/ml were embedded in low melting point (LMP) agarose at 37 ºC at a ratio of 1:10 (v/v). Cells/LMPagarose were then transferred onto microscope slides. After solidification at 4 °C for 30 min, slides were lysed with lysis buffer for 12 h at 4 °C. DNA was unwound by alkaline treatment in alkaline electrophoresis solution pH>13 (200 mM NaOH, 1 mM EDTA) for 20 min at RT. Slides were placed in an electrophoresis chamber and electrophoresis was performed in the same buffer at 25 V (adjusting the current to 300 mA with the volume of buffer). Slides were then washed with distilled water for 5 min at RT and dried for 30 min at 37 °C to remove alkali and detergent. Finally, DNA was stained with SYBR™ Green I Nucleic Acid Gel Stain 10,000X (Invitrogen) and images from randomly selected areas were taken using a Nikon Eclipse TS2 microscope with 10x objective lense. Zoom images from single comets were taken with 40x objective lense. Quantitative analysis of the tail moment (product of the DNA of the tail, given as a percentage, and the length of such tail) of at least 100 randomly selected comets for each sample was performed using CASPLAB software (available at http://casplab.com/download). Values were represented as the mean average of the tail moment of treated cells relative to the mean average of the tail moment of untreated cells.

Immunostaining, confocal microscopy and image quantification

18.1. Immunostaining

For all immunostainings, cells were seeded in 24-well plates containing sterile coverslips (Thermo Fisher Scientific). Cells grown at 60 % confluency and treated as required were immunostained following different protocols depending on the type of assay and the subcellular localization of the target of interest:

- For **colocalization assays,** cells were transiently transfected, fixed with 4 % p-formaldehyde, permeabilized with 0.05 % Triton-X 100 (v/v) and blocked with 5 % BSA in PBS for 1 h at RT. For co-localization analysis of MC1R-001 and Iso1 or Iso2 with the ER marker calnexin, HEK293T cells were labeled with anti-Flag M2 monoclonal antibody and with calnexin antibody followed by alexa 568-anti-mouse conjugated and alexa 488-anti-rabbit conjugated secondary antibodies. For co-localization of HA-MC1R-001 and Flag-

isoforms, cells were incubated simultaneously with anti-HA monoclonal and anti-Flag rabbit polyclonal, followed by alexa 568-anti-mouse conjugated and alexa 488-anti-rabbit conjugated secondary antibodies.

- For **8-oxodG staining**, cells were fixed with methanol followed by acetone at -20 °C. Fixed cells were treated with 0.05 N HCl for 5 min at 4 ºC and with 100 µg/ml RNAse for 1 h at 37 °C. DNA was denatured *in situ* with 0.15 N NaOH in 70 % EtOH. Then, cells were treated with 5 µg/ml proteinase K for 10 min at 37 °C, blocked with 5 % BSA in PBS for 1 h at RT and incubated with 8-oxodG primary antibody followed by an alexa 488-anti-mouse conjugated secondary antibody and with DAPI (10 µg/ml, Invitrogen Life Technologies) to stain DNA.

- For **nuclear markers staining (γ-H2AX and APE-1/Ref1)**, cells were fixed with 4% p-formaldehyde, permeabilized with 0.5% Triton-X 100 (v/v) and blocked with 5% BSA in PBS for 1 h at RT. Cells were labeled with anti-γH2A.X (phospho S139) monoclonal antibody, followed by an alexa 488-anti-rabbit conjugated secondary antibody. DAPI was used for nuclear staining.

Samples were mounted with a mounting medium from Dako (Glostrup, Denmark). Antibodies used for immunostaining are described in Table 9.

Primary Antibody	Cellular localization	Dilution	Secondary antibody
APE-1/Ref (Santa Cruz)	Nuclear	1:250	alexa 488-anti-mouse conjugated
Calnexin (Santa Cruz)	ER	1:1500	alexa 488-anti-rabbit conjugated
Flag monoclonal (Sigma-Aldrich)	———	1:7000	alexa 568-anti-mouse conjugated
Flag polyclonal (Sigma-Aldrich)	———	1:5000	alexa 488-anti-rabbit conjugated
HA monoclonal (Sigma-Aldrich)	———	1:7000	alexa 568-anti-mouse conjugated
γ-H2AX (Abcam)	Nuclear	1:250	alexa 488-anti-rabbit conjugated
8-oxodG (Trevigen)	Nuclear	1:250	alexa 488-anti-mouse conjugated

Table 9. Antibodies used for immunostaining. Manufacturer, dilution and secondary antibody used for each primary antibody are described. Antibodies were incubated in 1% BSA, 0.01% Tween PBS. Secondary antibodies used at 1:400 dilution were from Invitrogen.

18.2. Confocal image acquisition

Samples were examined with a SP8 Leica laser scanning confocal microscope and software (Leica Microsystems GmbH, Wetzlar, Germany) with HCXPL APO CS 40x or 63x objective lense.

Single plane images corresponding to Z positions of maximal DAPI signal were acquired. Pinhole was 1.00 AU. For colocalization analysis, images were taken in sequential scan mode between frames. Each fluorophore emission was collected separately and both images were acquired exactly in the same space conditions. To avoid crosstalk effects that may occur if two fluorophores are too close each other on the emission spectrum, appropriate laser and gate for excitacion spectrum were selected: the left side of the gate was always at least 10 nm away from the excitation laser's wavelength. Another important aspect considered was fluorescence intensity-related settings. Laser power, gain and offset were established for each fluorophore to minimize background, sample saturation and photobleaching. Laser power and offset were set up below 5 % and 3 %, respectively. Images from randomly selected areas were acquired.

18.3. Confocal image quantification

Colocalization of MC1R with calnexin, Isos, or HLA analysis was performed in single cells using the line scan analysis of ImageJ software.

Nuclear 8-oxodG, γ-H2AX and APE-1/Ref1 fluorescence signals were quantified calculating the pixel intensity in single cell nuclei relative to the nucleus area. At least, 200 randomly selected cells per condition were quantified using Qwin software (Leica Microsystems Ltd., Barcelona, Spain). For APE-1/Ref1 the number of positive cells was determined, considering as positive those cells with a fluorescence signal >25. The percentage of positive cells relative to the total number of cells for each condition was analyzed.

Statistical analysis

Experiments were performed with at least three biological replicates. The sample size was chosen using GRANMO (https://www.imim.es/ofertadeserveis/softwarepublic/granmo/index.html) and is indicated in figure legends. No samples were excluded from any analyses. Subpopulations of cells were randomly assigned to treatments. Blind analysis was not performed in this study. Statistical significance was assessed using GraphPad Software (San Diego California, USA). Data met the assumptions of the test used. We used D'Angostino-Pearson omnibus normality test for Gaussian distribution. Unpaired two-tailed Student's t test and one-way ANOVA with Tukey post-test for multiple comparisons were performed when variance among groups was not statistically different. Otherwise, we used one-way Kruskal–Wallis test. Results are expressed as mean±SEM; p values were calculated using two-sided tests.

RESULTS

Functional analysis of MC1R-TUBB3 chimerae

Expression of MC1R-TUBB3 splice variants

The Iso1 and Iso2 intergenic splicing chimerae were originally reported in HBL and M14 HMCs[213]. Since gene expression patterns in HMC lines are very variable[366], it was of interest to compare the occurrence and abundance of the chimeric transcripts in a wider panel of melanoma cell lines of known genetic characteristics, as well as in immortalized human melanocytes (Hermes cells). This was approached by RT-PCR (Figures 1A and 1B). We found detectable expression of the canonical MC1R-001 transcript in all cell lines, with large differences (~ 40-fold) between the cell lines with the highest and lowest levels (HBL and C8161 cells, respectively). The patterns of expression of Iso1 and Iso2 in the various cell lines were similar. However, when compared with MC1R-001, there where clear differences. For instance, the cell line expressing the highest level of MC1R-001 (HBL cells) was not the same as the one expressing more Iso1 and Iso2 (HMEL1 cells), and SKMEL28 cells with good expression of MC1R-001 had low levels of the intergenic splice variants. Accordingly, the ratio of expression of chimeric mRNA normalized for expression of MC1R-001 was variable, with an approximately 20-fold difference between the cells expressing the highest and lowest ratios (HMEL1 and C8161, Figure 1B). Furthermore, similar analysis in Hermes melanocytes revealed that basal expression of chimeric splice variants in non-stimulated normal melanocytes was very low, comparable to the melanoma cell line C8161 expressing the lowest levels of Iso1 and Iso2 (Figure 1A). In addition, when intergenic splice variants expression levels were normalized to MC1R-001 expression, we found that Hermes cells expressed mainly the canonical MC1R-001 (Figure 1B).

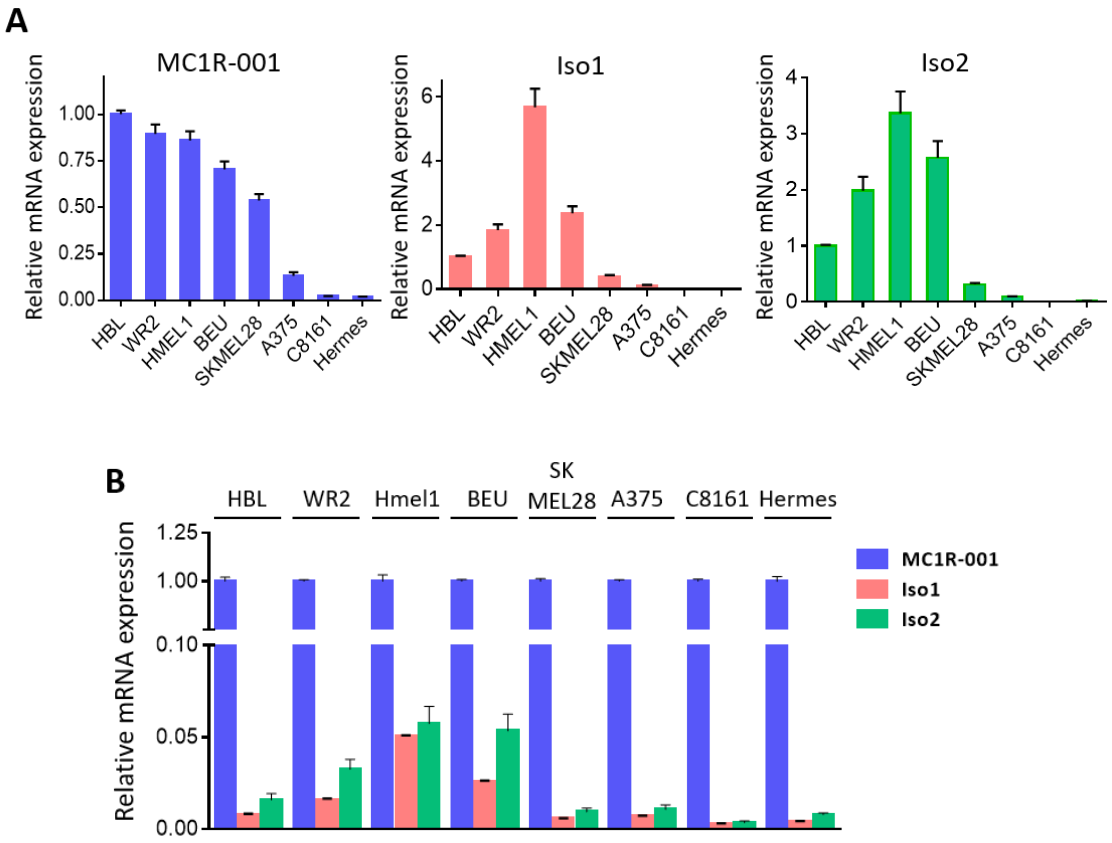

Figure 1. Expression of MC1R-001 and MC1R-TUBB3 splice variants in HMCs. (A) MC1R-001, Iso1 and Iso2 expression in HMCs. Data are shown as relative expression of each isoform (as indicated in each bar graph) as compared with the levels of the isoform in HBL cells. **(B) Expression of Iso1 and Iso2 mRNA as a function of the levels of the canonical MC1R-001 transcript in a panel of HMCs.** Data are represented as mRNA expression of the two intergenic splicing forms relative to MC1R-001 in each cell line.

MC1R-TUBB3 chimeric intergenic splice isoforms Iso1 and Iso2 contain the N-terminus and 7 TM domains from MC1R (Figures 19A and 19B in introduction). Thus, they are potentially able to perform MC1R functions. In order to compare the signaling properties of the chimeric proteins and MC1R-001, we cloned Iso1 and Iso2 (with or without an N-terminal fused Flag epitope) and expressed them in heterologous HEK293T cells, along with the canonical receptor (Figure 2A). As previously reported[161,318], MC1R migrated as a doublet with a majority band of apparent Mr ~ 29 kDa and a minority band of ~ 34 kDa, corresponding to *de novo* WT MC1R-001 and an Endo H-sensitive glycoform, respectively. Moreover, Iso1 migrated with the expected apparent molecular weight (Mr ~ 88 kDa) whereas Iso2 showed a Mr around 38 kDa, lower than predicted. As expected, the Iso1 in-frame fusion of MC1R and TUBB3 cross-reacted with anti-TUBB3 antibodies (Figure 2A) whereas the out-of-frame chimera Iso2 did not (blot below). Comparison of band intensities for the Flag-tagged proteins showed lower steady-state levels of

Iso1 and Iso2 compared with WT MC1R-001, suggesting a lower intracellular stability for the chimeric forms. A higher rate of intracellular proteolysis would also be consistent with the Mr of Iso2, lower than expected on the basis of its predicted amino acid sequence, as well as with the finding of more than one discrete immunoreactive band. We further analyzed the electrophoretic pattern of Iso1 and Iso2 intergenic chimerae expressed in the HMC line HBL (Figure 2B). We found a similar pattern of migration for Iso1, with an apparent Mr of 88 kDa and cross-reactivity with TUBB3 antibody. However, Iso2 was detected as a faint band of very high Mr, suggesting protein aggregation and/or ubiquitylation followed by degradation.

Therefore, we tested the possibility of a faster intracellular proteolytic degradation by following the decay of MC1R-001, Iso1 and Iso2 in HEK293T cells treated with the protein synthesis inhibitor Chx (Figures 2C and 2D). The decay rate of the proteins was faster for Iso2, intermediate for Iso1 and slower for MC1R-001, corresponding with half-life values of 1.6, 2.3 and 5.3 hs, respectively (Figures 2C and 2D), consistent with the steady state protein levels.

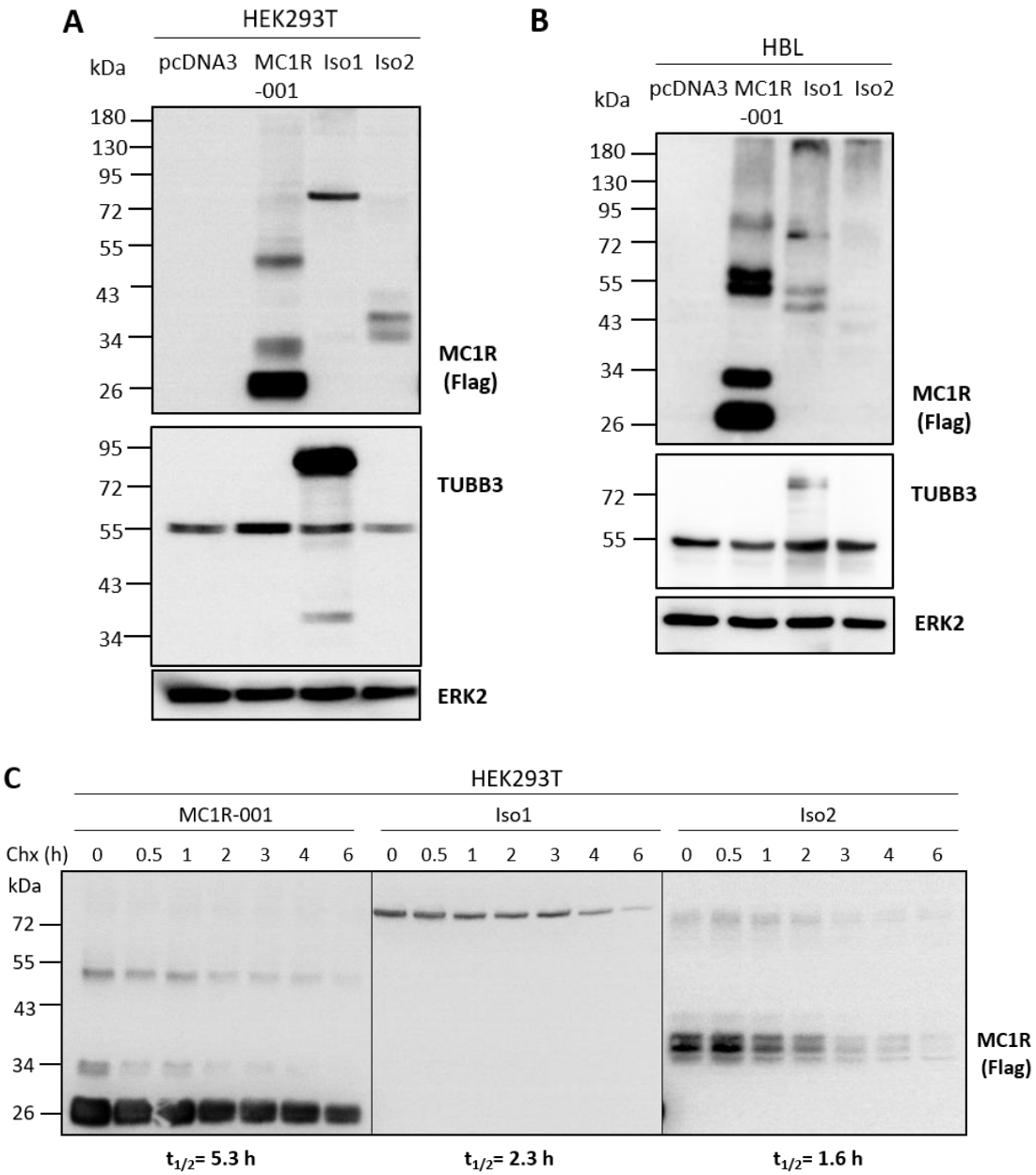
A
HEK293T
kDa
pcDNA3
MC1R -001
Iso1
Iso2
180
130
95
72
55
43
34
26
MC1R (Flag)
TUBB3
ERK2
B
HBL
MC1R (Flag)
TUBB3
ERK2
C
HEK293T
MC1R-001
Iso1
Iso2
Chx (h) 0 0.5 1 2 3 4 6
MC1R (Flag)
t1/2= 5.3 h
t1/2= 2.3 h
t1/2= 1.6 h
D
MC1R-001
Iso1
Iso2
log (% band intensity)
t (h)

Figure 2. Electrophoretic analysis and intracellular stability of MC1R-TUBB3 isoforms. (**A) Expression of canonical and chimeric MC1R proteins in heterologous HEK293T cells**. HEK293T cells were transiently transfected to express Flag-labelled WT MC1R-001, Iso1 and Iso2. Cells were detergent-solubilized, electrophoresed and blotted. For MC1R detection, cell lysates were probed with an anti-Flag monoclonal antibody (upper blot). Membranes were also probed for TUBB3 (middle blot) and ERK2 (lower blot), as loading control (n = 5, representative blots are shown). **(B) Electrophoretic pattern of MC1R-TUBB3 transcripts expressed in HBL HMCs**. Representative immunoblots for MC1R, TUBB3 and ERK2 are shown as in panel A (n = 5, representative blots are shown). **(C) Intracellular stability of MC1R-TUBB3 chimeric fusion proteins in HEK293T cells**. Flag-labelled MC1R-001, Iso1 and Iso2 were expressed in HEK293T cells. Cells were incubated with the protein synthesis inhibitor cycloheximide (Chx, 0.1 mM) for the times indicated, lysed and the levels of residual proteins in cell extracts were detected by Western blot. Representative immunoblots probed for MC1R-001, Iso1 or Iso2 with anti-Flag are shown. **(D) Semi-log graph for calculation of half-lives**. The intensity of receptor bands in the blots as in panel C was quantitated with ImageJ and the semi-log of residual signals was plotted against time. Half-life (t½) values correspond to the slope of the resulting lines.

Agonist binding and cell surface expression of MC1R-TUBB3 splice variants

We compared agonist binding parameters for MC1R-001, Iso1 and Iso2 expressed in HEK293T cells, by equilibrium binding assays using [I^{125}]-NDP-MSH as the radioactive tracer and unlabeled NDP-MSH as competing peptide. The data were plotted as specific binding normalized for protein to compare maximal levels of bound agonist in cells expressing each variant (Figure 3A) and as % of maximal binding to each isoform for an easier comparison of the relative affinity of the variants (Figure 3B). Both Iso1 and Iso2 bound radiolabeled agonist specifically, but maximal binding was low, with residual Bmax values of about 10% (Table 1). However, affinity remained high with IC50 and Kd values in the low nM range (Figure 3A and 3B and Table 1). In fact, the affinity for NDP-MSH was even slightly higher for the chimeric forms, as shown by left-shifted displacement curves (Figure 3B).

MC1R transcript	Bmax (fmoles/mg protein)	Kd (nM)
MC1R-001	3.47 ± 0.18	1.99 ± 0.49
Iso1	0.27 ± 0.03	0.59 ± 0.27
Iso2	0.37 ± 0.04	1.17 ± 0.52

Table 1. Binding parameters of WT MC1R-001 and chimeric transcripts Iso1 and Iso2. Equilibrium binding parameters of [^{125}I]-NDP-MSH to MC1R-001 or the MC1R-TUBB3 isoforms Iso1 and Iso2 expressed in HEK293T cells (n = 3, data are given as mean ±SEM).

These binding parameters suggested aberrant intracellular trafficking of MC1R-TUBB3 chimeric proteins with decreased cell surface expression of the fusion proteins. This was further tested by flow cytometry (Figure 3C). Non-permeabilized cells were stained with an anti-Flag antibody directed against the Flag epitope fused to the extracellular N-terminus of the protein. In these non-permeabilizing conditions, only receptor molecules inserted on the plasma membrane with the correct orientation should be detected. The intensity of staining was much lower for the chimeric proteins compared with WT receptor. Lower plasma membrane levels of Iso1 and Iso2 could in turn result from an inefficient forward movement or from an increased rate of sequestration away from the cell surface. Forward trafficking was assessed by confocal microscopy analysis of co-localization with calnexin, an ER-resident chaperone. Extensive co-localization with calnexin was found for Iso1 and Iso2, whereas expression of the isoforms on the cell surface was almost undetectable (Figure 3D). Conversely, co-localization of calnexin and MC1R-001 was much lower and presence of the receptor on the plasma membrane was easily detected. These results indicated massive intracellular retention and failure to escape the quality control mechanisms of the secretory pathway for Iso1 and Iso2 proteins. On the other hand, retrograde transport away from the cell surface was estimated by an acid-wash procedure that allows distinguishing external (acid-sensitive) binding sites and internalized (acid-resistant) radioligand-receptor complexes (Figure 3E). Internalization of Iso1 was also significantly impaired. Conversely, Iso2 was internalized at slightly higher rates than MC1R-001, which may contribute to its low cell surface expression.

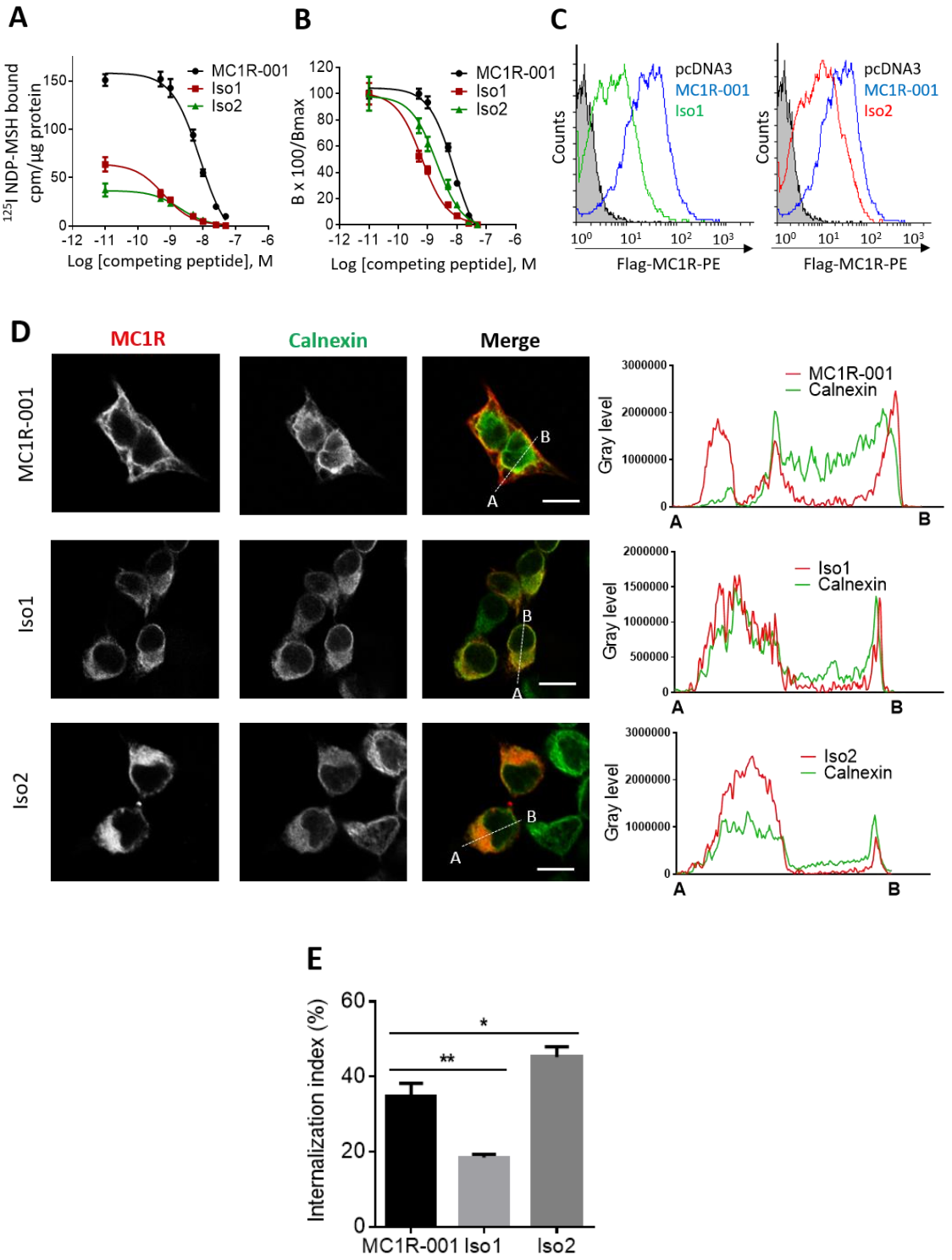

Figure 3. Radioligand binding and intracellular trafficking properties of MC1R-TUBB3 isoforms. (A-B) Competition binding assay of HEK293T cells transfected with MC1R-001, Iso1 and Iso2. Cells were incubated with ^{125}I-labelled NDP-MSH ($5x10^{-11}$ M) and increasing concentrations of non-labelled competing NDP-MSH, from 10^{-12} to 10^{-7} M, extensively washed and counted for radioactivity. Non-specific binding was determined with non-transfected cells or with transfected cells incubated with the radioactive tracer in the presence of excess (10^{-6} M) non-labelled peptide, with the same results. Values are represented as specifically bound [^{125}I]-NDP-MSH (A) and as percentage of residual binding (B) at the different ligand concentrations (n = 3, data are given as mean ±SEM). **(C) Flow cytometric analysis of HEK293T cells expressing MC1R-001 and MC1R-TUBB3 chimeric isoforms**. Non-permeabilized cells expressing the

indicated proteins were incubated with an anti-Flag antibody labelled with phycoerythrin. Histograms represent cell number (counts) as a function of Flag surface staining, on a logarithmic scale. The gray filled curve refers to cells transfected with an empty pcDNA3 (n = 3, representative histograms are shown). **(D) Co-localization analysis of MC1R-001, Iso1 or Iso2 and calnexin**. Left panel: Representative confocal images of MC1R-001 or the chimeric isoforms (red) and calnexin (green) immunostaining in HEK293T cells transiently transfected with Flag-labelled MC1R-001 and MC1R-TUBB3 constructs. Scale bar, 10 µm. Representative line scan (right panel) from multiple experimental repeats across the cell (location indicated in merged image) shows co-localization of MC1R-TUBB3 transcripts and calnexin. Line scan, 19 µm for MC1R-001, 17 µm for Iso1 and 18 µm for Iso2. **(E) Radioligand internalization assay performed on HEK293T cells expressing MC1R-001, Iso1 or Iso2 incubated with ^{125}I-labelled NDP-MSH**. The radioactive tracer was isotopically diluted to achieve a final concentration of $5x10^{-11}$ M and $5x10^{4}$ counts/well. Externally bound agonist was separated by an acid wash procedure. Both the externally bound ligand present in the acid washes and the internalized ligand associated with the cell pellets were counted. The internalization index represents the percentage of ligand internalized referred to total radioligand bound (n = 3, error bars are ±SEM, two-sided one-way ANOVA was used to generate p values, *p<0.05, **p<0.01).

Functional coupling

Activation of canonical MC1R potently stimulates cAMP synthesis and triggers ERK signaling through a cAMP-independent pathway[161,310]. We tested the chimeric proteins for activation of the cAMP and ERK pathways. For comparison, residual signaling from frequent hypomorphic MC1R variants associated with a RHC phenotype with lower ("r" variants V60L and V92M) or higher penetrance ("R" forms R151C and D294H) was also estimated. HEK293T cells were transfected with the MC1R forms, challenged with a saturating concentration of NDP-MSH for 30 min, and cAMP contents were determined. Functional coupling of Iso1 and Iso2 to the cAMP pathway was strongly impaired relative to MC1R-001, as shown by lower cAMP production upon stimulation with NDP-MSH (Figure 4A). The residual signaling potential of the chimeric fusions was lower than V60L and V92M, and comparable with R151C and D294H. On the other hand, MC1R activates the MAPKs ERK1 and ERK2 by a cKIT transactivation mechanism independent of cAMP, which is less sensitive to many natural mutations than activation of the cAMP cascade[177]. We analyzed ERK activation downstream of Iso1 and Iso2 in PC12 cells transfected to express the canonical or the chimeric receptors (Figure 4B). Signaling from the intergenic splice isoforms to ERK activation showed a decreasing trend compared with MC1R-001, but the differences in the maximal levels of active ERKs did not reach statistical significance (Figure 4B).

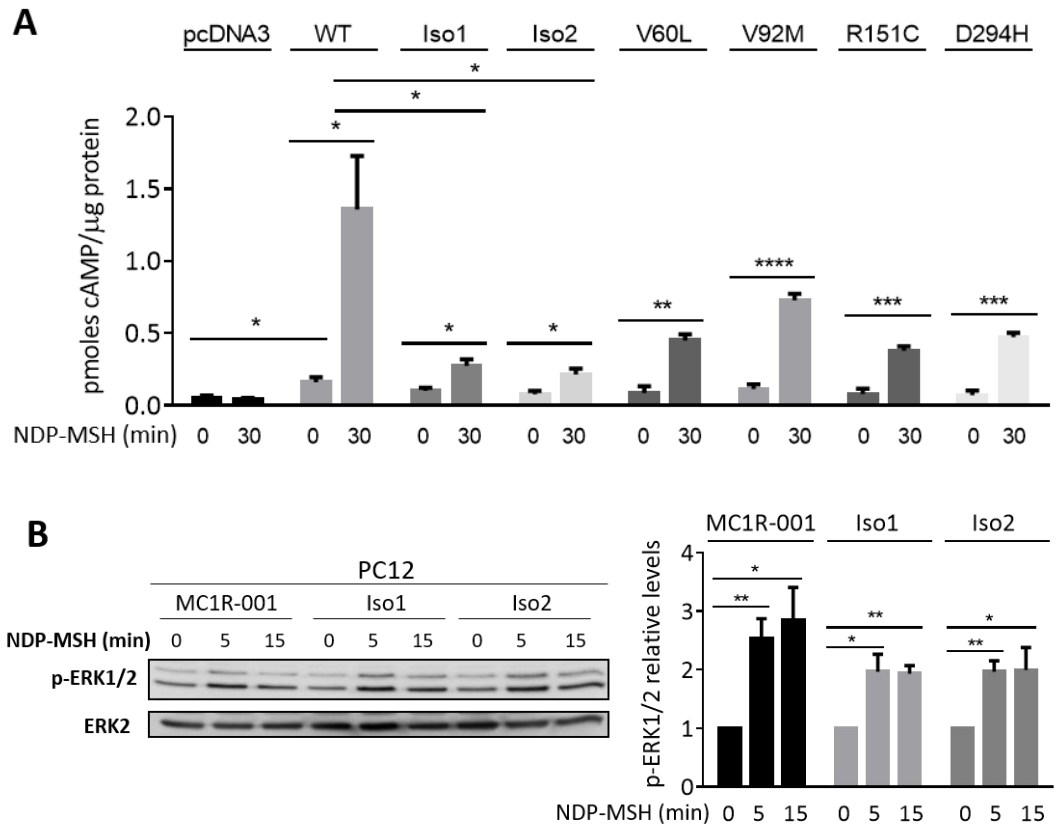

Figure 4. Effects of intergenic splicing on the functional coupling of MC1R to the cAMP and ERK1/2 pathways. (A) Agonist-induced cAMP production in HEK293T cells expressing MC1R-001, Iso1, Iso2, or the natural MC1R-001 variant alleles V60L, V92M, R151C and D294H. Cells were incubated with 10^{-7} M NDP-MSH for 30 min and cAMP levels were determined by an immunoassay (n = 6, error bars are ±SEM, two-sided Student´s t test was used to generate p values, *p< 0.05, *** p< 0.001). **(B) NDP-MSH-induced ERK signaling in PC12 cells expressing MC1R-001, Iso1, Iso2.** Representative immunoblots (left panel) and quantification (right panel) of ERK1 and ERK2 phosphorylation in PC12 cells transfected to express MC1R-001, Iso1 or Iso2 and stimulated with NDP-MSH (10^{-7} M) for the times indicated (n = 5, error bars are ±SEM, two-sided Student´s t test was used to generate p values, *p< 0.05, ** p< 0.01).

Functional interactions of WT MC1R and intergenic splice variants

We have previously shown that MC1R exists as dimeric species[171,221], and that heterodimerization of WT and mutant forms gives raise to dominant negative effects[171,316]. Since dimerization apparently proceeds through a domain swap mechanism involving the 7 TM fragments expressed in Iso1 and Iso2[221], *in vivo* formation of MC1R/Iso heteromeric species is likely. We analyzed the occurrence of heterodimerization by co-immunoprecipitation of differentially epitope-labelled variants. First, MC1R-001 tagged by in-frame fusion of the HA epitope to its N-terminus, and chimeric proteins (or MC1R-001 as positive control) labelled at the N-terminus with the Flag epitope were expressed alone or in combination in HEK293T cells. The intergenic chimerae were immunoprecipitated from detergent-solubilized extracts with anti-Flag

agarose beads, and the pellets were analyzed for MC1R-001 by Western blot probed with anti-HA (Figure 5A). Co-immunoprecipitation of MC1R-001 and the MC1R-TUBB3 chimeric proteins was readily detected, indicating efficient heterodimerization. In addition, to mimic a heterocygotic MC1R genetic background highly frequent in northern European population, we tested the heterodimerization capability of two common hypomorphic variant MC1R alleles with the WT MC1R-derived chimeric protein Iso1. We selected the frequent V60L and R151C alleles as representative of the r and R types of RHC alleles, respectively. Flag-labelled versions of these constructs were overexpressed alone or with Iso1 in HEK293T cells. The amount of chimeric Iso1 immunoprecipitated with MC1R was comparable for WT and the variant alleles V60L and R151C (Figure 5B). Therefore, in a RHC variant allele background, heterodimerization between MC1R variant alleles and splice variants Iso1 and Iso2 may occur.

Moreover, we examined the intracellular localization of MC1R-001 and Iso1 or Iso2 by confocal microscopy in HEK293T cells co-expressing MC1R-001 and one of the intergenic splice forms (Figure 5C). We found a high degree of co-localization of MC1R-001 and Iso1 or Iso2 in internal compartments, suggesting that heterodimerization impairs forward trafficking compared with MC1R-001 homodimers. Nevertheless, we also detected co-localization of MC1R-001 and Iso1 or Iso2 at the cell periphery, consistent with higher expression of the chimeric proteins on the cell surface when co-expressed with MC1R-001 compared with cells expressing the isoforms alone.

We next estimated agonist-induced cAMP production in HEK293T cells co-expressing WT MC1R or the variant alleles V60L or R151C and chimeric proteins Iso1 and Iso2 (Figure 5D). The cAMP response was similar in cells expressing WT or variant MC1R-001 alone, or MC1R-001 and the chimeric forms. On the other hand, co-expression of canonical MC1R and the chimerae slightly decreased cell surface expression of binding sites, although the differences did not reach statistical significance (Figure 5E). No effects on internalization rates were detected, with comparable results for cells expressing WT MC1R-001 alone, or in combination with Iso1 or Iso2 under conditions previously shown to result in efficient heterodimerization (Figure 5F).

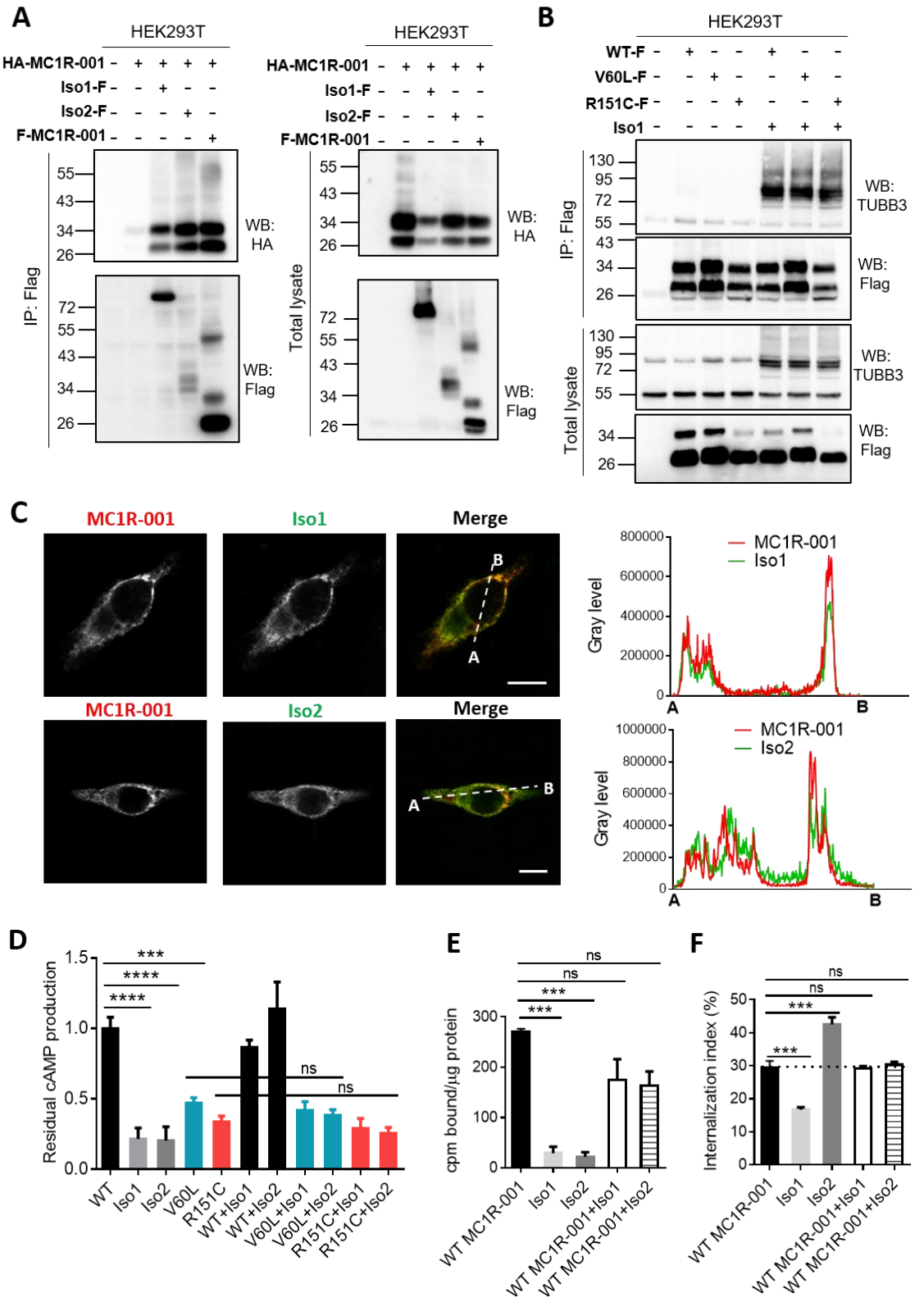

Figure 5. Heterodimerization of MC1R and MC1R-TUBB3 chimeric isoforms. (A) Co-immunoprecipitation of MC1R-001 and the MC1R-TUBB3 chimeric isoforms. HEK293T cells expressing the indicated constructs were lysed and immunoprecipitated for Flag-labelled MC1R-001, Iso1 or Iso2 using an anti-Flag monoclonal antibody. The pellets were electrophoresed and blotted for HA-labelled MC1R-001 (with a specific anti-HA monoclonal antibody) or for Flag-labelled MC1R-001, Iso1 or Iso2 (with anti-Flag monoclonal antibody) as a control for efficient immunoprecipitation. Total lysates were also electrophoresed and blotted as

expression controls (n = 3, representative blots are shown). **(B) Co-immunoprecipitation of V60L or R151C variant MC1R-001 and WT MC1R-TUBB3 intergenic splice isoform Iso1**. The indicated constructs were expressed in HEK293T cells and immunoprecipitated for Flag-labelled MC1R-001, V60L or R151C using an anti-Flag monoclonal antibody. Immunoblots for Flag-tagged constructs and TUBB3 are shown for immunoprecipitated and total lysates. **(C) Co-localization analysis of MC1R-001 and the chimeric isoforms**. Representative confocal images of MC1R-001 (red) and Iso1 or Iso2 (green) immunostaining in HBL cells transiently transfected with HA-labelled MC1R-001 and Flag-labelled MC1R-TUBB3 chimeric isoforms. Scale bar, 10 µm. Representative line scan (right panel) from multiple experimental repeats across the cell (location indicated in merged image) shows co-localization of canonical MC1R-001 and chimeric proteins. Line scan, 20 µm for MC1R-001+Iso1, and 31 µm for MC1R-001+Iso2. **(D) Effect of heterodimerization on functional coupling to cAMP**. Intracellular cAMP levels in HEK293T cells expressing MC1R-001, V60L or R151C alone or in combination with Iso1 and Iso2 upon stimulation with 10^{-7} M NDP-MSH for 30 min. Results are presented as residual cAMP production relative to MC1R-001 (for which cAMP levels were 0.096±0.043 and 0.889±0.071 pmol/µg protein in resting and stimulated conditions respectively) (n = 3, error bars are ±SEM, two-sided one-way ANOVA was used to generate p values *p< 0.05, **p< 0.01, ***p< 0.001). **(E) Analysis of MC1R agonist binding.** Specific binding of [^{125}I]-NDP-MSH ($5x10^{-11}$ M and $5x10^{4}$ cpm) to HEK293T cells expressing MC1R-001 or the MC1R-TUBB3 isoforms Iso1 and Iso2, alone or in combination (n = 3, error bars are ±SEM, two-sided one-way ANOVA was used to generate p values, ***p< 0.001). **(F) Radioligand internalization assay in HEL293T cells co-expressing MC1R-001 and MC1R-TUBB3 chimeric isoforms.** Agonist internalization index in HEK293T cells co-transfected with MC1R-001 and Iso1 or Iso2 upon incubation with [^{125}I]-labelled NDP-MSH ($5x10^{-11}$ M and $5x10^{4}$ cpm) for 90 min (n = 3, error bars are ±SEM, two-sided one-way ANOVA was used to generate p values, ***p< 0.001).

In summary, our analysis of the functional properties of MC1R-TUBB3 isoforms showed that they behave as R variants. However, the role of both R variants and Isos in the complex UVR response and in melanomagenesis is not completely understood. In this context, a better knowledge of the behaviour of R alleles in terms of promotion of genomic instability is required, and it would help to decipher the physiological relevance of the functionally similar MC1R-TUBB3 quimeric isoforms. R alleles confer increased melanoma susceptibility due to impaired pigmentary and non-pigmentary mechanisms compared to the MC1R WT but, although it has been demonstrated that R variants fail to efficiently activate eumelanogenesis, their role in regulating pigment-independent mechanisms against UVR-induced DNA damage requires further investigation.

Activation of repair of oxidative DNA damage by variant MC1R

In WT-MC1R melanocytes, activation of the pigment-independent mechanisms against DNA damage requires functional coupling to the cAMP signaling pathway and consequently, these responses are absent in R alleles. However, common R mutations with impaired cAMP signaling have little effect on ERK activation downstream of MC1R[161,177,310], and their possible effects on signaling to AKT remain largely unknown. Moreover, it has been shown that WT MC1R, but not several major RHC alleles, might prevent proteasomal degradation of PTEN[210], suggesting the possibility of a differential capability to activate AKT signaling. Both the ERKs[367–369] and AKT[370–372] play roles in DNA repair. Taken together, these observations suggest that variant *MC1R* with disrupted cAMP signaling might still be able to activate DDRs through cAMP-independent mechanisms. We aimed at analyzing the occurrence of MC1R-dependent protection against oxidative DNA damage in HMCs and epidermal melanocytes of variant *MC1R* genotype. We compared these responses with those triggered by MC1R-WT. Given the relevance of oxidatively-generated DNA damage in the presence of pheomelanic pigmentation associated with *MC1R* variants[140], we focused on major oxidative lesions, namely 8-oxodG and SSBs or DSBs[78].

MC1R genotype and signaling properties in model cell lines

To investigate the effect of *MC1R* genotype on susceptibility to oxidative DNA damage, we first used two HMC lines, HBL and A375. HBL cells are WT for *MC1R*, *NRAS* and *BRAF*, whereas A375 cells carry the V600E *BRAF* mutation and are homozygous for the R151C *MC1R* variant. We also analyzed three other melanocytic cell lines, SKMEL28 and C8161 HMCs, and immortalized Hermes melanocytes. The genotype of relevant genes in these cell lines is shown in Table 2.

Cell line	*MC1R*	*NRAS*	*BRAF* exon15	*PTEN*
HBL	WT	WT	WT	WT
A375	R151C/R151C	WT	V600E	WT
SKMEL28	I155T/S83P	WT	V600E	T167A
C8161	R151C/WT	WT	V600E	WT
Hermes	$C275^{STOP}$/WT	ND	ND	WT

Table 2. Genotype of Hermes melanocytes and HMCs. Full-length *MC1R, NRAS* and *PTEN* ORFs were amplified from cDNA and sequenced in both strands from two different PCR reactions to confirm each mutation. For *BRAF*, exon 15 was amplified using genomic DNA as template. ND: not determined.

C8161 cells are heterozygotes for R151C *MC1R* and bear the V600E *BRAF* mutation. SKMEL28 cells carry the V600E *BRAF* mutation and the T167A *PTEN* mutation (Figure 6A) causing partial LOF with retention of significant phosphatase activity[373]. SKMEL28 cells are compound heterozygotes for *MC1R*, bearing the I155T R-type variant[316] and another variant allele, S83P, of unknown functional behaviour. We cloned the S83P variant for functional analysis. Upon stimulation with the stable αMSH analogue, NDP-MSH, S83P MC1R expressed in HEK293T cells showed a strongly impaired ability to activate the cAMP pathway but retained full capacity to activate the ERKs (Figure 6B-D). Therefore, S83P behaved as a strong R allele.

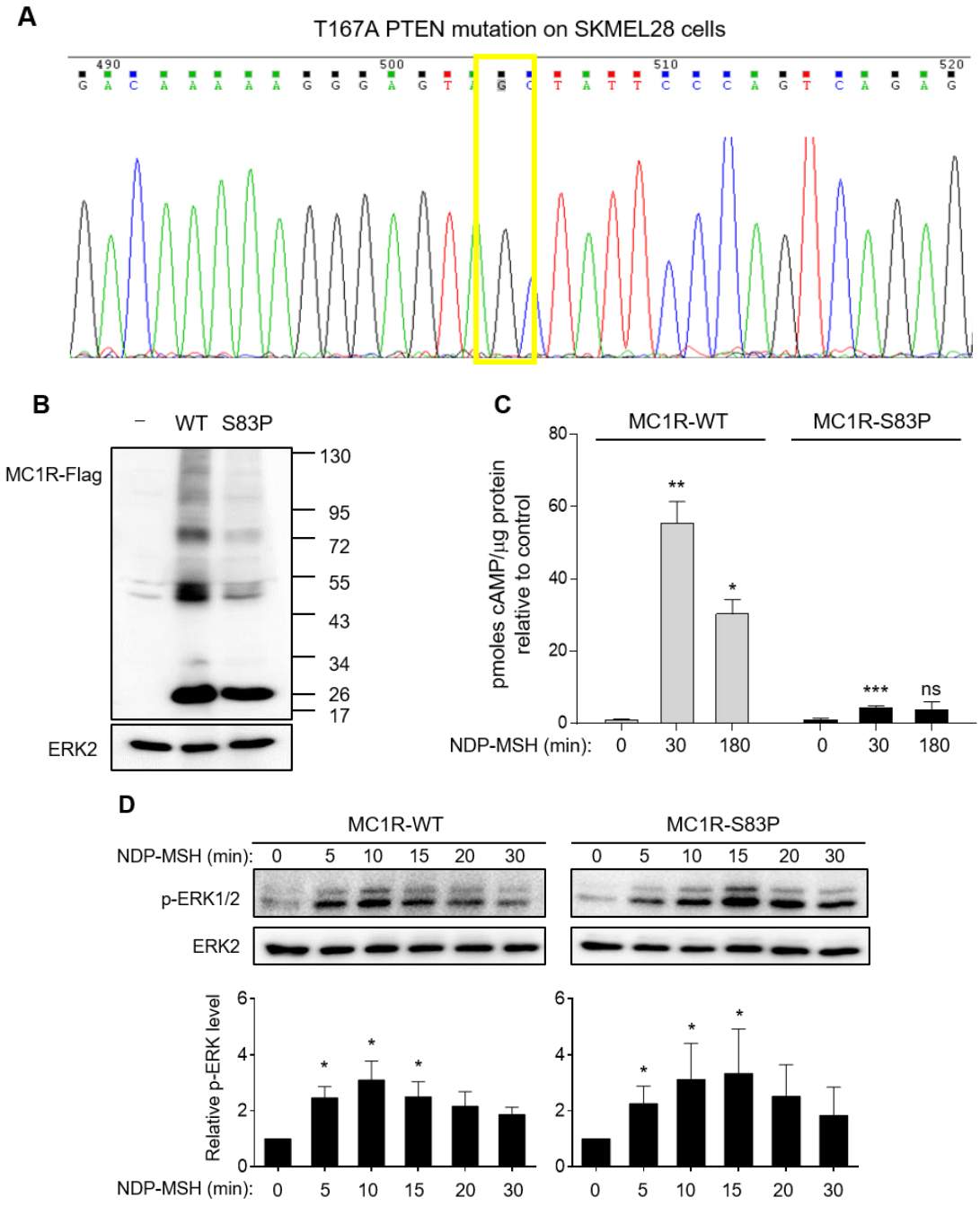

Figure 6. PTEN and MC1R status in SKMEL28 cells. (A) PTEN mutation status in SKEML28 cells. Electrophoregram of the *PTEN* sequence in SKMEL28 cells showing the position of the T167A mutation. **(B) Expression of WT or S83P MC1R in heterologous HEK293T cells**. Cells were transiently transfected to express Flag-tagged WT or S83P MC1R. Cells were detergent-solubilized, electrophoresed and blotted. A representative immunoblot stained for MC1R using an anti-Flag monoclonal antibody is shown. ERK2 was used as loading control (n = 3). **(C) Agonist-induced cAMP production in HEK293T cells expressing WT or S83P MC1R.** Intracellular cAMP levels were measured in cells transfected with WT or S83P MC1R and treated with 10^{-7} M NDP-MSH for 30 or 180 min (n = 3, error bars are mean±SEM, *p<0.05, **p<0.01, ****p<0.0001, ns stands for non-significant). **(D) MC1R-mediated ERK activation in PC12 cells transfected with WT MC1R or S83P MC1R**. Cells were serum-deprived, stimulated with NDP-MSH for the times shown and probed for phospho-ERK. Representative immunoblots (top), and quantification of 3 experiments (bottom) are shown (error bars and statistics as in panel C).

We also found that Hermes melanocytes were *MC1R* heterozygotes carrying a natural variant allele coding for a $C275^{STOP}$ truncated protein. Cys275 is located within the 3rd el of the receptor, and accordingly $C275^{STOP}$ lacks the complete 7th TM fragment and cytosolic extension of the native receptor. We did not analyze this variant for function since previous studies from our laboratory have shown that removal of the same regions in an artificial $C273^{STOP}$ mutant, or the C-terminal cytosolic extension in $Y298^{STOP}$ lead to complete loss of signaling to the cAMP pathway[221,315]. Consistent with their *MC1R* genotype, treatment of A375, SKMEL28, C8161 or Hermes cells with NDP-MSH did not increase intracellular cAMP levels (Figure 7A). On the other hand, NDP-MSH transiently stimulated the ERKs in Hermes melanocytes (Figure 7B), and the ERKs were constitutively activated in A375, SKMEL28 and C8161 cells in agreement with their *V600E-BRAF* genotype.

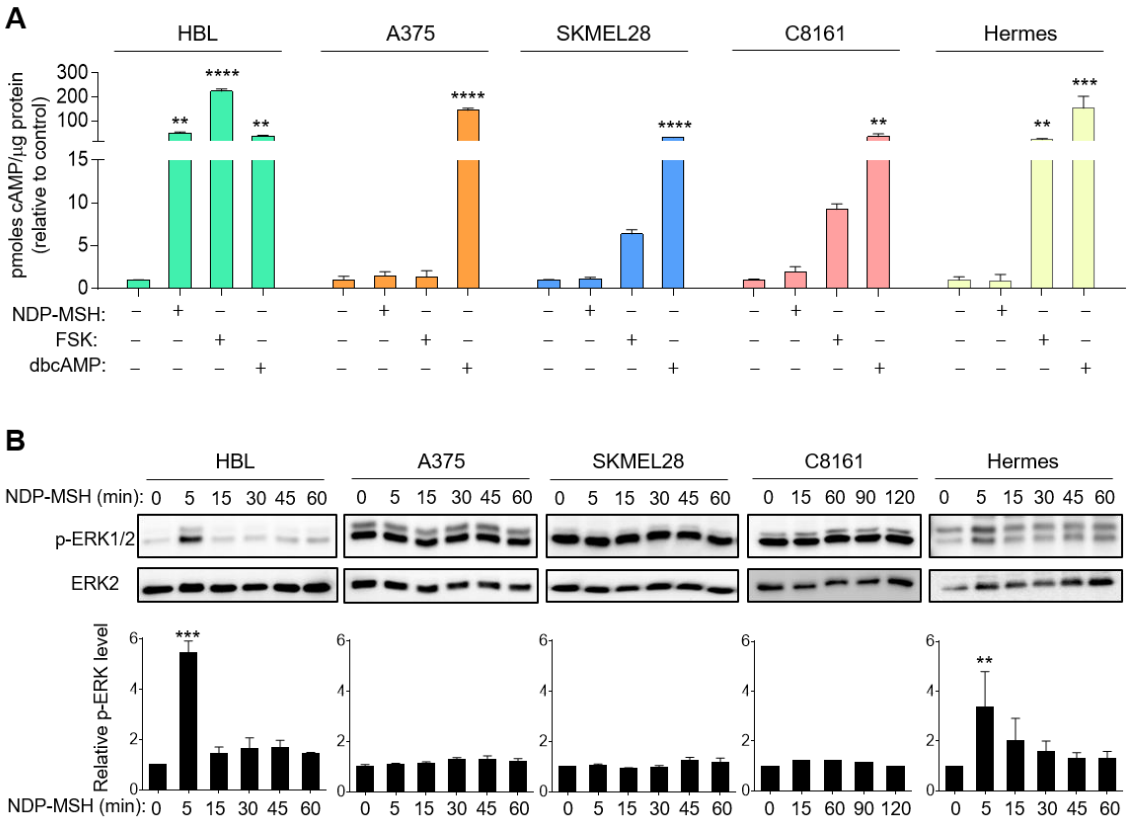

Figure 7. MC1R signaling to the cAMP and ERK pathways in HMCs and Hermes melanocytes. (A) Intracellular cAMP production in the indicated cell lines. Cells were serum-deprived and stimulated with 10^{-7} M NDP-MSH, 10^{-5} M FSK or $3x10^{-6}$ M dbcAMP for 30 min. **(B) Kinetics of ERK activation upon NDP-MSH stimulation in HMCs and Hermes**. Cells were serum-starved and challenged with 10^{-7} M NDP-MSH for the times indicated. Representative immunoblots (top panel) and quantification (bottom panel) for pERK1/2 are shown. Data shown as mean±SEM, *p<0.05, **p<0.01, ***p<0.001, ****p<0.0001.

Induction of repair of oxidative damage downstream of variant MC1R

After having characterized the genotype of *MC1R* in our panel of model cell lines as well as the pathways activated by MC1R agonists in these cells, we analyzed their sensitivity to oxidative DNA damage. To mimic transient oxidative stress, cells were pulsed with Luperox ($1.5x10^{-4}$ M, 30 min), used as a stable form of H_2O_2[374]. This treatment increased comparably ROS levels without significant effects on cell viability not only in A375 and HBL cells, but also in SKMEL28 and C8161 HMCs and in Hermes human melanocytes (Figures 8A and 8B). As expected, pretreatment of the cells with the antioxidant ebselen efficiently blocked the increase in ROS in HBL or A375 cells challenged with Luperox (Figure 8C). These data showed that melanoma cells can be submitted to short oxidative treatments that substantially increase intracellular ROS but that do not impair cell viability.

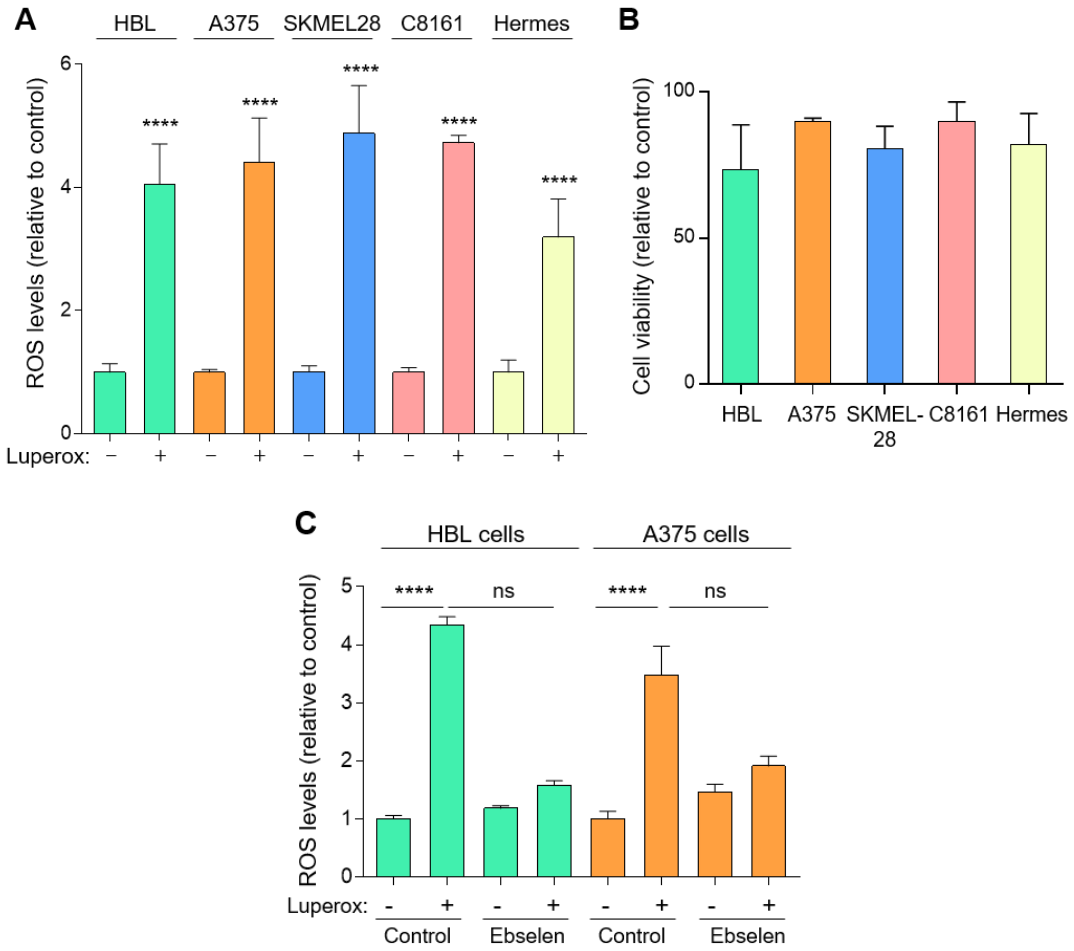

Figure 8. (A) Increased ROS levels in human melanocytes and melanoma cells following Luperox treatment. ROS levels were estimated with the H_2DCFDA assay. Data represent the mean fold-change of ROS-induced dichlorofluorescein fluorescence after a Luperox challenge ($1.5x10^{-4}$ M, 30 min), and are given as mean ±SEM (n = 3 with 6 replicate wells/experiment, ****p<0.0001). **(B) Effects of the Luperox challenge on cell viability**, as measured by the MTT assay after exposure to $1.5x10^{-4}$ M Luperox for 30 min. Data are shown as relative cell viability after Luperox treatment respect to untreated controls (n = 3, data given as mean±SEM). **(C) Effect of ebselen on ROS levels in HBL and A375 melanoma cells**. Both melanoma cell lines were treated with $4x10^{-5}$ M ebselen for 36 h prior to Luperox ($1.5x10^{-4}$ M, 30 min) treatment. ROS levels were estimated with the H_2DCFDA assay. Data as indicated for panel A.

To look for MC1R- and cAMP-dependent protective responses, the oxidative challenge was performed with or without pretreatment (36 h) with NDP-MSH, the AC activator FSK, or the cell-permeable cAMP precursor dbcAMP. Then, Luperox-treated cells were stained for 8-oxodG, a major product of UVR-induced oxidative DNA damage. For *MC1R*-WT HBL cells, Luperox strongly increased 8-oxodG staining. This increase was abolished by the non-selective antioxidant ebselen[375] or by pretreatment with NDP-MSH, FSK or dbcAMP (Figure 9A). These treatments dramatically increased intracellular cAMP levels (Figure 9B). Furthermore, the AC inhibitor DDA blocked NDP-MSH or FSK-dependent cAMP production and decreased markedly their protective

effect (Figures 9A and 9B). Therefore, in WT *MC1R* HBL cells, the cAMP pathway contributed most of the MC1R-dependent reduction of ROS-induced oxidative DNA damage as assessed by 8-oxodG staining, in agreement with reports by others[326,329,331].

Pretreatment of *MC1R*-variant A375 cells with NDP-MSH also decreased 8-oxodG levels compared with treatment with Luperox alone (Figure 9C), but NDP-MSH failed to activate cAMP signaling as demonstrated by lack of stimulation of cAMP levels or *MITF* gene expression (Figure 9D and 9E). Thus, in A375 cells homozygous for the R151C allele, MC1R activation triggered a significant protective response, most likely in a cAMP-independent manner. Interestingly, pretreatment of A375 HMCs with dbcAMP, but not FSK, achieved a strong increase in intracellular cAMP and had a strong protective effect against ROS-induced DNA oxidative damage (Figures 9C, 9D). This showed that the cAMP-activated pathway(s) responsible for protection against DNA oxidative insults remained operative in A375 cells, although these pathways could not be responsible for the protective effect of the MC1R agonists, since A375 cells are unable to activate cAMP synthesis in response to NDP-MSH.

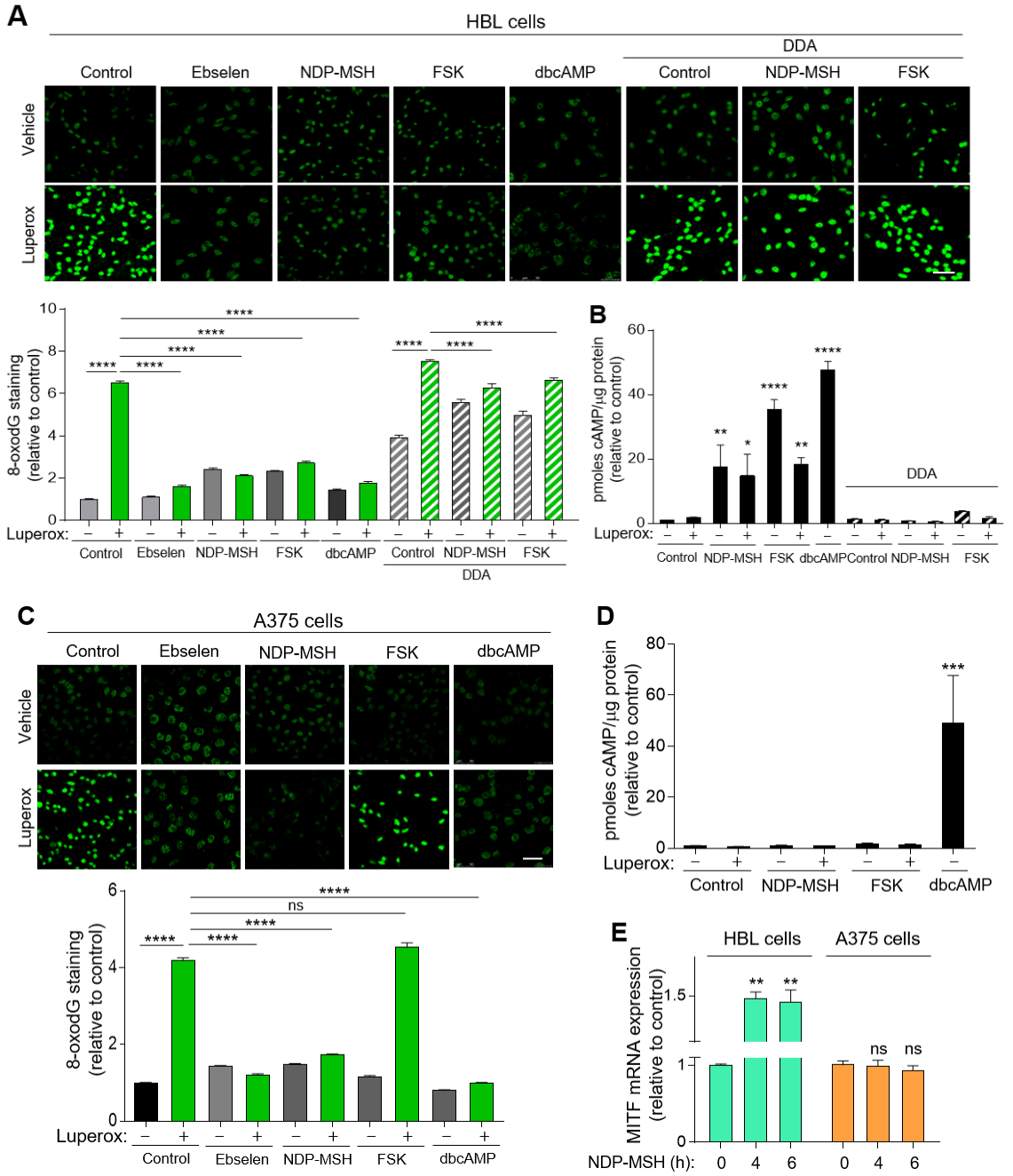

Figure 9. Effect of MC1R signaling on 8-oxodG levels induced by an oxidative challenge in HBL and A375 melanoma cells. (A) 8-oxodG levels in WT MC1R cells. HBL cells were serum-deprived for 12 h and stimulated with 10^{-7} M NDP-MSH, 10^{-5} M FSK or $3x10^{-6}$ M dbcAMP, for 36 h with or without pretreatment with $2.5x10^{-3}$ M DDA for 1 h, or incubated with ebselen ($4x10^{-5}$ M, 36 h prior to and during the oxidative challenge), then treated with Luperox ($1.5x10^{-4}$ M, 30 min). After 8-oxodG immunostaining, samples were mounted with a medium from Dako (Glostrup, Denmark), examined and quantified as explained in material and methods section 18. At least 200 randomly selected cells were quantified. Representative confocal images of 8-oxodG immunostaining are shown (bar size: 50 µm), as well as quantitative analysis of nuclear 8-oxodG fluorescence intensity in each condition. **(B) cAMP levels in HBL cells treated as above. (C) 8-oxodG and (D) cAMP levels in A375 cells treated as above** (n = 3 independent experiments, error bars are mean±SEM, two-sided one-way ANOVA was used to generate p values, *p<0.05, **p<0.01, ***p<0.001, ****p<0.0001). **(E) Activation of MITF gene expression by NDP-MSH in HBL cells, but not in A375 cells.** Cells were serum-starved (12 h), then treated with NDP-MSH (10^{-7} M) for the times shown. mRNA was extracted, reverse-transcribed and MITF mRNA levels were compared by RT-PCR (n = 3, **p<0.01).

Next, we analyzed variant MC1R-dependent protection against peroxide-generated DNA SBs. Exposure of cells to ROS such as peroxyl radicals increases SBs[376]. Whereas low micromolar peroxide concentrations mostly induce SSBs, relatively high concentrations such as those employed here also induce significant numbers of DSBs[377]. ROS-induced DSBs rapidly result in phosphorylation of histone H2AX. γH2AX attracts repair factors to DSB sites, forming foci enriched in repair proteins[378]. In the same experimental conditions as for determination of 8-oxodG, Luperox treatment augmented γH2AX staining in HBL and A375 cells (Figures 10A, 10B). Preincubation with NDP-MSH prevented the increase in γH2AX staining in both cell lines, suggesting reduction of DSBs. The possibility that γH2AX foci, which are poorly induced by SSBs, might arise by conversion of such lesions to DSBs on passage of a replication fork in proliferating cells appeared unlikely, since a clear majority of cells exhibited extensive and similar staining (Figures 10C and 10D). Moreover, incubation with NDP-MSH, which reduced strongly γH2AX staining, had little effect on cell cycle progression (Figure 10E).

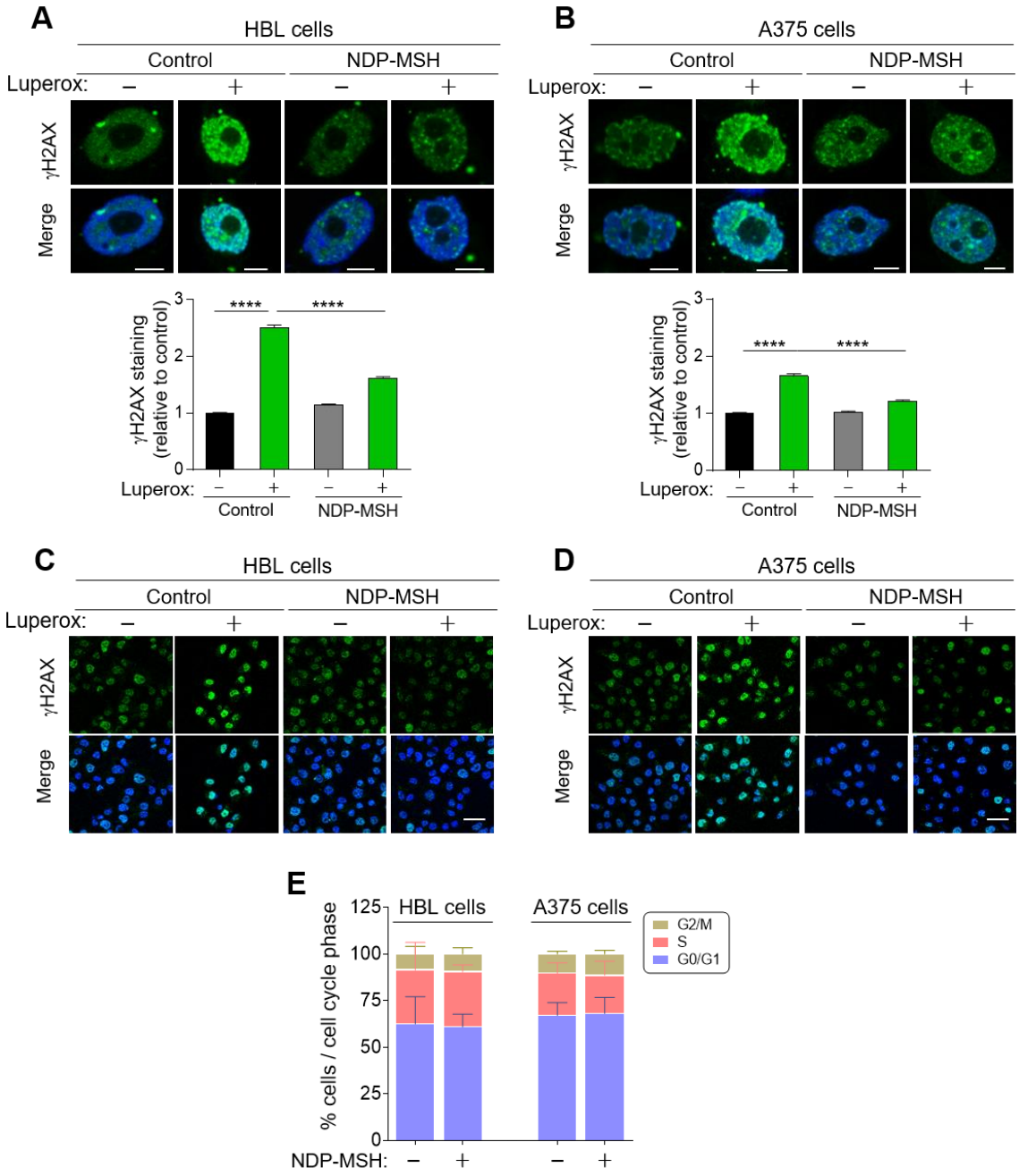

Figure 10. Effect of MC1R signaling on DNA strand breaks induced by Luperox in HBL and A375 melanoma cells. (A-B) γH2AX levels in HBL and A375 melanoma cells. HBL (A) and A375 (B) melanoma cells were serum-deprived for 12 h and then stimulated with 10^{-7} M NDP-MSH for 36 h prior to Luperox treatment. Cells were fixed, permeabilized and stained for γH2AX (green). DAPI was used for nuclear staining (blue). Representative confocal images of γH2AX immunostaining (bar size: 5 μm) and the quantification of the relative intensity of γH2AX signals are shown below. Immunostaining images and quantification were performed as described in material and methods section 18 (n = 3 independent experiments, error bars, statistical analysis and p values as in Figure 9). **(C-D) γH2AX immunostaining in HBL and A375 melanoma cells**. Representative images of HBL (C) and A375 (D) cells treated as above, obtained at lower magnification (bar size 50 μm) to show homogenous staining of the cellular population. **(E) Minor effect of NDP-MSH on cell cycle progression in HBL or A375 cells**.

On the other hand, pretreatment of HBL cells with either FSK or dbcAMP also decreased the γH2AX signal. Conversely, only dbcAMP afforded protection to A375 cells (Figure 11) but FSK was ineffective, in keeping with its previously observed inability to decrease peroxide-induced 8-oxodG or to activate significantly cAMP synthesis in these cells.

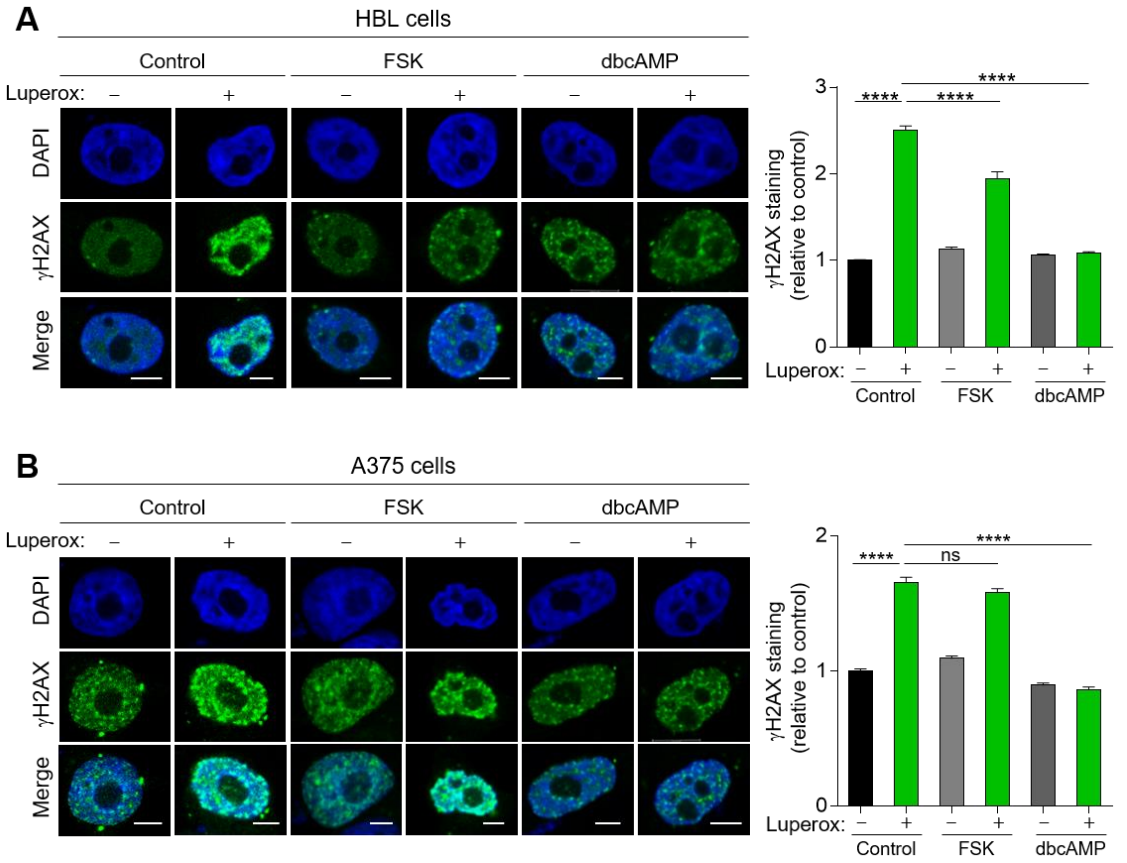

Figure 11. Effect of increased cAMP levels on γH2AX foci induced by Luperox in HBL (A) and A375 (B) melanoma cells. Both melanoma cell lines were serum-deprived for 12 h and stimulated with 10^{-5} M FSK or $3x10^{-6}$ M dbcAMP for 36 h prior to Luperox treatment (30 min). Cells were fixed, permeabilized and stained for γH2AX (green). DAPI was used for nuclear staining (blue). Representative confocal images of γH2AX immunostaining (bar size: 5 μm) and the quantification of the intensity of γH2AX signals are shown (n = 3, at least 200 cells randomly selected in each case, error bars are mean±SEM, ****p<0.0001, Tukey's test was used for multiple comparison).

We wished to confirm MC1R-mediated reduction of DNA SBs in MC1R-variant A375 cells. To this end, we assessed oxidative DNA fragmentation using the alkaline comet assay. In HBL and A375 cells, NDP-MSH reduced Luperox-induced DNA SBs (Figures 12A, 12B and Table 3). As for γH2AX staining, preincubation with FSK decreased Luperox-generated SBs in HBL cells but not in A375 HMCs, whereas dbcAMP reduced SBs in both cell types. These data confirmed the involvement of cAMP-independent pathways in protection against oxidative DNA damage

downstream of variant MC1R. Of note, the DNA damage repair response triggered by cAMP remained operative in these cell lines, as it could be evoked by dbcAMP.

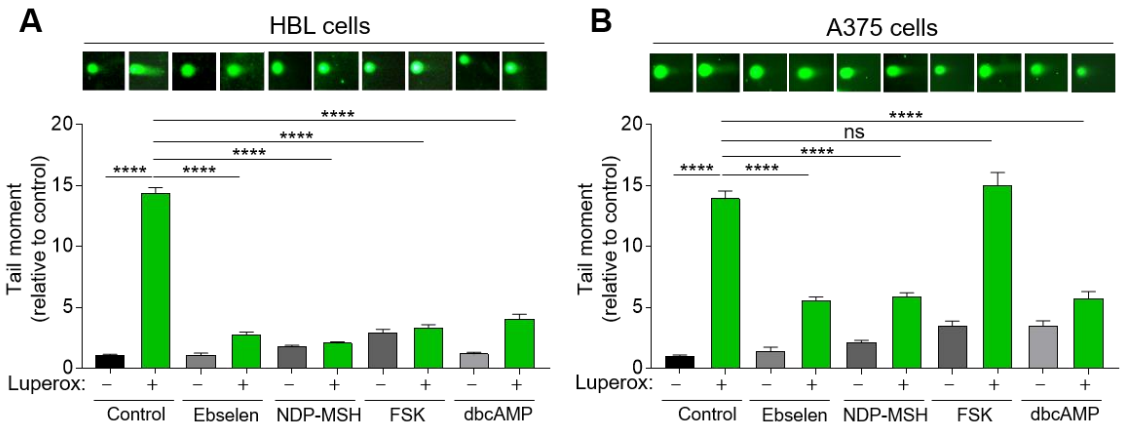

Figure 12. MC1R-dependent protection against Luperox-induced DNA SBs in HBL (A) and A375 (B) cells. Comet assays were performed on cells treated with NDP-MSH, pharmacological cAMP-elevating agents or ebselen under the standard conditions described in Figure 9. Then, cells were processed as explained in material and methods section 17. Quantitative analysis of at least 100 randomly selected comets was performed using a Leica fluorescence microscope and CASPLAB software. Histograms show the mean average of the tail moment of treated cells relative to untreated cells (n = 3 independent experiments, each one with at least 100 comets analysed. Error bars, statistical analysis and p values as in Figure 9). Representative images of comet tails acquired at 40X magnification are shown above each histogram.

To confirm the novel finding of cAMP-independent protective mechanisms downstream of variant MC1R, we analyzed three other melanocytic cell lines, SKMEL28 and C8161 HMCs and Hermes melanocytes. Preincubation of C8161, SKMEL28 or Hermes cells with NDP-MSH comparably decreased the steady state levels of DNA SBs generated by Luperox as estimated with comet assays (Figure 13A and Table 3). This suggested that the cAMP-independent protection against oxidative DNA fragmentation afforded by NDP-MSH in A375 cells was not an artefact of this cell type but was rather a general behaviour of MC1R-variant melanocytic cells.

Cell line	Control	Luperox	NDP-MSH	NDP-MSH+Luperox
HBL	1.11 +/- 0,11	12.58 +/- 0,53	1.64 +/- 0,13	3.02 +/- 0,23
A375	3.02 +/- 0,22	36.95 +/- 1,64	4.05 +/- 0,25	10.37 +/- 0,67
SKMEL 28	2.14 +/- 0,22	21.78 +/- 1,27	2.12 +/- 0,27	6.14 +/- 0,38
C8161	1.41 +/- 0,36	20.19 +/- 1,47	1.28 +/- 0,34	12.21 +/- 1,14
Hermes	1.58 +/- 0,23	10.56 +/- 1,22	2.74 +/- 0,50	3.91 +/- 0,44

Table 3. Mean tail moment values +/- SEM (a.u.) of Hermes melanocytes and HMCs. The indicated cells were serum-deprived for 12 h. If required, cells were stimulated with 10^{-7} M NDP-MSH then treated with Luperox ($1.5x10^{-4}$ M, 30 min). Cells were harvested for comet assays. At least 100 comets were scored in each case. Data are presents as mean±SEM (n = 3).

To further establish the ability of variant MC1R to protect against oxidative DNA damage, we transfected HEK293T cells with Flag epitope-labeled WT or R151C MC1R. At comparable expression levels, NDP-MSH elicited a similar protective response against Luperox-induced DNA fragmentation, as estimated by comet assays (Figure 13B).

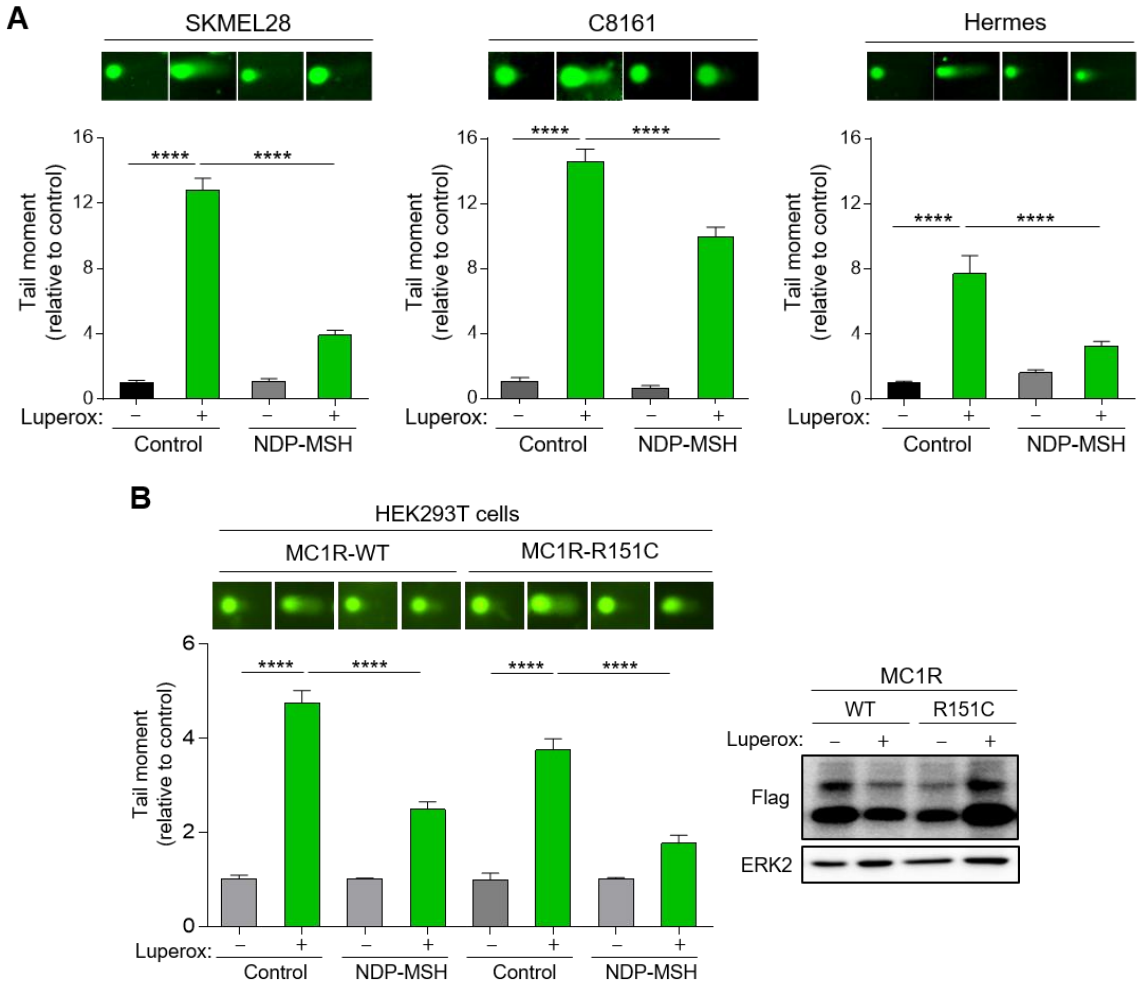

Figure 13. MC1R-dependent protection against Luperox-induced DNA SBs in HMCs, melanocytes and in heterologous HEK293T cells. Comet assays were performed on SKMEL28 and C8161 melanoma cells and Hermes melanocytes (A) and on HEK293T cells transfected with MC1R WT or MC1R R151C (B) treated with NDP-MSH under the standard conditions described in Figure 12. Then, cells were processed as explained in material and methods section 17. Histograms show the mean average of the tail moment of treated cells relative to untreated cells (n = 3, error bars are mean±SEM, Kruskal-Wallis test was used to generate p values, ****p<0.0001). Representative images of comet tails acquired at 40X magnification are shown above each histogram. Representative immunoblots of MC1R transfection in HEK293T cells are also shown to ascertain comparable expression of WT and variant MC1R.

The experiments described thus far were performed using a relatively long oxidative challenge (30 min) and a prolonged preincubation with NDP-MSH (36 h) that may allow for the induction of antioxidant enzymes. Therefore, the protective effect of MC1R activation could result from a combination of augmented clearance of oxidative lesions and decreased oxidative

damage due to improved antioxidant defenses. To assess the relative contribution of these non-mutually exclusive mechanisms, we investigated the extent and kinetics of induction of antioxidant enzymes downstream of WT or variant MC1R. HBL or A375 cells were treated with NDP-MSH, and the expression of *CAT*, *SOD1* and *GPx1* genes was assessed. For HBL cells, NDP-MSH caused a time-dependent induction of *CAT*, a faster stimulation of *SOD1* and a weaker increase in *GPx1* expression. These stimulatory effects were abolished by DDA-mediated inhibition of AC (Figure 14A). Moreover, upregulation of intracellular cAMP levels by FSK or dbcAMP also increased expression of *CAT*, *SOD1* and *GPx1* in HBL cells (Figure 14B). These data were consistent with reports of cAMP-dependent upregulation of antioxidant enzymes downstream of WT MC1R[326,329,331]. Concerning A375 cells, NDP-MSH (Figure 14C) or FSK (Figure 14D) had little, if any, effect on *CAT* expression and did not increase *GPx1* mRNA, whereas dbcAMP significantly stimulated *SOD* and *CAT* expression (Figure 14D). Surprisingly, in A375 cells NDP-MSH and FSK upregulated potently and transiently *SOD1* expression, suggesting that in these cells signaling mechanisms different from the cAMP pathway could be responsible for *SOD1* upregulation downstream of MC1R.

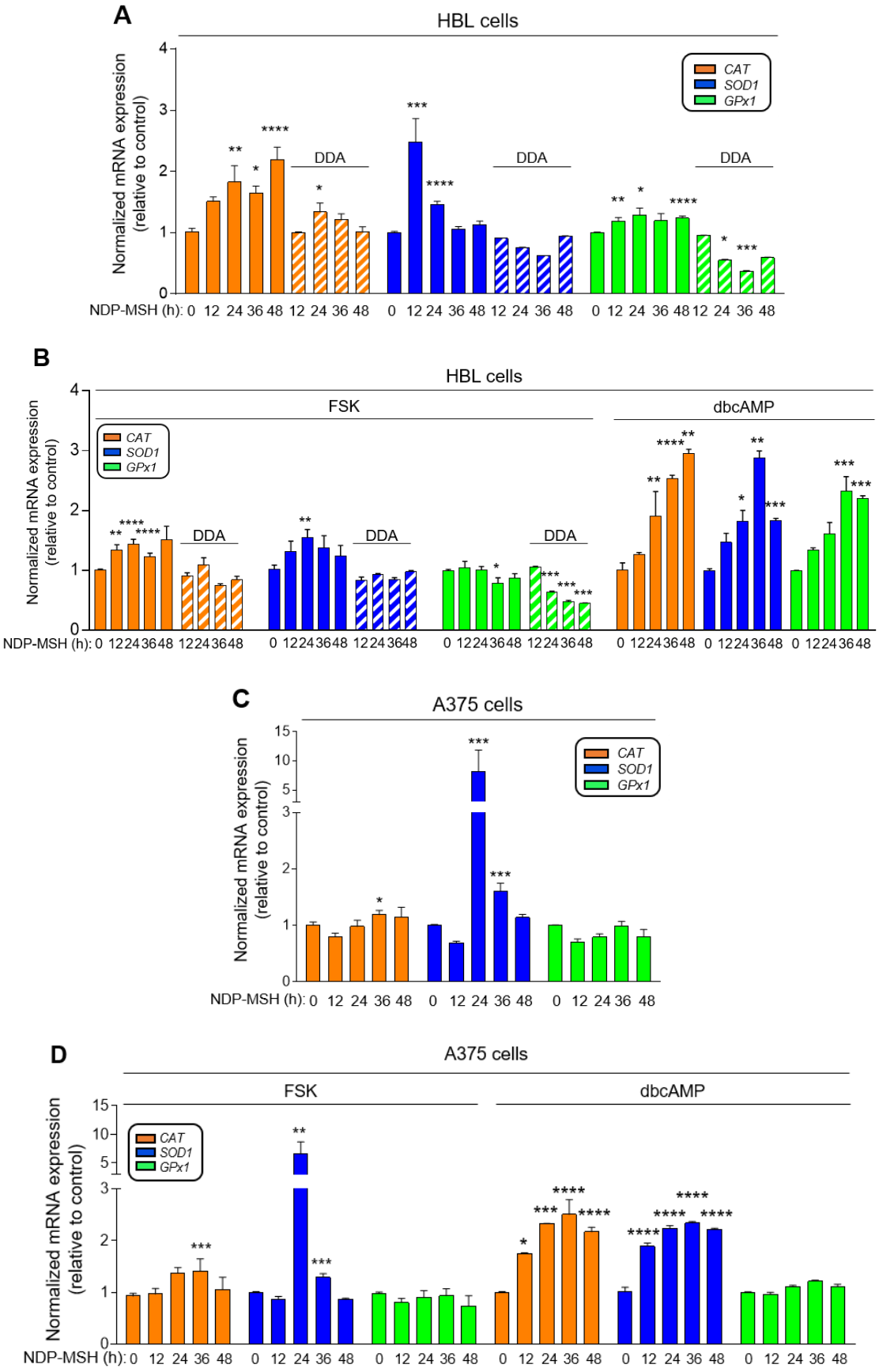
A
HBL cells
Normalized mRNA expression (relative to control)
CAT
SOD1
GPx1
DDA
DDA
DDA
NDP-MSH (h): 0 12 24 36 48 12 24 36 48 0 12 24 36 48 12 24 36 48 0 12 24 36 48 12 24 36 48
B
HBL cells
FSK
dbcAMP
Normalized mRNA expression (relative to control)
CAT
SOD1
GPx1
DDA
DDA
DDA
NDP-MSH (h): 0 12 24 36 48 12 24 36 48 0 12 24 36 48 12 24 36 48 0 12 24 36 48 12 24 36 48 0 12 24 36 48 12 24 36 48
C
A375 cells
Normalized mRNA expression (relative to control)
CAT
SOD1
GPx1
NDP-MSH (h): 0 12 24 36 48 0 12 24 36 48 0 12 24 36 48
D
A375 cells
FSK
dbcAMP
Normalized mRNA expression (relative to control)
CAT
SOD1
GPx1
NDP-MSH (h): 0 12 24 36 48 0 12 24 36 48 0 12 24 36 48 0 12 24 36 48 0 12 24 36 48

Figure 14. Induction of antioxidant enzymes by MSH, FSK and dbcAMP in HBL and A375 melanoma cells. HBL melanoma cells, with or without pretreatment with $2.5x10^{-3}$ M DDA (hatched bars) were stimulated with 10^{-7} M NDP-MSH (A), 10^{-5} M FSK or $3x10^{-6}$ M dbcAMP (B) at the indicated time points. A375 melanoma cells were treated with 10^{-7} M NDP-MSH (C), 10^{-5} M FSK or $3x10^{-6}$ M dbcAMP (D) for the times shown. Expression of *CAT* (orange bars), *SOD1* (blue) and *GPX1* (green) genes was estimated by RT-PCR. Data are shown as relative expression of each enzyme in treated cells relative to untreated controls calculated using the $2^{-\Delta\Delta Ct}$ method. β-actin was used as endogenous normalizer. These data were compiled from three separate experiments performed in triplicate (n = 3, error bars are mean±SEM, statistical analysis and p values as in Figure 9).

We analyzed catalase and SOD1 protein levels upon MC1R stimulation with NDP-MSH for up to 48 h. We observed a significant induction of catalase in agonist-treated HBL cells consistent with changes in mRNA levels, but A375 cells were unresponsive (Figure 15A). Expression of SOD1 did not change significantly in either cell type (Figure 15B). To find out whether upregulation of catalase led to a decreased ROS burden, we measured total ROS levels in NDP-MSH-treated cells. We found a trend towards lower ROS levels in NDP-MSH-stimulated cells that did not reach statistical significance (Figure 15C). Therefore, WT MC1R HMCs may cope only partially with oxidative stress by induction of antioxidant enzymes in response to activation of the cAMP pathway. This effect would be small or absent in *MC1R* variant HMCs. Accordingly, the protection against DNA damage in A375 cells treated with NDP-MSH most likely resulted from enhanced DNA repair.

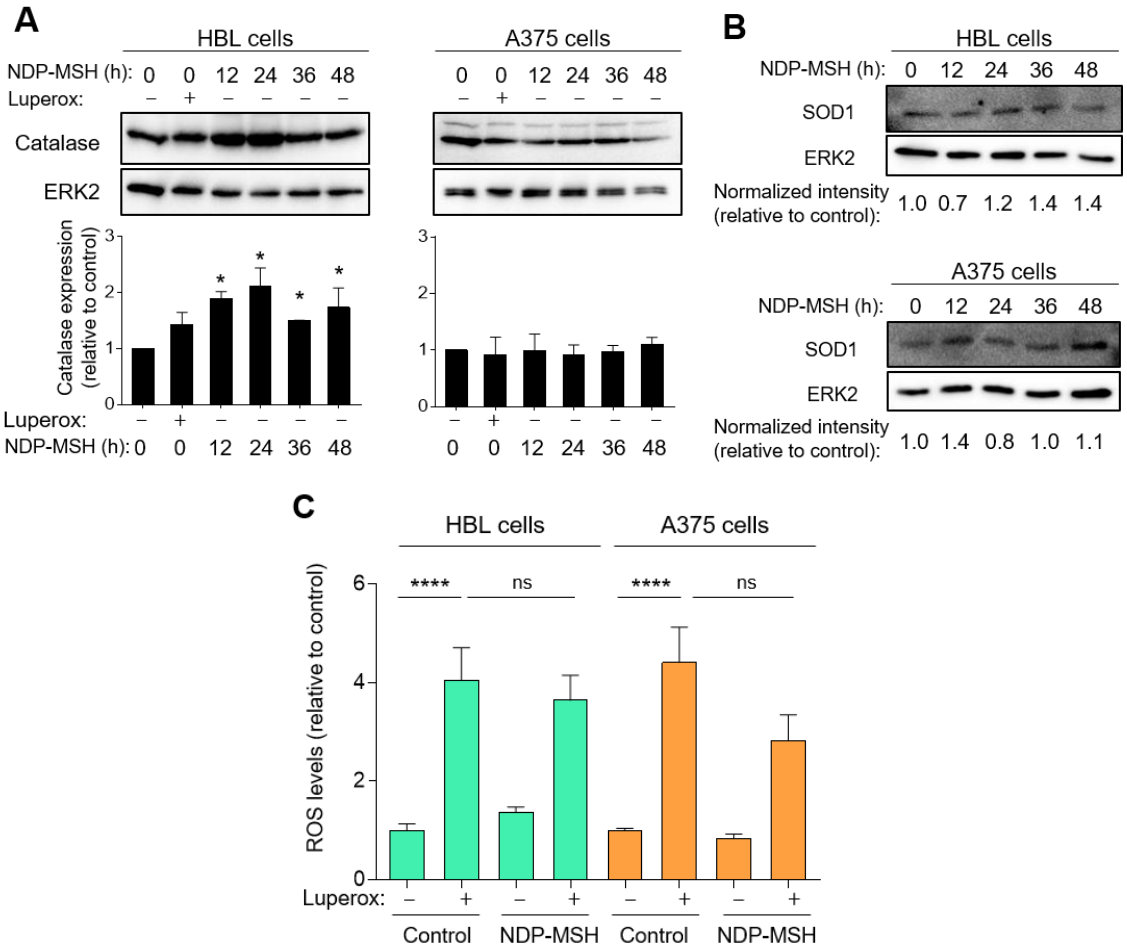

Figure 15. Induction of antioxidant enzymes by MSH in HBL and A375 melanoma cells. (A) Increased catalase expression in HBL melanoma cells stimulated with NDP-MSH. Representative immunoblots (top) and quantification (bottom) of catalase protein levels in HBL (left) and A375 (right) melanoma cells stimulated with 10^{-7} M NDP-MSH for the indicated times are shown. Quantification of 3 independent experiments using ERK2 signal as loading control is shown below the blots. Values were normalized to the 0 time-point (n = 3, error bars are mean±SEM, two-sided Student´s t test was used to generate p values, *p< 0.05). **(B) Expression of SOD1 in HBL and A375 melanoma cells**. Levels of SOD1 in HBL or A375 cells stimulated with 10^{-7} M NDP-MSH for the times shown, as analysed by Western blot. The number below each lane represents the normalized intensity of the SOD1 signals corrected for protein load (mean of two independent experiments). ERK2 was used as a control for protein load. **(C) Intracellular ROS levels in Luperox-treated HBL and A375 cells**. Cells were pretreated with NDP-MSH (10^{-7} M, 36 h), as indicated, then challenged with Luperox ($1.5x10^{-4}$ M, 30 min). Total ROS were measured with 2'7'dichlorodihydrofluorescein (n = 3, with 6 replicate wells for each experiment, error bars are mean±SEM, statistical analysis and p values as in Figure 9).

To confirm activation of DNA repair pathways downstream of variant MC1R, we compared the rate of clearance of oxidative DNA lesions in control cells or cells pretreated with NDP-MSH for 36 h. For this purpose, HBL and A375 HMCs kept on ice were challenged with Luperox for a shorter time (10 min), then quickly washed and incubated at 37ºC to follow the kinetics of 8-oxodG removal and comet tail clearance. In the absence of NDP-MSH, the intensity of 8-oxodG staining and the comet tail moments stayed constant for up to 15 min after removal

of the oxidizing agent in HBL cells or even increased slightly in A375 cells (Figure 16). Conversely, NDP-MSH-treated cells showed a progressive clearance of 8-oxodG and a reduction of the comet tail moments, already noticeable after a 5 min recovery, thus confirming active DNA repair.

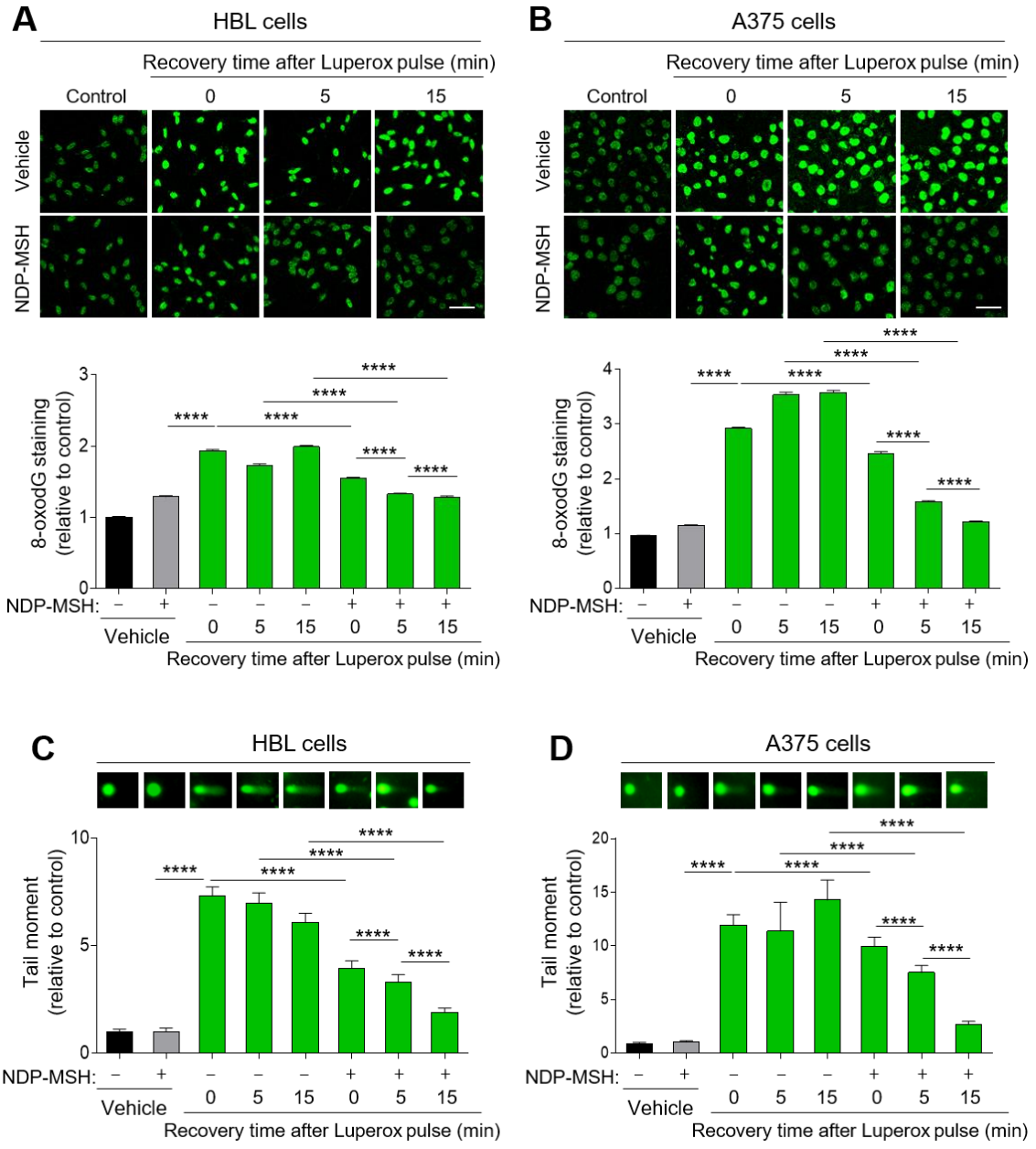

Figure 16. Effect of MC1R activation on the kinetics of oxidative DNA damage repair in HMCs. HBL and A375 cells, as indicated, were pretreated or not with NDP-MSH (10^{-7} M, 36 h) during a short challenge with Luperox ($1.5x10^{-4}$ M, 10 min, 4ºC). Cells were quickly washed and further incubated for up to 15 min either in the absence (vehicle) or in the presence of NDP-MSH. Then cells were processed for 8-oxodG staining (panels A and B) or for single cell electrophoresis and comet assay (panels C, D) performed and quantified as specified in Figures 9 and 12, respectively. Control stands for cells that were not challenged with Luperox.

In summary, thus far we have confirmed results from other laboratories showing that WT MC1R stimulation activates expression of antioxidant enzymes and repair of oxidative DNA lesions via cAMP-dependent mechanisms. On the other hand, we have shown for the first time that unexpectedly, variant MC1R activation also stimulates clearance of oxidatively generated DNA SBs and oxidized bases by cAMP-independent mechanisms. Indeed, even if MC1R-variant melanoma cells are able to trigger protective responses when cAMP is elevated by pharmacological agents, their variant *MC1R* genotype impedes activation of AMP synthesis upon treatment with MC peptides.

Involvement of AKT signaling in the protective effect of variant MC1R

AKT activation is required for variant MC1R-induced repair of oxidative DNA damage

We aimed at identifying MC1R-triggered, cAMP-independent signaling pathway(s) responsible for the protective effects of NDP-MSH in *MC1R*-variant cells. We showed previously that NDP-MSH triggers ERK activation by cAMP-independent transactivation of cKIT and that ERK activation is comparable in potency and kinetics for WT or variant MC1R[161,310]. Thus, we assessed the effect of the ERK pathway inhibitor PD98059 on MC1R-induced DNA repair. In HBL cells, PD98059 inhibited effectively basal and NDP-MSH-induced ERK activity and decreased slightly, but did not abolish, protection against oxidative DNA fragmentation afforded by NDP-MSH. Indeed, Luperox-challenged HBL cells pre-stimulated with NDP-MSH in the presence of PD98059 showed significant reductions of comet tail moments (Figure 17A). For A375 cells, NDP-MSH decreased comparably oxidative DNA SBs in the presence or absence of PD98059 (Figure 17B), despite nearly complete ERK inhibition. We obtained similar results for SKMEL28 cells (Figure 17C). These observations ruled out ERK activation as the major mechanism of protection against oxidative DNA fragmentation downstream of variant *MC1R*.

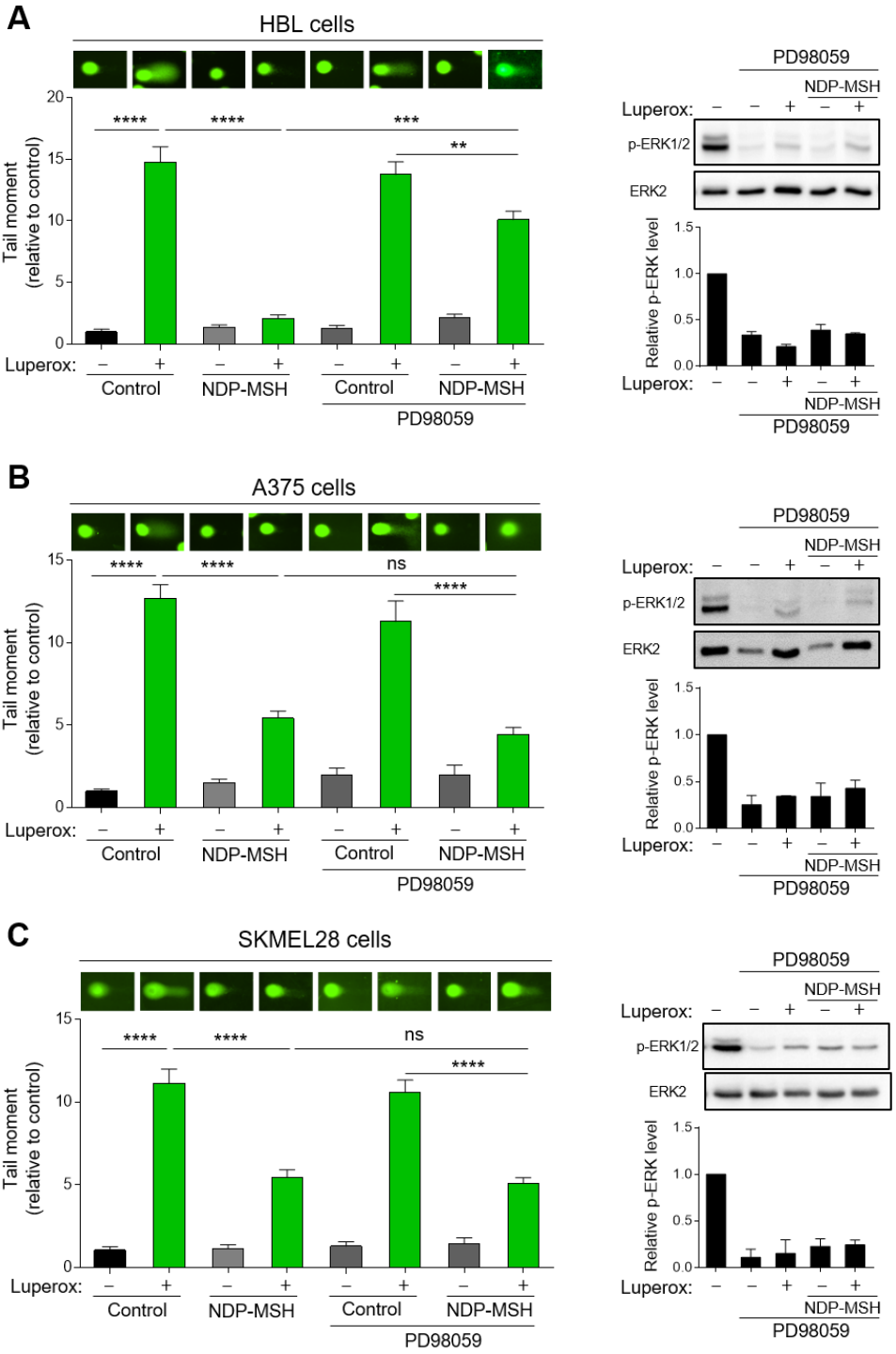

Figure 17. Lack of involvement of the ERK pathway in the protective effect of NDP-MSH in cells harboring *MC1R* variants. HBL (A), A375 (B) and SKMEL28 (C) melanoma cells were pretreated with the MEK1 inhibitor PD98059 ($5x10^{-5}$ M, 1h), then stimulated with NDP-MSH (10^{-7} M, 36 h) prior to a Luperox challenge ($1.5x10^{-4}$ M, 30 min). SBs were analyzed by comet assay. Histograms show the mean average of the tail moment of treated cells relative to the tail moment of untreated cells (n = 3 independent experiments with at least 100 comets analysed in each case. Error bars, statistical analysis and p values as in Figure 9). Representative immunoblots ascertaining ERK inhibition by PD98059 are shown on the right along with the quantification of ERK phosphorylation levels relative to the control (n = 3, error bars as above).

Next, we investigated a possible role of AKT in variant MC1R-dependent DNA repair. To this end, first we analyzed AKT activation downstream of variant MC1R. We challenged HBL and A375 cells with NDP-MSH and compared the levels of activatory AKT phosphorylation. NDP-MSH did not augment AKT phosphorylation in WT *MC1R* HBL cells but activated AKT in A375 cells (Figure 18A). We observed a comparable activation of AKT in NDP-MSH-treated SKMEL28, C8161 and Hermes cells, with peak levels at 60-90 min (Figure 18A). Therefore, variant MC1R activated AKT efficiently, but AKT activation downstream of MC1R was undetectable in cells expressing WT MC1R. This observation suggested an inverse relationship between AKT activation and the cAMP pathway. Since high cAMP levels inhibit AKT in B16 mouse melanoma cells[379], we reasoned that a similar inhibition might occur in human cells. To test this possibility, we blocked AC activation with DDA in HBL cells, and we increased cAMP levels in A375 cells with dbcAMP. Then, we challenged cells with NDP-MSH and compared pAKT levels. DDA allowed activation of AKT downstream of MC1R in HBL cells, whereas pharmacological elevation of cAMP in A375 melanoma cells abolished AKT phosphorylation (Figure 18B). Similar results were obtained for SKMEL28, C8161 and Hermes cells (Figure 18B).

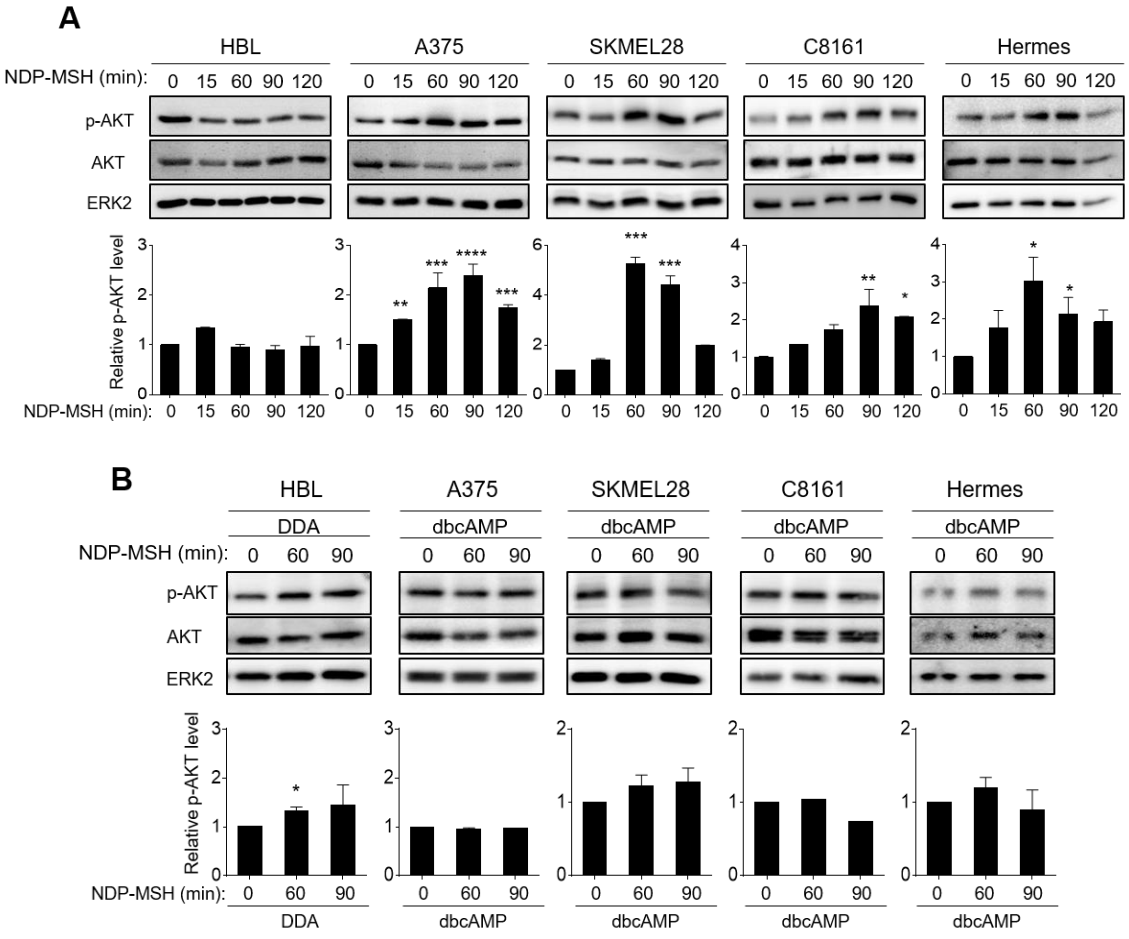

Figure 18. AKT activation upon NDP-MSH stimulation of variant MC1R. (A) Kinetics of AKT activation following stimulation with NDP-MSH. HBL, A375, SKMEL28, C8161 and Hermes melanocytic cells were challenged with 10^{-7} M NDP-MSH for the times shown. Representative immunoblots for pAKT1/2/3 are shown for each cell line. Quantification of the intensity of pAKT signal relative to the control is shown below. Total AKT1/2/3 was used as loading control (n = 3, error bars are mean±SEM, *p<0.05, **p<0.01 ***p<0.001, ****p<0.0001, calculated with a two-sided Student´s t test). **(B) Relationship between AKT activation and the cAMP pathway**. HBL cells were pretreated with DDA ($2.5x10^{-3}$ M, 1 h) to block cAMP production, and conversely, A375, SKMEL28, C8161 and Hermes melanocytic cells, were incubated with dbcAMP ($3x10^{-6}$ M, 30 min) to increase cAMP levels prior to stimulation with 10^{-7} M NDP-MSH for 60 and 90 min. Representative immunoblots and quantification of 3 independent blots for pAKT are shown (n = 3, error bars are mean±SEM, two-sided Student´s t test was used to generate p values, *p< 0.05,**p<0.01 ***p<0.001, ****p<0.0001).

Since AKT was activated downstream of variant MC1R, we checked its involvement in MC1R-dependent reduction of oxidative DNA damage. We blocked the AKT pathway with pharmacological inhibitors and analyzed comet tail moments in Luperox-pulsed cells. We used LY94002 and MK-2206 to block PI3K and AKT activation, respectively[380]. This treatment prevented AKT activation and abolished the protective action of NDP-MSH in A375 but not in HBL cells (Figures 19A, 19B). Moreover, this treatment also blocked protection in C8161, SKMEL28 and Hermes cells (Figure 19C-E). To confirm a protective effect of AKT signaling in MC1R-variant melanoma cells, the oxidative challenge was performed in cells pretreated with SC79, an agonist of the AKT pathway which binds to AKT to induce a conformation favorable for phosphorylation by upstream activatory kinases[381]. SC79 had no effect on tail moments in HBL cells, consistent with its inability to increase pAKT levels in these cells (Figure 19A). Conversely, SC79 activated AKT efficiently in A375 cells (Figure 19B) and reduced Luperox-induced comet tail moments. Again, we observed a similar behaviour in other melanocytic cells (Figure 19C-E). Therefore, the PI3K/AKT pathway was involved in NDP-MSH-induced clearance of DNA SBs downstream of variant MC1R.

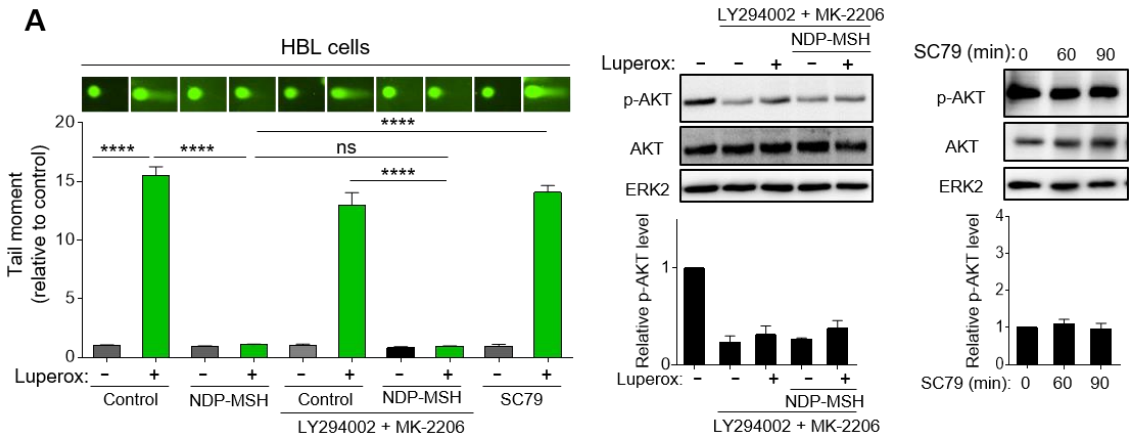

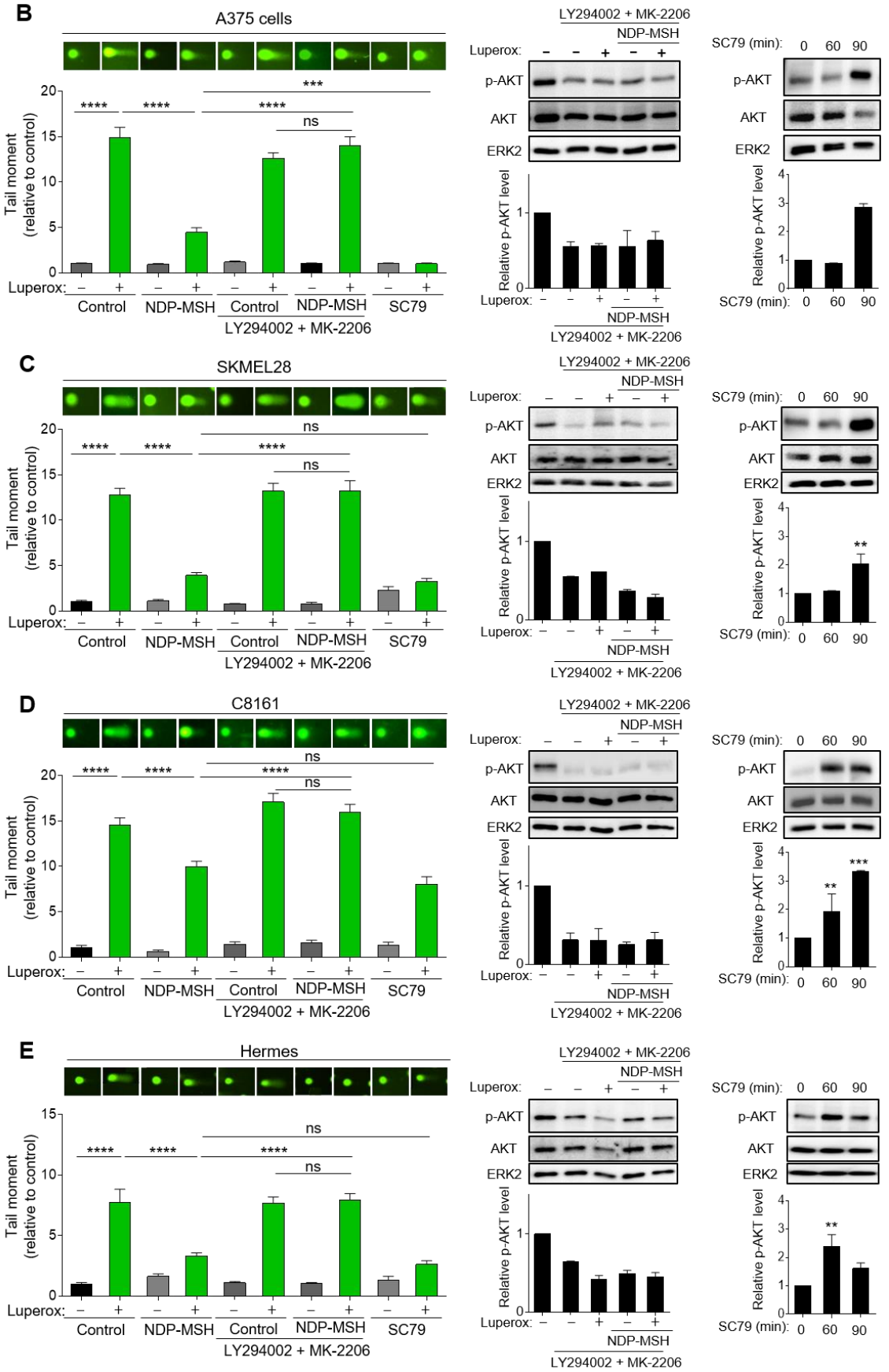
B
A375 cells
C
SKMEL28
D
C8161
E
Hermes
Tail moment (relative to control)
Luperox:
Control
NDP-MSH
SC79
LY294002 + MK-2206
p-AKT
AKT
ERK2
Relative p-AKT level
SC79 (min): 0 60 90

Figure 19. Involvement of AKT activation in the protective effect of NDP-MSH. HBL (A), A375 (B), SKMEL28 (C), C8161 (D) melanoma cells, and Hermes melanocytes (E) were pretreated for 1 h with LY294002 ($2x10^{-5}$ M) and MK-2206 ($5x10^{-6}$ M), to block AKT stimulation. Then cells were stimulated with NDP-MSH (10^{-7} M, 36 h) prior to treatment with Luperox ($1.5x10^{-4}$ M, 30 min) and collected for comet assay. Cells were also treated with 10 μg/ml SC79, an activator of AKT, before the Luperox challenge. Histograms show the mean average of the tail moment of treated cells relative to the tail moment of untreated cells (n = 3 independent experiments with at least 100 comets scored in each case, error bars and statistical analysis as in Figure 9). Representative immunoblots and their quantification for pAKT are shown to confirm AKT inhibition (n = 3, error bars and p values as above, Tukey's test was used for multiple comparison).

To confirm these results, we evaluated 8-oxodG levels under the same experimental conditions as for determination of SBs, using A375 and SKMEL28 melanoma cells. Again, NDP-MSH blocked Luperox-induced oxidative damage, whereas AKT inhibition abolished the reduction of 8-oxodG levels afforded by NDP-MSH stimulation in both MC1R-variant melanoma cell lines (Figure 20). In addition, activation of AKT prior to the oxidative challenge decreased 8-oxodG levels in A375 (Figure 20A) and SKMEL28 cells (Figure 20B).

Overall, these data show that: i) the AKT pathway is triggered by variant MC1R activation, but not downstream of WT MC1R; ii) activation of AKT signaling is blunted by high cAMP levels in human melanocytes and melanoma cells; and iii) activation of the AKT pathway is responsible for must, if not all, the clearance of DNA oxidative lesions mediated by variant MC1R signaling.

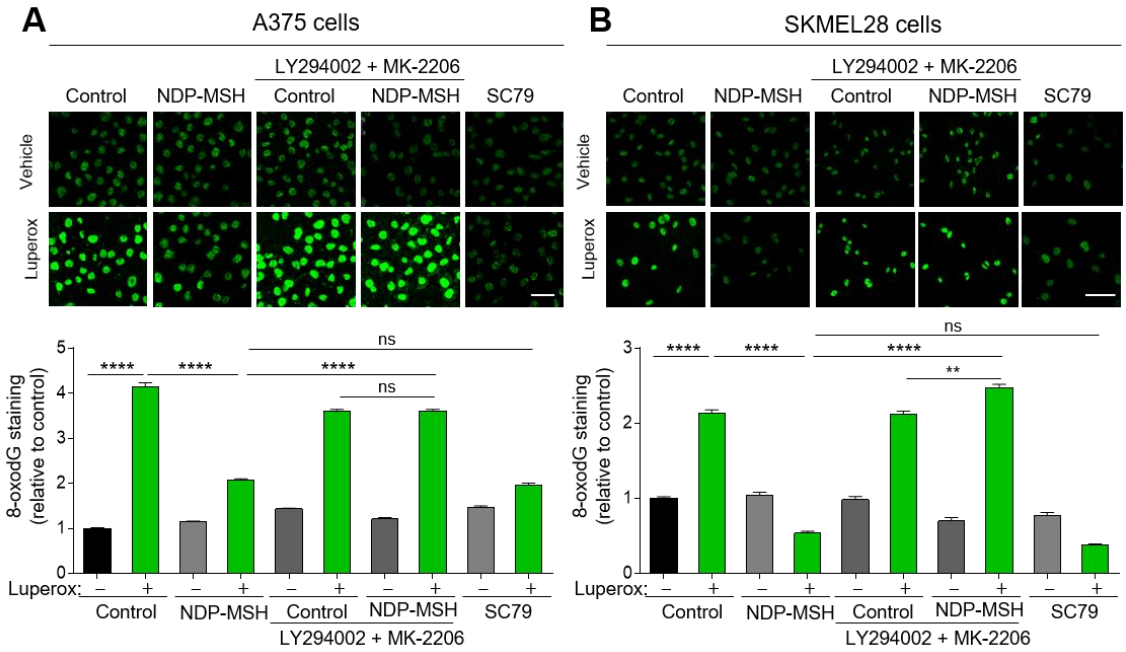

Figure 20. Involvement of AKT activation in variant MC1R-dependent reduction of oxidative DNA damage. A375 (A) and SKMEL28 (B) melanoma cells, were pretreated for 1 h with LY294002 ($2x10^{-5}$ M) and MK-2206 ($5x10^{-6}$ M), to block AKT stimulation. Then cells were stimulated with NDP-MSH (10^{-7} M, 36 h) prior to treatment with Luperox ($1.5x10^{-4}$ M, 30 min). Cells were also treated with 10 μg/ml SC79, an activator of AKT, before the Luperox challenge. After 8-oxodG immunostaining, samples were examined and quantified

as explained in material and methods section 18. At least 200 randomly selected cells were quantified. Representative confocal images of 8-oxodG immunostaining are shown (bar size: 50 μm), as well as quantitative analysis of nuclear 8-oxodG fluorescence intensity in each condition (n = 3 independent experiments, error bars are mean±SEM, two-sided one-way ANOVA was used to generate p values, **p<0.01, ****p<0.0001)

Since the BER pathway mediates clearance of most oxidative lesions, including 8-oxodG and SSBs, we hypothesized that at least one of the subtypes of this pathway should be involved in the protective action of variant MC1R. We compared the induction by NDP-MSH of two key BER enzymes, OGG and APE-1/Ref1 in HBL melanoma cells and melanoma cells carrying variant MC1R. OGG is the primary enzyme responsible for the BER rate-limiting recognition and excision of 8-oxodG. Mice lacking a functional *OGG1* gene have increased levels of 8-oxodG and a higher risk for cancer[382]. Alternative splicing of the C-terminal region of the gene classifies splice variants into two major groups (OGG1 and OGG2), depending on the last exon of the sequence. APE-1/Ref-1 creates a nick in the phosphodiester backbone of the abasic site created by OGG or other DNA glycosylases, which is further processed to repair the primary lesion[383]. Cells were stimulated with the MC1R agonist for up to 36 h and we determined the expression of BER enzymes by Western blot. In all cell types tested, treatment with NDP-MSH induced the two BER components (Figure 21). In WT MC1R HBL cells, NDP-MSH induced both OGG and APE-1/Ref-1 in a cAMP-dependent fashion, since the AC inhibitor DDA, abolished the increase of the two key components of BER triggered by the MC1R agonist (Figure 21A). These findings were consistent with previously reported studies that showed OGG and APE-1/Ref-1 induction in MC1R-WT melanocytes treated with αMSH[329].

In *MC1R*-variant HMCs with impaired cAMP signaling A375 and SKMEL28 cells, NDP-MSH also mediated a significant induction of OGG1/2 and APE-1/Ref1. (Figure 21B). Pharmacological inhibition of AKT abolished variant MC1R-dependent induction of OGG and APE-1/Ref1 (Figures 21B and 21C). We confirmed the results obtained by Western blot by assessing expression of APE-1/Ref1 enzyme in A375 and SKMEL28 melanoma cells by immunostaining under identical experimental conditions (Figure 21C). Analysis of APE-1//Ref1 expression by immunostaining confirmed that NDP-MSH mediated the AKT-dependent induction of the enzyme in MC1R variant cells.

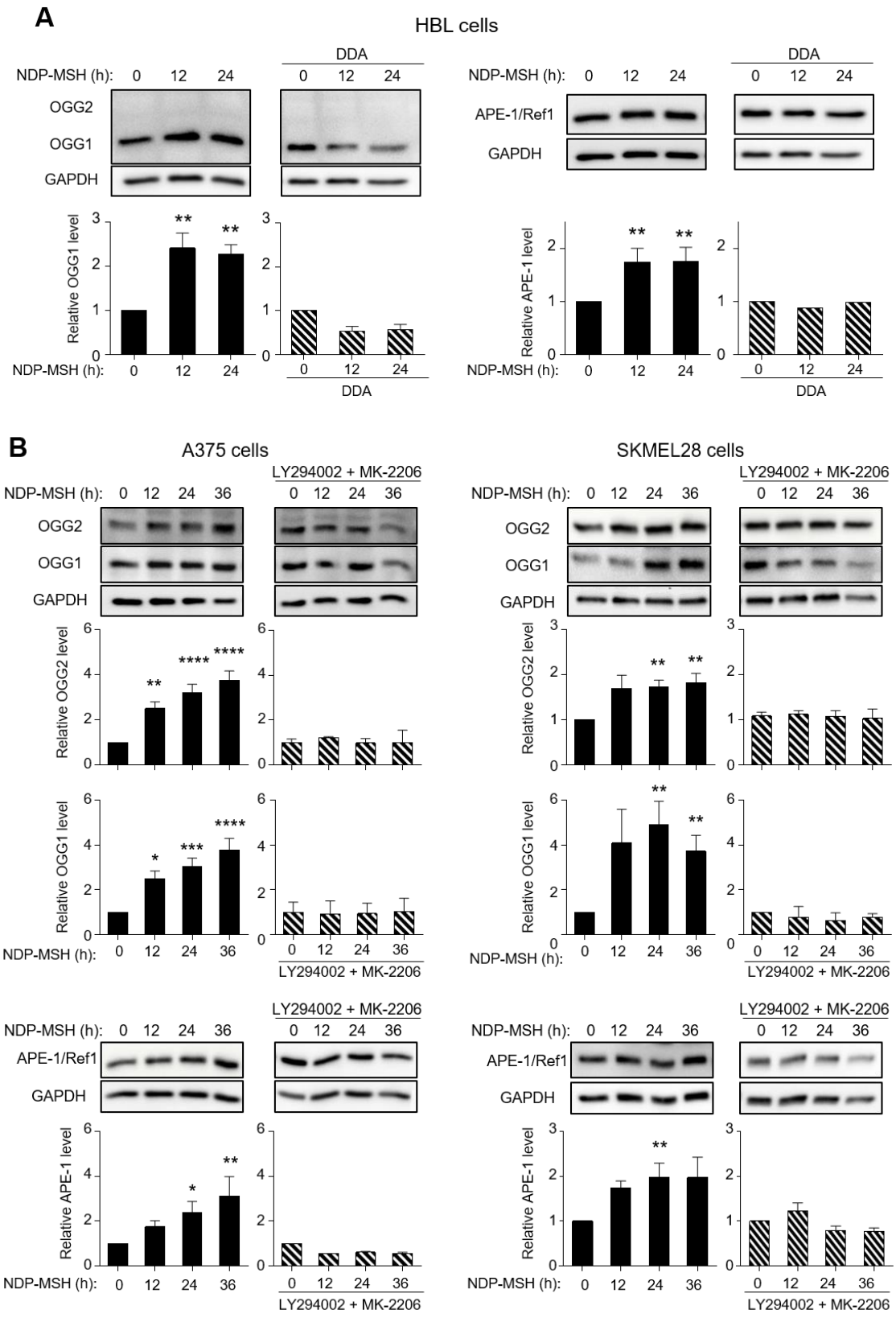
A
HBL cells
NDP-MSH (h): 0 12 24
DDA
OGG2
OGG1
GAPDH
Relative OGG1 level
APE-1/Ref1
Relative APE-1 level
B
A375 cells
SKMEL28 cells
LY294002 + MK-2206
NDP-MSH (h): 0 12 24 36
Relative OGG2 level

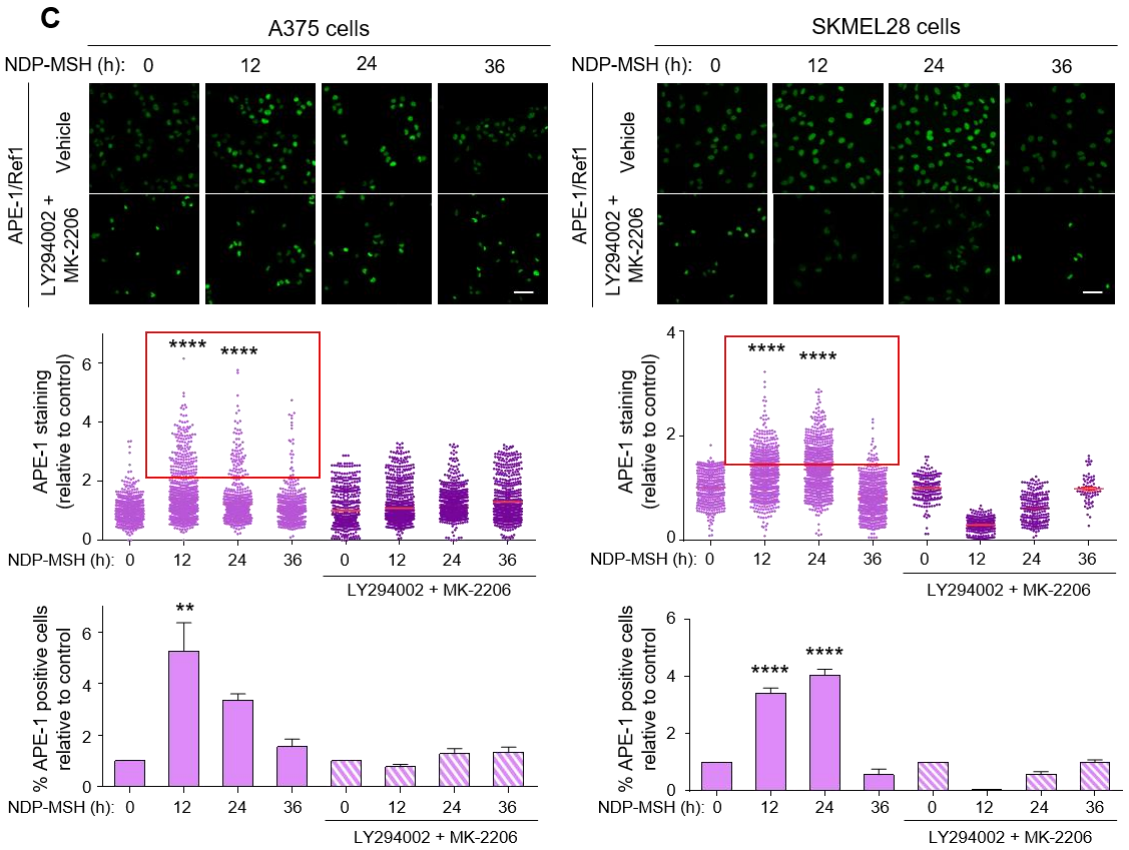

Figure 21. Induction of BER enzymes by NDP-MSH in HBL, A375 and SKMEL28 melanoma cells. HBL melanoma cells (A), with or without pretreatment with $2.5x10^{-3}$ M DDA (hatched bars) were stimulated with 10^{-7} M NDP-MSH at the indicated time points. Expression of OGG1/2(left) and APE-1/Ref-1 (right) was estimated by Western Blot. Representative immunoblots (top) and quantification (bottom) are shown. Quantification of 3 independent experiments using GAPDH signal as loading control is shown below the blots. Values were normalized to the 0 time-point (n = 3, error bars are mean±SEM, two-sided Student´s t test was used to generate p value **p<0.01). **(B) Effect of AKT inhibition on OGG (upper) or APE-1/Ref-1 (bottom) protein levels in A375 (left) or SKMEL28 (right) melanoma cells.** Cells were stimulated with 10^{-7} M NDP-MSH for the times shown, with or without pretreatment with LY294002 ($2x10^{-5}$ M) and MK-2206 ($5x10^{-6}$ M) (hatched bars) and analyzed by Western Blot. Representative immunoblots are shown for each cell line. Quantification of 3 independent experiments using GAPDH signal as loading control is shown below the blots (n = 4, error bars and statistics as in Figure 18). **(C) Effect of AKT inhibition on APE-1/Ref1 levels in A375 (left) or SKMEL28 (right) melanoma cells.** Both melanoma cell lines were treated as described in section B and stained for APE-1/Ref-1. At least 200 randomly selected nuclei were quantified as described in material and methods section 18. Representative confocal images (top) (bar size: 50 μm) and quantifications (bottom) are shown for each cell line. The upper histograms show the quantification of nuclear APE-1/Ref1 fluorescence intensity. In the lower histograms the data represent the number of positive cells relative to control, considering as positive cells those with a fluorescence intensity value higher than the threshold (n = 3 independent experiments, error bars are mean±SEM, two-sided one-way ANOVA was used to generate p values **p<0.01, ****p<0.0001).

Finally, we wished to confirm that AKT activation in MC1R-variant HMCs is sufficient to cause induction of BER enzymes. To this end, A375 or SKMEL28 cells were treated with SC79 for various times and OGG1/2 or APE-1/Ref1 were estimated by Western blot in cell-free lysates (Figure 22A). In both cell types, SC79 increased significantly the expression of OGG and APE-1/Ref1. Induction of APE-1/Ref1 was further confirmed by immunostaining of control and SC79-treated cells (Figure 22B).

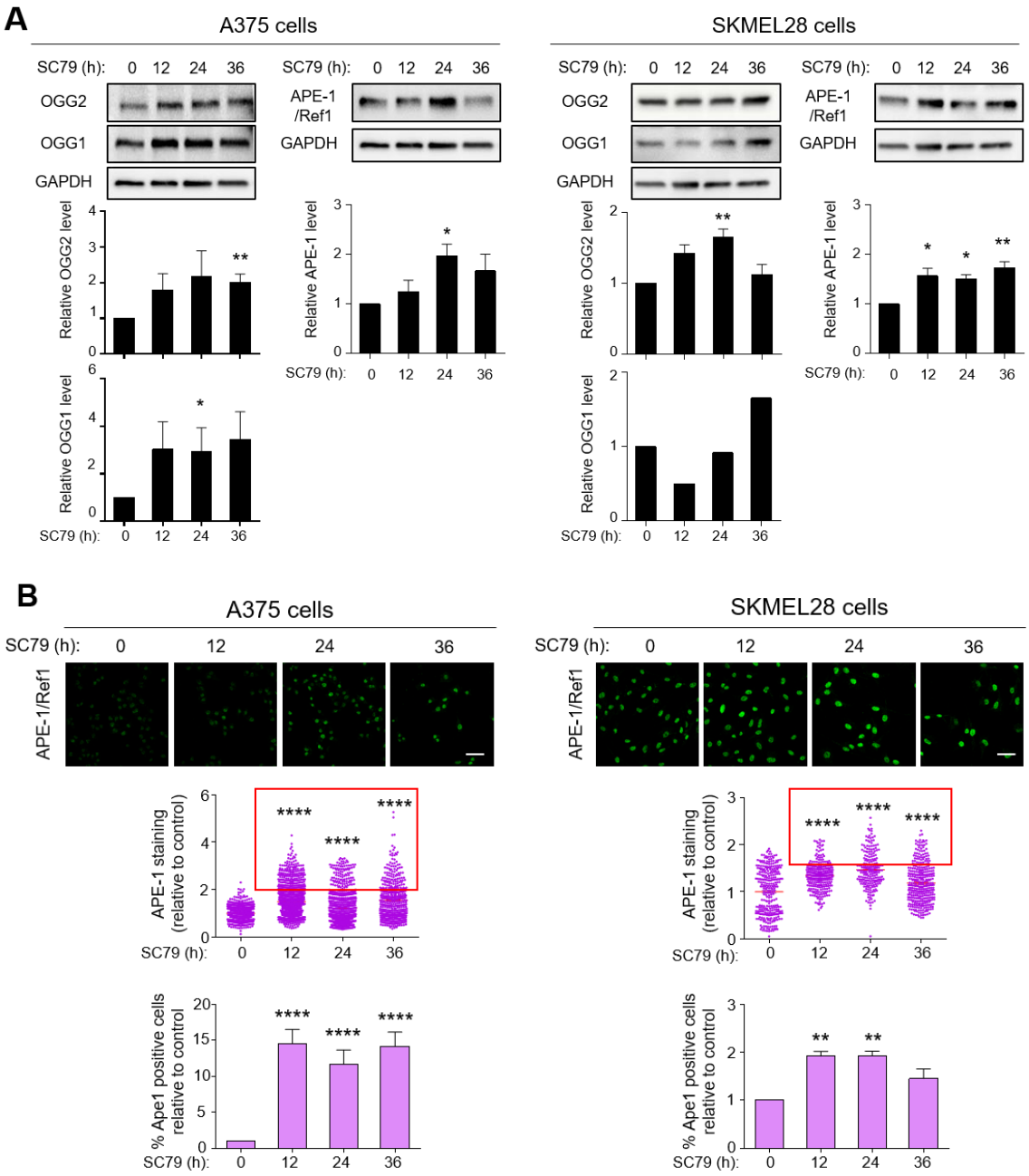

Figure 22. Effect of AKT activation in OGG and APE-1/Ref-1 expression. A375 (left) or SKMEL28 (right) cells were treated with 10 μg/ml SC79, an activator of AKT, for the times shown. **(A) OGG (left) and APE-1/Ref-1 (right) expression were estimated by Western Blot for each cell line**. Representative immunoblots (top) and quantification (bottom) of 4 independent experiments are shown. GAPDH signal was used as loading control. Values were normalized to the 0 time-point (n = 3, error bars are mean±SEM, two-sided Student´s t test was used to generate p values, *p<0.05, **p<0.01). **(B) APE-1/Ref-1 expression was analysed by immunostaining.** Representative confocal images (top) and quantification (bottom) are shown for each cell line. Histograms and statistics as described in Figure 21C.

Activation of AKT downstream of variant MC1R is mediated by ROS generation

Overall, the data reported above showed that AKT activation is sufficient to stimulate BER in MC1R-variant melanoma cells, and is necessary for NDP-MSH-mediated induction of BER enzymes in these cells. However, the molecular details of the pathway leading from variant MC1R to activation of AKT are unknown. Our group showed previously that variant MC1R stimulated with MC agonists transactivates cKIT RTK[310]. Since activated RTKs interact with PI3K to achieve AKT signaling, one obvious possibility was a variant MC1R → cKIT → PI3K → AKT pathway. However, this possibility was ruled out by the lack of cKIT expression in A375 and SKMEL28 melanoma cells (Figure 23), as opposed to HBL cells.

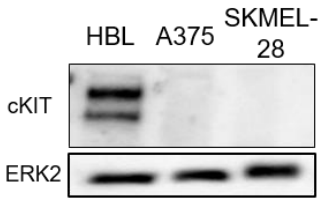

Figure 23. Expression of cKIT RTK in HBL, A375 and SMEL28 melanoma cells. Representative immunoblot of cKIT expression (n = 3).

On the other hand, although ROS have been considered as damaging agents, there is a growing body of evidence providing that, at low levels, they can act as signal molecules modulating activity, abundance and cellular localization of target proteins[384–386]. Redox signaling mediated by ROS can activate a number of protein kinases, including AKT, although it is often unclear whether this activation is carried out by direct induction by ROS of the kinases, or by inhibition of phosphatases[387,388]. In addition, it is well established that certain physiological effects of GPCRs are mediated by ROS acting as second messengers, and various signaling pathways linking GPCRs and activation of ROS-generating NADPH oxidases have been described (reviewed by[389]). Accordingly, we investigated a possible role of ROS in AKT activation downstream of MC1R.

Stimulation of MC1R-variant melanoma cells with NDP-MSH caused a rapid increase in intra- and extra- cellular ROS levels, as measured with H_2DCFDA and AmplexRed fluorescent dyes, respectively (Figures 24A and 24B). This observation supported the notion that ROS can act as second messengers for certain NDP-MSH physiological actions. To evaluate whether MSH-

induced ROS could be responsible for AKT activation, variant-MC1R HMCs were challenged with short pulses of low levels of Luperox ($8x10^{-5}$ M) (rather than with higher Luperox concentrations used for the induction of oxidative stress and DNA lesions) and the activatory AKT phosphorylation was analyzed by Western blot. In both A375 and SKMEL28 cell lines, treatment with exogenous ROS stimulated AKT efficiently (Figure 24C) Importantly, the low concentration of exogenous Luperox used in this experiment was optimal, as it increased intracellular and extracellular ROS to levels similar to those achieved by NDP-MSH stimulation.

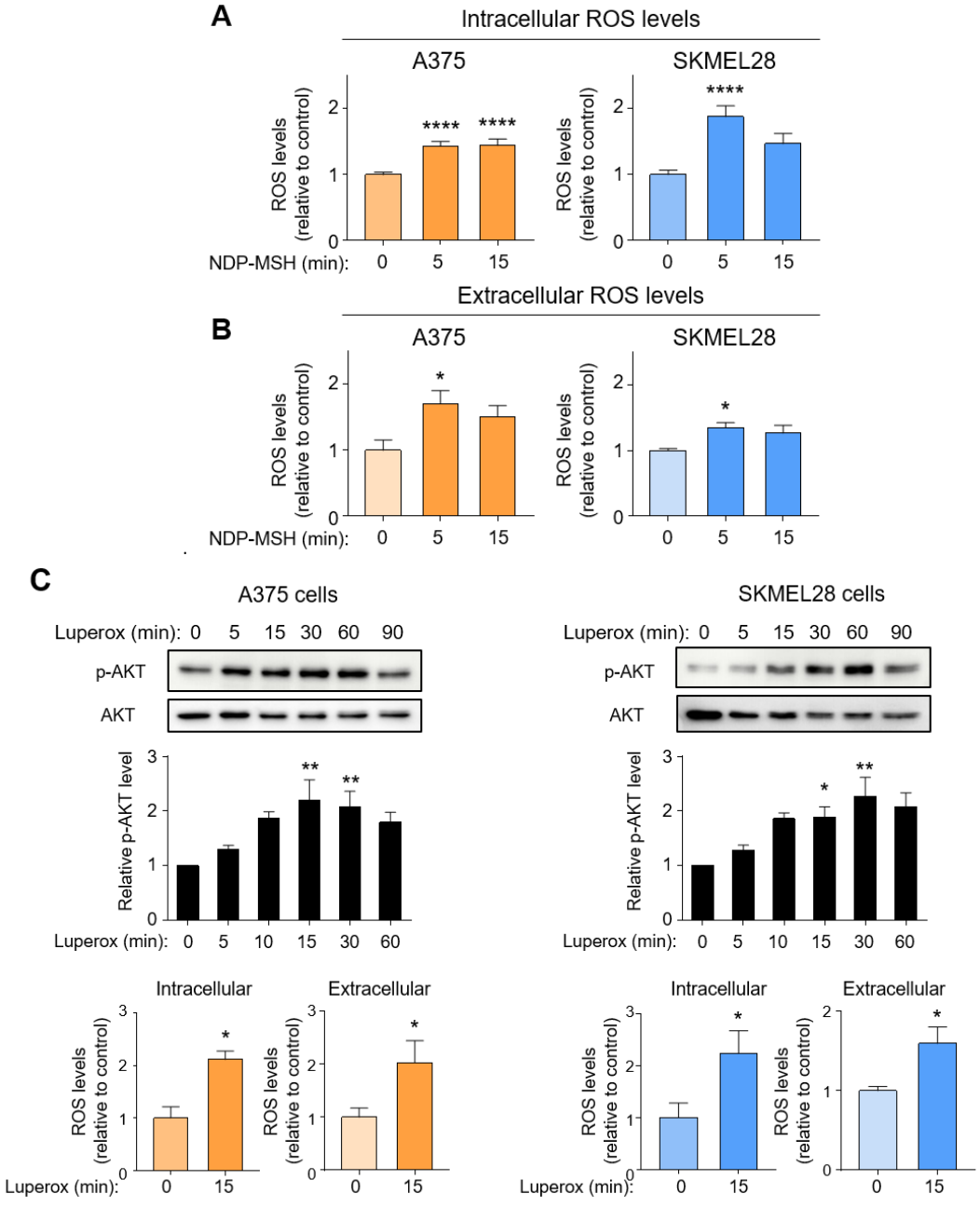

Figure 24. Involvement of ROS in variant MC1R-mediated AKT activation. (A-B) MSH-induced ROS production in A375 and SKMEL28 melanoma cells. A375 (left) and SKMEL28 (right) cells were pretreated with 10^{-7} M NDP-MSH for the times indicated and total ROS measurement was assessed with fluorescent dyes. (A) Intracellular ROS were measured with H_2DCFDA. Data represent the mean fold-change of ROS-induced dichlorofluorescein fluorescence and are given as mean ±SEM (n = 12, with 6 replicate wells for each experiment, error bars are mean±SEM, two-sided Student´s t test was used to generate p values, ****p<0.0001). (B) Extracellular ROS levels were measured with AmplexUltraRed assay. Data represent the mean fold-change of ROS-induced resorufin fluorescence and are given as mean ±SEM (n = 3, with 6 replicate wells for each experiment, statistical analysis as above, *p<0.05). **(C) Kinetics of AKT activation by Luperox treatment in MC1R-variant HMCs**. Cells were serum-starved and challenged with Luperox ($8x10^{-5}$ M) for the times indicated. Representative immunoblots (top panel) and quantification of the intensity of pAKT signal relative to the control (bottom panel) are shown. Total AKT1/2/3 was used as loading control (n = 6, error bars and statistic analysis as in Figure 18). Intracellular (left) and extracellular (right) ROS levels in Luperox-treated cells ($8x10^{-5}$ M, 15 min) are shown below the blots. ROS levels were measured as above (n = 3 with 6 replicate wells/experiment, *p<0.05).

MSH induces NOX activation in *MC1R* variant human melanoma cells

Having established that MSH stimulates ROS production to achieve intracellular levels capable to trigger AKT activation, we next tackled two questions, namely whether NDP-MSH-induced intracellular ROS are actually responsible for AKT activation downstream of MC1R and what is the source of these species. Within melanocytes and HMCs, ROS can be generated as byproducts of the activity of melanosomes and mitochondria, by certain enzymatic reactions or as the main product of the action of a family of enzymes, the NADPH oxidases[385,389]. Among these, NOX enzymes have been shown to be activated by various growth factors and cytokines to generate H_2O_2 or $O_2^{\bullet-}$ for signaling processes in non-phagocytic cell types[384]. The NOX family of NADPH oxidases comprises 7 members (NOX1 to NOX5, DUOX1 and DUOX2), among which NOX1 could be particularly relevant in our setting, since it is known to undergo regulation downstream of several GPCRs[57], it is inhibited by cAMP via PKA-mediated phosphorylation[341,342] and it has been involved in UVA- and UVB-induced signaling in human keratinocytes[56,57,87]. Accordingly, to answer the questions mentioned above, we decided to ascertain NOX1 expression in our cell lines and to compare ROS production and AKT activation by NDP-MSH in control conditions and in cells pretreated with the antioxidant ebselen (which would block ROS-dependent processes) or with inhibitors of NADPH oxidases.

All the cell lines tested, WT MC1R HBL cells, and A375 and SKMEL28 cells carrying MC1R variant alleles, expressed detectable protein levels of NOX1 enzyme, consistent with NOX1 as a source of ROS upon MSH stimulation (Figure 25A). To test this hypothesis, we used: i) DPI, a low specificity general NOX inhibitor and ii) GKT137831, a potent dual NOX1/4 inhibitor[390,391]. Cells were treated with these compounds for at least two hours prior to NDP-MSH stimulation, and ROS production was analyzed. We also used the antioxidant ebselen before the NDP-MSH

challenge to neutralize the increase of ROS triggered by the hormone. MC1R agonist-induced ROS production was blocked by NOX inhibition and antioxidant treatment in A375 (Figure 25B) and SKMEL28 (Figure 25C) cells.

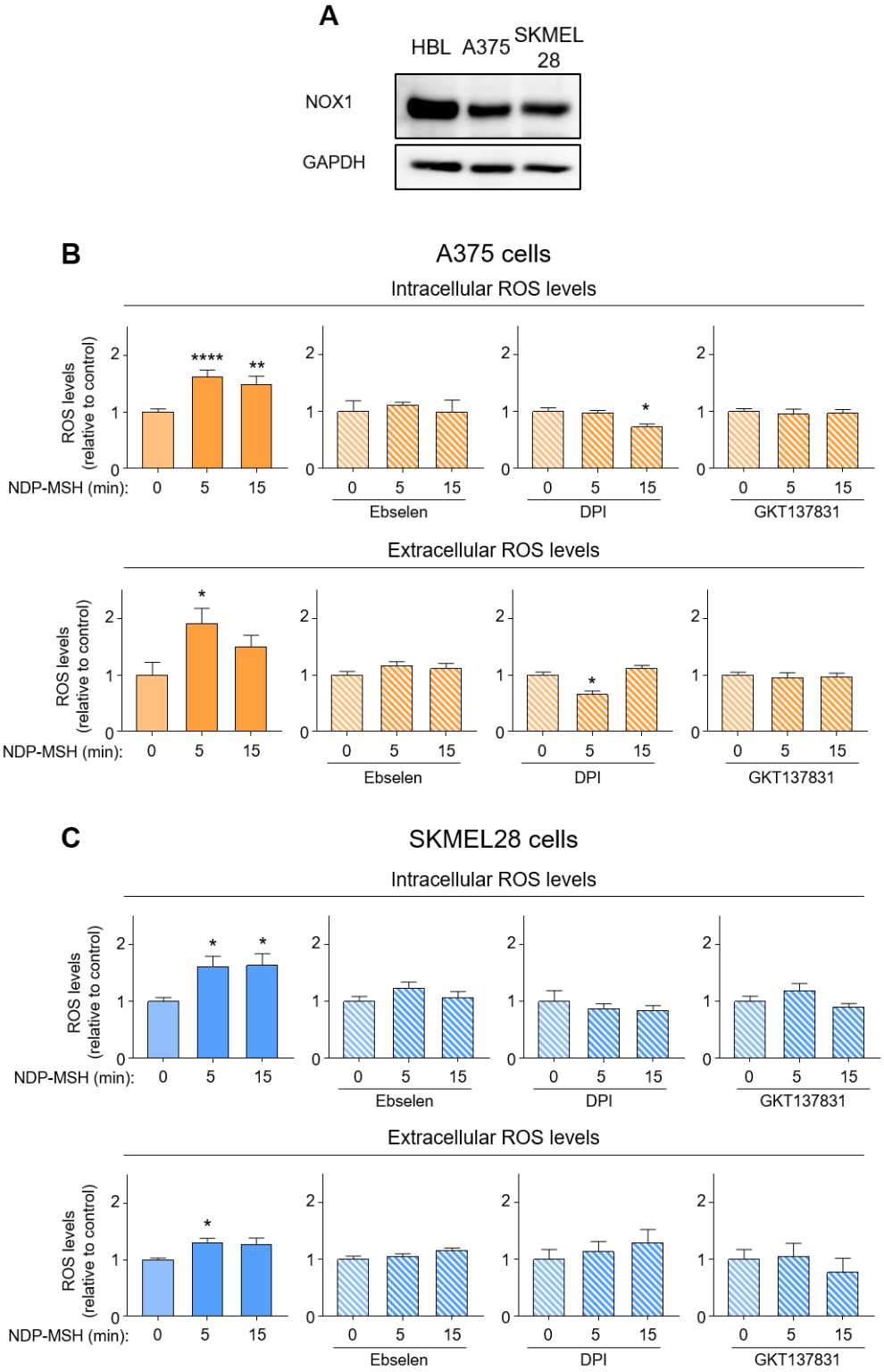

Figure 25. Effect of NOX inhibition on MSH-induced ROS generation in MC1R-variant melanoma cells. (A) NOX expression in HBL, A375 and SKMEL28 melanoma cells. Representative immunoblot showing NOX1 protein levels. **ROS production in A375 (B) and SKMEL28 (C) cells**. Both cell lines were pretreated with (from left to right) ebselen ($4x10^{-5}$ M, 12h), DPI ($2.5x10^{-5}$ M, 2h) or GKT137831 ($5x10^{-5}$ M, 2h) (hatched bars) prior to NDP-MSH stimulation (10^{-7}M, 5 and 15 min). Then, intracellular (upper) and extracellular (bottom) ROS levels were assessed with the H_2DCFDA and the AmplexUltraRed assays, respectively. Histograms showing the mean fold-change of ROS-induced dye fluorescence are shown. Data are given as mean ±SEM (n = 3 with 6 replicate wells/experiment, *p<0.05, **p<0.01, ****p<0.0001, calculated with a two-sided Student´s t test).

Next, pAKT induction was examined using the same experimental conditions as described for assessment of ROS production. Pharmacological inhibition of NOX enzymes and antioxidant treatment abolished AKT activation by MSH in A375 (Figure 26A) and SKMEL28 (Figure 26B) cells. Therefore, NOX-dependent signaling accounts for functional coupling of variant MC1R and AKT.

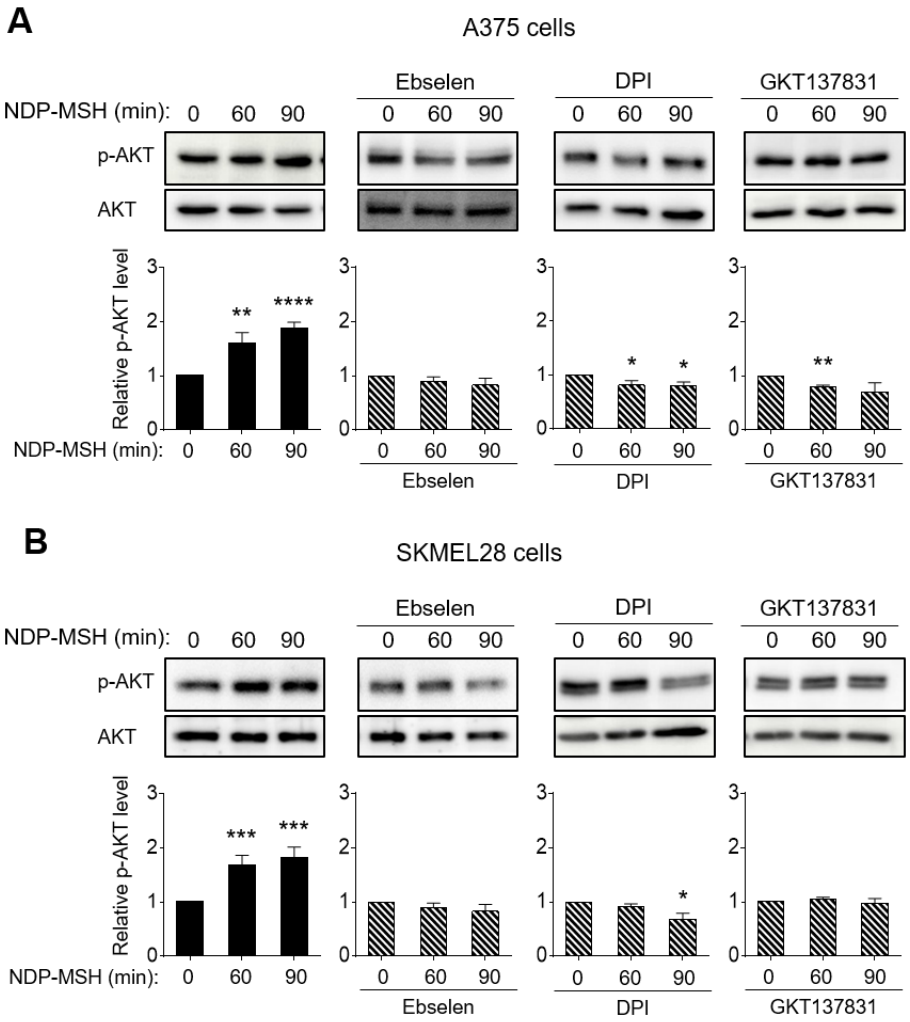

Figure 26. Effect of NOX inhibition on AKT activation triggered by MC1R variant. A375 (A) and SKMEL28 (B) cells were pretreated with (from left to right) ebselen ($4x10^{-5}$ M, 12h), DPI ($2.5x10^{-5}$ M, 2h) or GKT137831 ($5x10^{-5}$ M, 2h) (hatched bars) prior to NDP-MSH stimulation (10^{-7}M) for the times shown and pAKT levels were analyzed by Western blot. Representative immunoblots for pAKT1/2/3 are shown for each cell line. Quantification of the intensity of pAKT signal relative to the control is shown below. Total AKT1/2/3 was used as loading control (n = 4, error bars and statistics as in Figure 18).

Conversely, in HBL melanoma cells, NDP-MSH did not augment ROS levels (Figure 27A) consistent with its inability to increase pAKT levels in these cells (Figure 27B). In fact, MSH actually decreased ROS levels. This finding is consistent with the inhibition of NOX by cAMP-activated PKA reported by others[341,342] and suggests that basal NOX activity maintains a tonic level of ROS in HBL melanoma cells [208,216,329]. Moreover, the inhibition of NOX1/4 with GKT137831 had no effect on ROS or AKT phosphorylation levels in HBL cells (Figures 27A and 27B), which shows that neither NOX nor AKT are activated downstream of MC1R WT signaling. Therefore, activation of NOX by MSH is only efficiently triggered by MC1R variant to increase AKT signaling.

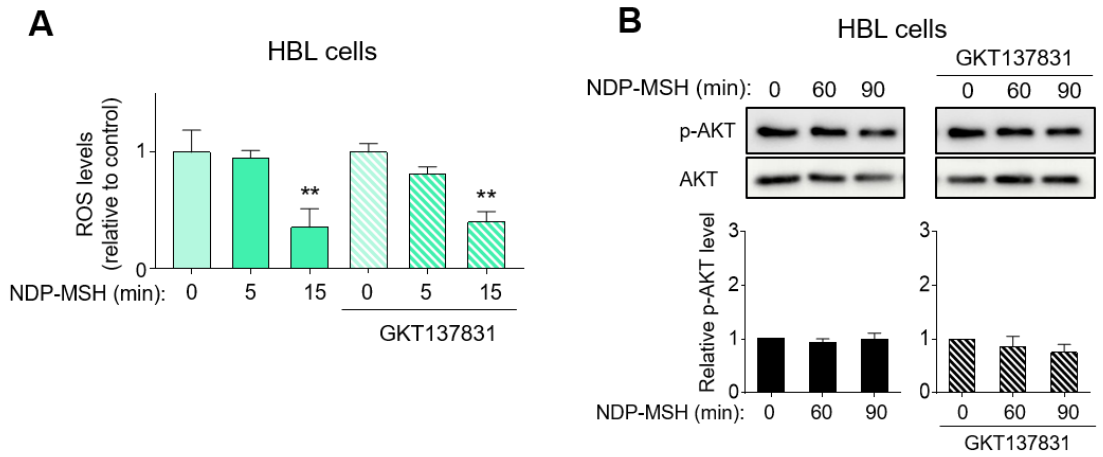

Figure 27. Effect of NOX inhibition in ROS production and AKT activation in MC1R-WT cells. Cells were serum-deprived for at least 3 h and stimulated with NDP-MSH (10^{-7} M) with or without pretreatment with GKT137831 ($5x10^{-5}$ M, 2h) (hatched bars). **(A) ROS levels were measured with the H_2DCFDA assay**. Data represent the mean fold-change of ROS-induced dichlorofluorescein fluorescence and are given as mean ±SEM (n = 3 with 6 replicate wells/experiment, **p<0.01). **(B) Activatory AKT phosphorylation was assessed by Western blot**. Immunoblots (top) and quantification of 3 independent blots for pAKT are shown (n = 3, error bars are mean±SEM).

On the other hand, we have shown previously that high cAMP levels blunt AKT activation in MC1R-variant HMCs stimulated with NDP-MSH (Figure 18), indicating a negative regulation of the AKT pathway by cAMP. Since MC1R WT does not promote ROS generation when stimulated with agonist (Figure 27A), but rather decreases ROS levels, we hypothesized that cAMP may act at this step to block AKT signaling. Accordingly, we examined the effects of cAMP on the functional status of NOX in MC1R-variant melanoma cells. We increased intracellular cAMP levels

with dbcAMP in A375 and SKMEL28 cells prior to NDP-MSH stimulation and then, ROS levels were measured. High levels of cAMP blocked ROS generation downstream of variant MC1R (Figure 28A). On the other hand, we also blocked AC activation with DDA in WT MC1R cells. AC inhibition allowed activation of ROS generation downstream of MC1R WT (Figure 28A). To extend these findings, we studied the effect of cAMP in AKT phosphorylation in A375 and SKMEL28 melanoma cells after treatment with low levels of Luperox ($8x10^{-5}$ M). As previously shown (Figure 24C), treatment with low levels of exogenous ROS activated AKT efficiently. Increasing the intracellular concentration of cAMP by treatment with dbcAMP did not affect the stimulatory effect of ROS (Figure 28B), thus suggesting that cAMP exerts its inhibitory effect upstream of ROS, likely at the level of ROS production by NOX1.

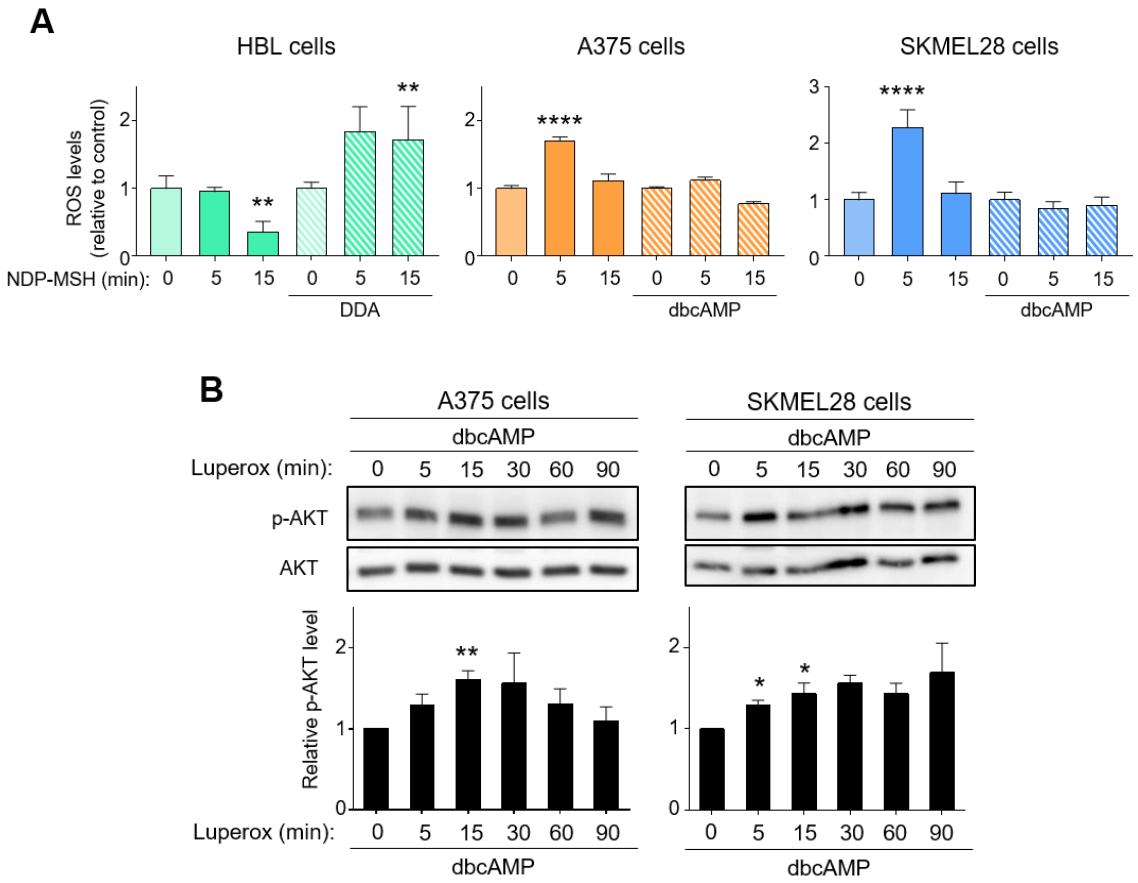

Figure 28. Relationship between ROS production and cAMP signaling. (A) Intracellular ROS levels in HBL, A375 and SKMEL28 melanoma cells. HBL cells were preincubated with DDA ($2.5x10^{-3}$ M, 1 h) to block cAMP production (hatched bars), and conversely, A375 and SKMEL28 cells, were incubated with dbcAMP ($3x10^{-6}$ M, 30 min) to increase cAMP levels (hatched bars) prior to stimulation with 10^{-7} M NDP-MSH for 5 and 15 min. ROS levels were measured with the H_2DCFDA assay. Data represent the mean fold-change of ROS-induced dichlorofluorescein fluorescence and are given as mean ±SEM (n = 3 with 6 replicate wells/experiment, **p<0.01, ****p<0.0001). **(B) Kinetics of AKT induction by Luperox**. A375 and SKMEL28 melanoma cells were incubated with dbcAMP ($3x10^{-6}$ M, 30 min) prior to Luperox treatment ($8x10^{-5}$ M).

Representative immunoblots and quantification of 3 independent blots for pAKT are shown (n = 3, error bars are mean±SEM *p<0.05, **p<0.01, calculated with a two-sided Student´s t test).

Role of NOX is required for variant MC1R-induced repair of oxidative DNA damage

So far, our results have shown, for the first time, that NOX-derived ROS led to AKT activation downstream of variant MC1R. As AKT activation downstream of MC1R induces clearance of oxidatively lesions such as 8-oxodG (Figure 20) it is reasonable to assume that a variant MC1R → NOX → AKT → BER axis is operative in melanocytes and melanoma cells. However, a formal link between NOX activation and induction of BER by NDP-MSH remains to be established. Therefore, we next explored NOX involvement in MC1R and AKT-dependent reduction of oxidative DNA damage. To this end, we prevented ROS generation with pharmacological NOX inhibitors and with ebselen and assessed 8-oxodG levels in Luperox-pulsed ($1.5x10^{-4}$ M, 30 min) cells. Of note, the antioxidant treatment with ebselen was performed before and during MSH stimulation, but ebselen was removed from the culture medium and cells were gently washed before the oxidative challenge. Under these experimental conditions, ebselen only exerts its antioxidant effect against rapidly generated (after 5-15min) NOX-induced ROS, but not during the oxidative challenge performed with Luperox. Both ebselen and the NOX inhibitors DPI and GKT137831 abolished MC1R-dependent clearance of 8-oxodG in A375 (Figure 29A) or SKMEL28 (Figure 29B) cells. Thus, NOX activation contributed to the MC1R-dependent reduction of oxidative DNA damage.

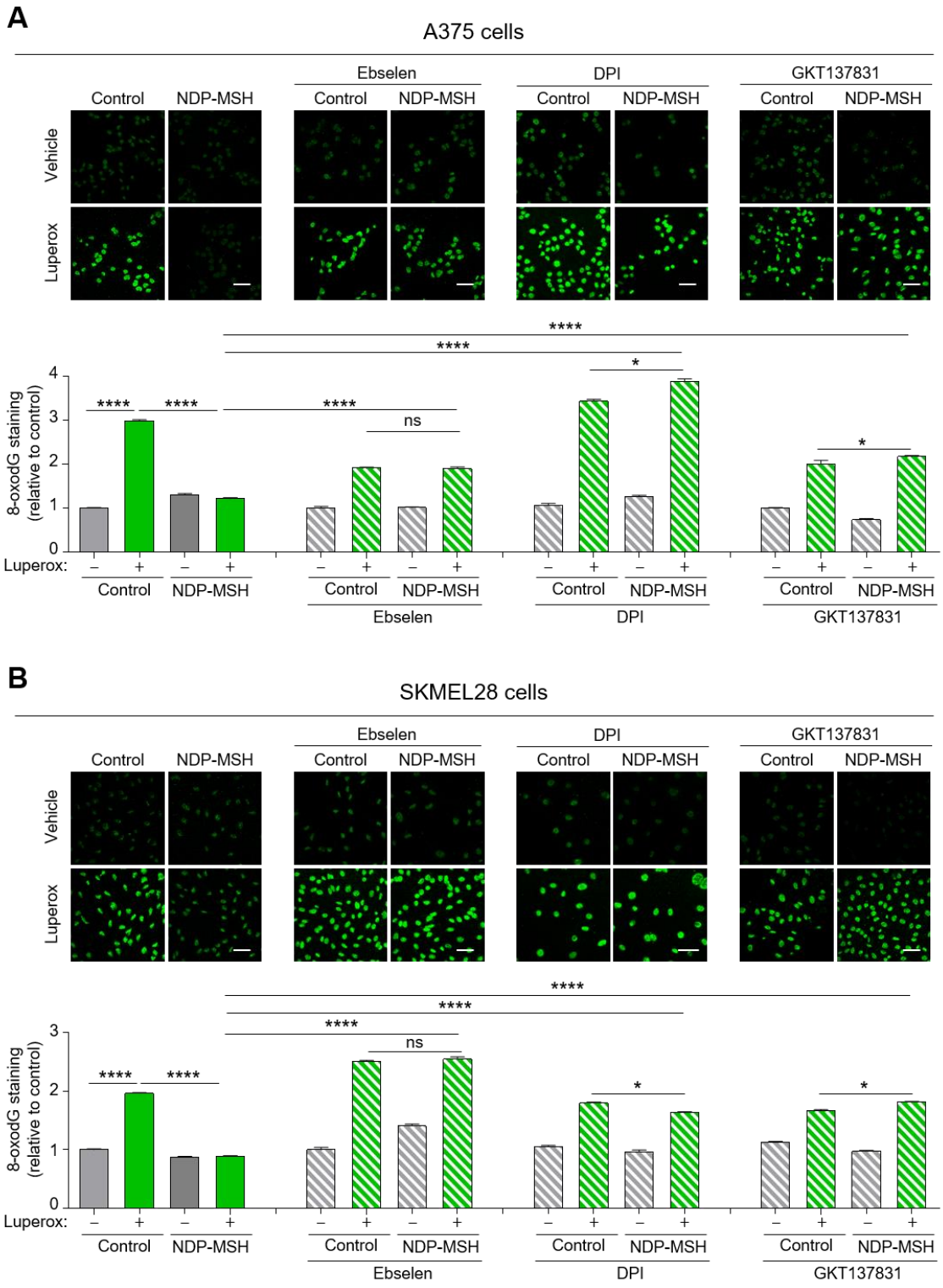

Figure 29. NOX-dependent protection against Luperox-induced oxidative DNA damage in A375 (A) and SKMEL28 (B) melanoma cells. ROS increase was neutralized with ebselen ($4x10^{-5}$ M, 12h) and NOX activation was blocked with the inhibitors DPI ($2.5x10^{-5}$ M, 2h) or GKT137831 ($5x10^{-5}$ M, 2h) (hatched bars). Then cells were stimulated with NDP-MSH (10^{-7}M, 24h) before the oxidative challenge with Luperox ($1.5x10^{-4}$ M, 30 min). Cells were fixed and immunostained for 8-oxodG. Quantitative analysis, error bars and statistics as in Figure 9 (n = 3 independent experiments).

Since we have shown that the variant MC1R-dependent protection against oxidative DNA damage relies on the activation of the BER pathway (Figures 21 and 22), we also evaluated the involvement of NOX in the induction of BER enzymes. We ascertained blockade of OGG and APE-1/Ref1 induction by NOX inhibitors and by the antioxidant ebselen (Figures 30A and 30B). Thus, a variant MC1R → NOX → ROS → AKT signaling axis enhances BER and reduces the levels of 8-oxodG. Moreover, in MC1R-WT HBL melanoma cells, induction of OGG and APE-1/Ref-1 by MSH was not blocked by GKT137831, ruling out the involvement of NOX in activation of DNA repair enzymes. Accordingly, activation of the BER pathway is independent of NOX and AKT in MC1R-WT cells. This is in accordance with the results reported in Figure 21, which showed that induction of BER enzymes required functional coupling of MC1R WT to the cAMP signaling pathway.

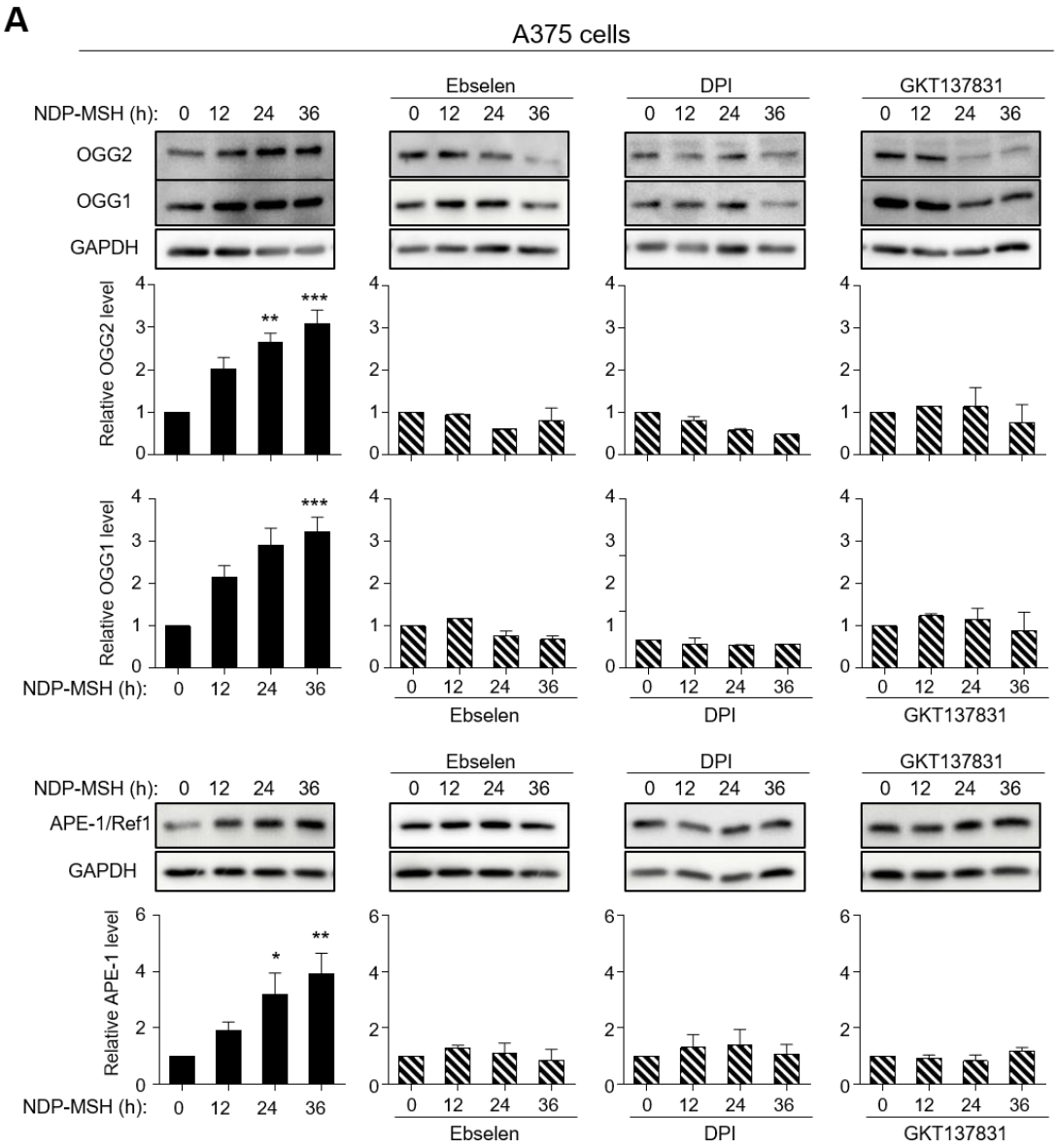

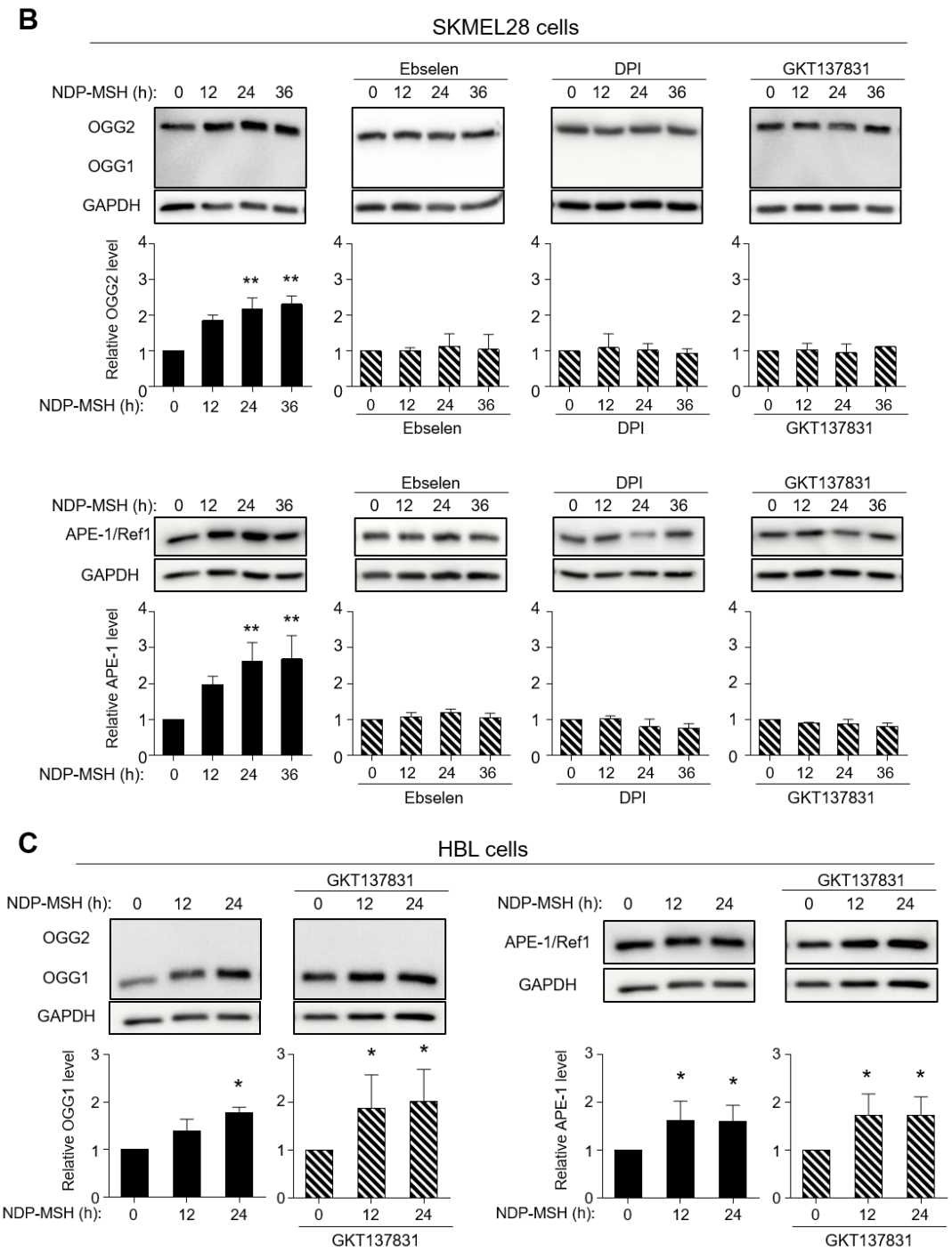

Figure 30. Effect of NOX inhibition in MSH-induced BER enzymes expression. (A-B) NOX-dependent activation of BER pathway in melanoma cells carrying MC1R-variant alleles. A375 (A) and SKMEL28 (B) melanoma cells were stimulated with NDP-MSH (10^{-7}M) for the times shown with or without pretreatment with (from left to right) ebselen ($4x10^{-5}$ M, 12h), DPI ($2.5x10^{-5}$ M, 2h) or GKT137831 ($5x10^{-5}$ M, 2h) (hatched bars) and the kinetics of induction of OGG1 (top) and APE-1/Ref1 (bottom) was followed by Western blot. Representative immunoblots (top), and quantification of 3 independent experiments (bottom) are shown for each cell line (error bars and statistics as in Figure 18). **(C) Effect of NOX1/4 inhibition in BER induction by activation of MC1R-WT**. OGG1 (left) and APE-1/Ref1 (right) induction was determined by Western blot. BER enzymes immunoblots (top) and quantification (bottom) are shown (n = 3, *p<0.05, calculated with two-sided t student test).

Overall, our results indicate that variant MC1R-dependent repair of oxidized bases most likely involves BER activation via NOX-mediated ROS signaling. Conversely, MC1R-WT activates the BER repair pathway by a cAMP-dependent and NOX-AKT-independent mechanism.

DISCUSSION

Discussion

It is widely accepted that the efficient UVR response of melanocytes is strongly dependent on MC1R function. The role of MC1R-TUBB3 isoforms and of R-type variants in the regulation of this response required further investigation. We have analyzed some of these issues. On the one hand, we explored the trafficking and signaling properties of the intergenic splice isoforms, which has contributed to a better understanding of their possible biological role. These MC1R-TUBB3 isoforms behave as R variants according to their lack of efficient functional coupling to the cAMP pathway and their decreased cell surface expression due to an aberrant intracellular trafficking. However, the possible role of R variants in protecting against UVR-induced DNA damage by pigment-independent mechanisms remained to be determined. In this respect, we have elucidated a NOX/AKT-mediated protective mechanism against oxidative DNA damage triggered by MC1R variants.

The genes encoding for most if not all GPCRs have been considered intronless for long[392]. However, recent progress in the analysis of the architecture of these genes has shown that they often contain several introns and can undergo alternative splicing events. On the other hand, intergenic splicing giving raise to chimeric molecules is a rare event[393] where transcription proceeds through the region between two adjacent genes to yield a non-canonical chimeric RNA which is further spliced to a final fusion product composed of sequences from the two neighboring genes. To the best of our knowledge, within the large GPCR superfamily, this process has been described only for the P2Y receptor and the SSF1 genes[394] on one hand, and the *MC1R* and *TUBB3* genes on the other[212,213].

We confirmed the occurrence of Iso1 and Iso2 MC1R-TUBB chimeric mRNA species in a panel of 8 HMC lines and a human epidermal melanocytic cell line. We were able to detect the corresponding transcripts in all of them even in the absence of external stimuli, thus showing that expression of Iso1 and Iso2 is a general phenomenon in human melanocytic cells occurring even in the absence of external stimuli such as UVR. We also observed that the ratio of Iso1 and Iso2 transcripts relative to the canonical MC1R-001 transcript was variable in different cell lines. This suggests that Iso1/2 may not merely result from an unregulated error of the transcriptional machinery occurring at a constant rate within the context of the crowded genomic region where *MC1R* is located. Should this be the case, a linear relationship between MC1R-001 and Iso1/2 mRNA would be expected. In keeping with these data, Dalziel and co-workers reported that Iso1/2 expression is a regulated process, activated by αMSH and by the p38 stress activated kinase[213].

When expressed in HEK293T heterologous cells or in human melanocytic cells, the in-frame Iso1 intergenic fusion protein exhibited the expected Mr and cross-reacted with anti-TUBB3 antibodies. Therefore, chimeric mRNA was adequately processed and the resulting protein accumulated at sufficient levels within transfected cells, although its intracellular stability was lower than the one of MC1R-001. On the other hand, Iso2 results from an out-of-frame fusion with *TUBB3* exon 3, skipping exon 1a in the MC1R 3'-UTR. Hence, Iso2 did not cross-react with anti-TUBB3 antibodies. Moreover, its intracellular levels and half-life were low. The shorter half-life of the chimeric proteins was consistent with impaired forward trafficking demonstrated by reduced cell surface expression and high co-localization with the ER marker calnexin. Thus, the ER-resident protein quality control system most likely recognized the chimeric proteins as aberrant, causing their ubiquitylation, extrusion to the cytosol and proteolytic degradation[395].

Both chimerae exhibited very poor ability to activate the cAMP pathway. This might be at least partially due to decreased cell surface expression of the chimeric receptor compared to WT MC1R. Residual cAMP levels after stimulation with a saturating concentration of the superpotent NDP-MSH analog of αMSH were lower than those obtained in cells expressing known RHC-associated MC1R variants with low (V60L and V92M) or high (R151C and D294H) penetrance[177]. Conceivably, chimeric proteins arising from variant MC1R may be even more severely reduced in signaling capacity, but we did not test directly this likely hypothesis. Functional impairment was nevertheless less evident for activation of the ERK cascade. Accordingly, signaling from the MC1R-TUBB3 intergenic splicing isoforms seemed biased in favor of the ERK pathway. A similar behavior has been shown for many natural MC1R variant alleles associated with the RHC phenotype and with increased skin cancer risk[177].

Therefore, when expressed following exposure to UVR, the chimeric isoforms might prevent excessive stimulation of the cAMP pathway without a parallel decrease in MC1R-dependent ERK activation. This effect might be enhanced by the ability of the isoforms to heterodimerize with MC1R-001, which seemed to impair forward trafficking of the canonical form and led to its partial intracellular retention. This was suggested by high co-localization of the canonical protein and the chimeric isoforms in intracellular locations as well as a by an apparently decreased number of αMSH binding sites on the cell surface of cells overexpressing both MC1R forms simultaneously. Although in this case the observed decrease did not reach statistical significance, it appears likely that under normal expression conditions it may become a significant factor.

The observation that expression of the intergenic splicing isoforms is a general feature in HMCs as well as a regulated process[213] strongly suggests that Iso1 and Iso2 might fulfil still

uncharacterized specific actions within melanocytes. Given that both isoforms are hypomorphic in terms of functional coupling to the cAMP pathway, these actions might likely be related with dampening MC1R signaling under specific physiological conditions. UVR-mediated direct transcriptional activation of the *MC1R* gene has been demonstrated in mouse and human melanocytic cells[214,396] as well as in human epidermis *in vivo*[397]. In addition, *MC1R* gene expression is upregulated, apparently via MITF, in human and mouse melanocytes stimulated with αMSH or the cAMP inducer forskolin[215,301,398]. UVR-induced DNA damage in keratinocytes has been shown to stabilize the p53 tumor suppressor, which activates transcription of *POMC* gene encoding for the precursor of αMSH. αMSH is then released from keratinocytes to activate MC1R in melanocytes[228]. Accordingly, UVR would increase MC1R expression by at least two types of processes: i) a direct stimulation of *MC1R* gene expression in irradiated melanocytes and ii) an indirect pathway whereby release of POMC-derived MC1R agonists by keratinocytes in UVR-exposed skin would activate MC1R signaling in melanocytes, followed by increased cAMP signaling and induction of *MC1R* transcription. This would further increase the responsiveness of melanocytes to the paracrine signals resulting in a positive feedback loop that may favor a potent tanning response, but that may also threaten melanocyte viability owing to the inherent cytotoxicity of the melanogenic pathway[399,400]. It has been shown that Iso1/2 expression increases following stimulation of melanocytes with αMSH or activation of the p38 kinase, in an isoform switch that favors their expression relative to the canonical transcript[213]. Thus, the same signaling cascades implicated in induction of *MC1R* gene expression have also been shown to promote Iso1 and Iso2 transcripts. The diversion of a fraction of the new transcriptional events towards formation of inactive and maybe even dominant-negative intergenic splice isoforms might endeavor the melanocytes with a mechanism to dampen and fine-tune this potentially dangerous positive feedback loop.

Since Iso1 and Iso2 behave as R *MC1R* isoforms, they may share with variant MC1R-001 most of their physiological functions. However, the role of these R variants in the protection against melanomagenesis is not completely understood. It is generally accepted that WT *MC1R* protects against melanomagenesis by a combination of pigmentation-dependent and independent mechanisms[4]. The main external etiologic factor for melanoma is solar UVR, which causes direct DNA damage through its UVB component, or ROS-induced lesions through less energetic UVA radiation, resulting in high mutational rates[84,274,292]. The pigmentation-dependent component of *MC1R* protective action is accounted for by a switch from basal pheomelanogenesis to eumelanogenesis. Eumelanin is a photoprotective pigment owing to its absorption properties in the UVR spectrum and its free radical scavenging properties[8].

Conversely, pheomelanin is a photosensitizer promoting ROS production upon exposure to UVR[114,120,401,402], that can reduce the intracellular antioxidant pool even in the absence of UVR[142]. Concerning non-pigmentary actions, WT MC1R signaling activates antioxidant enzymes[216,326] and DNA repair pathways[336,360]. Owing to this combination of pigment-dependent and -independent effects, the mutation load in WT *MC1R* melanomas is lower compared with *MC1R*-variant melanomas[275,276,338] .

MC1R triggers several signaling pathways, and most *MC1R* alleles associated with higher melanoma risk are not LOF variants *sensu stricto,* since they activate the ERKs with an efficiency comparable with WT, despite impaired cAMP signaling[4,161,177,310]. The pheomelanogenesis/eumelanogenesis switch depends upon activation of the cAMP pathway[32,112,165,403]. Therefore, inefficient cAMP signaling accounts for the pigmentary component of the association of *MC1R* variants and melanoma risk. Moreover, cAMP signaling stimulates non-pigmentary protective responses, including activation of BER and NER[326,329,331,357]. The complex molecular mechanisms accounting for the acceleration of NER downstream of MC1R involve phosphorylation of ATR at Ser435 by cAMP-activated PKA[334], followed by nuclear translocation of a AKAP12-ATRpS435 complex, and recruitment to UVB-damaged DNA sites of XPA[357], Thus, deficient cAMP signaling downstream of variant MC1R would impair NER by blunting ATR phosphorylation. Activation of BER downstream of WT MC1R has also been demonstrated[329]. In mammalian cells, this pathway most often depends on the sequential action of broad specificity glycosylases such as OGG followed by APE-1/Ref-1. Notably, two key components of BER, OGG1 and APE-1/Ref-1 are induced in MSH-treated melanocytes[329] in a cAMP-dependent manner.

However, ERK and AKT signaling play important roles in the activation of cell cycle checkpoints in response to DNA damage and in the induction of DNA repair mechanisms[370,404]. Therefore, *MC1R* alleles unable to promote cAMP-dependent eumelanogenesis might still be able to trigger cAMP-independent non-pigmentary responses. To test this hypothesis, and given the relevance of oxidative stress in pheomelanic MC1R-variant melanocytes, we compared the response of HMCs of defined *MC1R* genotype to oxidative challenges. We also analyzed the enzymatic machinery and signaling pathway(s) responsible for these protective responses downstream of MC1R.

We found that NDP-MSH reduced significantly and comparably oxidative DNA damage in HMCs of WT or variant *MC1R* genotype, as shown by decreased steady-state levels of 8-oxodG, γH2AX foci and DNA SBs in cells submitted to an oxidative challenge. In HBL cells expressing WT MC1R, this protective effect may be partially accounted for by increased antioxidant defenses, since a significant induction of catalase by NDP-MSH was detected. However, in A375 cells

expressing the hypomorphic R151C MC1R variant, this protective effect occurred without induction of antioxidant enzymes, pointing to activation of DNA repair, which was confirmed by kinetic analysis of clearance of oxidative DNA lesions after short Luperox challenges. The repair of oxidative lesions was accounted for by induction of two key BER enzymes OGG and APE-1/Ref1 downstream of both WT and variant MC1R. Therefore, our data showed that variant MC1R could activate DNA repair to cope with oxidative damage.

Since *MC1R*-variant melanocytic cells used in this study failed to activate the cAMP pathway downstream of MC1R, we looked for the signaling pathways responsible for their pigment-independent protective action. In MC1R-variant cells, NDP-MSH decreased comparably Luperox-induced DNA fragmentation in the absence or presence of the MEK inhibitor PD98059, thus excluding ERK signaling as the main pathway responsible for the DNA protective effect. On the other hand, NDP-MSH significantly activated AKT in cells of variant *MC1R* genetic background. AKT is directly involved in DNA repair processes[370,404], as it promotes NHEJ-mediated repair of DSBs after irradiation of cancer cells[124], it activates APE-1/Ref-1 to decrease oxidative lesions[405] and it induces BER through activation of Nrf2 and subsequent upregulation of OGG1[406,407]. This mechanism has been recently shown to account for the protection against UVB-induced damage afforded by melatonin treatment of cultured human melanocytes[408]. In keeping with the protective role of AKT in melanocytic cells, the AKT activator SC79 decreased the number of DNA SBs and 8-oxodG levels in Luperox-treated *MC1R*-variant HMCs and induced BER enzymes in these cells. Moreover, blocking AKT signaling with LY94002 and MK-2206 abolished variant *MC1R*-dependent clearance of SBs and 8-oxodG DNA lesions, and prevented the induction of BER enzymes.

On the other hand, we gained insight into the mechanism of AKT activation downstream of variant MC1R. There is strong evidence that ROS act as cellular signaling molecules to modulate different signaling pathways and to ultimately regulate relevant biological processes such as proliferation, migration and survival[384–386]. The PI3K/AKT signaling pathway has been shown to be regulated by ROS[386,387,409]. Moreover, it is well established that ROS act as second messengers to convey signals downstream of GPCRs[389]. In this respect, we have shown a rapid increase of ROS production in MC1R variant cells treated with NDP-MSH whereas the presence of the antioxidant ebselen prior to MSH stimulation blocked the increase of ROS and the activation of AKT in these cells. In addition, treatment with low concentrations of Luperox ($8x10^{-5}$ M) comparable to those achieved by NDP-MSH, mimicked the effect of NDP-MSH on AKT activation downstream of variant MC1R. Therefore, ROS fulfill three major criteria defining them as potential second messengers acting downstream of MC1R: i) their intracellular concentration increases rapidly and transiently

upon treatment with MC1R agonists, ii) blocking their accumulation in response to the hormone also blunts some of the actions of MSH and iii) their increase by addition to the cells mimics these hormonal responses.

We have also identified NOX as the source of these MSH-induced ROS. Several reports show that the NADPH oxidases can be activated downstream of GPCRs[57,389] as well as by growth factors and hormones[384], and after UVB[56,410–412] and UVA[87] exposure in keratinocytes. In this respect, we have shown that NOX inhibition with DPI or GKT137831 abolished the MSH-induced ROS increase as well as AKT activation in MC1R variant melanocytic cells. On the contrary, in MC1R-WT cells NDP-MSH decreased intracellular ROS levels and was unable to activate AKT. This finding is in accordance with a rapid PKA-mediated activation of catalase[326] and/or with the inhibition of NOX by a cAMP-dependent mechanism[341,342]. Notably, blocking cAMP production in these cells with DDA rescued NOX and AKT activation downstream of MC1R. On the other hand, pharmacological elevation of cAMP levels in *MC1R* variant HMCs also blocked NOX-AKT signaling axis downstream of MC1R. Therefore, cAMP inhibited AKT signaling in melanocytic cells, as previously shown for mouse melanoma cells[32,379]. Therefore, our data are consistent with a model whereby variant MC1R stimulation by NDP-MSH leads to NOX activation, increased intracellular concentration of ROS and ROS-dependent activation of AKT.

Conversely, in WT MC1R melanocytic cells, NDP-MSH activation of the cAMP pathway would interfere with AKT activation, likely by blocking NOX-dependent increases in intracellular ROS. Consistent with lack of NOX and AKT activation downstream of WT MC1R, induction of protective responses by NDP-MSH in cells of WT *MC1R* genotype was not affected by LY94002 and MK-2206. Conversely, these responses were blocked by DDA and mimicked by FSK or dbcAMP, confirming their dependence on cAMP. In addition, NOX inhibition with GKT137831 had no effect in BER induction by NDP-MSH whereas DDA blocked this effect. These data demonstrate the involvement of cAMP pathway in activation of BER in MC1R-WT HMCs. Accordingly, our results show that MC1R activation promotes protection against oxidative DNA damage at least by two mechanisms. One of them depends on cAMP and is operative in MC1R-WT cells, whereas the other would depend on AKT and would be restricted to *MC1R*-variant cells (Figure 31). Moreover, in MC1R-WT cells cAMP would efficiently induce antioxidant enzymes, mainly catalase, and the BER enzymes OGG and APE-1/Ref1 whereas variant MC1R would augment efficiently the expression of the two key BER enzymes but should have no effect on catalase levels or activity.

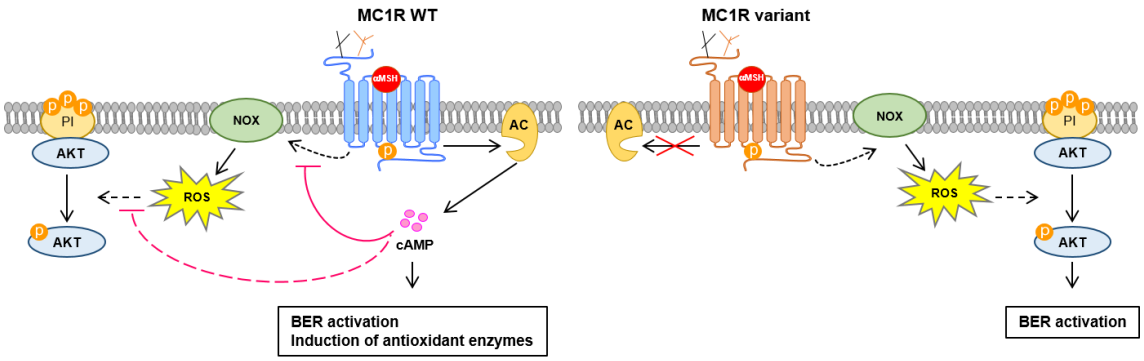

Figure 31. Proposed model for the differential coupling of WT and variant MC1R to different DNA repair pathways. In MC1R WT melanocytic cells, MC1R agonists induce high cAMP levels that block NOX and thus, AKT activation, so that cAMP-dependent DNA repair pathways are predominantly operative. In MC1R-variant melanocytes, failure to increase high cAMP levels enables NOX-AKT activation downstream of MC1R and AKT-dependent repair pathways would prevail. The BER pathway is induced downstream of both MC1Rs whereas induction of antioxidant enzymes, mainly catalase, is only achieved by MC1R-WT in a cAMP-dependent manner.

Taken together, our results clearly support the involvement of NOX in MC1R variant-dependent activation of AKT. However, the molecular players downstream of NOX and upstream of AKT remain unknown. NOX-induced ROS have been shown to activate the PI3K/AKT signaling pathway by inhibition of phosphatases or activation of kinases[386–388] through the reversible oxidation of redox sensitive Cys residues[386,413]. There is evidence of ROS-mediated activation of the non-RTK Src[414,415] and this kinase has been shown to be activated by NDP-MSH independently of cAMP in melanoma cells[161]. Therefore, we considered Src as a possible target of MSH-induced ROS. We confirmed activation of Src downstream of variant MC1R in A375 and SKMEL28 melanoma cells (data not shown). When stimulated with NDP-MSH, a transient increase in Src activity was detected, which was maximal slightly sooner than peak pAKT levels were reached. Moreover, treatment with low levels of Luperox ($8x10^{-5}$ M) also activated Src, (preliminary data not shown here). These data are compatible with a role for Src in transmitting the MSH signal to AKT in MC1R variant cells, although this point needs further confirmation by additional pharmacological and molecular approaches.

On the other hand, downregulation of a phosphatase responsible for removal of the activatory phosphorylation of AKT would be perhaps more consistent with the slow kinetics of AKT activation by NDP-MSH in MC1R-variant cells. Notably, PTEN inhibition by NOX has been demonstrated[416]. On the other hand, in MSH-treated UV-irradiated melanocytes, WT MC1R recruits PTEN in an interaction that prevents PTEN ubiquitination by WWP2, thereby protecting the phosphatase from proteasomal degradation[210]. The resulting PTEN stabilization partially downregulates AKT signaling. Conversely, MC1R variants such as R151C interact poorly with

PTEN, allowing for PTEN degradation and higher AKT activity. On the other hand, attenuation of PP2A activity by NOX has been reported to increase AKT signaling[417] and cAMP can activate PP2A leading to inactivation of AKT[418–422] which would provide another mechanism for cAMP-dependent inhibition of AKT signaling in MC1R-WT cells. However, stimulation of A375 and SKMEL28 cells with the MC1R agonist did not produce a significant modification of PP2A activity although these cells express detectable levels of the enzyme (data not shown). Nevertheless, involvement of other phosphatases, such as PTP-1B, PHLPP phosphatases or the serine/threonine phosphatases PP1, PP2B and PP2C cannot be ruled out. In fact, several studied reported inhibition of PTP-1B[423] and PP1α[417] by NOX in order to regulate AKT signaling in other cell types. In summary, a differential regulation of the levels or activity of specific kinases or phosphatases might underlie the different effect of WT and variant MC1R on AKT. These possibilities are currently under investigation.

Overall, we have shown that ROS play an important role in triggering the signaling pathway that leads from variant MC1R to AKT activation, to ultimately induce BER and increase DNA repair. Paradoxically, these mechanisms are activated in order to cope with the genotoxic effects of excessive ROS levels. Therefore, ROS seem to play a dual role in melanocyte biology by promoting DNA repair at the low concentrations induced by variant MC1R signaling on the one hand, but causing DNA damage and genomic instability at higher levels induced by excessive UVR or oxidative stress on the other. This suggests that ROS levels might be tightly regulated in melanocytes in order to keep them under toxic ranges. In fact, there is increasing evidence supporting that oxidative stress is important for melanoma formation, especially in a pheomelanogenic context[93,138–140]. Moreover, dysregulation of NOX levels and activity has been associated with melanoma initiation and progression[385,424]. On the other hand, the presence of a specific mechanism to cope with oxidative DNA damage in melanocytes of variant MC1R genotype might be important given the prooxidant properties of the pheomelanic pigments synthesized by these cells. Indeed, pheomelanic MC1R-variant melanocytes are likely to be more exposed to ROS-induced DNA lesions, thus requiring specific and efficient ways to repair them. The lifespan of melanocytes in the epidermis is long and continuous exposure to mutagenic UVR and oxidative stress would result in excessive accumulation of oxidative damage. The inability of these cells to cope with oxidative lesions through the cAMP-dependent mechanisms operative in MC1R-WT cells might be at least partially compensated by the occurrence of AKT-dependent and cAMP-independent repair pathways. These pathways of DNA repair would allow MC1R-variant cells to maintain sufficient genomic stability to avoid unsustainable rates of cell death or

malignant transformation under the conditions of continuously high oxidative stress imposed by their pheomelanogenic activity.

In summary, we have shown that AKT was activated via NOX stimulation downstream of variant MC1R in human melanocytic cells. This activation was blunted downstream of the WT receptor due to a suppressive effect of cAMP. We also showed that variant MC1R accelerated the NOX- and AKT-dependent clearance of 8-oxodG and DNA SBs, suggesting that it activated at least the BER pathway and maybe also either HR or NHEJ. The possibility of activation of HR and NHEJ is currently under investigation. It remains to be seen how these observations can be reconciled with the higher mutation load in melanomas of variant *MC1R* genetic background compared with *MC1R*-WT melanomas[275,276]. In this respect, several possibilities can be considered. Variant MC1R may not activate NER-mediated clearance of UVB-produced lesions such as CPDs as effectively as WT. Moreover, the precise cAMP-dependent DNA damage responses triggered by WT MC1R to repair DSBs may not be the same as the AKT-dependent pathways activated by variant MC1R. AKT plays opposite roles in the two major types of NER by promoting transcription-coupled NER while inhibiting global genome NER[370]. Concerning repair of DSBs, AKT was shown to inhibit high fidelity HR while activating error-prone NHEJ[370,425]. Importantly, NHEJ may be particularly important for DSB clearance in UVR-irradiated melanocytes, since UVR induces G1 cell cycle arrest[426] and HR is restricted to the S and G2 phases[427]. The possibility of a differential engagement of DSB repair pathways by WT and variant MC1R clearly deserves further investigation, as it may impinge on the fidelity of repair.

In addition, the higher mutation load of MC1R-variant melanomas might be explained in simpler kinetic terms, without invoking occurrence of less efficient MC1R-activated repair pathways, or even absence of them. Indeed, the steady-state levels of DNA lesions result from the balance of their rate of production on one hand, and the rate of their clearance on the other. Accordingly, an increase in the abundance of mutations might simply reflect an increased rate of lesion formation at a constant rate of removal. It is generally agreed that oxidative stress under basal conditions or after UVR exposure is higher in pheomelanic MC1R variant melanocytes compared with MC1R-WT cells. In MC1R-WT cells, MSH mediates induction of antioxidant enzymes (as reported by our group and by others[326,331]) and non-enzymatic antioxidants including the ROS-scavenger eumelanin. However, in MC1R variant cells MSH is unable to induce antioxidant enzymes. Moreover, in these cells pro-oxidant pheomelanins have been shown to deplete the pool of intracellular antioxidants and to behave as photosensitizers augmenting the deleterious effects of UVR. Thus, the ROS balance might be easily upset in MC1R-variant cells compared to MC1R-WT, thus augmenting the rate of generation of oxidative lesions in the

former. Therefore, even under conditions of comparable repair activation downstream of variant or WT MC1R, a higher amount of oxidative lesions should be expected in MC1R-variant melanocytes.

The results of our work therefore show that variant MC1R cells retain a significant potential to activate repair of DNA oxidative lesions in response to MSH, and suggest that this potential may be important to allow for a sufficient level of genomic stability under conditions of persistent oxidative stress. On the other hand, WT MC1R would trigger a more efficient protection against UVR, involving not only induction BER but also stimulation of antioxidant defenses and activation of NER. Activation of NER downstream of variant MC1R remains to be investigated in depth. In this respect, a deeper study of DNA damage responses downstream of variant MC1R is critical in order to understand the higher mutation burden in melanomas of variant *MC1R* genotype and the molecular bases of the association of variant MC1R to melanoma risk. In any case, our demonstration of AKT-dependent DNA repair downstream of variant MC1R may be important for the design of rational melanoma prevention treatments such as a recently suggested treatment with NOX1 inhbitors[424] and application of topical agents increasing cAMP levels in sun-exposed skin.

CONCLUSIONS

Conclusions

1. MC1R-TUBB3 chimerae expressed in all human melanoma cells tested and are able to bind agonist with the same affinity as MC1R-001, but their plasma membrane expression is strongly reduced, mostly as a result from aberrant forward trafficking.

2. Iso1 and Iso2 heterodimerize efficiently with MC1R-001 and may behave as dominant-negative forms by promoting intracellular retention of the canonical form.

3. MC1R-TUBB3 chimerae behave as R variants in terms of signaling, as their functional coupling to the cAMP pathway is dramatically compromised, but activation of the ERKs remains efficient.

4. Activation of MC1R-WT increases expression of the antioxidant enzymes catalase and superoxide dismutase in a cAMP-dependent fashion.

5. NDP-MSH significantly and comparably induces repair of oxidative DNA damage in human melanoma cells of WT or variant *MC1R* genotype, as shown by clearance of oxidative DNA lesions (8-oxodG and DNA strand breaks) in cells submitted to an oxidative challenge.

6. The repair of oxidative lesions is, at least partially, accounted for by induction of two key BER enzymes, OGG and APE-1/Ref1, downstream of both WT and variant MC1R.

7. In *MC1R*-WT melanocytic cells, the DNA-protective responses are mediated by the cAMP signaling pathway whereas in *MC1R*-variant melanocytic cells, AKT is responsible for inducing DNA repair.

8. In human melanocytic cells carrying MC1R variants, non-canonical signaling from MC1R to AKT is cAMP-independent and relies on the activation of NOX.

9. NOX is required for induction of the BER enzymes OGG and APE-1/Ref1 and repair of oxidative DNA damage in variant MC1R human melanoma cells.

10. High cAMP levels inhibit MC1R-mediated AKT activation in MC1R-variant human melanoma cells, likely by blocking NOX-dependent increases in intracellular ROS.

REFERENCES

References

1 Fuchs E. Epithelial Skin Biology. In: *Current topics in developmental biology*. 2016, pp 357–374.

2 Yamaguchi Y, Hearing VJ. Melanocytes and their diseases. *Cold Spring Harb Perspect Med* 2014; **4**: a017046–a017046.

3 Plonka PM, Passeron T, Brenner M, Tobin DJ, Shibahara S, Thomas A *et al.* What are melanocytes really doing all day long...? *Exp Dermatol* 2009; **18**: 799–819.

4 Garcia-Borron JC, Abdel-Malek Z, Jimenez-Cervantes C. MC1R, the cAMP pathway, and the response to solar UV: extending the horizon beyond pigmentation. *Pigment Cell Melanoma Res* 2014; **27**: 699–720.

5 D'Orazio J, Jarrett S, Amaro-Ortiz A, Scott T. UV radiation and the skin. *Int J Mol Sci* 2013; **14**: 12222–48.

6 Slominski A, Paus R, Schadendorf D. Melanocytes as Sensory and Regulatory Cells in the Epidermis. *J Theor Biol* 1993; **164**: 103–120.

7 Ito S, Wakamatsu K. Melanin chemistry and melanin precursors in melanoma. *J Invest Dermatol* 1989; **92**: 261S–265S.

8 d'Ischia M, Wakamatsu K, Cicoira F, Di Mauro E, Garcia-Borron JC, Commo S *et al.* Melanins and melanogenesis: from pigment cells to human health and technological applications. *Pigment Cell Melanoma Res* 2015; **28**: 520–544.

9 Kondo T, Hearing VJ. Update on the regulation of mammalian melanocyte function and skin pigmentation. *Expert Rev Dermatol* 2011; **6**: 97–108.

10 García-Borrón JC, Solano F. Molecular anatomy of tyrosinase and its related proteins: beyond the histidine-bound metal catalytic center. *Pigment cell Res* 2002; **15**: 162–73.

11 Prota G. The chemistry of melanins and melanogenesis. *Fortschr Chem Org Naturst* 1995; **64**: 93–148.

12 Ito S, Wakamatsu K. Diversity of human hair pigmentation as studied by chemical analysis of eumelanin and pheomelanin. *J Eur Acad Dermatol Venereol* 2011; **25**: 1369–80.

13 Olivares C, Solano F. New insights into the active site structure and catalytic mechanism of tyrosinase and its related proteins. *Pigment Cell Melanoma Res* 2009; **22**: 750–760.

14 Lai X, Wichers HJ, Soler-Lopez M, Dijkstra BW. Structure and Function of Human Tyrosinase and Tyrosinase-Related Proteins. *Chemistry* 2018; **24**: 47–55.

15 Hida T, Wakamatsu K, Sviderskaya E V, Donkin AJ, Montoliu L, Lynn Lamoreux M *et al.* Agouti protein, mahogunin, and attractin in pheomelanogenesis and melanoblast-like alteration of melanocytes: a cAMP-independent pathway. *Pigment Cell Melanoma Res* 2009; **22**: 623–34.

16 Aroca P, Garcia-Borron JC, Solano F, Lozano JA. Regulation of mammalian melanogenesis. I: Partial purification and characterization of a dopachrome converting factor: dopachrome tautomerase. *Biochim Biophys Acta* 1990; **1035**: 266–75.

17 Jiménez-Cervantes C, Solano F, Kobayashi T, Urabe K, Hearing VJ, Lozano JA *et al.* A new enzymatic function in the melanogenic pathway. The 5,6-dihydroxyindole-2-carboxylic acid oxidase activity of tyrosinase-related protein-1 (TRP1). *J Biol Chem* 1994; **269**: 17993–8000.

18 Kobayashi T, Urabe K, Winder A, Jiménez-Cervantes C, Imokawa G, Brewington T *et al.* Tyrosinase related protein 1 (TRP1) functions as a DHICA oxidase in melanin biosynthesis. *EMBO J* 1994; **13**: 5818–25.

19 Olivares C, Jiménez-Cervantes C, Lozano JA, Solano F, García-Borrón JC. The 5,6-dihydroxyindole-2-carboxylic acid (DHICA) oxidase activity of human tyrosinase. *Biochem J* 2001; **354**: 131–9.

20 Di Donato P, Napolitano A. 1,4-benzothiazines as key intermediates in the biosynthesis of red hair pigment pheomelanins. *Pigment cell Res* 2003; **16**: 532–9.

21 Greco G, Wakamatsu K, Panzella L, Ito S, Napolitano A, d'Ischia M. Isomeric cysteinyldopas provide a (photo)degradable bulk component and a robust structural element in red human hair pheomelanin. *Pigment Cell Melanoma Res* 2009; **22**: 319–27.

22 Hirobe T, Abe H. Genetic and epigenetic control of the proliferation and differentiation of mouse epidermal melanocytes in culture. *Pigment cell Res* 1999; **12**: 147–63.

23 Sakurai T, Ochiai H, Takeuchi T. Ultrastructural change of melanosomes associated with agouti pattern formation in mouse hair. *Dev Biol* 1975; **47**: 466–71.

24 D'Alba L, Shawkey MD. Melanosomes: Biogenesis, Properties, and Evolution of an Ancient Organelle. *Physiol Rev* 2019; **99**: 1–19.

25 Jimbow K, Ishida O, Ito S, Hori Y, Witkop CJ, King RA. Combined chemical and electron microscopic studies of pheomelanosomes in human red hair. *J Invest Dermatol* 1983; **81**: 506–11.

26 Fuller BB, Spaulding DT, Smith DR. Regulation of the Catalytic Activity of Preexisting Tyrosinase in Black and Caucasian Human Melanocyte Cell Cultures. *Exp Cell Res* 2001; **262**: 197–208.

27 Smith DR, Spaulding DT, Glenn HM, Fuller BB. The relationship between Na+/H+ exchanger expression and tyrosinase activity in human melanocytes. *Exp Cell Res* 2004; **298**: 521–534.

28 Raposo G, Marks MS, Cutler DF. Lysosome-related organelles: driving post-Golgi compartments into specialisation. *Curr Opin Cell Biol* 2007; **19**: 394–401.

29 Marks MS, Heijnen HFG, Raposo G. Lysosome-related organelles: unusual compartments become mainstream. *Curr Opin Cell Biol* 2013; **25**: 495–505.

30 Nordlund JJ. The pigmentary system and inflammation. *Pigment cell Res* 1992; **5**: 362–5.

31 Wu XS, Rao K, Zhang H, Wang F, Sellers JR, Matesic LE *et al.* Identification of an organelle receptor for myosin-Va. *Nat Cell Biol* 2002; **4**: 271–8.

32 Slominski A, Tobin DJ, Shibahara S, Wortsman J. Melanin pigmentation in mammalian skin and its hormonal regulation. *Physiol Rev* 2004; **84**: 1155–1228.

33 FITZPATRICK TB, BREATHNACH AS. [THE EPIDERMAL MELANIN UNIT SYSTEM]. *Dermatol Wochenschr* 1963; **147**: 481–9.

34 Costin G-E, Hearing VJ. Human skin pigmentation: melanocytes modulate skin color in response to stress. *FASEB J* 2007; **21**: 976–94.

35 Thong H-Y, Jee S-H, Sun C-C, Boissy RE. The patterns of melanosome distribution in keratinocytes of human skin as one determining factor of skin colour. *Br J Dermatol* 2003; **149**: 498–505.

36 Hurbain I, Romao M, Sextius P, Bourreau E, Marchal C, Bernerd F *et al.* Melanosome Distribution in Keratinocytes in Different Skin Types: Melanosome Clusters Are Not Degradative Organelles. *J Invest Dermatol* 2018; **138**: 647–656.

37 Hirobe T. How are proliferation and differentiation of melanocytes regulated? *Pigment Cell Melanoma Res* 2011; **24**: 462–78.

38 Kielbassa C, Roza L, Epe B. Wavelength dependence of oxidative DNA damage induced by UV and visible light. *Carcinogenesis* 1997; **18**: 811–6.

39 Douki T. The variety of UV-induced pyrimidine dimeric photoproducts in DNA as shown by chromatographic quantification methods. *Photochem Photobiol Sci* 2013; **12**: 1286–302.

40 Cadet J, Mouret S, Ravanat J-L, Douki T. Photoinduced damage to cellular DNA: direct and photosensitized reactions. *Photochem Photobiol* 2012; **88**: 1048–65.

41 Taylor JS, Cohrs MP. DNA, light, and Dewar pyrimidinones: the structure and biological significance to TpT3. *J Am Chem Soc* 1987; **109**: 2834–2835.

42 Zhao X, Nadji S, Kao JL, Taylor JS. The structure of d(TpA), the major photoproduct of thymidylyl-(3'5')-deoxyadenosine. *Nucleic Acids Res* 1996; **24**: 1554–60.

43 Banyasz A, Martinez-Fernandez L, Ketola T-M, Muñoz-Losa A, Esposito L, Markovitsi D *et al.* Excited State Pathways Leading to Formation of Adenine Dimers. *J Phys Chem Lett* 2016; **7**: 2020–3.

44 Koning TM, Davies RJ, Kaptein R. The solution structure of the intramolecular photoproduct of d(TpA) derived with the use of NMR and a combination of distance geometry and molecular dynamics. *Nucleic Acids Res* 1990; **18**: 277–84.

45 Asgatay S, Martinez A, Coantic-Castex S, Harakat D, Philippe C, Douki T *et al.* UV-induced TA photoproducts: formation and hydrolysis in double-stranded DNA. *J Am Chem Soc* 2010; **132**: 10260–1.

46 Schuch AP, Moreno NC, Schuch NJ, Menck CFM, Garcia CCM. Sunlight damage to cellular DNA: Focus on oxidatively generated lesions. *Free Radic Biol Med* 2017; **107**: 110–124.

47 Douki T, Cadet J. Individual determination of the yield of the main UV-induced dimeric pyrimidine photoproducts in DNA suggests a high mutagenicity of CC photolesions. *Biochemistry* 2001; **40**: 2495–501.

48 Mitchell DL, Allison JP, Nairn RS. Immunoprecipitation of pyrimidine(6-4)pyrimidone photoproducts and cyclobutane pyrimidine dimers in UV-irradiated DNA. *Radiat Res* 1990; **123**: 299–303.

49 Yasui H, Hakozaki T, Date A, Yoshii T, Sakurai H. Real-time chemiluminescent imaging and detection of reactive oxygen species generated in the UVB-exposed human skin equivalent model. *Biochem Biophys Res Commun* 2006; **347**: 83–8.

50 Hakozaki T, Date A, Yoshii T, Toyokuni S, Yasui H, Sakurai H. Visualization and characterization of UVB-induced reactive oxygen species in a human skin equivalent model. *Arch Dermatol Res* 2008; **300 Suppl 1**: S51-6.

51 Schallreuter KU, Wood JM. Thioredoxin reductase - its role in epidermal redox status. *J Photochem Photobiol B* 2001; **64**: 179–84.

52 Kalyanaraman B, Darley-Usmar V, Davies KJA, Dennery PA, Forman HJ, Grisham MB *et al.* Measuring reactive oxygen and nitrogen species with fluorescent probes: challenges and limitations. *Free Radic Biol Med* 2012; **52**: 1–6.

53 Wang H, Kochevar IE. Involvement of UVB-induced reactive oxygen species in TGF-beta biosynthesis and activation in keratinocytes. *Free Radic Biol Med* 2005; **38**: 890–7.

54 Jin G-H, Liu Y, Jin S-Z, Liu X-D, Liu S-Z. UVB induced oxidative stress in human keratinocytes and protective effect of antioxidant agents. *Radiat Environ Biophys* 2007; **46**: 61–68.

55 Yogianti F, Kunisada M, Nakano E, Ono R, Sakumi K, Oka S *et al.* Inhibitory effects of dietary Spirulina platensis on UVB-induced skin inflammatory responses and carcinogenesis. *J Invest Dermatol* 2014; **134**: 2610–2619.

56 Beak SM, Lee YS, Kim J-A. NADPH oxidase and cyclooxygenase mediate the ultraviolet B-induced generation of reactive oxygen species and activation of nuclear factor-kappaB in HaCaT human keratinocytes. *Biochimie* 2004; **86**: 425–9.

57 Glady A, Tanaka M, Moniaga CS, Yasui M, Hara-Chikuma M. Involvement of NADPH oxidase 1 in UVB-induced cell signaling and cytotoxicity in human keratinocytes. *Biochem Biophys reports* 2018; **14**: 7–15.

58 Katiyar SK, Meeran SM. Obesity increases the risk of UV radiation-induced oxidative stress and activation of MAPK and NF-kappaB signaling. *Free Radic Biol Med* 2007; **42**: 299–310.

59 Wölfle U, Esser PR, Simon-Haarhaus B, Martin SF, Lademann J, Schempp CM. UVB-induced DNA damage, generation of reactive oxygen species, and inflammation are effectively attenuated by the flavonoid luteolin in vitro and in vivo. *Free Radic Biol Med* 2011; **50**: 1081–93.

60 Bickers DR, Athar M. Oxidative Stress in the Pathogenesis of Skin Disease. *J Invest Dermatol* 2006; **126**: 2565–2575.

61 Suschek CV, Mahotka C, Schnorr O, Kolb-Bachofen V. UVB radiation-mediated expression of inducible nitric oxide synthase activity and the augmenting role of co-induced TNF-alpha in human skin endothelial cells. *J Invest Dermatol* 2004; **123**: 950–7.

62 Wei H, Cai Q, Tian L, Lebwohl M. Tamoxifen reduces endogenous and UV light-induced oxidative damage to DNA, lipid and protein in vitro and in vivo. *Carcinogenesis* 1998; **19**: 1013–8.

63 Rosen JE, Prahalad AK, Williams GM. 8-Oxodeoxyguanosine formation in the DNA of cultured cells after exposure to H2O2 alone or with UVB or UVA irradiation. *Photochem Photobiol* 1996; **64**: 117–22.

64 Stewart MS, Cameron GS, Pence BC. Antioxidant nutrients protect against UVB-induced oxidative damage to DNA of mouse keratinocytes in culture. *J Invest Dermatol* 1996; **106**:

1086–9.

65 Douki T, Perdiz D, Gróf P, Kuluncsics Z, Moustacchi E, Cadet J *et al.* Oxidation of guanine in cellular DNA by solar UV radiation: biological role. *Photochem Photobiol* 1999; **70**: 184–90.

66 Pelle E, Huang X, Mammone T, Marenus K, Maes D, Frenkel K. Ultraviolet-B-induced oxidative DNA base damage in primary normal human epidermal keratinocytes and inhibition by a hydroxyl radical scavenger. *J Invest Dermatol* 2003; **121**: 177–83.

67 Garcin G, Douki T, Stoebner P-E, Guesnet J, Guezennec A, Martinez J *et al.* Cell surface expression of melanocortin-1 receptor on HaCaT keratinocytes and alpha-melanocortin stimulation do not affect the formation and repair of UVB-induced DNA photoproducts. *Photochem Photobiol Sci* 2007; **6**: 585–93.

68 Kielbassa C, Epe B. DNA damage induced by ultraviolet and visible light and its wavelength dependence. *Methods Enzymol* 2000; **319**: 436–45.

69 Orimo H, Tokura Y, Hino R, Kasai H. Formation of 8-hydroxy-2'-deoxyguanosine in the DNA of cultured human keratinocytes by clinically used doses of narrowband and broadband ultraviolet B and psoralen plus ultraviolet A. *Cancer Sci* 2006; **97**: 99–105.

70 Cadet J, Davies KJA, Medeiros MH, Di Mascio P, Wagner JR. Formation and repair of oxidatively generated damage in cellular DNA. *Free Radic Biol Med* 2017; **107**: 13–34.

71 Kunisada M, Sakumi K, Tominaga Y, Budiyanto A, Ueda M, Ichihashi M *et al.* 8-Oxoguanine formation induced by chronic UVB exposure makes Ogg1 knockout mice susceptible to skin carcinogenesis. *Cancer Res* 2005; **65**: 6006–10.

72 Garinis GA, Mitchell JR, Moorhouse MJ, Hanada K, de Waard H, Vandeputte D *et al.* Transcriptome analysis reveals cyclobutane pyrimidine dimers as a major source of UV-induced DNA breaks. *EMBO J* 2005; **24**: 3952–62.

73 Lucas RM, Norval M, Neale RE, Young AR, de Gruijl FR, Takizawa Y *et al.* The consequences for human health of stratospheric ozone depletion in association with other environmental factors. *Photochem Photobiol Sci* 2015; **14**: 53–87.

74 De Fabo EC, Noonan FP, Fears T, Merlino G. Ultraviolet B but not Ultraviolet A Radiation Initiates Melanoma. *Cancer Res* 2004; **64**: 6372–6376.

75 Sage E, Girard P-M, Francesconi S. Unravelling UVA-induced mutagenesis. *Photochem Photobiol Sci* 2012; **11**: 74–80.

76 Cadet J, Douki T. Formation of UV-induced DNA damage contributing to skin cancer development. *Photochem Photobiol Sci* 2018; **17**: 1816–1841.

77 Mouret S, Forestier A, Douki T. The specificity of UVA-induced DNA damage in human melanocytes. *Photochem Photobiol Sci* 2012; **11**: 155–162.

78 Cadet J, Douki T, Ravanat J-L. Oxidatively Generated Damage to Cellular DNA by UVB and UVA Radiation ·. *Photochem Photobiol* 2015; **91**: 140–155.

79 Lawrence KP, Douki T, Sarkany RPE, Acker S, Herzog B, Young AR. The UV/Visible Radiation Boundary Region (385-405 nm) Damages Skin Cells and Induces 'dark' Cyclobutane Pyrimidine Dimers in Human Skin in vivo. *Sci Rep* 2018; **8**: 12722.

80 Tewari A, Sarkany RP, Young AR. UVA1 induces cyclobutane pyrimidine dimers but not 6-

4 photoproducts in human skin in vivo. *J Invest Dermatol* 2012; **132**: 394–400.

81 Noonan FP, Zaidi MR, Wolnicka-Glubisz A, Anver MR, Bahn J, Wielgus A *et al.* Melanoma induction by ultraviolet A but not ultraviolet B radiation requires melanin pigment. *Nat Commun* 2012; **3**: 884.

82 BEUKERS R, BERENDS W. Isolation and identification of the irradiation product of thymine. *Biochim Biophys Acta* 1960; **41**: 550–1.

83 van Steeg H, Kraemer KH. Xeroderma pigmentosum and the role of UV-induced DNA damage in skin cancer. *Mol Med Today* 1999; **5**: 86–94.

84 Zhang T, Dutton-Regester K, Brown KM, Hayward NK. The genomic landscape of cutaneous melanoma. *Pigment Cell Melanoma Res* 2016; **29**: 266–283.

85 Douki T, Reynaud-Angelin A, Cadet J, Sage E. Bipyrimidine photoproducts rather than oxidative lesions are the main type of DNA damage involved in the genotoxic effect of solar UVA radiation. *Biochemistry* 2003; **42**: 9221–6.

86 Premi S, Wallisch S, Mano CM, Weiner AB, Bacchiocchi A, Wakamatsu K *et al.* Chemiexcitation of melanin derivatives induces DNA photoproducts long after UV exposure. *Science (80-)* 2015; **347**: 842–847.

87 Valencia A, Kochevar IE. Nox1-based NADPH oxidase is the major source of UVA-induced reactive oxygen species in human keratinocytes. *J Invest Dermatol* 2008; **128**: 214–22.

88 Birch-Machin MA, Swalwell H. How mitochondria record the effects of UV exposure and oxidative stress using human skin as a model tissue. *Mutagenesis* 2010; **25**: 101–7.

89 Wenczl E, Van der Schans GP, Roza L, Kolb RM, Timmerman AJ, Smit NP *et al.* (Pheo)melanin photosensitizes UVA-induced DNA damage in cultured human melanocytes. *J Invest Dermatol* 1998; **111**: 678–82.

90 Wondrak GT, Jacobson MK, Jacobson EL. Endogenous UVA-photosensitizers: mediators of skin photodamage and novel targets for skin photoprotection. *Photochem Photobiol Sci* 2006; **5**: 215–237.

91 Wischermann K, Popp S, Moshir S, Scharfetter-Kochanek K, Wlaschek M, de Gruijl F *et al.* UVA radiation causes DNA strand breaks, chromosomal aberrations and tumorigenic transformation in HaCaT skin keratinocytes. *Oncogene* 2008; **27**: 4269–80.

92 Boorstein RJ, Cummings A, Marenstein DR, Chan MK, Ma Y, Neubert TA *et al.* Definitive identification of mammalian 5-hydroxymethyluracil DNA N-glycosylase activity as SMUG1. *J Biol Chem* 2001; **276**: 41991–7.

93 Pleasance ED, Cheetham RK, Stephens PJ, McBride DJ, Humphray SJ, Greenman CD *et al.* A comprehensive catalogue of somatic mutations from a human cancer genome. *Nature* 2010; **463**: 191–196.

94 Armstrong BK, Kricker A. How much melanoma is caused by sun exposure? *Melanoma Res* 1993; **3**: 395–401.

95 Agar NS, Halliday GM, Barnetson RS, Ananthaswamy HN, Wheeler M, Jones AM. The basal layer in human squamous tumors harbors more UVA than UVB fingerprint mutations: a role for UVA in human skin carcinogenesis. *Proc Natl Acad Sci U S A* 2004; **101**: 4954–9.

96 Young AR, Chadwick CA, Harrison GI, Nikaido O, Ramsden J, Potten CS. The similarity of action spectra for thymine dimers in human epidermis and erythema suggests that DNA is the chromophore for erythema. *J Invest Dermatol* 1998; **111**: 982–8.

97 Mouret S, Baudouin C, Charveron M, Favier A, Cadet J, Douki T. Cyclobutane pyrimidine dimers are predominant DNA lesions in whole human skin exposed to UVA radiation. *Proc Natl Acad Sci U S A* 2006; **103**: 13765–70.

98 Ikehata H, Kawai K, Komura J, Sakatsume K, Wang L, Imai M *et al.* UVA1 genotoxicity is mediated not by oxidative damage but by cyclobutane pyrimidine dimers in normal mouse skin. *J Invest Dermatol* 2008; **128**: 2289–96.

99 Brigelius-Flohé R. Tissue-specific functions of individual glutathione peroxidases. *Free Radic Biol Med* 1999; **27**: 951–65.

100 Toppo S, Flohé L, Ursini F, Vanin S, Maiorino M. Catalytic mechanisms and specificities of glutathione peroxidases: Variations of a basic scheme. *Biochim Biophys Acta - Gen Subj* 2009; **1790**: 1486–1500.

101 Lubos E, Loscalzo J, Handy DE. Glutathione peroxidase-1 in health and disease: from molecular mechanisms to therapeutic opportunities. *Antioxid Redox Signal* 2011; **15**: 1957–97.

102 Forman HJ. Redox signaling: An evolution from free radicals to aging. *Free Radic Biol Med* 2016; **97**: 398–407.

103 Schärer OD. Nucleotide excision repair in eukaryotes. *Cold Spring Harb Perspect Biol* 2013; **5**: a012609.

104 Shah P, He Y-Y. Molecular Regulation of UV-Induced DNA Repair. *Photochem Photobiol* 2015; **91**: 254–264.

105 Bradford PT, Goldstein AM, Tamura D, Khan SG, Ueda T, Boyle J *et al.* Cancer and neurologic degeneration in xeroderma pigmentosum: long term follow-up characterises the role of DNA repair. *J Med Genet* 2011; **48**: 168–76.

106 Dahle J, Brunborg G, Svendsrud DH, Stokke T, Kvam E. Overexpression of human OGG1 in mammalian cells decreases ultraviolet A induced mutagenesis. *Cancer Lett* 2008; **267**: 18–25.

107 Del Bino S, Duval C, Bernerd F. Clinical and Biological Characterization of Skin Pigmentation Diversity and Its Consequences on UV Impact. *Int J Mol Sci* 2018; **19**. doi:10.3390/ijms19092668.

108 Scherer D, Kumar R. Genetics of pigmentation in skin cancer--a review. *Mutat Res* 2010; **705**: 141–53.

109 Kaidbey KH, Agin PP, Sayre RM, Kligman AM. Photoprotection by melanin--a comparison of black and Caucasian skin. *J Am Acad Dermatol* 1979; **1**: 249–60.

110 O'Rahilly R. The Structure and Function of Skin. William Montagna. *Q Rev Biol* 1962; **37**: 186–186.

111 Miller DL, Weinstock MA. Nonmelanoma skin cancer in the United States: incidence. *J Am Acad Dermatol* 1994; **30**: 774–8.

112 Ito S, Wakamatsu K. Quantitative analysis of eumelanin and pheomelanin in humans,

mice, and other animals: a comparative review. *Pigment cell Res* 2003; **16**: 523–31.

113 Vincensi MR, d'Ischia M, Napolitano A, Procaccini EM, Riccio G, Monfrecola G *et al.* Phaeomelanin versus eumelanin as a chemical indicator of ultraviolet sensitivity in fair-skinned subjects at high risk for melanoma: a pilot study. *Melanoma Res* 1998; **8**: 53–8.

114 Napolitano A, Panzella L, Monfrecola G, d'Ischia M. Pheomelanin-induced oxidative stress: bright and dark chemistry bridging red hair phenotype and melanoma. *Pigment Cell Melanoma Res* 2014; **27**: 721–733.

115 Nasti TH, Timares L. MC1R, eumelanin and pheomelanin: their role in determining the susceptibility to skin cancer. *Photochem Photobiol* 2015; **91**: 188–200.

116 Swope V, Abdel-Malek Z. MC1R: Front and Center in the Bright Side of Dark Eumelanin and DNA Repair. *Int J Mol Sci* 2018; **19**: 2667.

117 Ham WT, Ruffolo JJ, Mueller HA, Guerry D. The nature of retinal radiation damage: Dependence on wavelength, power level and exposure time. *Vision Res* 1980; **20**: 1105–1111.

118 Meredith P, Sarna T. The physical and chemical properties of eumelanin. *Pigment Cell Res* 2006; **19**: 572–594.

119 Kobayashi N, Nakagawa A, Muramatsu T, Yamashina Y, Shirai T, Hashimoto MW *et al.* Supranuclear Melanin Caps Reduce Ultraviolet Induced DNA Photoproducts in Human Epidermis. *J Invest Dermatol* 1998; **110**: 806–810.

120 Chedekel MR, Smith SK, Post PW, Pokora A, Vessell DL. Photodestruction of pheomelanin: role of oxygen. *Proc Natl Acad Sci U S A* 1978; **75**: 5395–9.

121 Menon IA, Persad S, Haberman HF, Kurian CJ. A comparative study of the physical and chemical properties of melanins isolated from human black and red hair. *J Invest Dermatol* 1983; **80**: 202–6.

122 Sarna T, Menon IA, Sealy RC. Photosensitization of melanins: a comparative study. *Photochem Photobiol* 1985; **42**: 529–32.

123 Bustamante J, Bredeston L, Malanga G, Mordoh J. Role of melanin as a scavenger of active oxygen species. *Pigment cell Res* 1993; **6**: 348–53.

124 Toulany M, Kehlbach R, Florczak U, Sak A, Wang S, Chen J *et al.* Targeting of AKT1 enhances radiation toxicity of human tumor cells by inhibiting DNA-PKcs-dependent DNA double-strand break repair. *Mol Cancer Ther* 2008; **7**: 1772–1781.

125 Herrling T, Jung K, Fuchs J. The role of melanin as protector against free radicals in skin and its role as free radical indicator in hair. *Spectrochim Acta Part A Mol Biomol Spectrosc* 2008; **69**: 1429–1435.

126 Krol ES, Liebler DC. Photoprotective Actions of Natural and Synthetic Melanins. *Chem Res Toxicol* 1998; **11**: 1434–1440.

127 Tadokoro T, Kobayashi N, Zmudzka BZ, Ito S, Wakamatsu K, Yamaguchi Y *et al.* UV-induced DNA damage and melanin content in human skin differing in racial/ethnic origin. *FASEB J* 2003; **17**: 1177–9.

128 Hauser JE, Kadekaro AL, Kavanagh RJ, Wakamatsu K, Terzieva S, Schwemberger S *et al.* Melanin content and MC1R function independently affect UVR-induced DNA damage in

cultured human melanocytes. *Pigment Cell Res* 2006; **19**: 303–314.

129 Wakamatsu K, Nakanishi Y, Miyazaki N, Kolbe L, Ito S. UVA-induced oxidative degradation of melanins: fission of indole moiety in eumelanin and conversion to benzothiazole moiety in pheomelanin. *Pigment Cell Melanoma Res* 2012; **25**: 434–445.

130 Ye TY, Simon J. Ultrafast Spectroscopic Study of Pheomelanin: Implications on the Mechanism of Superoxide Anion Formation. 2002. doi:10.1021/JP025672L.

131 Bennett DC. Ultraviolet wavebands and melanoma initiation. *Pigment Cell Melanoma Res* 2008; **21**: 520–524.

132 Panzella L, Szewczyk G, d'Ischia M, Napolitano A, Sarna T. Zinc-induced structural effects enhance oxygen consumption and superoxide generation in synthetic pheomelanins on UVA/visible light irradiation. *Photochem Photobiol* 2010; **86**: 757–64.

133 Maresca V, Flori E, Briganti S, Camera E, Cario-André M, Taïeb A *et al.* UVA-induced modification of catalase charge properties in the epidermis is correlated with the skin phototype. *J Invest Dermatol* 2006; **126**: 182–90.

134 Zadlo A, Szewczyk G, Sarna M, Camenisch TG, Sidabras JW, Ito S *et al.* Photobleaching of pheomelanin increases its phototoxic potential: Physicochemical studies of synthetic pheomelanin subjected to aerobic photolysis. *Pigment Cell Melanoma Res* 2018; : pcmr.12752.

135 Maresca V, Flori E, Briganti S, Mastrofrancesco A, Fabbri C, Mileo AM *et al.* Correlation between melanogenic and catalase activity in in vitro human melanocytes: a synergic strategy against oxidative stress. *Pigment Cell Melanoma Res* 2007; **21**: 200–205.

136 Fajuyigbe D, Lwin SM, Diffey BL, Baker R, Tobin DJ, Sarkany RPE *et al.* Melanin distribution in human epidermis affords localized protection against DNA photodamage and concurs with skin cancer incidence difference in extreme phototypes. *FASEB J* 2018; **32**: 3700–3706.

137 Takeuchi S, Zhang W, Wakamatsu K, Ito S, Hearing VJ, Kraemer KH *et al.* Melanin acts as a potent UVB photosensitizer to cause an atypical mode of cell death in murine skin. *Proc Natl Acad Sci* 2004; **101**: 15076–15081.

138 Pavel S, van Nieuwpoort F, van der Meulen H, Out C, Pizinger K, Cetkovská P *et al.* Disturbed melanin synthesis and chronic oxidative stress in dysplastic naevi. *Eur J Cancer* 2004; **40**: 1423–30.

139 Bauer J, Büttner P, Murali R, Okamoto I, Kolaitis NA, Landi MT *et al.* BRAF mutations in cutaneous melanoma are independently associated with age, anatomic site of the primary tumor, and the degree of solar elastosis at the primary tumor site. *Pigment Cell Melanoma Res* 2011; **24**: 345–351.

140 Mitra D, Luo X, Morgan A, Wang J, Hoang MP, Lo J *et al.* An ultraviolet-radiation-independent pathway to melanoma carcinogenesis in the red hair/fair skin background. *Nature* 2012; **491**: 449–453.

141 Morgan AM, Lo J, Fisher DE. How does pheomelanin synthesis contribute to melanomagenesis?: Two distinct mechanisms could explain the carcinogenicity of pheomelanin synthesis. *Bioessays* 2013; **35**: 672–6.

142 Panzella L, Leone L, Greco G, Vitiello G, D'Errico G, Napolitano A *et al.* Red human hair

pheomelanin is a potent pro-oxidant mediating UV-independent contributory mechanisms of melanomagenesis. *Pigment Cell Melanoma Res* 2014; **27**: 244–252.

143 Kim E, Panzella L, Micillo R, Bentley WE, Napolitano A, Payne GF. Reverse Engineering Applied to Red Human Hair Pheomelanin Reveals Redox-Buffering as a Pro-Oxidant Mechanism. *Sci Rep* 2015; **5**: 18447.

144 Lembo S, Di Caprio R, Micillo R, Balato A, Monfrecola G, Panzella L *et al.* Light-independent pro-inflammatory and pro-oxidant effects of purified human hair melanins on keratinocyte cell cultures. *Exp Dermatol* 2017; **26**: 592–594.

145 Płonka PM, Picardo M, Slominski AT. Does melanin matter in the dark? *Exp Dermatol* 2017; **26**: 595–597.

146 Brenner M, Degitz K, Besch R, Berking C. Differential expression of melanoma-associated growth factors in keratinocytes and fibroblasts by ultraviolet A and ultraviolet B radiation. *Br J Dermatol* 2005; **153**: 733–739.

147 Abdel-Malek ZA, Knittel J, Kadekaro AL, Swope VB, Starner R. The Melanocortin 1 Receptor and the UV Response of Human Melanocytes—A Shift in Paradigm. *Photochem Photobiol* 2008; **84**: 501–508.

148 Imokawa G, Yada Y, Miyagishi M. Endothelins secreted from human keratinocytes are intrinsic mitogens for human melanocytes. *J Biol Chem* 1992; **267**: 24675–80.

149 Tada A, Pereira E, Beitner-Johnson D, Kavanagh R, Abdel-Malek ZA. Mitogen- and ultraviolet-B-induced signaling pathways in normal human melanocytes. *J Invest Dermatol* 2002; **118**: 316–22.

150 Mizuno N, Kokubu H, Sato M, Nishimura A, Yamauchi J, Kurose H *et al.* G protein-coupled receptor signaling through Gq and JNK negatively regulates neural progenitor cell migration. *Proc Natl Acad Sci U S A* 2005; **102**: 12365–70.

151 Yada Y, Higuchi K, Imokawa G. Effects of endothelins on signal transduction and proliferation in human melanocytes. *J Biol Chem* 1991; **266**: 18352–7.

152 Imokawa G, Yada Y, Kimura M. Signalling mechanisms of endothelin-induced mitogenesis and melanogenesis in human melanocytes. *Biochem J* 1996; **314 (Pt 1**: 305–12.

153 Halaban R, Langdon R, Birchall N, Cuono C, Baird A, Scott G *et al.* Basic fibroblast growth factor from human keratinocytes is a natural mitogen for melanocytes. *J Cell Biol* 1988; **107**: 1611–9.

154 Hachiya A, Kobayashi A, Ohuchi A, Takema Y, Imokawa G. The paracrine role of stem cell factor/c-kit signaling in the activation of human melanocytes in ultraviolet-B-induced pigmentation. *J Invest Dermatol* 2001; **116**: 578–86.

155 Easty DJ, Gray SG, O'Byrne KJ, O'Donnell D, Bennett DC. Receptor tyrosine kinases and their activation in melanoma. *Pigment Cell Melanoma Res* 2011; **24**: 446–461.

156 Tsao H, Chin L, Garraway LA, Fisher DE. Melanoma: from mutations to medicine. *Genes Dev* 2012; **26**: 1131–55.

157 Suzuki I, Cone RD, Im S, Nordlund J, Abdel-Malek ZA. Binding of melanotropic hormones to the melanocortin receptor MC1R on human melanocytes stimulates proliferation and melanogenesis. *Endocrinology* 1996; **137**: 1627–33.

158 Tada A, Suzuki I, Im S, Davis MB, Cornelius J, Babcock G *et al.* Endothelin-1 is a paracrine growth factor that modulates melanogenesis of human melanocytes and participates in their responses to ultraviolet radiation. *Cell Growth Differ* 1998; **9**: 575–84.

159 Halaban R. The Regulation of Normal Melanocyte Proliferation. *Pigment Cell Res* 2000; **13**: 4–14.

160 Swope VB, Medrano EE, Smalara D, Abdel-Malek ZA. Long-term proliferation of human melanocytes is supported by the physiologic mitogens alpha-melanotropin, endothelin-1, and basic fibroblast growth factor. *Exp Cell Res* 1995; **217**: 453–9.

161 Herraiz C, Journe F, Abdel-Malek Z, Ghanem G, Jimenez-Cervantes C, Garcia-Borron JC. Signaling from the human melanocortin 1 receptor to ERK1 and ERK2 mitogen-activated protein kinases involves transactivation of cKIT. *Mol Endocrinol* 2011; **25**: 138–156.

162 Rousseau K, Kauser S, Pritchard LE, Warhurst A, Oliver RL, Slominski A *et al.* Proopiomelanocortin (POMC), the ACTH/melanocortin precursor, is secreted by human epidermal keratinocytes and melanocytes and stimulates melanogenesis. *FASEB J* 2007; **21**: 1844–1856.

163 Slominski A, Pawelek J. Animals under the sun: effects of ultraviolet radiation on mammalian skin. *Clin Dermatol* 1998; **16**: 503–15.

164 Chakraborty AK, Funasaka Y, Slominski A, Bolognia J, Sodi S, Ichihashi M *et al.* UV light and MSH receptors. *Ann N Y Acad Sci* 1999; **885**: 100–16.

165 Abdel-Malek Z, Swope VB, Suzuki I, Akcali C, Harriger MD, Boyce ST *et al.* Mitogenic and melanogenic stimulation of normal human melanocytes by melanotropic peptides. *Proc Natl Acad Sci U S A* 1995; **92**: 1789–93.

166 Garcia-Borron JC, Sanchez-Laorden BL, Jimenez-Cervantes C. Melanocortin-1 receptor structure and functional regulation. *Pigment Cell Res* 2005; **0**: 051103015727002.

167 Sanchez-Mas J, Hahmann C, Gerritsen I, Garcia-Borron JC, Jimenez-Cervantes C. Agonist-Independent, High Constitutive Activity of the Human Melanocortin 1 Receptor. *Pigment Cell Res* 2004; **17**: 386–395.

168 Böhm M, Luger TA, Tobin DJ, García-Borrón JC. Melanocortin Receptor Ligands: New Horizons for Skin Biology and Clinical Dermatology. *J Invest Dermatol* 2006; **126**: 1966–1975.

169 Wallin E, von Heijne G. Properties of N-terminal tails in G-protein coupled receptors: a statistical study. *Protein Eng* 1995; **8**: 693–8.

170 Sanchez-Mas J, Sanchez-Laorden BL, Guillo LA, Jimenez-Cervantes C, Garcia-Borron JC. The melanocortin-1 receptor carboxyl terminal pentapeptide is essential for MC1R function and expression on the cell surface. *Peptides* 2005; **26**: 1848–1857.

171 Sanchez-Laorden BL, Sanchez-Mas J, Martinez-Alonso E, Martinez-Menarguez JA, Garcia-Borron JC, Jimenez-Cervantes C. Dimerization of the human melanocortin 1 receptor: functional consequences and dominant-negative effects. *J Invest Dermatol* 2006; **126**: 172–181.

172 Sánchez Más J, Olivares Sánchez C, Ghanem G, Haycock J, Lozano Teruel JA, García-Borrón JC *et al.* Loss-of-function variants of the human melanocortin-1 receptor gene in melanoma cells define structural determinants of receptor function. *Eur J Biochem* 2002;

269: 6133–41.

173 Herraiz C, Sánchez-Laorden BL, Jiménez-Cervantes C, García-Borrón JC. N-glycosylation of the human melanocortin 1 receptor: occupancy of glycosylation sequons and functional role. *Pigment Cell Melanoma Res* 2011; **24**: 479–489.

174 Holst B, Schwartz TW. Molecular mechanism of agonism and inverse agonism in the melanocortin receptors: Zn(2+) as a structural and functional probe. *Ann N Y Acad Sci* 2003; **994**: 1–11.

175 Sanchez-Laorden BL, Jimenez-Cervantes C, Garcia-Borron JC. Regulation of human melanocortin 1 receptor signaling and trafficking by Thr-308 and Ser-316 and its alteration in variant alleles associated with red hair and skin cancer. *J Biol Chem* 2006; **282**: 3241–3251.

176 Sanchez-Laorden BL, Herraiz C, Valencia JC, Hearing VJ, Jimenez-Cervantes C, Garcia-Borron JC. Aberrant trafficking of human melanocortin 1 receptor variants associated with red hair and skin cancer: Steady-state retention of mutant forms in the proximal golgi. *J Cell Physiol* 2009; **220**: 640–654.

177 Herraiz C, Journe F, Ghanem G, Jimenez-Cervantes C, Garcia-Borron JC. Functional status and relationships of melanocortin 1 receptor signaling to the cAMP and extracellular signal-regulated protein kinases 1 and 2 pathways in human melanoma cells. *Int J Biochem Cell Biol* 2012; **44**: 2244–2252.

178 Yang Y k, Dickinson C, Haskell-Luevano C, Gantz I. Molecular basis for the interaction of [Nle4,D-Phe7]melanocyte stimulating hormone with the human melanocortin-1 receptor. *J Biol Chem* 1997; **272**: 23000–10.

179 Strader CD, Fong TM, Tota MR, Underwood D, Dixon RAF. Structure and Function of G Protein-Coupled Receptors. *Annu Rev Biochem* 1994; **63**: 101–132.

180 Katritch V, Cherezov V, Stevens RC. Structure-function of the G protein-coupled receptor superfamily. *Annu Rev Pharmacol Toxicol* 2013; **53**: 531–556.

181 Chen S, Zhu B, Yin C, Liu W, Han C, Chen B *et al.* Palmitoylation-dependent activation of MC1R prevents melanomagenesis. *Nature* 2017; **549**: 399–403.

182 Garcia-Borron JC, Jimenez-Cervantes C. Sticky fingers at work: Palmitoylation-dependent MC1R activation. *Pigment Cell Melanoma Res* 2018; **31**: 238–240.

183 Ringholm A, Klovins J, Rudzish R, Phillips S, Rees JL, Schiöth HB. Pharmacological characterization of loss of function mutations of the human melanocortin 1 receptor that are associated with red hair. *J Invest Dermatol* 2004; **123**: 917–923.

184 Herraiz C, Garcia-Borron JC, Jiménez-Cervantes C, Olivares C. MC1R signaling. Intracellular partners and pathophysiological implications. *Biochim Biophys Acta - Mol Basis Dis* 2017. doi:10.1016/j.bbadis.2017.02.027.

185 D'Orazio J, Fisher DE. Central role for cAMP signaling in pigmentation and UV resistance. *Cell Cycle* 2011; **10**: 8–9.

186 Levy C, Khaled M, Fisher DE. MITF: master regulator of melanocyte development and melanoma oncogene. *Trends Mol Med* 2006; **12**: 406–414.

187 Yasumoto K, Yokoyama K, Shibata K, Tomita Y, Shibahara S. Microphthalmia-associated

transcription factor as a regulator for melanocyte-specific transcription of the human tyrosinase gene. *Mol Cell Biol* 1994; **14**: 8058–70.

188 Bentley NJ, Eisen T, Goding CR. Melanocyte-specific expression of the human tyrosinase promoter: activation by the microphthalmia gene product and role of the initiator. *Mol Cell Biol* 1994; **14**: 7996–8006.

189 Bertolotto C, Bille K, Ortonne JP, Ballotti R. Regulation of tyrosinase gene expression by cAMP in B16 melanoma cells involves two CATGTG motifs surrounding the TATA box: implication of the microphthalmia gene product. *J Cell Biol* 1996; **134**: 747–55.

190 Hume AN, Collinson LM, Rapak A, Gomes AQ, Hopkins CR, Seabra MC. Rab27a regulates the peripheral distribution of melanosomes in melanocytes. *J Cell Biol* 2001; **152**: 795–808.

191 Hume AN, Ushakov DS, Tarafder AK, Ferenczi MA, Seabra MC. Rab27a and MyoVa are the primary Mlph interactors regulating melanosome transport in melanocytes. *J Cell Sci* 2007; **120**: 3111–22.

192 Passeron T, Bahadoran P, Bertolotto C, Chiaverini C, Buscà R, Valony G *et al.* Cyclic AMP promotes a peripheral distribution of melanosomes and stimulates melanophilin/Slac2-a and actin association. *FASEB J* 2004; **18**: 989–91.

193 Shoag J, Haq R, Zhang M, Liu L, Rowe GC, Jiang A *et al.* PGC-1 Coactivators Regulate MITF and the Tanning Response. *Mol Cell* 2013; **49**: 145–157.

194 Rodgers JT, Lerin C, Gerhart-Hines Z, Puigserver P. Metabolic adaptations through the PGC-1α and SIRT1 pathways. *FEBS Lett* 2008; **582**: 46–53.

195 Villena JA. New insights into PGC-1 coactivators: redefining their role in the regulation of mitochondrial function and beyond. *FEBS J* 2015; **282**: 647–672.

196 Seifert R, Wenzel-Seifert K. Constitutive activity of G-protein-coupled receptors: cause of disease and common property of wild-type receptors. *Naunyn Schmiedebergs Arch Pharmacol* 2002; **366**: 381–416.

197 Parnot C, Miserey-Lenkei S, Bardin S, Corvol P, Clauser E. Lessons from constitutively active mutants of G protein-coupled receptors. *Trends Endocrinol Metab* 2002; **13**: 336–43.

198 Walker WP, Gunn TM. Shades of meaning: the pigment-type switching system as a tool for discovery. *Pigment Cell Melanoma Res* 2010; **23**: 485–95.

199 Sulem P, Gudbjartsson DF, Stacey SN, Helgason A, Rafnar T, Jakobsdottir M *et al.* Two newly identified genetic determinants of pigmentation in Europeans. *Nat Genet* 2008; **40**: 835–7.

200 Nix MA, Kaelin CB, Ta T, Weis A, Morton GJ, Barsh GS *et al.* Molecular and functional analysis of human β-defensin 3 action at melanocortin receptors. *Chem Biol* 2013; **20**: 784–95.

201 Swope VB, Jameson JA, McFarland KL, Supp DM, Miller WE, McGraw DW *et al.* Defining MC1R regulation in human melanocytes by its agonist α-melanocortin and antagonists agouti signaling protein and β-defensin 3. *J Invest Dermatol* 2012; **132**: 2255–62.

202 Newton RA, Roberts DW, Leonard JH, Sturm RA. Human melanocytes expressing MC1R

variant alleles show impaired activation of multiple signaling pathways. *Peptides* 2007; **28**: 2387–2396.

203 Smalley KSM, Eisen TG. Differentiation of human melanoma cells through p38 MAP kinase is associated with decreased retinoblastoma protein phosphorylation and cell cycle arrest. *Melanoma Res* 2002; **12**: 187–92.

204 Wu M, Hemesath TJ, Takemoto CM, Horstmann MA, Wells AG, Price ER *et al.* c-Kit triggers dual phosphorylations, which couple activation and degradation of the essential melanocyte factor Mi. *Genes Dev* 2000; **14**: 301–12.

205 Xu W, Gong L, Haddad MM, Bischof O, Campisi J, Yeh ET *et al.* Regulation of microphthalmia-associated transcription factor MITF protein levels by association with the ubiquitin-conjugating enzyme hUBC9. *Exp Cell Res* 2000; **255**: 135–43.

206 Vasudevan KM, Garraway LA. AKT signaling in physiology and disease. *Curr Top Microbiol Immunol* 2010; **347**: 105–33.

207 Shtivelman E, Davies MQA, Hwu P, Yang J, Lotem M, Oren M *et al.* Pathways and therapeutic targets in melanoma. *Oncotarget* 2014; **5**: 1701–52.

208 Kadekaro AL, Kavanagh R, Kanto H, Terzieva S, Hauser J, Kobayashi N *et al.* alpha-Melanocortin and endothelin-1 activate antiapoptotic pathways and reduce DNA damage in human melanocytes. *Cancer Res* 2005; **65**: 4292–4299.

209 Cheng L, Cheng L, Bi H, Zhang Z, Yao J, Zhou X *et al.* Alpha-melanocyte stimulating hormone protects retinal pigment epithelium cells from oxidative stress through activation of melanocortin 1 receptor-Akt-mTOR signaling. *Biochem Biophys Res Commun* 2014; **443**: 447–52.

210 Cao J, Wan L, Hacker E, Dai X, Lenna S, Jimenez-Cervantes C *et al.* MC1R is a potent regulator of PTEN after UV exposure in melanocytes. *Mol Cell* 2013; **51**: 409–422.

211 Guo J, Jie W, Shen Z, Li M, Lan Y, Kong Y *et al.* SCF increases cardiac stem cell migration through PI3K/AKT and MMP-2/-9 signaling. *Int J Mol Med* 2014; **34**: 112–8.

212 Dalziel M, Nunes NM, Furger A. Two G-rich regulatory elements located adjacent to and 440 nucleotides downstream of the core poly(A) site of the intronless melanocortin receptor 1 gene are critical for efficient 3' end processing. *Mol Cell Biol* 2007; **27**: 1568–1580.

213 Dalziel M, Kolesnichenko M, das Neves RP, Iborra F, Goding C, Furger A. Alpha-MSH regulates intergenic splicing of MC1R and TUBB3 in human melanocytes. *Nucleic Acids Res* 2011; **39**: 2378–2392.

214 Funasaka Y, Chakraborty AK, Hayashi Y, Komoto M, Ohashi A, Nagahama M *et al.* Modulation of melanocyte-stimulating hormone receptor expression on normal human melanocytes: evidence for a regulatory role of ultraviolet B, interleukin-1alpha, interleukin-1beta, endothelin-1 and tumour necrosis factor-alpha. *Br J Dermatol* 1998; **139**: 216–224.

215 Scott MC, Suzuki I, Abdel-Malek ZA. Regulation of the human melanocortin 1 receptor expression in epidermal melanocytes by paracrine and endocrine factors and by ultraviolet radiation. *Pigment Cell Res* 2002; **15**: 433–439.

216 Kadekaro AL, Leachman S, Kavanagh RJ, Swope V, Cassidy P, Supp D *et al.* Melanocortin 1

receptor genotype: an important determinant of the damage response of melanocytes to ultraviolet radiation. *FASEB J* 2010; **24**: 3850–3860.

217 Aoki H, Moro O. Involvement of microphthalmia-associated transcription factor (MITF) in expression of human melanocortin-1 receptor (MC1R). *Life Sci* 2002; **71**: 2171–9.

218 Martínez-Esparza M, Jiménez-Cervantes C, Solano F, Lozano JA, García-Borrón JC. Mechanisms of melanogenesis inhibition by tumor necrosis factor-alpha in B16/F10 mouse melanoma cells. *Eur J Biochem* 1998; **255**: 139–46.

219 Martínez-Esparza M, Jiménez-Cervantes C, Beermann F, Aparicio P, Lozano JA, García-Borrón JC. Transforming growth factor-beta1 inhibits basal melanogenesis in B16/F10 mouse melanoma cells by increasing the rate of degradation of tyrosinase and tyrosinase-related protein-1. *J Biol Chem* 1997; **272**: 3967–72.

220 Jiménez-Cervantes C, Martínez-Esparza M, Pérez C, Daum N, Solano F, García-Borrón JC. Inhibition of melanogenesis in response to oxidative stress: transient downregulation of melanocyte differentiation markers and possible involvement of microphthalmia transcription factor. *J Cell Sci* 2001; **114**: 2335–44.

221 Zanna PT, Sanchez-Laorden BL, Perez-Oliva AB, Turpin MC, Herraiz C, Jimenez-Cervantes C *et al.* Mechanism of dimerization of the human melanocortin 1 receptor. *Biochem Biophys Res Commun* 2008; **368**: 211–216.

222 Perez Oliva AB, Fernendez LP, Detorre C, Herraiz C, Martinez-Escribano JA, Benitez J *et al.* Identification and functional analysis of novel variants of the human melanocortin 1 receptor found in melanoma patients. *Hum Mutat* 2009; **30**: 811–822.

223 Rajagopal S, Shenoy SK. GPCR desensitization: Acute and prolonged phases. *Cell Signal* 2018; **41**: 9–16.

224 Sánchez-Más J, Guillo LA, Zanna P, Jiménez-Cervantes C, García-Borrón JC. Role of G protein-coupled receptor kinases in the homologous desensitization of the human and mouse melanocortin 1 receptors. *Mol Endocrinol* 2005; **19**: 1035–48.

225 Abrisqueta M, Herraiz C, Perez Oliva AB, Sanchez-Laorden BL, Olivares C, Jimenez-Cervantes C *et al.* Differential and competitive regulation of human melanocortin 1 receptor signaling by beta-arrestin isoforms. *J Cell Sci* 2013; **126**: 3724–3737.

226 Pérez-Oliva AB, Olivares C, Jiménez-Cervantes C, García-Borrón JC. Mahogunin Ring Finger-1 (MGRN1) E3 Ubiquitin Ligase Inhibits Signaling from Melanocortin Receptor by Competition with $G\alpha_s$. *J Biol Chem* 2009; **284**: 31714–31725.

227 Abrisqueta M, Olivares C, Herraiz C, Castejón-Griñán M, Sirés-Campos J, García-Borrón JC *et al.* Human melanocortin 1 receptor-mediated ubiquitination of nonvisual arrestins. Role of Mahogunin Ring Finger 1 E3 ligase. *Biochim Biophys Acta - Mol Cell Res* 2018; **1865**: 76–94.

228 Cui R, Widlund HR, Feige E, Lin JY, Wilensky DL, Igras VE *et al.* Central role of p53 in the suntan response and pathologic hyperpigmentation. *Cell* 2007; **128**: 853–864.

229 Scott MC, Wakamatsu K, Ito S, Kadekaro AL, Kobayashi N, Groden J *et al.* Human melanocortin 1 receptor variants, receptor function and melanocyte response to UV radiation. *J Cell Sci* 2002; **115**: 2349–2355.

230 Park HY, Perez JM, Laursen R, Hara M, Gilchrest BA. Protein kinase C-beta activates

tyrosinase by phosphorylating serine residues in its cytoplasmic domain. *J Biol Chem* 1999; **274**: 16470–8.

231 Kosary CL, Altekruse SF, Ruhl J, Lee R, Dickie L. Clinical and prognostic factors for melanoma of the skin using SEER registries: Collaborative stage data collection system, version 1 and version 2. *Cancer* 2014; **120**: 3807–3814.

232 Matthews NH, Li W-Q, Qureshi AA, Weinstock MA, Cho E. *Epidemiology of Melanoma*. Codon Publications, 2017 doi:10.15586/CODON.CUTANEOUSMELANOMA.2017.CH1.

233 SEER. Cancer Stat Facts: Melanoma of the Skin. Natl. Cancer Institute. Bethesda MD. 2016; : https://seer.cancer.gov/statfacts/html/amyl.html.

234 Siegel RL, Miller KD, Jemal A. Cancer statistics, 2018. *CA Cancer J Clin* 2018; **68**: 7–30.

235 IARC. International Agency for Research on Cancer. Globocan. 2018.https://www.iccp-portal.org/news/globocan-2018.

236 Guy GP, Thomas CC, Thompson T, Watson M, Massetti GM, Richardson LC *et al.* Vital signs: melanoma incidence and mortality trends and projections - United States, 1982-2030. *MMWR Morb Mortal Wkly Rep* 2015; **64**: 591–6.

237 ECIS. European Cancer Information System. Incid. moratlity Estim. 2018. 2018.https://ecis.jrc.ec.europa.eu/.

238 Clark WH, Elder DE, Guerry D, Epstein MN, Greene MH, Van Horn M. A study of tumor progression: the precursor lesions of superficial spreading and nodular melanoma. *Hum Pathol* 1984; **15**: 1147–65.

239 Miller AJ, Mihm MC. Melanoma. *N Engl J Med* 2006; **355**: 51–65.

240 Gogas H, Eggermont AMM, Hauschild A, Hersey P, Mohr P, Schadendorf D *et al.* Biomarkers in melanoma. *Ann Oncol Off J Eur Soc Med Oncol* 2009; **20 Suppl 6**: vi8-13.

241 Horn S, Figl A, Rachakonda PS, Fischer C, Sucker A, Gast A *et al.* TERT Promoter Mutations in Familial and Sporadic Melanoma. *Science (80-)* 2013; **339**: 959–961.

242 Shain AH, Yeh I, Kovalyshyn I, Sriharan A, Talevich E, Gagnon A *et al.* The Genetic Evolution of Melanoma from Precursor Lesions. *N Engl J Med* 2015; **373**: 1926–1936.

243 Gray-Schopfer V, Wellbrock C, Marais R. Melanoma biology and new targeted therapy. *Nature* 2007; **445**: 851–857.

244 Goydos JS, Shoen SL. Acral Lentiginous Melanoma. In: *Cancer treatment and research*. 2016, pp 321–329.

245 Alasadi AH, Alsafy B. Diagnosis of Malignant Melanoma of Skin Cancer Types. *Int J Interact Multimed Artif Intell* 2017; **4**: 44.

246 Dermatoweb. Web docente de Dermatología. *Serv Dermatología Hosp Univ Arnau Vilanova Univ Lleida* 1997.http://dermatoweb.udl.es/.

247 Rodríguez A, Dueñas-Gonzalez A, Delgado-Pelayo S. Clinical presentation and management of uveal melanoma. *Mol Clin Oncol* 2016; **5**: 675–677.

248 Tetzlaff MT, Reuben A, Billings SD, Prieto VG, Curry JL. Toward a Molecular-Genetic Classification of Spitzoid Neoplasms. *Clin Lab Med* 2017; **37**: 431–448.

249 Marques PC, Diniz LM, Spelta K, Nogueira PSE. Desmoplastic melanoma: a rare variant with challenging diagnosis. *An Bras Dermatol* 2019; **94**: 82–85.

250 Boniol M, Autier P, Boyle P, Gandini S. Cutaneous melanoma attributable to sunbed use: systematic review and meta-analysis. *BMJ* 2012; **345**: e4757.

251 Gandini S, Sera F, Cattaruzza MS, Pasquini P, Picconi O, Boyle P *et al.* Meta-analysis of risk factors for cutaneous melanoma: II. Sun exposure. *Eur J Cancer* 2005; **41**: 45–60.

252 Kricker A, Armstrong BK, Goumas C, Litchfield M, Begg CB, Hummer AJ *et al.* Ambient UV, personal sun exposure and risk of multiple primary melanomas. *Cancer Causes Control* 2007; **18**: 295–304.

253 Wu S, Han J, Laden F, Qureshi AA. Long-term Ultraviolet Flux, Other Potential Risk Factors, and Skin Cancer Risk: A Cohort Study. *Cancer Epidemiol Biomarkers Prev* 2014; **23**: 1080–1089.

254 Mire L, Hollowood K, Gray D, Bordea C, Wojnarowska F. Melanomas in renal transplant recipients. *Br J Dermatol* 2006; **154**: 472–477.

255 Sullivan AN, Bryant EA, Mark LA. Malignant melanoma in transplant patients: a case report and review of the literature. *Cutis* 2012; **89**: 133–6.

256 American Cancer Society. Cancer Facts &Figures 2018. *Am Cancer Soc* 2018. doi:10.1182/blood-2015-12-687814.

257 Hussussian CJ, Struewing JP, Goldstein AM, Higgins PAT, Ally DS, Sheahan MD *et al.* Germline p16 mutations in familial melanoma. *Nat Genet* 1994; **8**: 15–21.

258 Kamb A, Shattuck-Eidens D, Eeles R, Liu Q, Gruis NA, Ding W *et al.* Analysis of the p16 gene (CDKN2) as a candidate for the chromosome 9p melanoma susceptibility locus. *Nat Genet* 1994; **8**: 23–6.

259 Rizos H, Darmanian AP, Holland EA, Mann GJ, Kefford RF. Mutations in the INK4a/ARF melanoma susceptibility locus functionally impair p14ARF. *J Biol Chem* 2001; **276**: 41424–34.

260 Puntervoll HE, Yang XR, Vetti HH, Bachmann IM, Avril MF, Benfodda M *et al.* Melanoma prone families with CDK4 germline mutation: phenotypic profile and associations with MC1R variants. *J Med Genet* 2013; **50**: 264–70.

261 Hayward NK. Genetics of melanoma predisposition. *Oncogene* 2003; **22**: 3053–3062.

262 Robles-Espinoza CD, Harland M, Ramsay AJ, Aoude LG, Quesada V, Ding Z *et al.* POT1 loss-of-function variants predispose to familial melanoma. *Nat Genet* 2014; **46**: 478–481.

263 Aoude LG, Wadt KAW, Pritchard AL, Hayward NK. Genetics of familial melanoma: 20 years after *CDKN2A*. *Pigment Cell Melanoma Res* 2015; **28**: 148–160.

264 Duffy DL, Box NF, Chen W, Palmer JS, Montgomery GW, James MR *et al.* Interactive effects of MC1R and OCA2 on melanoma risk phenotypes. *Hum Mol Genet* 2004; **13**: 447–61.

265 Palmer JS, Duffy DL, Box NF, Aitken JF, O'Gorman LE, Green AC *et al.* Melanocortin-1 Receptor Polymorphisms and Risk of Melanoma: Is the Association Explained Solely by Pigmentation Phenotype? *Am J Hum Genet* 2000; **66**: 176–186.

266 Raimondi S, Sera F, Gandini S, Iodice S, Caini S, Maisonneuve P *et al.* MC1R variants, melanoma and red hair color phenotype: A meta-analysis. *Int J Cancer* 2008; **122**: 2753–2760.

267 Tagliabue E, Gandini S, Bellocco R, Maisonneuve P, Newton-Bishop J, Polsky D *et al.* MC1R variants as melanoma risk factors independent of at-risk phenotypic characteristics: a pooled analysis from the M-SKIP project. *Cancer Manag Res* 2018; **10**: 1143–1154.

268 Pasquali E, Garcia-Borron JC, Fargnoli MC, Gandini S, Maisonneuve P, Bagnardi V *et al.* MC1R variants increased the risk of sporadic cutaneous melanoma in darker-pigmented Caucasians: a pooled-analysis from the M-SKIP project. *Int J Cancer* 2015; **136**: 618–631.

269 Sturm RA. Skin colour and skin cancer - MC1R, the genetic link. *Melanoma Res* 2002; **12**: 405–16.

270 van der Velden PA, Sandkuijl LA, Bergman W, Pavel S, van Mourik L, Frants RR *et al.* Melanocortin-1 receptor variant R151C modifies melanoma risk in Dutch families with melanoma. *Am J Hum Genet* 2001; **69**: 774–9.

271 Box NF, Duffy DL, Chen W, Stark M, Martin NG, Sturm RA *et al.* MC1R Genotype Modifies Risk of Melanoma in Families Segregating CDKN2A Mutations. *Am J Hum Genet* 2001; **69**: 765–773.

272 Hayward NK, Wilmott JS, Waddell N, Johansson PA, Field MA, Nones K *et al.* Whole-genome landscapes of major melanoma subtypes. *Nature* 2017; **545**: 175–180.

273 Lawrence MS, Stojanov P, Polak P, Kryukov G V, Cibulskis K, Sivachenko A *et al.* Mutational heterogeneity in cancer and the search for new cancer-associated genes. *Nature* 2013; **499**: 214–218.

274 Krauthammer M, Kong Y, Ha BH, Evans P, Bacchiocchi A, McCusker JP *et al.* Exome sequencing identifies recurrent somatic RAC1 mutations in melanoma. *Nat Genet* 2012; **44**: 1006–1014.

275 Johansson PA, Pritchard AL, Patch A-M, Wilmott JS, Pearson J V., Waddell N *et al.* Mutation load in melanoma is affected by *MC1R* genotype. *Pigment Cell Melanoma Res* 2017; **30**: 255–258.

276 Robles-Espinoza CD, Roberts ND, Chen S, Leacy FP, Alexandrov LB, Pornputtapong N *et al.* Germline MC1R status influences somatic mutation burden in melanoma. *Nat Commun* 2016; **7**: 12064.

277 Akbani R, Akdemir KC, Aksoy BA, Albert M, Ally A, Amin SB *et al.* Genomic Classification of Cutaneous Melanoma. *Cell* 2015; **161**: 1681–1696.

278 Gorden A, Osman I, Gai W, He D, Huang W, Davidson A *et al.* Analysis of BRAF and N-RAS mutations in metastatic melanoma tissues. *Cancer Res* 2003; **63**: 3955–7.

279 Kiuru M, Busam KJ. The NF1 gene in tumor syndromes and melanoma. *Lab Invest* 2017; **97**: 146–157.

280 Cirenajwis H, Lauss M, Ekedahl H, Törngren T, Kvist A, Saal LH *et al.* NF1-mutated melanoma tumors harbor distinct clinical and biological characteristics. *Mol Oncol* 2017; **11**: 438–451.

281 Lo JA, Fisher DE. The melanoma revolution: From UV carcinogenesis to a new era in therapeutics. *Science (80-)* 2014; **346**: 945–949.

282 Johnpulle RAN, Johnson DB, Sosman JA. Molecular Targeted Therapy Approaches for BRAF Wild-Type Melanoma. *Curr Oncol Rep* 2016; **18**: 6.

283 Krauthammer M, Kong Y, Bacchiocchi A, Evans P, Pornputtapong N, Wu C *et al.* Exome sequencing identifies recurrent mutations in NF1 and RASopathy genes in sun-exposed melanomas. *Nat Genet* 2015; **47**: 996–1002.

284 Shain AH, Garrido M, Botton T, Talevich E, Yeh I, Sanborn JZ *et al.* Exome sequencing of desmoplastic melanoma identifies recurrent NFKBIE promoter mutations and diverse activating mutations in the MAPK pathway. *Nat Genet* 2015; **47**: 1194–1199.

285 Omholt K, Kröckel D, Ringborg U, Hansson J. Mutations of PIK3CA are rare in cutaneous melanoma. *Melanoma Res* 2006; **16**: 197–200.

286 Davies MA, Stemke-Hale K, Tellez C, Calderone TL, Deng W, Prieto VG *et al.* A novel AKT3 mutation in melanoma tumours and cell lines. *Br J Cancer* 2008; **99**: 1265–1268.

287 Tsao H, Zhang X, Benoit E, Haluska FG. Identification of PTEN/MMAC1 alterations in uncultured melanomas and melanoma cell lines. *Oncogene* 1998; **16**: 3397–402.

288 Jönsson G, Dahl C, Staaf J, Sandberg T, Bendahl P-O, Ringnér M *et al.* Genomic profiling of malignant melanoma using tiling-resolution arrayCGH. *Oncogene* 2007; **26**: 4738–48.

289 Berger MF, Hodis E, Heffernan TP, Deribe YL, Lawrence MS, Protopopov A *et al.* Melanoma genome sequencing reveals frequent PREX2 mutations. *Nature* 2012; **485**: 502–506.

290 Weinhold N, Jacobsen A, Schultz N, Sander C, Lee W. Genome-wide analysis of noncoding regulatory mutations in cancer. *Nat Genet* 2014; **46**: 1160–1165.

291 Fredriksson NJ, Ny L, Nilsson JA, Larsson E. Systematic analysis of noncoding somatic mutations and gene expression alterations across 14 tumor types. *Nat Genet* 2014; **46**: 1258–63.

292 Hodis E, Watson IR, Kryukov G V, Arold ST, Imielinski M, Theurillat JP *et al.* A landscape of driver mutations in melanoma. *Cell* 2012; **150**: 251–263.

293 Stefansson B, Brautigan DL. Protein Phosphatase PP6 N Terminal Domain Restricts G_1 to S Phase Progression in Human Cancer Cells. *Cell Cycle* 2007; **6**: 1386–1392.

294 Zeng K, Bastos RN, Barr FA, Gruneberg U. Protein phosphatase 6 regulates mitotic spindle formation by controlling the T-loop phosphorylation state of Aurora A bound to its activator TPX2. *J Cell Biol* 2010; **191**: 1315–32.

295 Barr FA, Elliott PR, Gruneberg U. Protein phosphatases and the regulation of mitosis. *J Cell Sci* 2011; **124**: 2323–34.

296 Nikolaev SI, Rimoldi D, Iseli C, Valsesia A, Robyr D, Gehrig C *et al.* Exome sequencing identifies recurrent somatic MAP2K1 and MAP2K2 mutations in melanoma. *Nat Genet* 2011; **44**: 133–9.

297 Wei X, Walia V, Lin JC, Teer JK, Prickett TD, Gartner J *et al.* Exome sequencing identifies GRIN2A as frequently mutated in melanoma. *Nat Genet* 2011; **43**: 442–446.

298 Stark MS, Woods SL, Gartside MG, Bonazzi VF, Dutton-Regester K, Aoude LG *et al.* Frequent somatic mutations in MAP3K5 and MAP3K9 in metastatic melanoma identified by exome sequencing. *Nat Genet* 2011; **44**: 165–9.

299 Smith AG, Box NF, Marks LH, Chen W, Smit DJ, Wyeth JR *et al.* The human melanocortin-1 receptor locus: analysis of transcription unit, locus polymorphism and haplotype evolution. *Gene* 2001; **281**: 81–94.

300 Tan CP, McKee KK, Weinberg DH, MacNeil T, Palyha OC, Feighner SD *et al.* Molecular analysis of a new splice variant of the human melanocortin-1 receptor. *FEBS Lett* 1999; **451**: 137–141.

301 Rouzaud F, Costin GE, Yamaguchi Y, Valencia JC, Berens WF, Chen KG *et al.* Regulation of constitutive and UVR-induced skin pigmentation by melanocortin 1 receptor isoforms. *FASEB J* 2006; **20**: 1927–1929.

302 Valverde P, Healy E, Jackson I, Rees JL, Thody a J. Variants of the melanocyte-stimulating hormone receptor gene are associated with red hair and fair skin in humans. *Nat Genet* 1995; **11**: 328–330.

303 Healy E, Jordan SA, Budd PS, Suffolk R, Rees JL, Jackson IJ. Functional variation of MC1R alleles from red-haired individuals. *Hum Mol Genet* 2001; **10**: 2397–2402.

304 Gerstenblith MR, Goldstein AM, Fargnoli MC, Peris K, Landi MT. Comprehensive evaluation of allele frequency differences of MC1R variants across populations. *Hum Mutat* 2007; **28**: 495–505.

305 Savage SA, Gerstenblith MR, Goldstein AM, Mirabello L, Fargnoli MC, Peris K *et al.* Nucleotide diversity and population differentiation of the Melanocortin 1 Receptor gene, MC1R. *BMC Genet* 2008; **9**: 31.

306 John PR, Makova K, Li W-H, Jenkins T, Ramsay M. DNA Polymorphism and Selection at the Melanocortin-1 Receptor Gene in Normally Pigmented Southern African Individuals. *Ann N Y Acad Sci* 2003; **994**: 299–306.

307 Harding RM, Healy E, Ray AJ, Ellis NS, Flanagan N, Todd C *et al.* Evidence for Variable Selective Pressures at MC1R. *Am J Hum Genet* 2000; **66**: 1351–1361.

308 Martínez-Cadenas C, López S, Ribas G, Flores C, García O, Sevilla A *et al.* Simultaneous Purifying Selection on the Ancestral MC1R Allele and Positive Selection on the Melanoma-Risk Allele V60L in South Europeans. *Mol Biol Evol* 2013; **30**: 2654–2665.

309 Jablonski NG, Chaplin G. Human skin pigmentation as an adaptation to UV radiation. *Proc Natl Acad Sci* 2010; **107**: 8962–8968.

310 Herraiz C, Jimenez-Cervantes C, Zanna P, Garcia-Borron JC. Melanocortin 1 receptor mutations impact differentially on signalling to the cAMP and the ERK mitogen-activated protein kinase pathways. *FEBS Lett* 2009; **583**: 3269–3274.

311 Frandberg PA, Doufexis M, Kapas S, Chhajlani V. Human pigmentation phenotype: a point mutation generates nonfunctional MSH receptor. *Biochem Biophys Res Commun* 1998; **245**: 490–492.

312 Newton RA, Smit SE, Barnes CC, Pedley J, Parsons PG, Sturm RA. Activation of the cAMP pathway by variant human MC1R alleles expressed in HEK and in melanoma cells. *Peptides* 2005; **26**: 1818–1824.

313 Schiöth HB, Phillips SR, Rudzish R, Birch-Machin M a, Wikberg JE, Rees JL. Loss of function mutations of the human melanocortin 1 receptor are common and are associated with red hair. *Biochem Biophys Res Commun* 1999; **260**: 488–491.

314 Garcia-Borron JC, Olivares C. Melanocortin 1 receptor and skin pathophysiology: beyond colour, much more than meets the eye. *Exp Dermatol* 2014; **23**: 387–388.

315 Shahzad M, Sires Campos J, Tariq N, Herraiz Serrano C, Yousaf R, Jiménez-Cervantes C *et al.* Identification and functional characterization of natural human melanocortin 1 receptor mutant alleles in Pakistani population. *Pigment Cell Melanoma Res* 2015; **28**: 730–5.

316 Beaumont KA, Shekar SL, Newton RA, James MR, Stow JL, Duffy DL *et al.* Receptor function, dominant negative activity and phenotype correlations for MC1R variant alleles. *Hum Mol Genet* 2007; **16**: 2249–2260.

317 Beaumont KA, Newton RA, Smit DJ, Leonard JH, Stow JL, Sturm RA. Altered cell surface expression of human MC1R variant receptor alleles associated with red hair and skin cancer risk. *Hum Mol Genet* 2005; **14**: 2145–2154.

318 Sanchez-Laorden BL, Sanchez-Mas J, Turpin MC, Garcia-Borron JC, Jimenez-Cervantes C. Variant amino acids in different domains of the human melanocortin 1 receptor impair cell surface expression. *Cell Mol Biol* 2006; **52**: 39–46.

319 Chatzinasiou F, Lill CM, Kypreou K, Stefanaki I, Nicolaou V, Spyrou G *et al.* Comprehensive Field Synopsis and Systematic Meta-analyses of Genetic Association Studies in Cutaneous Melanoma. *JNCI J Natl Cancer Inst* 2011; **103**: 1227–1235.

320 Williams PF, Olsen CM, Hayward NK, Whiteman DC. Melanocortin 1 receptor and risk of cutaneous melanoma: a meta-analysis and estimates of population burden. *Int J Cancer* 2011; **129**: 1730–1740.

321 Barnetson RS, Ooi TKT, Zhuang L, Halliday GM, Reid CM, Walker PC *et al.* [Nle4-D-Phe7]-α-Melanocyte-Stimulating Hormone Significantly Increased Pigmentation and Decreased UV Damage in Fair-Skinned Caucasian Volunteers. *J Invest Dermatol* 2006; **126**: 1869–1878.

322 Kadekaro AL, Wakamatsu K, Ito S, Abdel-Malek ZA. Cutaneous photoprotection and melanoma susceptibility: reaching beyond melanin content to the frontiers of DNA repair. *Front Biosci* 2006; **11**: 2157–73.

323 Bastiaens MT, ter Huurne J a, Kielich C, Gruis N a, Westendorp RG, Vermeer BJ *et al.* Melanocortin-1 receptor gene variants determine the risk of nonmelanoma skin cancer independently of fair skin and red hair. *Am J Hum Genet* 2001; **68**: 884–894.

324 Kennedy C, ter Huurne J, Berkhout M, Gruis N, Bastiaens M, Bergman W *et al.* Melanocortin 1 Receptor (MC1R) Gene Variants are Associated with an Increased Risk for Cutaneous Melanoma Which is Largely Independent of Skin Type and Hair Color. *J Invest Dermatol* 2001; **117**: 294–300.

325 Landi MT, Kanetsky PA, Tsang S, Gold B, Munroe D, Rebbeck T *et al.* MC1R, ASIP, and DNA Repair in Sporadic and Familial Melanoma in a Mediterranean Population. *JNCI J Natl Cancer Inst* 2005; **97**: 998–1007.

326 Maresca V, Flori E, Bellei B, Aspite N, Kovacs D, Picardo M. MC1R stimulation by alpha-MSH induces catalase and promotes its re-distribution to the cell periphery and

dendrites. *Pigment Cell Melanoma Res* 2010; **23**: 263–75.

327 Swope VB, Abdel-Malek ZA. Significance of the Melanocortin 1 and Endothelin B Receptors in Melanocyte Homeostasis and Prevention of Sun-Induced Genotoxicity. *Front Genet* 2016; **7**: 146.

328 Bohm M, Wolff I, Scholzen TE, Robinson SJ, Healy E, Luger TA *et al.* alpha-Melanocyte-stimulating hormone protects from ultraviolet radiation-induced apoptosis and DNA damage. *J Biol Chem* 2005; **280**: 5795–5802.

329 Kadekaro AL, Chen J, Yang J, Chen S, Jameson J, Swope VB *et al.* Alpha-Melanocyte-Stimulating Hormone Suppresses Oxidative Stress through a p53-Mediated Signaling Pathway in Human Melanocytes. *Mol Cancer Res* 2012; **10**: 778–786.

330 Denat L, Kadekaro AL, Marrot L, Leachman SA, Abdel-Malek ZA. Melanocytes as instigators and victims of oxidative stress. *J Invest Dermatol* 2014; **134**: 1512–1518.

331 Song X, Mosby N, Yang J, Xu A, Abdel-Malek Z, Kadekaro AL. alpha-MSH activates immediate defense responses to UV-induced oxidative stress in human melanocytes. *Pigment Cell Melanoma Res* 2009; **22**: 809–18.

332 Kadekaro AL, Kavanagh R, Kanto H, Terzieva S, Hauser J, Kobayashi N *et al.* alpha-Melanocortin and endothelin-1 activate antiapoptotic pathways and reduce DNA damage in human melanocytes. *Cancer Res* 2005; **65**: 4292–9.

333 D'Orazio JA, Nobuhisa T, Cui R, Arya M, Spry M, Wakamatsu K *et al.* Topical drug rescue strategy and skin protection based on the role of Mc1r in UV-induced tanning. *Nature* 2006; **443**: 340–4.

334 Jarrett SG, Horrell EMW, Christian PA, Vanover JC, Boulanger MC, Zou Y *et al.* PKA-Mediated Phosphorylation of ATR Promotes Recruitment of XPA to UV-Induced DNA Damage. *Mol Cell* 2014; **54**: 999–1011.

335 Kokot A, Metze D, Mouchet N, Galibert M-D, Schiller M, Luger TA *et al.* α-Melanocyte-Stimulating Hormone Counteracts the Suppressive Effect of UVB on Nrf2 and Nrf-Dependent Gene Expression in Human Skin. *Endocrinology* 2009; **150**: 3197–3206.

336 Abdel-Malek ZA, Swope VB, Starner RJ, Koikov L, Cassidy P, Leachman S. Melanocortins and the melanocortin 1 receptor, moving translationally towards melanoma prevention. *Arch Biochem Biophys* 2014; **563**: 4–12.

337 Jarrett SG, Carter KM, Shelton BJ, D'Orazio JA. The melanocortin signaling cAMP axis accelerates repair and reduces mutagenesis of platinum-induced DNA damage. *Sci Rep* 2017; **7**: 11708.

338 Jarrett SG, Carter KM, D'Orazio JA. Paracrine regulation of melanocyte genomic stability: a focus on nucleotide excision repair. *Pigment Cell Melanoma Res* 2017; **30**: 284–293.

339 Wolf Horrell EM, Jarrett SG, Carter KM, D'Orazio JA. Divergence of cAMP signalling pathways mediating augmented nucleotide excision repair and pigment induction in melanocytes. *Exp Dermatol* 2017; **26**: 577–584.

340 Cotter MA, Thomas J, Cassidy P, Robinette K, Jenkins N, Florell SR *et al.* N-acetylcysteine protects melanocytes against oxidative stress/damage and delays onset of ultraviolet-induced melanoma in mice. *Clin Cancer Res* 2007; **13**: 5952–8.

341 Kim J-S, Diebold BA, Babior BM, Knaus UG, Bokoch GM. Regulation of Nox1 Activity via Protein Kinase A-mediated Phosphorylation of NoxA1 and 14-3-3 Binding. *J Biol Chem* 2007; **282**: 34787–34800.

342 Henri P, Beaumel S, Guezennec A, Poumès C, Stoebner P-E, Stasia M-J *et al.* MC1R expression in HaCaT keratinocytes inhibits UVA-induced ROS production via NADPH oxidase- and cAMP-dependent mechanisms. *J Cell Physiol* 2012; **227**: 2578–85.

343 Matés JM, Sánchez-Jiménez FM. Role of reactive oxygen species in apoptosis: implications for cancer therapy. *Int J Biochem Cell Biol* 2000; **32**: 157–70.

344 Arosio P, Levi S. Ferritin, iron homeostasis, and oxidative damage. *Free Radic Biol Med* 2002; **33**: 457–63.

345 Njålsson R, Norgren S. Physiological and pathological aspects of GSH metabolism. *Acta Paediatr* 2005; **94**: 132–7.

346 Hanawalt PC. Subpathways of nucleotide excision repair and their regulation. *Oncogene* 2002; **21**: 8949–8956.

347 Yin K, Sturm RA, Smith AG. MC1R and NR4A receptors in cellular stress and DNA repair: implications for UVR protection. *Exp Dermatol* 2014; **23**: 449–452.

348 Jagirdar K, Yin K, Harrison M, Lim W, Muscat GEO, Sturm RA *et al.* The NR4A2 Nuclear Receptor Is Recruited to Novel Nuclear Foci in Response to UV Irradiation and Participates in Nucleotide Excision Repair. *PLoS One* 2013; **8**: e78075.

349 Abdel-Malek ZA, Ruwe A, Kavanagh-Starner R, Kadekaro AL, Swope V, Haskell-Luevano C *et al.* alpha-MSH tripeptide analogs activate the melanocortin 1 receptor and reduce UV-induced DNA damage in human melanocytes. *Pigment Cell Melanoma Res* 2009; **22**: 635–44.

350 Swope V, Alexander C, Starner R, Schwemberger S, Babcock G, Abdel-Malek ZA. Significance of the melanocortin 1 receptor in the DNA damage response of human melanocytes to ultraviolet radiation. *Pigment Cell Melanoma Res* 2014; **27**: 601–610.

351 Wong SS, Ainger SA, Leonard JH, Sturm RA. MC1R variant allele effects on UVR-induced phosphorylation of p38, p53, and DDB2 repair protein responses in melanocytic cells in culture. *J Invest Dermatol* 2012; **132**: 1452–61.

352 Ray A, Milum K, Battu A, Wani G, Wani AA. NER initiation factors, DDB2 and XPC, regulate UV radiation response by recruiting ATR and ATM kinases to DNA damage sites. *DNA Repair (Amst)* 2013; **12**: 273–283.

353 Hanasoge S, Ljungman M. H2AX phosphorylation after UV irradiation is triggered by DNA repair intermediates and is mediated by the ATR kinase. *Carcinogenesis* 2007; **28**: 2298–304.

354 Blackford AN, Jackson SP. ATM, ATR, and DNA-PK: The Trinity at the Heart of the DNA Damage Response. *Mol Cell* 2017; **66**: 801–817.

355 Jarrett SG, D'Orazio JA. Hormonal Regulation of the Repair of UV Photoproducts in Melanocytes by the Melanocortin Signaling Axis. *Photochem Photobiol* 2017; **93**: 245–258.

356 Cassidy PB, Abdel-Malek ZA, Leachman SA. Beyond Red Hair and Sunburns: Uncovering

the Molecular Mechanisms of MC1R Signaling and Repair of UV-Induced DNA Damage. *J Invest Dermatol* 2015; **135**: 2918–2921.

357 Jarrett SG, Wolf Horrell EM, D'Orazio JA. AKAP12 mediates PKA-induced phosphorylation of ATR to enhance nucleotide excision repair. *Nucleic Acids Res* 2016; **44**: 10711–10726.

358 Strub T, Giuliano S, Ye T, Bonet C, Keime C, Kobi D *et al.* Essential role of microphthalmia transcription factor for DNA replication, mitosis and genomic stability in melanoma. *Oncogene* 2011; **30**: 2319–2332.

359 April CS, Barsh GS. Skin layer-specific transcriptional profiles in normal and recessive yellow (Mc1re/Mc1re) mice. *Pigment Cell Res* 2006; **19**: 194–205.

360 Wolf Horrell EM, Boulanger MC, D'Orazio JA. Melanocortin 1 Receptor: Structure, Function, and Regulation. *Front Genet* 2016; **7**: 95.

361 Cadet J, Douki T. Oxidatively Generated Damage to DNA by UVA Radiation in Cells and Human Skin. *J Invest Dermatol* 2011; **131**: 1005–1007.

362 Kinner A, Wu W, Staudt C, Iliakis G. Gamma-H2AX in recognition and signaling of DNA double-strand breaks in the context of chromatin. *Nucleic Acids Res* 2008; **36**: 5678–5694.

363 Malewicz M, Kadkhodaei B, Kee N, Volakakis N, Hellman U, Viktorsson K *et al.* Essential role for DNA-PK-mediated phosphorylation of NR4A nuclear orphan receptors in DNA double-strand break repair. *Genes Dev* 2011; **25**: 2031–40.

364 Fernandez-Capetillo O, Lee A, Nussenzweig M, Nussenzweig A. H2AX: the histone guardian of the genome. *DNA Repair (Amst)* 2004; **3**: 959–967.

365 Smith AG, Luk N, Newton RA, Roberts DW, Sturm RA, Muscat GEO. Melanocortin-1 receptor signaling markedly induces the expression of the NR4A nuclear receptor subgroup in melanocytic cells. *J Biol Chem* 2008; **283**: 12564–70.

366 Hoek KS. DNA microarray analyses of melanoma gene expression: a decade in the mines. *Pigment Cell Res* 2007; **20**: 466–484.

367 Cohen-Armon M. PARP-1 activation in the ERK signaling pathway. *Trends Pharmacol Sci* 2007; **28**: 556–60.

368 Wei F, Yan J, Tang D. Extracellular signal-regulated kinases modulate DNA damage response - a contributing factor to using MEK inhibitors in cancer therapy. *Curr Med Chem* 2011; **18**: 5476–82.

369 Hawkins AJ, Golding SE, Khalil A, Valerie K. DNA double-strand break - induced pro-survival signaling. *Radiother Oncol* 2011; **101**: 13–7.

370 Liu Q, Turner KM, Alfred Yung WK, Chen K, Zhang W. Role of AKT signaling in DNA repair and clinical response to cancer therapy. *Neuro Oncol* 2014; **16**: 1313–1323.

371 Toulany M, Rodemann HP. Phosphatidylinositol 3-kinase/Akt signaling as a key mediator of tumor cell responsiveness to radiation. *Semin Cancer Biol* 2015; **35**: 180–190.

372 Singh P, Dar MS, Dar MJ. p110α and p110β isoforms of PI3K signaling: are they two sides of the same coin? *FEBS Lett* 2016; **590**: 3071–3082.

373 Rodríguez-Escudero I, Oliver MD, Andrés-Pons A, Molina M, Cid VJ, Pulido R. A

comprehensive functional analysis of PTEN mutations: implications in tumor- and autism-related syndromes. *Hum Mol Genet* 2011; **20**: 4132–4142.

374 Monaghan RM, Barnes RG, Fisher K, Andreou T, Rooney N, Poulin GB *et al.* A nuclear role for the respiratory enzyme CLK-1 in regulating mitochondrial stress responses and longevity. *Nat Cell Biol* 2015; **17**: 782–792.

375 Luo Z, Chen Y, Chen S, Welch W, Andresen B, Jose P *et al.* Comparison of inhibitors of superoxide generation in vascular smooth muscle cells. *Br J Pharmacol* 2009; **157**: 935–943.

376 Altieri F, Grillo C, Maceroni M, Chichiarelli S. DNA Damage and Repair: From Molecular Mechanisms to Health Implications. *Antioxid Redox Signal* 2008; **10**: 891–938.

377 Löbrich M, Shibata A, Beucher A, Fisher A, Ensminger M, Goodarzi AA *et al.* gammaH2AX foci analysis for monitoring DNA double-strand break repair: strengths, limitations and optimization. *Cell Cycle* 2010; **9**: 662–9.

378 Podhorecka M, Skladanowski A, Bozko P. H2AX Phosphorylation: Its Role in DNA Damage Response and Cancer Therapy. *J Nucleic Acids* 2010; **2010**: 1–9.

379 Khaled M. Glycogen Synthase Kinase 3beta Is Activated by cAMP and Plays an Active Role in the Regulation of Melanogenesis. *J Biol Chem* 2002; **277**: 33690–33697.

380 Gharbi SI, Zvelebil MJ, Shuttleworth SJ, Hancox T, Saghir N, Timms JF *et al.* Exploring the specificity of the PI3K family inhibitor LY294002. *Biochem J* 2007; **404**: 15–21.

381 Jo H, Mondal S, Tan D, Nagata E, Takizawa S, Sharma AK *et al.* Small molecule-induced cytosolic activation of protein kinase Akt rescues ischemia-elicited neuronal death. *Proc Natl Acad Sci* 2012; **109**: 10581–10586.

382 Sakumi K, Tominaga Y, Furuichi M, Xu P, Tsuzuki T, Sekiguchi M *et al.* Ogg1 knockout-associated lung tumorigenesis and its suppression by Mth1 gene disruption. *Cancer Res* 2003; **63**: 902–5.

383 Hegde ML, Izumi T, Mitra S. Oxidized Base Damage and Single-Strand Break Repair in Mammalian Genomes. In: *Progress in molecular biology and translational science*. 2012, pp 123–153.

384 Groeger G, Quiney C, Cotter TG. Hydrogen peroxide as a cell-survival signaling molecule. *Antioxid Redox Signal* 2009; **11**: 2655–71.

385 Liu-Smith F, Dellinger R, Meyskens FL. Updates of reactive oxygen species in melanoma etiology and progression. *Arch Biochem Biophys* 2014; **563**: 51–5.

386 Gough DR, Cotter TG. Hydrogen peroxide: a Jekyll and Hyde signalling molecule. *Cell Death Dis* 2011; **2**: e213–e213.

387 Koundouros N, Poulogiannis G. Phosphoinositide 3-Kinase/Akt Signaling and Redox Metabolism in Cancer. *Front Oncol* 2018; **8**: 160.

388 Krylatov A V, Maslov LN, Voronkov NS, Boshchenko AA, Popov S V, Gomez L *et al.* Reactive Oxygen Species as Intracellular Signaling Molecules in the Cardiovascular System. *Curr Cardiol Rev* 2018; **14**: 290–300.

389 Petry A, Görlach A. Regulation of NADPH Oxidases by G Protein-Coupled Receptors. *Antioxid Redox Signal* 2019; **30**: 74–94.

390 Altenhöfer S, Radermacher KA, Kleikers PWM, Wingler K, Schmidt HHHW. Evolution of NADPH Oxidase Inhibitors: Selectivity and Mechanisms for Target Engagement. *Antioxid Redox Signal* 2015; **23**: 406–427.

391 Teixeira G, Szyndralewiez C, Molango S, Carnesecchi S, Heitz F, Wiesel P *et al.* Therapeutic potential of NADPH oxidase 1/4 inhibitors. *Br J Pharmacol* 2017; **174**: 1647–1669.

392 Markovic D, Challiss RAJ. Alternative splicing of G protein-coupled receptors: physiology and pathophysiology. *Cell Mol Life Sci* 2009; **66**: 3337–52.

393 Jividen K, Li H. Chimeric RNAs generated by intergenic splicing in normal and cancer cells. *Genes Chromosom Cancer* 2014; **53**: 963–971.

394 Communi D, Suarez-Huerta N, Dussossoy D, Savi P, Boeynaems JM. Cotranscription and intergenic splicing of human P2Y11 and SSF1 genes. *J Biol Chem* 2001; **276**: 16561–6.

395 Needham PG, Brodsky JL. How early studies on secreted and membrane protein quality control gave rise to the ER associated degradation (ERAD) pathway: the early history of ERAD. *Biochim Biophys Acta* 2013; **1833**: 2447–2457.

396 Corre S, Primot A, Sviderskaya E, Bennett DC, Vaulont S, Goding CR *et al.* UV-induced expression of key component of the tanning process, the POMC and MC1R genes, is dependent on the p-38-activated upstream stimulating factor-1 (USF-1). *J Biol Chem* 2004; **279**: 51226–51233.

397 Corre S, Mekideche K, Adamski H, Mosser J, Watier E, Galibert MD. In vivo and ex vivo UV-induced analysis of pigmentation gene expressions. *J Invest Dermatol* 2006; **126**: 916–918.

398 Rouzaud F, Annereau JP, Valencia JC, Costin GE, Hearing VJ. Regulation of melanocortin 1 receptor expression at the mRNA and protein levels by its natural agonist and antagonist. *FASEB J* 2003; **17**: 2154–2156.

399 Sarangarajan R, Apte SP. The polymerization of melanin: a poorly understood phenomenon with egregious biological implications. *Melanoma Res* 2006; **16**: 3–10.

400 Urabe K, Aroca P, Tsukamoto K, Mascagna D, Palumbo A, Prota G *et al.* The inherent cytotoxicity of melanin precursors: a revision. *Biochim Biophys Acta* 1994; **1221**: 272–278.

401 Felix CC, Hyde JS, Sarna T, Sealy RC. Melanin photoreactions in aerated media: electron spin resonance evidence for production of superoxide and hydrogen peroxide. *Biochem Biophys Res Commun* 1978; **84**: 335–41.

402 Simon JD, Peles DN. The Red and the Black. *Acc Chem Res* 2010; **43**: 1452–1460.

403 Buscà R, Ballotti R. Cyclic AMP a key messenger in the regulation of skin pigmentation. *Pigment cell Res* 2000; **13**: 60–9.

404 Hein A, Ouellette M, Yan Y. Radiation-induced signaling pathways that promote cancer cell survival (Review). *Int J Oncol* 2014. doi:10.3892/ijo.2014.2614.

405 Yang J-L, Chen W-Y, Chen Y-P, Kuo C-Y, Chen S-D. Activation of GLP-1 Receptor Enhances Neuronal Base Excision Repair via PI3K-AKT-Induced Expression of Apurinic/Apyrimidinic Endonuclease 1. *Theranostics* 2016; **6**: 2015–2027.

406 Habib SL, Yadav A, Kidane D, Weiss RH, Liang S. Novel protective mechanism of reducing renal cell damage in diabetes: Activation AMPK by AICAR increased NRF2/OGG1 proteins and reduced oxidative DNA damage. *Cell Cycle* 2016; **15**: 3048–3059.

407 Piao MJ, Kim KC, Choi J-Y, Choi J, Hyun JW. Silver nanoparticles down-regulate Nrf2-mediated 8-oxoguanine DNA glycosylase 1 through inactivation of extracellular regulated kinase and protein kinase B in human Chang liver cells. *Toxicol Lett* 2011; **207**: 143–148.

408 Janjetovic Z, Jarrett SG, Lee EF, Duprey C, Reiter RJ, Slominski AT. Melatonin and its metabolites protect human melanocytes against UVB-induced damage: Involvement of NRF2-mediated pathways. *Sci Rep* 2017; **7**: 1274.

409 Rhee SG. Cell signaling. H2O2, a necessary evil for cell signaling. *Science* 2006; **312**: 1882–3.

410 Raad H, Serrano-Sanchez M, Harfouche G, Mahfouf W, Bortolotto D, Bergeron V *et al.* NADPH Oxidase-1 Plays a Key Role in Keratinocyte Responses to UV Radiation and UVB-Induced Skin Carcinogenesis. *J Invest Dermatol* 2017; **137**: 1311–1321.

411 Rezvani HR, Mazurier F, Cario-André M, Pain C, Ged C, Taïeb A *et al.* Protective effects of catalase overexpression on UVB-induced apoptosis in normal human keratinocytes. *J Biol Chem* 2006; **281**: 17999–8007.

412 Rezvani HR, Dedieu S, North S, Belloc F, Rossignol R, Letellier T *et al.* Hypoxia-inducible Factor-1α, a Key Factor in the Keratinocyte Response to UVB Exposure. *J Biol Chem* 2007; **282**: 16413–16422.

413 Meng T-C, Fukada T, Tonks NK. Reversible oxidation and inactivation of protein tyrosine phosphatases in vivo. *Mol Cell* 2002; **9**: 387–99.

414 Giannoni E, Buricchi F, Raugei G, Ramponi G, Chiarugi P. Intracellular Reactive Oxygen Species Activate Src Tyrosine Kinase during Cell Adhesion and Anchorage-Dependent Cell Growth. *Mol Cell Biol* 2005; **25**: 6391–6403.

415 Giannoni E, Buricchi F, Grimaldi G, Parri M, Cialdai F, Taddei ML *et al.* Redox regulation of anoikis: reactive oxygen species as essential mediators of cell survival. *Cell Death Differ* 2008; **15**: 867–78.

416 Coant N, Ben Mkaddem S, Pedruzzi E, Guichard C, Tréton X, Ducroc R *et al.* NADPH oxidase 1 modulates WNT and NOTCH1 signaling to control the fate of proliferative progenitor cells in the colon. *Mol Cell Biol* 2010; **30**: 2636–50.

417 Naughton R, Quiney C, Turner SD, Cotter TG. Bcr-Abl-mediated redox regulation of the PI3K/AKT pathway. *Leukemia* 2009; **23**: 1432–1440.

418 Ahn J-H, McAvoy T, Rakhilin S V, Nishi A, Greengard P, Nairn AC. Protein kinase A activates protein phosphatase 2A by phosphorylation of the B56delta subunit. *Proc Natl Acad Sci U S A* 2007; **104**: 2979–84.

419 Cho E-A, Kim E-J, Kwak S-J, Juhnn Y-S. cAMP signaling inhibits radiation-induced ATM phosphorylation leading to the augmentation of apoptosis in human lung cancer cells. *Mol Cancer* 2014; **13**: 36.

420 Musante V, Li L, Kanyo J, Lam TT, Colangelo CM, Cheng SK *et al.* Reciprocal regulation of ARPP-16 by PKA and MAST3 kinases provides a cAMP-regulated switch in protein phosphatase 2A inhibition. *Elife* 2017; **6**. doi:10.7554/eLife.24998.

421 Feschenko MS, Stevenson E, Nairn AC, Sweadner KJ. A novel cAMP-stimulated pathway in protein phosphatase 2A activation. *J Pharmacol Exp Ther* 2002; **302**: 111–8.

422 Usui H, Inoue R, Tanabe O, Nishito Y, Shimizu M, Hayashi H *et al.* Activation of protein phosphatase 2A by cAMP-dependent protein kinase-catalyzed phosphorylation of the 74-kDa B'' (delta) regulatory subunit in vitro and identification of the phosphorylation sites. *FEBS Lett* 1998; **430**: 312–6.

423 Chen K, Kirber MT, Xiao H, Yang Y, Keaney JF. Regulation of ROS signal transduction by NADPH oxidase 4 localization. *J Cell Biol* 2008; **181**: 1129–1139.

424 Meyskens FL, Liu-Smith F. Redox-Redux and NADPH Oxidase (NOX): Even More Complicated than We Thought it Might Be. *J Invest Dermatol* 2017; **137**: 1208–1210.

425 Xu N, Lao Y, Zhang Y, Gillespie DA. Akt: a double-edged sword in cell proliferation and genome stability. *J Oncol* 2012; **2012**: 951724.

426 Medrano EE, Im S, Yang F, Abdel-Malek ZA. Ultraviolet B light induces G1 arrest in human melanocytes by prolonged inhibition of retinoblastoma protein phosphorylation associated with long-term expression of the p21Waf-1/SDI-1/Cip-1 protein. *Cancer Res* 1995; **55**: 4047–52.

427 Hustedt N, Durocher D. The control of DNA repair by the cell cycle. *Nat Cell Biol* 2016; **19**: 1–9.

RESUMEN

Introducción

La radiación ultravioleta (RUV) es el principal factor etiológico del cáncer de piel, ya que provoca lesiones en el ADN de forma directa o por generación de especies reactivas de oxígeno (ROS)[1,2]. El estrés oxidativo resultante se asocia a fotoenvejecimiento y carcinogénesis cutánea[3]. Los melanocitos epidérmicos son las células responsables de establecer una serie de acciones fotoprotectoras que limitan el riesgo de adquirir cáncer de piel en general, y melanoma en particular[4]. Además de la pigmentación cutánea, el principal mecanismo fotoprotector frente al daño en el ADN inducido por RUV, los melanocitos utilizan otros procesos para limitar o reparar dicho daño, entre los que destacan la activación de mecanismos de reparación de ADN y defensas antioxidantes. En conjunto, estos procesos contribuyen a la estabilidad genómica y previenen la transformación maligna de las células expuestas a la RUV.

El receptor de melanocortinas 1 (MC1R) es un receptor acoplado a la proteína Gs implicado en el control de la proliferación y diferenciación de los melanocitos. Se activa por hormonas peptídicas llamadas melanocortinas (MCs), derivadas de proopiomelanocortina (POMC) y emplea varias vías de transducción de señales, siendo las principales las del AMPc y las quinasas ERK1 y ERK2[1,5]. El gen que codifica para el *MC1R* humano (MIM# 155555, Ensembl ID ENSG00000258839) presenta una estructura compleja, ya que es capaz de dar lugar a varias variantes de *splicing* y presenta un alto grado de polimorfismo. Se han descrito dos variantes de *splicing* intergénico entre el *MC1R* y su gen vecino aguas abajo *Tubulin-β-III* (*TUBB3)*[6,7]. Estas quimeras MC1R-TUBB3 denominadas Iso1 e Iso2, contienen la secuencia completa del MC1R fusionada con extensiones en C-terminal derivadas de TUBB, con marco de lectura correcto para Iso1 y alterado para Iso2[7].

Además, el tratamiento con αMSH o la activación de la quinasa p38, ambas moléculas clave asociadas con las respuestas a la RUV, promueve un cambio de isoformas a favor de la expresión de las variantes de *splicing* alternativo intergénico MC1R-TUBB3 con propiedades funcionales desconocidas[6,7], lo que daría lugar a nuevos fenotipos necesarios para el bronceado. Sin embargo, existe poca información disponible sobre las propiedades funcionales de estas proteínas quiméricas.

Por otra parte, el gran polimorfismo del gen *MC1R*, con más de 200 variantes descritas, es la principal fuente de variación normal de la pigmentación y el fototipo humanos, ya que la activación de MC1R estimula la síntesis de eumelaninas fotoprotectoras de color oscuro, mientras que la falta de actividad del receptor se relaciona con la síntesis de feomelaninas rojizas fotosensibilizadoras[8]. Ciertas variantes de *MC1R* se asocian al fenotipo RHC (*red hair color*) con

una penetrancia baja (variantes de tipo "r") o alta (variantes de tipo "R")[9]. Además, MC1R es el determinante principal de la respuesta cutánea a la RUV, ya que ésta induce la expresión del gen POMC en los queratinocitos, y la liberación de MCs que activan de forma paracrina el MC1R y promueven un incremento de la síntesis de eumelaninas en los melanocitos (bronceado).

Estudios recientes sugieren que, además de la pigmentación, algunas de las acciones protectoras de MC1R consisten en: i) la inducción de defensas antioxidantes, que limitan el daño oxidativo provocado por la RUV[10–14], ii) la activación de mecanismos de reparación de ADN, que corrigen lesiones provocadas por dicha radiación, principalmente la activación de las vía de reparación por escisión de bases (*base excision repair*, BER) y por escisión de nucleótidos (*nucleotide excision repair*, NER). La vía BER repara las lesiones oxidativas de rotura de hebra simple de ADN y 8-oxo-7,8-dihidroguanina (8-oxodG) y la vía NER es responsable del aclaramiento de dímeros de pirimidina (*cyclobutane pyrimidine dimers*, CPDs) y fotoproductos de pirimidinas (*pyrimidine (6-4) pyrimidone photoproducts*, 6-4PPs)[12–15]. Los mecanismos moleculares responsables de la activación de NER aguas abajo de MC1R silvestre incluyen la fosforilación de ATR en Ser435 por la quinasa PKA activada por AMPc[16], seguida de la translocación a núcleo de complejos AKAP12-ATRpS435, y reclutamiento de XPA a los sitios de daño inducido por la RUV[15]. Además, se ha demostrado la activación de BER aguas abajo del MC1R silvestre[12]. Esta vía depende de la acción secuencial de glicosilasas de amplio espectro de acción como la glicosilasa de ADN 8-oxoguanina (*8-oxoguanine ADN glycosylase*, OGG) seguida de AP-endonucleasa (*AP-endonuclease 1*, APE-1/Ref-1). Estas dos enzimas clave en la vía BER son inducidas en melanocitos tratados con MSH de manera dependiente de AMPc[12]. Así, se considera que todos los mecanismos protectores son activados a través de la vía del AMPc, por activación del MC1R silvestre. Puesto que las variantes de *MC1R* asociadas a fenotipo RHC presentan una capacidad disminuida de acoplamiento a la vía del AMPc se suele admitir que dichas variantes no activan eficientemente los mecanismos protectores mencionados. De acuerdo con esta premisa, la carga mutacional en los melanomas de genotipo *MC1R* silvestre es menor que en los melanomas con *MC1R* variante[17–19].

Por lo tanto, la activación eficiente de las respuestas frente a la RUV parece depender del genotipo del *MC1R*. En este contexto, aún existen aspectos que deben ser estudiados. Por un lado, se desconoce el papel biológico de las variantes de *splicing* intra- e intergénico, cuya expresión parece condicionada por la exposición a RUV. Por otro lado, aunque se ha descubierto que las variantes RHC de MC1R no incrementan la eumelanogénesis, su papel en la inducción de efectos independientes de la pigmentación requiere mayor investigación.

Objetivos

A la vista de estos antecedentes, propusimos los siguientes objetivos:

1. **Caracterizar el tráfico a través de la vía secretora y el acoplamiento funcional a las vías de señalización de las proteínas quiméricas MC1R-TUBB3** con el fin de descifrar su posible papel fisiológico.

2. **Evaluar la protección dependiente de MC1R contra el daño oxidativo en ADN en células de melanoma humano y melanocitos epidérmicos de genotipo *MC1R* definido**, mediante la comparación de la capacidad de MC1R silvestre y las variantes RHC de promover:
   2a – Inducción de enzimas antioxidantes.
   2b- Reparación de bases oxidadas.
   2c- Aclaramiento de roturas de hebra simple de ADN.

3. **Identificar las vías de señalización, si existen, responsables de la activación de la reparación de ADN aguas abajo de MC1R variante.** Esto ayudará a entender mejor el papel del *MC1R* como gen de susceptibilidad a melanoma.

Resultados y Discusión

1. Análisis funcional de las quimeras MC1R-TUBB3

Los genes que codifican para la mayoría de GPCRs han sido considerados carentes de intrones durante mucho tiempo[20]. Sin embargo, el reciente avance en el análisis de la arquitectura de estos genes ha mostrado que a menudo contienen varios intrones y pueden ser sometidos a eventos de *splicing* alternativo. Por otra parte, el proceso de *splicing* intergénico que da lugar a proteínas quiméricas es un evento poco frecuente[21] donde la transcripción ocurre a través de una región entre dos genes adyacentes para sintetizar un ARN quimérico no canónico que es posteriormente cortado y empalmado para dar lugar a un producto de fusión final compuesto de secuencias codificadas por los dos genes vecinos. En la enorme superfamilia de los GPCRs, este proceso sólo ha sido descrito para los genes que codifican para el receptor *P2Y* y el *SSF1*[22] por una parte, y los genes *MC1R* y *TUBB3* por otra[6,7].

Expresión y procesamiento de variantes de *splicing* MC1R-TUBBIII

Confirmamos la presencia de las formas quiméricas de MC1R-TUBB3 Iso1 e Iso2 en un panel de 8 líneas de melanoma humano y en una línea de melanocitos humanos epidérmicos. Hemos detectado los transcritos correspondientes en todas ellas incluso en ausencia de estímulos externos, demostrando que la expresión de Iso1 e Iso2 es un fenómeno general de células melanocíticas humanas que ocurre incluso en ausencia de exposición a la RUV. Además, observamos que el ratio de los transcritos Iso1 e Iso2 relativo al transcrito de MC1R-001 canónico fue variable en diferentes líneas celulares.

Cuando expresamos las isoformas en células heterólogas HEK293T o en células melanocíticas humanas, la proteína de fusión intergénica Iso1 exhibió el peso molecular esperado y fue reconocida por anticuerpos frente a TUBB3. Por lo tanto, el ARNm quimérico fue procesado adecuadamente y la proteína resultante se acumuló a niveles suficientes en células transfectadas, aunque la estabilidad intracelular fue menor que la del MC1R-001. Por otra parte, Iso2 resultó de una fusión con pauta de lectura alterada del exon 3 del *MC1R* y el exon 3 del gen *TUBB3* dando lugar a una proteína de 432 aminoácidos cuyos primeros 316 residuos coinciden con la secuencia del MC1R-001. Por ello, Iso2 no presenta reactividad cruzada con anticuerpos anti-TUBB3. Además, sus niveles intracelulares y su vida media fueron bajos. La menor vida media de las proteínas quiméricas fue consistente con su tráfico anterógrado alterado demostrado por una expresión en la superficie celular reducida y una alta co-localización con el marcador de retículo endoplásmico (RE) calnexina. Por tanto, el control de calidad de las proteínas de RE reconoció las proteínas quiméricas como aberrantes, causando probablemente su ubiquitinación, extrusión al citosol y degradación proteolítica[23].

Acoplamiento funcional

Ambas quimeras mostraron baja capacidad de activar la vía del AMPc. Esto puede explicarse, al menos parcialmente, por una expresión disminuida en superficie celular de las quimeras con respecto al MC1R silvestre. Los niveles de AMPc residuales tras estimulación con una concentración saturante del análogo superpotente de αMSH, NDP-MSH, fueron menores que aquellos obtenidos en células que expresan variantes hipomórficas asociadas a fenotipo RHC conocidas con baja (V60L y V92M) o alta (R151C y D294H) penetrancia[9]. Sin embargo, la disminución funcional fue menos evidente para la activación de la cascada de las ERK. De acuerdo con esto, la señalización de las isoformas de *splicing* intergénico MC1R-TUBB3 parece sesgada a favor de la vía de las ERK. Muchos alelos variantes naturales de MC1R asociados con un fenotipo RHC y un riesgo incrementado de cáncer de piel han mostrado un comportamiento similar[9].

Interacciones funcionales del MC1R silvestre y las variantes de *splicing* alternativo

Por otra parte, el grupo de investigación en el que se integra la doctoranda ha demostrado previamente que MC1R existe en forma dimérica[24,25], y que la heterodimerización de la forma silvestre con mutantes hipomórficas da lugar a efectos de dominancia negativa[24,26]. Como la dimerización se produce aparentemente a través de un mecanismos "swap" que implica los fragmentos siete hebras transmembrana expresados en Iso1 e Iso2[25], la formación *in vivo* de las especies heterodiméricas MC1R/Iso parece posible. Demostramos la existencia de heterodimerización entre las Isos y el MC1R silvestre marcados diferencialmente con epítopos mediante experimentos de co-immunoprecipitación. Además, mediante el estudio de localización intracelular del MC1R-001 e Iso1 o Iso2 por microscopía confocal en células HEK293T co-expresando MC1R-001 y las formas de *splicing* intergénico encontramos un alto grado de co-localización del MC1R-001 con Iso1 o Iso2 en compartimentos internos, sugiriendo que la heterodimerización disminuye el tráfico anterógrado comparado con los homodímeros del MC1R-001. También se detectó co-localización de MC1R-001 e Iso1 o Iso2 en la periferia celular. Examinamos la producción de AMPc dependiente de agonista sin observar cambios significativos en la respuesta del AMPc en células expresando MC1R silvestre sólo o con las quimeras. Sin embargo, la co-expresión del MC1R silvestre con las formas quiméricas provocó una disminución en el número de sitios de unión a MSH en la superficie celular de células que sobreexpresaban ambas formas de MC1R simultáneamente. Aunque en este caso la disminución observada no fue estadísticamente significativa, parece muy posible que bajo condiciones normales de expresión la retención intracelular de MC1R-001 por heterodimerización con formas Iso pueda llegar a ser un factor significativo. Por lo tanto, cuando las isoformas quiméricas se expresan tras exposición a la RUV, puede que prevengan una estimulación excesiva de la vía del AMPc sin disminuir paralelamente la activación de las ERK dependiente de MC1R.

La observación de que la expresión de las isoformas de *splicing* intergénico es una característica común en células de melanoma humano así como un proceso regulado[7] sugiere que Iso1 e Iso2 pueden desempeñar acciones específicas en melanocitos que aún no se han caracterizado. Dado que ambas isoformas son hipomóficas en términos de acoplamiento funcional a la vía del AMPc, estas acciones pueden estar relacionadas con una disminución de la señalización por MC1R bajo condiciones fisiológicas concretas. Se ha demostrado que la RUV incrementaría la expresión del MC1R al menos a través de dos tipos de procesos: i) una estimulación directa de la expresión del gen *MC1R* en melanocitos irradiados[27,28] y ii) una vía indirecta donde la liberación de los agonistas de MC1R derivados del precursor POMC por los

queratinocitos en la piel expuesta a la RUV activaría la señalización mediada por MC1R en los melanocitos, y la transcripción del gen *MC1R*[29]. Esto incrementaría la sensibilidad de los melanocitos a las señales paracrinas resultando en una retroalimentación positiva a favor de la potente respuesta de bronceado, pero podría comprometer la viabilidad de los melanocitos de acuerdo a la inherente citotoxicidad de la vía melanogénica[30,31]. Se ha demostrado que la expresión de las isoformas Iso1/2 se incrementa tras estimulación de los melanocitos con αMSH o por activación de la quinasa p38, en un cambio de isoformas que favorece su expresión respecto a la del MC1R-001[7]. Por lo tanto, las mismas vías de señalización implicadas en la inducción de la expresión del gen *MC1R* han demostrado promover la expresión de los transcritos *Iso1* e *Iso2*. La desviación de una fracción de nuevos eventos transcripcionales hacia la formación de isoformas de *splicing* intergénico inactivas e incluso dominantes-negativas podría proporcionar a los melanocitos un mecanismo para amortiguar o afinar este bucle de retroalimentación positiva potencialmente peligroso.

2. Activación de la reparación del daño oxidativo en ADN por variantes de MC1R

Genotipo para *MC1R* y propiedades de señalización de los modelos celulares empleados

En melanocitos portadores de *MC1R* silvestre, la activación de mecanismos independientes de pigmentación contra el daño en ADN es dependiente de un acoplamiento funcional eficiente a la vía del AMPc y, en consecuencia, se asume que estas respuestas están ausentes en melanocitos portadores de alelos R. Sin embargo, las mutaciones R comunes con señalización disminuida por AMPc tienen un efecto escaso o nulo en la activación de las ERK aguas abajo del MC1R[5,9,32], y sus posibles efectos en la señalización de AKT son desconocidos. Ambas quinasas, las ERKs[33–35] y AKT[36–38], participan en la reparación del ADN en algunos tipos celulares. En consecuencia, estas observaciones sugieren que las variantes de MC1R con capacidad disminuida de acoplamiento a la vía del AMPc podrían activar algunas respuestas no pigmentarias frente al daño en ADN a través de mecanismos independientes de AMPc. Para verificar esta hipótesis y dada la relevancia del estrés oxidativo en melanocitos feomelánicos portadores de variantes de *MC1R*, comparamos las respuestas frente al estrés oxidativo de células de melanoma humano y melanocitos de genotipo definido para *MC1R*. Además, analizamos la maquinaria enzimática y las vías de señalización responsables de estas respuestas protectoras aguas abajo del MC1R.

Para ello, usamos la línea celular de melanoma humano HBL portadora de alelos silvestres para *MC1R*, *NRAS* y *BRAF*, las líneas de melanoma humano portadoras de variantes R para *MC1R* A375, SKMEL28 y C8161, y los melanocitos epidérmicos inmortalizados Hermes. De acuerdo con

su genotipo para *MC1R*, el tratamiento con NDP-MSH de células A375, SKMEL28, C8161 o Hermes no incrementó los niveles de AMPc intracelulares. Además, NDP-MSH estimuló transitoriamente las ERKs en melanocitos Hermes y las ERKs aparecieron constitutivamente activas en células A375, SKMEL28 y C8161 en consonancia con su genotipo *V600E-BRAF*.

Inducción de la reparación del daño oxidativo aguas abajo de variantes de MC1R

La estimulación con NDP-MSH redujo significativamente y de forma comparable el daño oxidativo en ADN en células de melanoma humano de genotipo *MC1R* silvestre o variante, como mostró la disminución de los niveles de 8-oxodG, de los focos de la histona H2AX fosforilada (γH2AX) y de las roturas de hebra de ADN en células sometidas a un tratamiento oxidativo. En células HBL portadoras de MC1R silvestre, se observó un incremento en las defensas antioxidantes ya que se detectó una inducción de catalasa por NDP-MSH. Sin embargo, en células A375 que expresan la variante hipomórfica RHC R151C, este efecto protector ocurrió sin inducción de enzimas antioxidantes, lo que apunta a una activación de reparación de ADN, que fue confirmada por el análisis de la cinética de aclaramiento de lesiones oxidativas de ADN tras tratamiento con pulsos de Luperox (análogo estable de peróxido de hidrógeno) de corta duración. La reparación de lesiones oxidativas fue debida a la inducción de dos enzimas clave de la vía BER, OGG y APE-1/Ref1 aguas abajo tanto del MC1R silvestre como de las variantes de MC1R. Por lo tanto, nuestros datos mostraron que las variantes de MC1R podrían activar la reparación de ADN para cooperar con el daño oxidativo, contrariamente a la idea predominante en el campo.

3. Implicación de la señalización por AKT en las respuestas protectoras mediadas por MC1R variante

La activación de AKT es necesaria para la reparación del daño oxidativo en ADN inducida por variantes del MC1R

Como las células melanocíticas con *MC1R* variante usadas en este estudio no activaron la vía del AMPc aguas abajo del MC1R, buscamos las vías de señalización responsables de la acción protectora independiente de la pigmentación. En células con MC1R variante, NDP-MSH disminuyó de forma comparable la fragmentación de ADN inducida por Luperox en ausencia o presencia del inhibidor de MEK PD98059, lo que excluye a la señalización por ERK como la principal vía responsable del efecto protector de ADN. Por otra parte, NDP-MSH activó significativamente AKT en células de fondo genético *MC1R* variante. AKT está directamente

implicada en procesos de reparación de ADN[36,39] ya que promueve la reparación de rotura de doble hebra de ADN mediada por vía de recombinación no homóloga (*non-homologous-end-joining*, NHEJ) tras irradiación celular[40], activa la enzima APE-1/Ref-1 para disminuir lesiones oxidativas[41] e induce BER a través de la activación de Nrf2 y la consecuente regulación al alza de OGG[42,43]. En relación con el posible papel protector de AKT en células melanocíticas, el activador de AKT SC79 disminuyó el número de roturas de cadena de ADN y los niveles de 8-oxodG, en células con MC1R variante tratadas con Luperox e indujo las enzimas BER en estas células. Además, el bloqueo de la señalización por AKT con los inhibidores LY94002 and MK-2206 abolió el aclaramiento de lesiones oxidativas y la inducción de las enzimas de la vía BER.

La activación de AKT aguas abajo de MC1R variante es mediada por la generación de ROS

Por otra parte, hemos estudiado el mecanismo de activación de AKT aguas abajo de las variantes de MC1R. Existe una fuerte evidencia de que las ROS actúan como moléculas de señalización celular para modular diferentes vías de señalización y regular procesos biológicos relevantes como proliferación, migración y supervivencia[44–46]. Concretamente, se ha demostrado que la vía de señalización PI3K/AKT es regulada por ROS[46–48]. Además, también se ha demostrado que ROS actúan como segundos mensajeros para transmitir las señales aguas abajo de los GPCRs[49]. En este sentido, hemos observado un rápido incremento en la producción de ROS en células portadoras de MC1R variante tratadas con NDP-MSH mientras que la presencia del antioxidante ebselen previa a la estimulación con MSH bloqueó este incremento de ROS y la activación de AKT en estas células. Además, el tratamiento con bajas concentraciones de Luperox ($8x10^{-5}$ M) comparables a las alcanzadas por estimulación con NDP-MSH, mimetizó el efecto de NDP-MSH en la activación de AKT aguas abajo de MC1R variante. Por lo tanto, las ROS cumplen tres criterios principales para ser consideradas segundos mensajeros actuando aguas abajo del MC1R: i) su concentración intracelular se incrementa rápida y transitoriamente tras tratamiento con agonistas del MC1R, ii) el bloqueo de su acumulación en respuesta a la hormona mitiga algunas de las acciones de MSH y iii) su incremento mediante adición exógena a las células mimetiza estas respuestas hormonales.

MSH induce la activación de NOX en células de melanoma humano con *MC1R* variante

Además, hemos identificado la enzima NOX como la fuente de estos ROS inducidos por MSH. Varios estudios muestran que las NADPH oxidasas pueden ser activadas aguas abajo de GPCRs[49,50] así como por factores de crecimiento y hormonas[44], y tras exposición a UVB[51–54] y UVA[55] en queratinocitos. Hemos demostrado que la inhibición de NOX con DPI o GKT137831 abolió el

incremento de ROS inducido por MSH así como la activación de AKT en células melanocíticas con MC1R variante. Por el contrario, en células portadoras de *MC1R* silvestre, NDP-MSH disminuyó los niveles intracelulares de ROS y fue incapaz de activar AKT. Este descubrimiento es acorde con la rápida activación de catalasa mediada por PKA[13] y/o con la inhibición de NOX por un mecanismo dependiente de AMPc[56,57]. El bloqueo en la producción de AMPc en estas células con DDA rescató la activación de NOX y AKT aguas abajo de MC1R. Por otra parte, la elevación farmacológica de los niveles de AMPc en células portadoras de variantes de *MC1R* bloqueó el eje de señalización NOX-AKT aguas abajo de MC1R. Por lo tanto, AMPc inhibió la señalización de AKT en células melanocíticas a nivel de NOX, como se ha demostrado previamente para células de melanoma de ratón[58,59]. Además, nuestros datos son consistentes con un modelo donde la estimulación con NDP-MSH de MC1R variante provoca la activación de NOX, un incremento en la concentración intracelular de ROS y la activación de AKT dependiente de ROS. Por el contrario, en células melanocíticas con MC1R silvestre, la activación de la vía del AMPc por NDP-MSH interferiría con la activación de AKT, principalmente por el bloqueo del incremento de ROS intracelulares dependiente de NOX.

En consonancia con la falta de activación de NOX y AKT aguas abajo del MC1R silvestre, la inducción de las respuestas protectoras por NDP-MSH en células de genotipo *MC1R* silvestre no estuvo afectado por LY94002 y MK-2206. Por el contrario, estas respuestas fueron bloqueadas por DDA y mimetizadas por FSK y dbcAMP, confirmando su dependencia de AMPc. Además, la inhibición de NOX con GKT137831 no tuvo efecto en la inducción de BER por NDP-MSH mientras que DDA bloqueó este efecto. Estos datos demuestran la implicación de la vía del AMPc en la activación de BER en células de melanoma humano con *MC1R* silvestre.

En conjunto, nuestros resultados muestran que la activación del MC1R promueve protección contra el daño oxidativo en ADN al menos mediante dos mecanismos. Uno de ellos es dependiente de AMPc y está operativo en células con *MC1R* silvestre mientras que el otro dependería de AKT y estaría limitado a las células con variantes de *MC1R*. Además, en células con *MC1R* silvestre, el AMPc induciría eficazmente enzimas antioxidantes, principalmente catalasa, y las enzimas de la vía BER OGG and APE-1/Ref1 mientras que variantes del MC1R incrementarían eficazmente la expresión de las dos enzimas clave de la vía BER, pero no tendrían efecto en los niveles o actividad de catalasa. La demostración de la activación de la reparación de ADN dependiente de AKT aguas abajo de MC1R puede ser importante para el diseño de estrategias racionales de prevención y tratamiento de melanoma como el tratamiento con inhibidores de NOX1[60] y la aplicación de agentes tópicos que incrementen los niveles de AMPc en la piel expuesta al sol.

Conclusiones

1. Las quimeras MC1R-TUBB3 se expresaron en todas las líneas de melanoma humano estudiadas y son capaces de unir agonista con la misma afinidad que el MC1R-001, pero su expresión en la membrana plasmática está drásticamente reducida, principalmente como resultado de un tráfico anterógrado aberrante.

2. Iso1 and Iso2 heterodimerizan eficientemente con MC1R-001 y se comportan como isoformas dominantes negativas promoviendo retención intracelular de la forma canónica.

3. Las quimeras MC1R-TUBB3 se comportan como variantes R de acuerdo con su señalización intracelular, ya que su acoplamiento funcional a la vía del AMPc está fuertemente disminuido, pero son capaces de activar eficientemente las ERK.

4. La activación del MC1R silvestre incrementa la expresión de las enzimas antioxidantes catalasa y superóxido dismutasa de forma dependiente de AMPc.

5. NDP-MSH induce de forma comparable y significativa la reparación de daño oxidativo en ADN en células de melanoma humano de genotipo *MC1R* silvestre o variante, como se muestra por el aclaramiento de lesiones oxidativas en ADN (8-oxodG y roturas de ADN) en células sometidas a un estrés oxidativo.

6. La reparación de lesiones oxidativas es debida, al menos parcialmente, a la inducción de dos enzimas clave de la vía BER, OGG y APE-1/Ref1, aguas abajo de MC1R silvestre o variante.

7. En células melanocíticas de genotipo *MC1R* silvestre, las respuestas protectoras de ADN son mediadas por la vía de señalización de AMPc mientras que en células de genotipo variante para *MC1R*, AKT es responsable de la inducción de la reparación de ADN.

8. En células de melanoma humano portadoras de variantes de *MC1R*, la señalización no canónica de MC1R a AKT es independiente de AMPc y está mediada por la activación de NOX.

9. NOX es necesaria para la inducción de las enzimas de la vía BER, OGG y APE-1/Ref1, y para la reparación del daño oxidativo en ADN en células de melanoma humano con *MC1R* variante.

10. Altos niveles de AMPc inhiben la activación de AKT mediada por el MC1R en células de melanoma humano con *MC1R* variante, principalmente por el bloqueo en el incremento de ROS intracelulares dependiente de NOX.

Referencias

1. Garcia-Borron, J. C., Abdel-Malek, Z. & Jimenez-Cervantes, C. MC1R, the cAMP pathway, and the response to solar UV: extending the horizon beyond pigmentation. *Pigment Cell Melanoma Res* **27**, 699–720 (2014).

2. Hauser, J. E. *et al.* Melanin content and MC1R function independently affect UVR-induced DNA damage in cultured human melanocytes. *Pigment Cell Res.* **19**, 303–314 (2006).

3. Napolitano, A., Panzella, L., Monfrecola, G. & d'Ischia, M. Pheomelanin-induced oxidative stress: bright and dark chemistry bridging red hair phenotype and melanoma. *Pigment Cell Melanoma Res* **27**, 721–733 (2014).

4. Kadekaro, A. L. *et al.* Melanocortin 1 receptor genotype: an important determinant of the damage response of melanocytes to ultraviolet radiation. *FASEB J.* **24**, 3850–3860 (2010).

5. Herraiz, C. *et al.* Signaling from the human melanocortin 1 receptor to ERK1 and ERK2 mitogen-activated protein kinases involves transactivation of cKIT. *Mol Endocrinol* **25**, 138–156 (2011).

6. Dalziel, M., Nunes, N. M. & Furger, A. Two G-rich regulatory elements located adjacent to and 440 nucleotides downstream of the core poly(A) site of the intronless melanocortin receptor 1 gene are critical for efficient 3' end processing. *Mol Cell Biol* **27**, 1568–1580 (2007).

7. Dalziel, M. *et al.* Alpha-MSH regulates intergenic splicing of MC1R and TUBB3 in human melanocytes. *Nucleic Acids Res* **39**, 2378–2392 (2011).

8. Panzella, L. *et al.* Red human hair pheomelanin is a potent pro-oxidant mediating UV-independent contributory mechanisms of melanomagenesis. *Pigment Cell Melanoma Res* **27**, 244–252 (2014).

9. Herraiz, C., Journe, F., Ghanem, G., Jimenez-Cervantes, C. & Garcia-Borron, J. C. Functional status and relationships of melanocortin 1 receptor signaling to the cAMP and extracellular signal-regulated protein kinases 1 and 2 pathways in human melanoma cells. *Int J Biochem Cell Biol* **44**, 2244–2252 (2012).

10. Bohm, M. *et al.* alpha-Melanocyte-stimulating hormone protects from ultraviolet radiation-induced apoptosis and DNA damage. *J Biol Chem* **280**, 5795–5802 (2005).

11. Kadekaro, A. L. *et al.* alpha-Melanocortin and endothelin-1 activate antiapoptotic pathways and reduce DNA damage in human melanocytes. *Cancer Res* **65**, 4292–4299 (2005).

12. Kadekaro, A. L. *et al.* Alpha-Melanocyte-Stimulating Hormone Suppresses Oxidative Stress through a p53-Mediated Signaling Pathway in Human Melanocytes. *Mol. Cancer Res.* **10**, 778–786 (2012).

13. Maresca, V. *et al.* MC1R stimulation by alpha-MSH induces catalase and promotes its re-distribution to the cell periphery and dendrites. *Pigment Cell Melanoma Res.* **23**, 263–75 (2010).

14. Song, X. *et al.* alpha-MSH activates immediate defense responses to UV-induced oxidative stress in human melanocytes. *Pigment Cell Melanoma Res.* **22**, 809–18 (2009).

15. Jarrett, S. G., Wolf Horrell, E. M. & D'Orazio, J. A. AKAP12 mediates PKA-induced phosphorylation of ATR to enhance nucleotide excision repair. *Nucleic Acids Res.* **44**, 10711–10726 (2016).

16. Jarrett, S. G. *et al.* PKA-Mediated Phosphorylation of ATR Promotes Recruitment of XPA to UV-Induced DNA Damage. *Mol. Cell* **54**, 999–1011 (2014).

17. Robles-Espinoza, C. D. *et al.* Germline MC1R status influences somatic mutation burden in melanoma. *Nat. Commun.* **7**, 12064 (2016).

18. Johansson, P. A. *et al.* Mutation load in melanoma is affected by *MC1R* genotype. *Pigment Cell Melanoma Res.* **30**, 255–258 (2017).

19. Jarrett, S. G., Carter, K. M. & D'Orazio, J. A. Paracrine regulation of melanocyte genomic stability: a focus on nucleotide excision repair. *Pigment Cell Melanoma Res.* **30**, 284–293 (2017).

20. Markovic, D. & Challiss, R. A. J. Alternative splicing of G protein-coupled receptors: physiology and pathophysiology. *Cell. Mol. Life Sci.* **66**, 3337–52 (2009).

21. Jividen, K. & Li, H. Chimeric RNAs generated by intergenic splicing in normal and cancer cells. *Genes Chromosom. Cancer* **53**, 963–971 (2014).

22. Communi, D., Suarez-Huerta, N., Dussossoy, D., Savi, P. & Boeynaems, J. M. Cotranscription and intergenic splicing of human P2Y11 and SSF1 genes. *J. Biol. Chem.* **276**, 16561–6 (2001).

23. Needham, P. G. & Brodsky, J. L. How early studies on secreted and membrane protein quality control gave rise to the ER associated degradation (ERAD) pathway: the early history of ERAD. *Biochim Biophys Acta* **1833**, 2447–2457 (2013).

24. Sanchez-Laorden, B. L. *et al.* Dimerization of the human melanocortin 1 receptor: functional consequences and dominant-negative effects. *J Invest Dermatol* **126**, 172–181 (2006).

25. Zanna, P. T. *et al.* Mechanism of dimerization of the human melanocortin 1 receptor. *Biochem Biophys Res Commun* **368**, 211–216 (2008).

26. Beaumont, K. A. *et al.* Receptor function, dominant negative activity and phenotype correlations for MC1R variant alleles. *Hum. Mol. Genet.* **16**, 2249–2260 (2007).

27. Corre, S. *et al.* UV-induced expression of key component of the tanning process, the POMC and MC1R genes, is dependent on the p-38-activated upstream stimulating factor-1 (USF-1). *J Biol Chem* **279**, 51226–51233 (2004).

28. Funasaka, Y. *et al.* Modulation of melanocyte-stimulating hormone receptor expression on normal human melanocytes: evidence for a regulatory role of ultraviolet B, interleukin-1alpha, interleukin-1beta, endothelin-1 and tumour necrosis factor-alpha. *Br J Dermatol* **139**, 216–224 (1998).

29. Cui, R. *et al.* Central role of p53 in the suntan response and pathologic hyperpigmentation. *Cell* **128**, 853–864 (2007).

30. Sarangarajan, R. & Apte, S. P. The polymerization of melanin: a poorly understood phenomenon with egregious biological implications. *Melanoma Res* **16**, 3–10 (2006).

31. Urabe, K. *et al.* The inherent cytotoxicity of melanin precursors: a revision. *Biochim Biophys Acta* **1221**, 272–278 (1994).

32. Herraiz, C., Jimenez-Cervantes, C., Zanna, P. & Garcia-Borron, J. C. Melanocortin 1 receptor mutations impact differentially on signalling to the cAMP and the ERK mitogen-activated protein kinase pathways. *FEBS Lett* **583**, 3269–3274 (2009).

33. Cohen-Armon, M. PARP-1 activation in the ERK signaling pathway. *Trends Pharmacol. Sci.* **28**, 556–60 (2007).

34. Wei, F., Yan, J. & Tang, D. Extracellular signal-regulated kinases modulate DNA damage response - a contributing factor to using MEK inhibitors in cancer therapy. *Curr. Med. Chem.* **18**, 5476–82 (2011).

35. Hawkins, A. J., Golding, S. E., Khalil, A. & Valerie, K. DNA double-strand break - induced pro-survival signaling. *Radiother. Oncol.* **101**, 13–7 (2011).

36. Liu, Q., Turner, K. M., Alfred Yung, W. K., Chen, K. & Zhang, W. Role of AKT signaling in DNA repair and clinical response to cancer therapy. *Neuro. Oncol.* **16**, 1313–1323 (2014).

37. Toulany, M. & Rodemann, H. P. Phosphatidylinositol 3-kinase/Akt signaling as a key mediator of tumor cell responsiveness to radiation. *Semin. Cancer Biol.* **35**, 180–190 (2015).

38. Singh, P., Dar, M. S. & Dar, M. J. p110α and p110β isoforms of PI3K signaling: are they two sides of the same coin? *FEBS Lett.* **590**, 3071–3082 (2016).

39. Hein, A., Ouellette, M. & Yan, Y. Radiation-induced signaling pathways that promote cancer cell survival (Review). *Int. J. Oncol.* (2014). doi:10.3892/ijo.2014.2614

40. Toulany, M. *et al.* Targeting of AKT1 enhances radiation toxicity of human tumor cells by inhibiting DNA-PKcs-dependent DNA double-strand break repair. *Mol. Cancer Ther.* **7**, 1772–1781 (2008).

41. Yang, J.-L., Chen, W.-Y., Chen, Y.-P., Kuo, C.-Y. & Chen, S.-D. Activation of GLP-1 Receptor Enhances Neuronal Base Excision Repair via PI3K-AKT-Induced Expression of Apurinic/Apyrimidinic Endonuclease 1. *Theranostics* **6**, 2015–2027 (2016).

42. Habib, S. L., Yadav, A., Kidane, D., Weiss, R. H. & Liang, S. Novel protective mechanism of reducing renal cell damage in diabetes: Activation AMPK by AICAR increased NRF2/OGG1 proteins and reduced oxidative DNA damage. *Cell Cycle* **15**, 3048–3059 (2016).

43. Piao, M. J., Kim, K. C., Choi, J.-Y., Choi, J. & Hyun, J. W. Silver nanoparticles down-regulate Nrf2-mediated 8-oxoguanine DNA glycosylase 1 through inactivation of extracellular regulated kinase and protein kinase B in human Chang liver cells. *Toxicol. Lett.* **207**, 143–148 (2011).

44. Groeger, G., Quiney, C. & Cotter, T. G. Hydrogen peroxide as a cell-survival signaling molecule. *Antioxid. Redox Signal.* **11**, 2655–71 (2009).

45. Liu-Smith, F., Dellinger, R. & Meyskens, F. L. Updates of reactive oxygen species in melanoma etiology and progression. *Arch. Biochem. Biophys.* **563**, 51–5 (2014).

46. Gough, D. R. & Cotter, T. G. Hydrogen peroxide: a Jekyll and Hyde signalling molecule. *Cell Death Dis.* **2**, e213–e213 (2011).

47. Rhee, S. G. Cell signaling. H2O2, a necessary evil for cell signaling. *Science* **312**, 1882–3 (2006).

48. Koundouros, N. & Poulogiannis, G. Phosphoinositide 3-Kinase/Akt Signaling and Redox Metabolism in Cancer. *Front. Oncol.* **8**, 160 (2018).

49. Petry, A. & Görlach, A. Regulation of NADPH Oxidases by G Protein-Coupled Receptors. *Antioxid. Redox Signal.* **30**, 74–94 (2019).

50. Glady, A., Tanaka, M., Moniaga, C. S., Yasui, M. & Hara-Chikuma, M. Involvement of NADPH oxidase 1 in UVB-induced cell signaling and cytotoxicity in human keratinocytes. *Biochem. Biophys. reports* **14**, 7–15 (2018).

51. Raad, H. *et al.* NADPH Oxidase-1 Plays a Key Role in Keratinocyte Responses to UV Radiation and UVB-Induced Skin Carcinogenesis. *J. Invest. Dermatol.* **137**, 1311–1321 (2017).

52. Rezvani, H. R. *et al.* Protective effects of catalase overexpression on UVB-induced apoptosis in normal human keratinocytes. *J. Biol. Chem.* **281**, 17999–8007 (2006).

53. Rezvani, H. R. *et al.* Hypoxia-inducible Factor-1α, a Key Factor in the Keratinocyte Response to UVB Exposure. *J. Biol. Chem.* **282**, 16413–16422 (2007).

54. Beak, S. M., Lee, Y. S. & Kim, J.-A. NADPH oxidase and cyclooxygenase mediate the ultraviolet B-induced generation of reactive oxygen species and activation of nuclear factor-kappaB in HaCaT human keratinocytes. *Biochimie* **86**, 425–9 (2004).

55. Valencia, A. & Kochevar, I. E. Nox1-based NADPH oxidase is the major source of UVA-induced reactive oxygen species in human keratinocytes. *J. Invest. Dermatol.* **128**, 214–22 (2008).

56. Kim, J.-S., Diebold, B. A., Babior, B. M., Knaus, U. G. & Bokoch, G. M. Regulation of Nox1 Activity via Protein Kinase A-mediated Phosphorylation of NoxA1 and 14-3-3 Binding. *J. Biol. Chem.* **282**, 34787–34800 (2007).

57. Henri, P. *et al.* MC1R expression in HaCaT keratinocytes inhibits UVA-induced ROS production via NADPH oxidase- and cAMP-dependent mechanisms. *J. Cell. Physiol.* **227**, 2578–85 (2012).

58. Khaled, M. Glycogen Synthase Kinase 3beta Is Activated by cAMP and Plays an Active Role in the Regulation of Melanogenesis. *J. Biol. Chem.* **277**, 33690–33697 (2002).

59. Slominski, A., Tobin, D. J., Shibahara, S. & Wortsman, J. Melanin pigmentation in mammalian skin and its hormonal regulation. *Physiol Rev* **84**, 1155–1228 (2004).

60. Meyskens, F. L. & Liu-Smith, F. Redox-Redux and NADPH Oxidase (NOX): Even More Complicated than We Thought it Might Be. *J. Invest. Dermatol.* **137**, 1208–1210 (2017).

APPENDIX

Composition of Buffers

A. General buffers:

Phosphate buffered saline (PBS): 137 mM NaCl, 2.7 mM KCl, 10 mM Na_2HPO_4, 1 mM KH_2PO_4, pH 7.2.

Tris Buffer Saline (TBS): 20 mM Tris, 137 mM NaCl, pH 7.4.

Trypsin-EDTA solution: 0.5% trypsin, 0.2% EDTA in PBS.

Lysis buffer I: 50 mM Tris-HCl pH 8, 1% Igepal, 1 mM EDTA, 0.1 mM PMSF.

Lysis buffer II: 150 mM sodium chloride, 1.0 Triton X-100, 0.5% sodium deoxycholate, 0.1% SDS, 50 mM Tris, pH 8.0.

Phosphatase inhibitors: 200 mM imidazol, 100 mM NaF, 100 mM sodium o-vanadate and 1 M β-Glycerol phosphate.

B. DNA Buffers:

Tris-acetate-EDTA buffer (TAE): 40 mM Tris, 1 mM EDTA, and 30 mM acetic acid (0.175% v/v).

C. Reagents and buffers used for SDS-PAGE and protein transfer:

Loading sample buffer (4X): 250 mM Tris pH 6.8, 8% SDS, 20% glycerol, 0.08% bromophenol blue and 3.2 M β-mercaptoethanol.

Running buffer: 25 mM Tris, 190 mM glicine, 0.1% SDS, pH 8.3.

Transfer buffer: 48 mM Tris, 39 mM Glicine, 0.04% SDS, 20% methanol pH 9.2.

Polyacrylamide Gels:

Acrylamide/bisacrylamide (AA/bAA) mix was used in a ratio 30:0.8. The composition of the gels used for SDS-PAGE are described below:

- **Stacking gel (10% acrylamide):**

  1.6 ml H_2O

  1.33 ml AA/bAA

  1.25ml 1.5 M Tris-HCl 0.4% SDS pH 8.8 10%

  40 µl 10% $(NH_4)_2S_2O_8$

  5 µl TEMED

- **Resolving gel (4% acrylamide):**

  1.2 ml H_2O

  270 µl AA/bAA

  0.5 ml 1.5 M Tris-HCl 0.4% SDS pH 8.8 10%

  20 µl 10% APS

  2.5 µl TEMED

D. Other buffers:

Washing buffer: 1%Tween20 1x PBS or 1%Tween20 1x TBS.

Blocking buffer: 5% milk in TBST or 2% BSA in TBST or 2% BSA in PBST.

Acid wash buffer: 0.5 ml of 50 mM glycine and 150 mM NaCl, pH 3.0.

Krebs-Ringer phosphate (KRPG): 145 mM NaCl, 5.7 mM sodium phosphate, 4.86 mM KCl, 0.54 mM $CaCl_2$, 1.22 mM $MgSO_4$, 5.5 mM glucose, pH 7.35).

Alkaline electrophoresis solution: 200 mM NaOH, 1 mM EDTA pH>13.